

# **Influence of temperature and wind on moisture transport in cementitious materials**

**Salman Zafar**

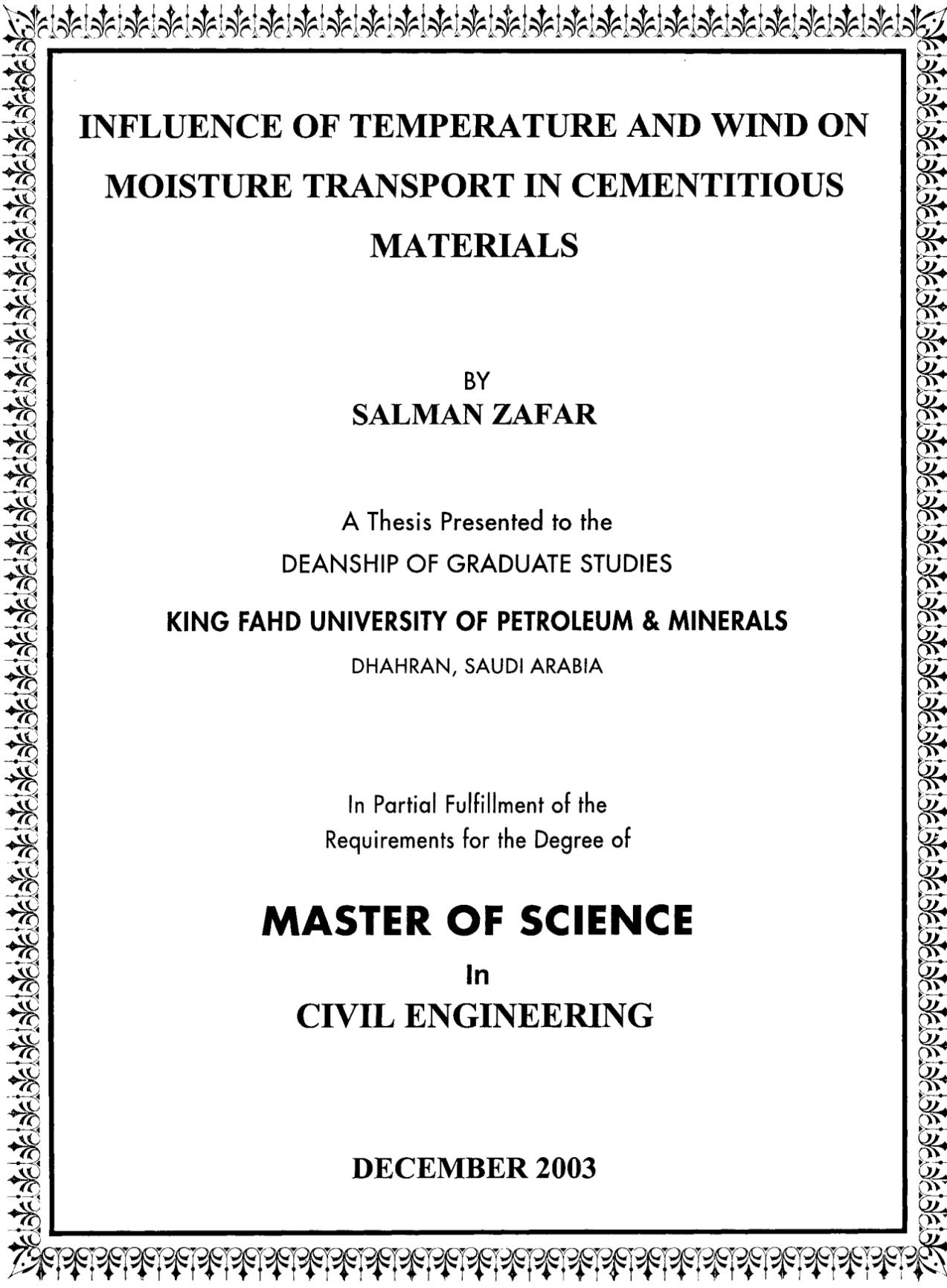
Civil Engineering

December 2003

## **Abstract**

Moisture diffusivity is a key physical parameter linked to the early deterioration of concrete structures, requiring repairs. The effect of hot arid climate of Saudi Arabia, characterized by high ambient temperature ( $T$ ) and high wind speed ( $\omega$ ), is investigated on the coefficient of moisture diffusivity ( $D$ ) and convective surface transfer coefficient ( $h(f)$ ) respectively, for ordinary concrete with varying water-cement ratio and selected repair materials. A combined experimental-numerical approach is adopted involving experimental investigation of moisture loss evolution under controlled exposure conditions in conjunction with an existing finite element based model DIANA-2D to calibrate values of  $D$  &  $h(f)$ . In addition, shrinkage strains were also recorded on specimens under similar environmental regimes. It is found that moisture diffusivity increases significantly with the increase in ambient temperature and water-cement ratio of concrete.

The salient feature of the work is a proposed model for mix design of a crack free concrete subject to environmental conditions defined by temperature ( $T$ ), wind speed ( $\omega$ ) and R.H. of 40%. This model has been postulated in terms of three invariant surfaces relating the primary variables. Also included are directions for further research to generalize the model for non-standard and new generation concretes.



**INFLUENCE OF TEMPERATURE AND WIND ON  
MOISTURE TRANSPORT IN CEMENTITIOUS  
MATERIALS**

BY  
**SALMAN ZAFAR**

A Thesis Presented to the  
DEANSHIP OF GRADUATE STUDIES  
**KING FAHD UNIVERSITY OF PETROLEUM & MINERALS**  
DHAHRAN, SAUDI ARABIA

In Partial Fulfillment of the  
Requirements for the Degree of

**MASTER OF SCIENCE**  
In  
**CIVIL ENGINEERING**

**DECEMBER 2003**

UMI Number: 1420766

## INFORMATION TO USERS

The quality of this reproduction is dependent upon the quality of the copy submitted. Broken or indistinct print, colored or poor quality illustrations and photographs, print bleed-through, substandard margins, and improper alignment can adversely affect reproduction.

In the unlikely event that the author did not send a complete manuscript and there are missing pages, these will be noted. Also, if unauthorized copyright material had to be removed, a note will indicate the deletion.

**UMI<sup>®</sup>**

---

UMI Microform 1420766

Copyright 2004 by ProQuest Information and Learning Company.

All rights reserved. This microform edition is protected against unauthorized copying under Title 17, United States Code.

ProQuest Information and Learning Company  
300 North Zeeb Road  
P.O. Box 1346  
Ann Arbor, MI 48106-1346

KING FAHD UNIVERSITY OF PETROLEUM & MINERALS  
DHAHRAN 31261, SAUDI ARABIA

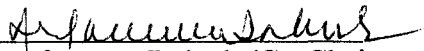
DEANSHIP OF GRADUATE STUDIES

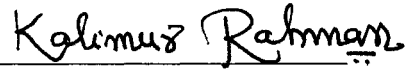
This thesis, written by SALMAN ZAFAR under the direction of his thesis advisor and approved by his thesis committee, has been presented to and accepted by the Dean of Graduate Studies, in partial fulfillment of the requirements for the degree of

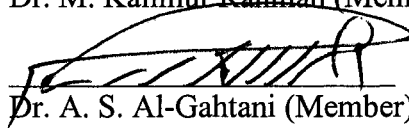
MASTER OF SCIENCE IN CIVIL ENGINEERING

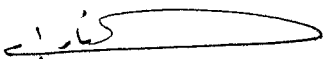
Thesis Committee

  
Dr. Ali H. Al-Gadhib (Chairman)

  
Prof. M. H. Baluch (Co-Chairman)


  
Dr. M. Kalimur Rahman (Member)

  
Dr. A. S. Al-Gahtani (Member)

  
Prof. Alfarabi M. Sharif (Member)



Prof. H.I. Al-Abdul Wahhab  
Department Chairman

  
Prof. Osama Ahmed Jannadi  
Dean of Graduate Studies

20-03-2004  
Date



Dedicated to My  
Brother, Parents &  
Sisters

# ACKNOWLEDGEMENT

All praise is for Almighty Allah who alone made this accomplishment possible and Salaam on His Prophet (PBUH). Acknowledgements are due to Civil Engineering Department and King Fahd University of Petroleum & Minerals for the support in carrying out this research.

I would like to express my gratitude to my main thesis advisor Dr. Ali H. Al-Gadhib for his encouragement and help throughout this work. My deepest thanks are offered to my thesis Co-advisor Dr. M.H. Baluch for his supervision, guidance and continuous involvement throughout this research. I am also highly thankful to Dr. M. Kalimur Rahman for his continuous support, emphasis on the practical aspects of the work and efforts to ensure high quality work. Thanks are due to the members of my thesis committee, Dr. A.S. Al-Gahtani and Dr. Alfarabi M. Sharif for their cooperation and support.

I also appreciate the assistance and encouragement received from the Chairman, faculty members, staff and graduate students of the department. Special thanks to Mr. Hassan for his continuous and untiring efforts to upgrade and maintain the equipment, Mr. Nahhash, Mr. Younus, Mr. Abu Abbas, Mr. Anwar, Mr. Mukarram, Mr. Omer and Mr. Esa for their assistance during the experimental work

Finally, I am deeply indebted to my Brother, Parents and Sisters for their love, prayers, extreme moral support, encouragement and patience during the course of my research.

# TABLE OF CONTENTS

<b>Acknowledgement</b>	<b>iv</b>
<b>List of Tables</b>	<b>xi</b>
<b>List of Figures</b>	<b>xii</b>
<b>Thesis Abstract (English)</b>	<b>xxv</b>
<b>Thesis Abstract (Arabic)</b>	<b>xxvi</b>
<b>1. INTRODUCTION</b>	<b>1</b>
1.1 Durability and Deterioration of Concrete .....	1
1.2 Repair of Concrete Structures .....	3
1.3 Moisture Transport and Durability of Cementitious Materials .....	6
1.4 Parameters Affecting Moisture Transport in Cementitious Materials .....	9
1.5 Need for Research .....	11
1.6 Aims and Objectives of Research .....	12
1.7 Research Methodology .....	13
<b>2. LITERATURE REVIEW</b>	<b>16</b>
2.1 Types of Moisture Transport in Cementitious Materials .....	16
2.2 Microstructure & Transport Properties of Cementitious Materials .....	20
2.2.1 Introduction .....	20
2.2.2 Microstructure and Diffusivity of Hydrated Cement Paste .....	21

2.2.3	Microstructure and Diffusivity of Mortar & Concrete .....	26
2.3	Mechanism of Moisture Transport in Cementitious Materials .....	29
2.3.1	Moisture Transport at Microscopic Level .....	30
2.3.2	Moisture Transport at Macroscopic Level .....	31
2.4	Moisture Diffusivity & Surface Transfer Coefficient .....	35
2.5	Effect of Temperature & Wind on Moisture Transport .....	38
2.6	Review of Methods for Measuring Moisture Profiles/Diffusivity .....	39
2.6.1	DIN Dry & Wet Cup Method .....	40
2.6.2	Slice-Dry-Weigh Method .....	42
2.6.3	Electrical Methods .....	43
2.6.4	Gamma Ray Attenuation .....	44
2.6.5	Neutron Radiography .....	46
2.6.6	Nuclear Magnetic Resonance (NMR) .....	47
2.6.7	Computer Tomography .....	48
2.6.8	Microwave Beam .....	48
2.6.9	Thermal Conductivity .....	49
2.6.10	Thermal Imaging .....	50
2.6.11	Capillary Water Uptake .....	51
2.6.12	Moisture Loss/Drying .....	52
2.7	Review of Methods Used for Computing Moisture Diffusivity .....	53
2.7.1	Boltzmann-Matano Method .....	53
2.7.2	Profile/Gradient Method .....	55
2.7.3	Difference Method .....	55

2.7.4	Double Integration Method .....	57
2.7.5	Numerical Methods .....	58
2.8	Types of Repair Materials .....	59
2.9	Properties of Repair Materials .....	61
2.10	Shrinkage of Concrete .....	63
2.11	Factors Affecting Drying Shrinkage of Concrete .....	66
2.11.1	Ambient Conditions .....	66
2.11.2	Curing of Concrete .....	68
2.11.3	Member Geometry .....	68
2.11.4	Cement Content, Type & Fineness .....	68
2.11.5	Water-Cement Ratio & Water Content .....	69
2.11.6	Aggregates .....	69
2.11.7	Admixtures .....	69
2.11.8	Construction Practice .....	70
2.12	Water Permeability of Concrete .....	71
2.13	Factors Affecting Water Permeability of Concrete .....	74
2.13.1	Water-Cement Ratio .....	74
2.13.2	Degree of Hydration .....	74
2.13.3	Properties of Cement .....	74
2.13.4	Curing Time .....	75
2.13.5	Temperature .....	75
2.13.6	Aggregate Properties .....	76
2.13.7	Mineral Admixtures .....	76

<b>3. Experimental Program for the Research</b>	<b>77</b>
3.1 Scope of the Experimental Work .....	77
3.2 Selected Repair Materials .....	78
3.2.1 Fluid Micro-Concrete (FMC1) .....	78
3.2.2 Flowing Precision Concrete (FMC2) .....	79
3.3 Concrete Mix Design .....	80
3.4 Shape and Size of Test Specimens .....	81
3.5 Moulds for Specimens .....	82
3.6 Manufacturing of Specimens .....	82
3.6.1 Mixing Procedures .....	84
3.6.2 Placing of Concrete & Repair Mortars .....	85
3.6.3 Curing Regimes for the Test Specimens .....	86
3.7 Test Procedure for Compressive Strength .....	86
3.8 Test Procedure for Water Permeability .....	88
3.9 Procedure for Drying Tests .....	91
3.9.1 Specimen Preparation .....	91
3.9.2 Environmental Chambers .....	94
3.9.3 Weight Loss Measurements .....	99
3.9.4 Testing Regimes .....	99
3.9.5 Moisture Content Determination .....	101
3.10 Shrinkage Test Procedure .....	101

<b>4. Analysis and Discussion of Results</b>	<b>104</b>
4.1 Properties of Concrete .....	104
4.1.1 Evolution of Compressive Strength .....	104
4.1.2 Water Permeability .....	107
4.2 Drying Tests for Moisture Diffusivity .....	109
4.2.1 Moisture Loss in Concrete .....	109
4.2.1.1 Effect of Water-Cement Ratio .....	109
4.2.1.2 Effect of Wind Speed .....	122
4.2.1.3 Effect of Temperature .....	131
4.2.2 Moisture Loss in Repair Materials .....	139
4.2.2.1 Influence of Wind .....	143
4.2.2.2 Influence of Temperature and Relative Humidity .....	146
4.3 Drying Shrinkage .....	148
4.3.1 Shrinkage Strains in Concrete .....	148
4.3.2 Shrinkage Strain in Repair Materials .....	152
<b>5. Numerical Computation of Moisture Diffusivity</b>	<b>154</b>
5.1 Introduction .....	154
5.2 Description of DIANA-2D .....	156
5.2.1 Governing Finite Element Equations .....	156
5.2.2 Functional Form of Diffusivity .....	159
5.2.3 Role of Convective Transfer Coefficient .....	161
5.2.4 Procedure for Computation of Diffusivity .....	161

5.3 Best Fit Diffusivity Law Parameters for Concrete .....	166
5.3.1 Parameters at 50 °C & 6 Km/hr Wind .....	166
5.3.2 Parameters at 50 °C & 22 Km/hr Wind .....	167
5.3.3 Parameters at 35 °C & 6 Km/hr Wind .....	174
5.3.4 Parameters at 35 °C & 22 Km/hr Wind .....	174
5.4 Moisture Diffusivity of Concrete .....	181
5.4.1 Effect of Water-Cement Ratio .....	187
5.4.2 Effect of Ambient Temperature .....	189
5.5 Diffusivity versus Strength & Permeability of Concrete .....	194
5.6 A New Approach to Mix Design based upon Moisture Diffusivity .....	197
5.7 Best Fit Diffusivity Law Parameters for Repair Materials .....	202
5.7.1 Diffusivity Parameters for FMC1 .....	202
5.7.2 Diffusivity Parameters for FMC2 .....	203
5.7.3 Effect of Temperature .....	207
5.8 Effect of Wind Speed on Convective Transfer Coefficient .....	210
<b>6. Conclusions and Recommendations</b>	<b>212</b>
6.1 Conclusions .....	212
6.2 Recommendations for Future Research .....	217
<b>APPENDIX-A</b>	<b>218</b>
<b>REFERENCES</b>	<b>228</b>

## LIST OF TABLES

3.1	Concrete Mix Design .....	81
3.2	Description of Test Specimens .....	82
3.3	Drying Test Regime for FMC1 & FMC2 .....	100
3.4	Drying Test Regime for Each Concrete Mix .....	101
4.1	Compressive Strength of Concrete .....	106
4.2	Regression Coefficients for ACI Compressive Strength Evolution Equation .....	106
5.1	Parameters for Diffusivity Law of Concrete, $D(C) = b_0 \tan (b_1 c^n)$ .....	182
5.2	Parameters for Diffusivity Law of Repair Materials, $D(C) = b_0 \tan (b_1 c^n)$ .....	208
5.3	Convective Transfer Coefficient at Various Wind Speeds .....	211

## LIST OF FIGURES

1.1	Phases in the Life Cycle of a Concrete Structure .....	4
1.2	Anatomy of the Life Cycle of a Concrete Structure .....	4
1.3	Freeze Thaw Action in Concrete due to Moisture Penetration .....	8
1.4	Drying Shrinkage Cracks in Concrete due to Moisture Loss .....	8
1.5	Carbonation in Concrete due to Moisture Loss .....	8
1.6	Phases of the Research .....	15
2.1	Electron Microscope Image of Concrete (top left), Mortar (top right), Hydrated Cement Paste (bottom left) & CSH (bottom right) .....	23
2.2	High Resolution Electron Microscope Image of Hydrated Cement Paste .....	23
2.3	SEI of Interfacial Transition Zone between Coarse Aggregate and Hydrated Cement Paste .....	27
2.4	SEI of Interfacial Transition Zone b/w Hydrated Cement Paste and Sand Grain .....	27
2.5	Equilibrium Vapor Pressure for Capillary Pores .....	32
2.6	De-sorption Isotherms in Cement Paste & Dense Concrete .....	32
2.7	Three Phases of Moisture Transport at Macroscopic Level .....	34

2.8	Principal of Boltzmann-Matano Method (Left), Profile/Gradient Method (Right) .....	56
2.9	Classification of Cement Based Repair Materials .....	60
2.10	Factors Affecting Drying Shrinkage of Concrete .....	67
2.11	Illustration of Permeability and Porosity, Porous-Impermeable (Top Left), Porous-Permeable (Top Right), Highly Porous-Less Permeable (Bottom Left), Less Porous-Highly Permeable material (Bottom Right) .....	73
3.1	Moulds for Drying & Shrinkage Tests on Concrete .....	83
3.2	Arrangement for Compressive Strength Test .....	87
3.3	Sketch of the Test Cell for Water Permeability by DIN 1048 .....	89
3.4	Water Permeability Specimens in the Test Cells Assembly .....	90
3.5	Water Tank, Valve & Pressure Meter Arrangement for Permeability Test .....	90
3.6	Splitting Arrangement for Water Permeability Specimens .....	92
3.7	Split Permeability Specimen showing Depth of Water Penetration .....	92
3.8	Sealed Diffusivity Specimens of Repair in Pyrex Chamber .....	93
3.9	Sealed Diffusivity Specimens of Concrete in Pyrex Chamber .....	93
3.10	Pyrex Glass Environmental Chamber in its Old Form .....	96
3.11	Outside view of the Steel Environmental Chamber & Control Unit (Old) .....	96
3.12	Inside view of Old Steel Chamber with Diffusivity Specimens .....	97
3.13	Set Up for Generating Very High Wind Speeds in Steel Chamber .....	97

3.14	Inside View of Up Graded Steel Chamber with Shaft & Fan Blade .....	98
3.15	Up Graded Pyrex Glass Chamber with Diffusivity & Shrinkage Specimens .....	98
3.16	Shrinkage Specimens Connected to Data Logger & Computer .....	103
4.1	Evolution of Compressive Strength of Concrete .....	106
4.2	Comparison of Water Permeability of Concrete Mixes .....	108
4.3	Relationship b/w Concrete Compressive Strength at 28 days and Water Penetration Depth .....	108
4.4	Effect of W/C Ratio on Moisture Loss (%) for 25 mm Specimen at 50 °C and 6 km/hr Wind .....	111
4.5	Effect of W/C Ratio on Moisture Loss (%) for 50 mm Specimen at 50 °C and 6 km/hr Wind .....	111
4.6	Effect of W/C Ratio on Moisture Loss (%) for 75 mm Specimen at 50 °C and 6 km/hr Wind .....	112
4.7	Effect of W/C Ratio on Moisture Loss (%) for 100 mm Specimen at 50 °C and 6 km/hr Wind .....	112
4.8	Effect of W/C Ratio on Moisture Loss (%) for 25 mm Specimen at 50 °C and 22 km/hr Wind .....	114
4.9	Effect of W/C Ratio on Moisture Loss (%) for 50 mm Specimen at 50 °C and 22 km/hr Wind .....	114
4.10	Effect of W/C Ratio on Moisture Loss (%) for 75 mm Specimen at 50 °C and 22 km/hr Wind .....	115

4.11	Effect of W/C Ratio on Moisture Loss (%) for 100 mm Specimen at 50 °C and 22 km/hr Wind .....	115
4.12	Effect of W/C Ratio on Moisture Loss (%) for 25 mm Specimen at 35 °C and 6 km/hr Wind .....	118
4.13	Effect of W/C Ratio on Moisture Loss (%) for 50 mm Specimen at 35 °C and 6 km/hr Wind .....	118
4.14	Effect of W/C Ratio on Moisture Loss (%) for 75 mm Specimen at 35 °C and 6 km/hr Wind .....	119
4.15	Effect of W/C Ratio on Moisture Loss (%) for 100 mm Specimen at 35 °C and 6 km/hr Wind .....	119
4.16	Effect of W/C Ratio on Moisture Loss (%) for 25 mm Specimen at 35 °C and 22 km/hr Wind .....	120
4.17	Effect of W/C Ratio on Moisture Loss (%) for 50 mm Specimen at 35 °C and 22 km/hr Wind .....	120
4.18	Effect of W/C Ratio on Moisture Loss (%) for 75 mm Specimen at 35 °C and 22 km/hr Wind .....	121
4.19	Effect of W/C Ratio on Moisture Loss (%) for 100 mm Specimen at 35 °C and 22 km/hr Wind .....	121
4.20	Effect of Wind Speed on Moisture Loss (%) for 25 mm Specimens for W/C Ratio 0.45 at 50 °C .....	124
4.21	Effect of Wind Speed on Moisture Loss (%) for 75 mm Specimens for W/C Ratio 0.45 at 50 °C .....	124

4.22	Effect of Wind Speed on Moisture Loss (%) for 25 mm Specimens for W/C Ratio 0.5 at 50 °C .....	125
4.23	Effect of Wind Speed on Moisture Loss (%) for 75 mm Specimens for W/C Ratio 0.5 at 50 °C .....	125
4.24	Effect of Wind Speed on Moisture Loss (%) for 25 mm Specimens for W/C Ratio 0.6 at 50 °C .....	126
4.25	Effect of Wind Speed on Moisture Loss (%) for 75 mm Specimens for W/C Ratio 0.6 at 50 °C .....	126
4.26	Effect of Wind Speed on Moisture Loss (%) for 25 mm Specimens for W/C Ratio 0.45 at 35 °C .....	128
4.27	Effect of Wind Speed on Moisture Loss (%) for 75 mm Specimens for W/C Ratio 0.45 at 35 °C .....	128
4.28	Effect of Wind Speed on Moisture Loss (%) for 25 mm Specimens for W/C Ratio 0.5 at 35 °C .....	129
4.29	Effect of Wind Speed on Moisture Loss (%) for 75 mm Specimens for W/C Ratio 0.5 at 35 °C .....	129
4.30	Effect of Wind Speed on Moisture Loss (%) for 25 mm Specimens for W/C Ratio 0.6 at 35 °C .....	130
4.31	Effect of Wind Speed on Moisture Loss (%) for 75 mm Specimens for W/C Ratio 0.6 at 35 °C .....	130
4.32	Effect of Temperature on Moisture Loss (%) at Wind Speed 6 km/hr W/C Ratio 0.45 Specimen Thickness 50 mm .....	133

4.33	Effect of Temperature on Moisture Loss (%) at Wind Speed 6 km/hr	
	W/C Ratio 0.45 Specimen Thickness 100 mm .....	133
4.34	Effect of Temperature on Moisture Loss (%) at Wind Speed 6 km/hr	
	W/C Ratio 0.5 Specimen Thickness 50 mm .....	134
4.35	Effect of Temperature on Moisture Loss (%) at Wind Speed 6 km/hr	
	W/C Ratio 0.5 Specimen Thickness 100 mm .....	134
4.36	Effect of Temperature on Moisture Loss (%) at Wind Speed 6 km/hr	
	W/C Ratio 0.6 Specimen Thickness 50 mm .....	135
4.37	Effect of Temperature on Moisture Loss (%) at Wind Speed 6 km/hr	
	W/C Ratio 0.6 Specimen Thickness 100 mm .....	135
4.38	Effect of Temperature on Moisture Loss (%) at Wind Speed 22 km/hr	
	W/C Ratio 0.45 Specimen Thickness 50 mm .....	136
4.39	Effect of Temperature on Moisture Loss (%) at Wind Speed 22 km/hr	
	W/C Ratio 0.45 Specimen Thickness 100 mm .....	136
4.40	Effect of Temperature on Moisture Loss (%) at Wind Speed 22 km/hr	
	W/C Ratio 0.5 Specimen Thickness 50 mm .....	137
4.41	Effect of Temperature on Moisture Loss (%) at Wind Speed 22 km/hr	
	W/C Ratio 0.5 Specimen Thickness 100 mm .....	137
4.42	Effect of Temperature on Moisture Loss (%) at Wind Speed 22 km/hr	
	W/C Ratio 0.6 Specimen Thickness 50 mm .....	138
4.43	Effect of Temperature on Moisture Loss (%) at Wind Speed 22 km/hr	
	W/C Ratio 0.6 Specimen Thickness 100 mm .....	138

4.44	Evolution of Moisture Loss (grams) for FMC2 at 30 °C & 60 % R.H .....	140
4.45	Evolution of Moisture Loss (%) for FMC2 at 30 °C & 60 % R.H .....	140
4.46	Evolution of Moisture Loss (%) for FMC1 at 50 °C & 50 % R.H .....	141
4.47	Evolution of Moisture Loss (%) for FMC2 at 50 °C & 50 % R.H .....	141
4.48	Evolution of Moisture Loss (%) for FMC1 at 50 °C, 50 % R.H & 12 km/hr wind .....	142
4.49	Evolution of Moisture Loss (%) for FMC2 at 50 °C, 50 % R.H & 12 km/hr wind .....	142
4.50	Effect of Wind on Moisture Loss (%) for FMC1, Specimen Thickness-40 mm .....	144
4.51	Effect of Wind on Moisture Loss (%) for FMC1, Specimen Thickness-50 mm .....	144
4.52	Effect of Wind on Moisture Loss (%) for FMC2, Specimen Thickness-40 mm .....	145
4.53	Effect of Wind on Moisture Loss (%) for FMC2, Specimen Thickness-50 mm .....	145
4.54	Effect of Temperature & Relative Humidity on Moisture Loss (%) for FMC2, Specimen Thickness-30 mm .....	147
4.55	Effect of Temperature & Relative Humidity on Moisture Loss (%) for FMC2, Specimen Thickness 40 mm .....	147
4.56	Shrinkage strain in Concrete at 50 °C, 40 % R.H & 6 km/hr Wind .....	150
4.57	Shrinkage strain in Concrete at 50 °C, 40 % R.H & 22 km/hr Wind ....	150

4.58	Shrinkage strain in Concrete at 35 °C, 40 % R.H & 6 km/hr Wind .....	151
4.59	Shrinkage strain in Concrete at 35 °C, 40 % R.H & 22 km/hr Wind .....	151
4.60	Shrinkage strain in FMC1 & FMC2 at 50 °C & 50 % R.H .....	153
5.1	Influence of Convective Transfer Coefficient on Moisture Loss .....	163
5.2	Finite Element Discretization of Diffusivity Specimen for DIANA-2D .....	163
5.3	Flow Chart for Time Step Computations of Moisture Content in DIANA-2D .....	164
5.4	Basic Flow Chart of Finite Element Program DIANA-2D .....	165
5.5	Computed & Experimental Mean Moisture Loss (%) for W/C 0.45 - 100x100x75 mm Specimen at 50 °C & 6 km/hr Wind .....	168
5.6	Computed & Experimental Mean Moisture Loss (%) for W/C 0.45 - 100x100x100 mm Specimen at 50 °C & 6 km/hr Wind .....	168
5.7	Computed & Experimental Mean Moisture Loss (%) for W/C 0.5 - 100x100x75 mm Specimen at 50 °C & 6 km/hr Wind .....	169
5.8	Computed & Experimental Mean Moisture Loss (%) for W/C 0.5 - 100x100x100 mm Specimen at 50 °C & 6 km/hr Wind .....	169
5.9	Computed & Experimental Mean Moisture Loss (%) for W/C 0.6 - 100x100x75 mm Specimen at 50 °C & 6 km/hr Wind .....	170
5.10	Computed & Experimental Mean Moisture Loss (%) for W/C 0.6 - 100x100x100 mm Specimen at 50 °C & 6 km/hr Wind .....	170
5.11	Computed & Experimental Mean Moisture Loss (%) for W/C 0.45 - 100x100x75 mm Specimen at 50 °C & 22 km/hr Wind .....	171

5.12	Computed & Experimental Mean Moisture Loss (%) for W/C 0.45 - 100x100x100 mm Specimen at 50 °C & 22 km/hr Wind	.... 171
5.13	Computed & Experimental Mean Moisture Loss (%) for W/C 0.5 - 100x100x75 mm Specimen at 50 °C & 22 km/hr Wind	..... 172
5.14	Computed & Experimental Mean Moisture Loss (%) for W/C 0.5 - 100x100x100 mm Specimen at 50 °C & 22 km/hr Wind	..... 172
5.15	Computed & Experimental Mean Moisture Loss (%) for W/C 0.6 - 100x100x75 mm Specimen at 50 °C & 22 km/hr Wind	..... 173
5.16	Computed & Experimental Mean Moisture Loss (%) for W/C 0.6 - 100x100x100 mm Specimen at 50 °C & 22 km/hr Wind	..... 173
5.17	Computed & Experimental Mean Moisture Loss (%) for W/C 0.45 - 100x100x75 mm Specimen at 35 °C & 6 km/hr Wind	..... 175
5.18	Computed & Experimental Mean Moisture Loss (%) for W/C 0.45 - 100x100x100 mm Specimen at 35 °C & 6 km/hr Wind	..... 175
5.19	Computed & Experimental Mean Moisture Loss (%) for W/C 0.5 - 100x100x75 mm Specimen at 35 °C & 6 km/hr Wind	..... 176
5.20	Computed & Experimental Mean Moisture Loss (%) for W/C 0.5 - 100x100x100 mm Specimen at 35 °C & 6 km/hr Wind	..... 176
5.21	Computed & Experimental Mean Moisture Loss (%) for W/C 0.6 - 100x100x75 mm Specimen at 35 °C & 6 km/hr Wind	..... 177
5.22	Computed & Experimental Mean Moisture Loss (%) for W/C 0.6 - 100x100x100 mm Specimen at 35 °C & 6 km/hr Wind	..... 177

5.23	Computed & Experimental Mean Moisture Loss (%) for W/C 0.45 - 100x100x75 mm Specimen at 35 °C & 22 km/hr Wind .....	178
5.24	Computed & Experimental Mean Moisture Loss (%) for W/C 0.45 - 100x100x100 mm Specimen at 35 °C & 22 km/hr Wind ....	178
5.25	Computed & Experimental Mean Moisture Loss (%) for W/C 0.5 - 100x100x75 mm Specimen at 35 °C & 22 km/hr Wind .....	179
5.26	Computed & Experimental Mean Moisture Loss (%) for W/C 0.5 - 100x100x100 mm Specimen at 35 °C & 22 km/hr Wind .....	179
5.27	Computed & Experimental Mean Moisture Loss (%) for W/C 0.6 - 100x100x75 mm Specimen at 35 °C & 22 km/hr Wind .....	180
5.28	Computed & Experimental Mean Moisture Loss (%) for W/C 0.6 - 100x100x100 mm Specimen at 35 °C & 22 km/hr Wind ....	180
5.29	Diffusivity-Normalized Moisture Content for Concrete, W/C 0.45 at 50 °C .....	183
5.30	Diffusivity-Normalized Moisture Content for Concrete, W/C 0.5 at 50 °C .....	183
5.31	Diffusivity-Normalized Moisture Content for Concrete, W/C 0.6 at 50 °C .....	184
5.32	Diffusivity-Normalized Moisture Content for Concrete, W/C 0.45 at 35 °C .....	184
5.33	Diffusivity-Normalized Moisture Content for Concrete, W/C 0.5 at 35 °C .....	185

5.34	Diffusivity-Normalized Moisture Content for Concrete, W/C 0.6 at 35 °C .....	185
5.35	Generic Curves for Effect of 'n' on Diffusivity ~ Normalized Moisture Content .....	186
5.36	Effect of Water-Cement Ratio on Diffusivity-Normalized Moisture Content for Concrete at 50 °C .....	188
5.37	Effect of Water-Cement Ratio on Diffusivity-Normalized Moisture Content for Concrete at 35 °C .....	188
5.38	Average Diffusivity at 35 °C ~ Water Cement Ratio of Concrete .....	190
5.39	Average Diffusivity at 50 °C ~ Water Cement Ratio of Concrete .....	190
5.40	Effect of Temperature on Diffusivity-Normalized Moisture Content for W/C 0.45 .....	192
5.41	Effect of Temperature on Diffusivity-Normalized Moisture Content for W/C 0.5 .....	192
5.42	Effect of Temperature on Diffusivity-Normalized Moisture Content for W/C 0.6 .....	193
5.43	Average Diffusivity at 50 °C ~ 35 °C for Concrete .....	193
5.44	Average Diffusivity at 50 °C ~ 28 day Compressive Strength of Concrete .....	195
5.45	Average Diffusivity at 35 °C ~ 28 day Compressive Strength of Concrete .....	195
5.46	Average Diffusivity at 50 °C ~ Permeability of Concrete .....	196
5.47	Average Diffusivity at 35 °C ~ Permeability of Concrete .....	196

5.48	Shrinkage Strain in Concrete at 45 days ~ Mean Moisture Loss at 28 days [Specimen size 100x100x75 mm] .....	200
5.49	Average Moisture Diffusivity of Concrete ~ Mean Moisture Loss at 28 days and Ambient Wind Speed [Specimen size 100x100x75 mm] ....	200
5.50	Water Cement Ratio of Concrete ~ Average Moisture Diffusivity and Ambient Temperature .....	201
5.51	Water Cement Ratio of Concrete ~ Ambient Temperature and Wind Speed .....	201
5.52	Computed & Experimental Mean Moisture Loss (%) for FMC1 - 100x100x40 mm Specimen at 30 °C & 60 % R.H .....	204
5.53	Computed & Experimental Mean Moisture Loss (%) for FMC1 - 100x100x40 mm Specimen at 50 °C & 50 % R.H .....	204
5.54	Computed & Experimental Mean Moisture Loss (%) for FMC1, 100x100x40 mm Specimen at 50 °C, 50 % R.H & 12 km/hr Wind .....	205
5.55	Computed & Experimental Mean Moisture Loss (%) for FMC2, 100x100x40 mm Specimen at 30 °C & 60 % R.H .....	205
5.56	Computed & Experimental Mean Moisture Loss (%) for FMC2, 100x100x40 mm Specimen at 50 °C & 50 % R.H .....	206
5.57	Computed & Experimental Mean Moisture Loss (%) for FMC2, 100x100x40 mm Specimen at 50 °C, 50 % R.H & 12 km/hr Wind .....	206
5.58	Effect of Temperature on Diffusivity-Normalized Moisture Content for FMC1 .....	209

5.59	Effect of Temperature on Diffusivity-Normalized Moisture Content for FMC2 .....	209
5.60	Convective Transfer Coefficient ~ Wind Speed .....	211

# THESIS ABSTRACT

<b>Full Name</b>	<b>Salman Zafar</b>
<b>Title of Study</b>	<b>Influence of Temperature and Wind on Moisture Transport in Cementitious Materials</b>
<b>Degree</b>	<b>Master of Science</b>
<b>Major Field</b>	<b>Civil Engineering (Structures)</b>
<b>Date of Degree</b>	<b>December 2003</b>

Moisture diffusivity is a key physical parameter linked to the early deterioration of concrete structures, requiring repairs. The effect of hot and arid climate of Saudi Arabia, characterized by high ambient temperature ( $T$ ) and high wind speed ( $\omega$ ), is investigated on the coefficient of moisture diffusivity ( $D$ ) and convective surface transfer coefficient ( $h_f$ ) respectively, for ordinary concrete with varying water-cement ratio and selected repair materials. A combined experimental-numerical approach is adopted involving experimental investigation of moisture loss evolution under controlled exposure conditions in conjunction with an existing finite element based model DIANA-2D to calibrate values of  $D$  &  $h_f$ . In addition, shrinkage strains were also recorded on specimens under similar environmental regimes. It is found that moisture diffusivity increases significantly with the increase in ambient temperature and water-cement ratio of concrete.

The salient feature of the work is a proposed model for mix design of a crack free concrete subject to environmental conditions defined by temperature ( $T$ ), wind speed ( $\omega$ ) and R.H of 40%. This model has been postulated in terms of three invariant surfaces relating the primary variables. Also included are directions for further research to generalize the model for non-standard and new generation concretes.

**Master of Science Degree**  
**King Fahd University of Petroleum and Minerals**  
**Dhahran, Saudi Arabia**  
**December 2003**

## الملخص

الاسم الكامل: سلمان ظفر

عنوان الدراسة: تأثير الحرارة والرياح على عملية انتقال الرطوبة في المواد الاسمنتية.

الدرجة: ماجستير

المجال: هندسة مدنية (إنشاء)

تاريخ التخرج : ديسمبر 2003 م

خاصية الانتشار الرطوبي تلعب دورا هاما في عملية التدهور المبكر للمباني الخرسانية الخاضعة لعملية الإصلاح الخرساني . إن تأثير الطقس الحار والجاف في المملكة العربية السعودية متمثلا بالحرارة العالية وسرعة الرياح القوية تم التحقق منها وتأثيرها على كلا من خاصية الانتشار الرطوبي للخرسانة العادية حيث المتغير هو نسبة الماء الى الاسمنت وكذلك المعامل الحملي لسطح المادة الصلاحية للخرسانة هنا تجدر الإشارة بان الدراسة عبارة عن دمج التجارب العملية والتحليل الرقمي من خلال قياس معدل التبخر وانخفاض الرطوبة داخل المواد تحت تأثير محيط بيئي محدد وعن طريق التحليل باستخدام العناصر المحددة تم معايرة كلا من خاصية الانتشار والمعامل الحملي للسطح . كما تم تسجيل الانفعال ذات الصلة بالنقل على العينات التي كانت تحت الدراسة وخاضعة لنفس الظروف البيئية .

لقد وجد ان خاصية الانتشار الرطوبي تتزايد بشكل ملحوظ مع زيادة كلا من الحرارة ونسبة الماء الى الاسمنت وهذا ما يفاقم عملية التدهور المبكر للخرسانة والمواد الإصلاحية .

ان ما يميز هذه الدراسة هو اتمام عمل نموذج لتصميم خلطة الخرسانة من اجل الحصول على خرسانة خالية من العيوب والشروخ عند تعرضها الى نفس الظروف التي تمت التجارب فيها من حرارة وسرعة رياح ونسبة الرطوبة 40 % هذا النموذج مبني على أساس الشكل العام لثلاثة سطوح . كما ختمت هذه الدراسة بتوصية من اجل توسيع مجال الدراسة وعمل نموذج عام لجميع انواع الخرسانة بما في ذلك الخرسانة المطورة ذات الأداء الجيد .

ماجستير علوم

جامعة الملك فهد للبترول والمعادن

الظهران - المملكة العربية السعودية

ديسمبر 2003 م

# **CHAPTER 1**

## **INTRODUCTION**

### **1.1 Durability and Deterioration of Concrete**

Concrete in many respects is the wonder material of this century. Among all the construction materials, it has the best ecological profile for a given engineering property such as strength or elastic modulus. It is probably the most widely and extensively used building material in the world, due to its relatively low cost, easy availability of constituents, versatility and adaptability. It is estimated that the present consumption of concrete is of the order of 4.5 billion tons every year [1]. It is easily prepared and fabricated into many conceivable shapes and structural systems in the realms of infrastructure, transport and habitation. It is often identified with a nation's stability and economic progress and the quality of human life. It thus seems reasonable to assume that in a rapidly changing world, the concrete industry and technology can offer one of the best ways forward to satisfy the social and human needs and aspirations.

In spite of these intrinsic technical and economical advantages of the material, and in spite of the tremendous scientific advances that have been made in our understanding of its microstructure and engineering, deterioration of concrete has become a major global problem, and there is widespread concern about its lack of durability [2]. The damage to

concrete structures can be attributed to a wide variety of causes including, but not limited to the following [3]:

- Lack of quality control in construction.
- Design defects including insufficient concrete strength, cover, structural depth and reinforcement.
- A phenomenal increase in loading spectra on infrastructure like bridges, associated with impact and vibration, abrasion, wear and fatigue.
- Damage in concrete under physical and chemical attack from:
  - Air borne chlorides and sulfates
  - Soil borne chlorides and sulfates
  - Leeching of salts
  - Salt crystal expansion
  - Alkali aggregate reaction
  - Chemical exposure
  - Thermal movement
  - Erosion
  - Humidity dynamics
  - Freeze and thaw reactions
- Damage due to concrete reinforcement under attack from
  - Chloride
  - Carbonation, resulting in destruction of steel passivity layer

The consequences of such a diverse and aggressive warfare on living and breathing concrete is tremendous. The concrete responds to such an attack with a

softening behavior associated with extensive cracking, de-lamination of concrete cover and dilution of reinforcement. It loses the prime characteristics of being a dense material. The porous concrete consequently becomes vulnerable to more profound attack, which if allowed continuing, results in disastrous failures.

In the international sphere, deterioration has been attributed to aging and degradation of concrete, carbonation, chloride contamination due to use of deicing salts, freeze and thaw action and alkali-aggregate reaction. The environment in Arabian Gulf region and Eastern province of Saudi Arabia is characterized by high humidity, high temperature and wind speeds, and excessive air/soil borne salinity, which has resulted in deterioration and subsequent cracking and spalling of concrete.

## **1.2 Repair of Concrete Structures**

The anatomy of the life cycle of a concrete structure indicates three different phases [4]:

- An early stage of trouble free life
- Problem initiation and incubation period
- Damage propagation period

As the damage propagates a time comes when the safety and serviceability of the structure gets seriously impaired, hence necessitating repair work to restore it [Figure 1.1, 1.2]. Repair, rehabilitation and strengthening of deteriorated concrete structures, is economically the most viable solution. In the United States repair and improvement to infrastructure will amount to \$ 3.3 trillions over the next two decades and has become the

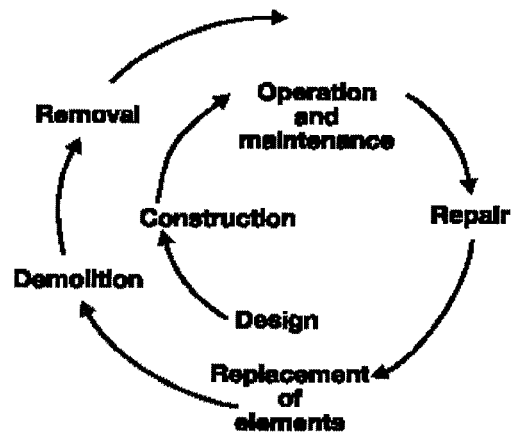


Figure 1.1: Phases in the Life Cycle of a Concrete Structure

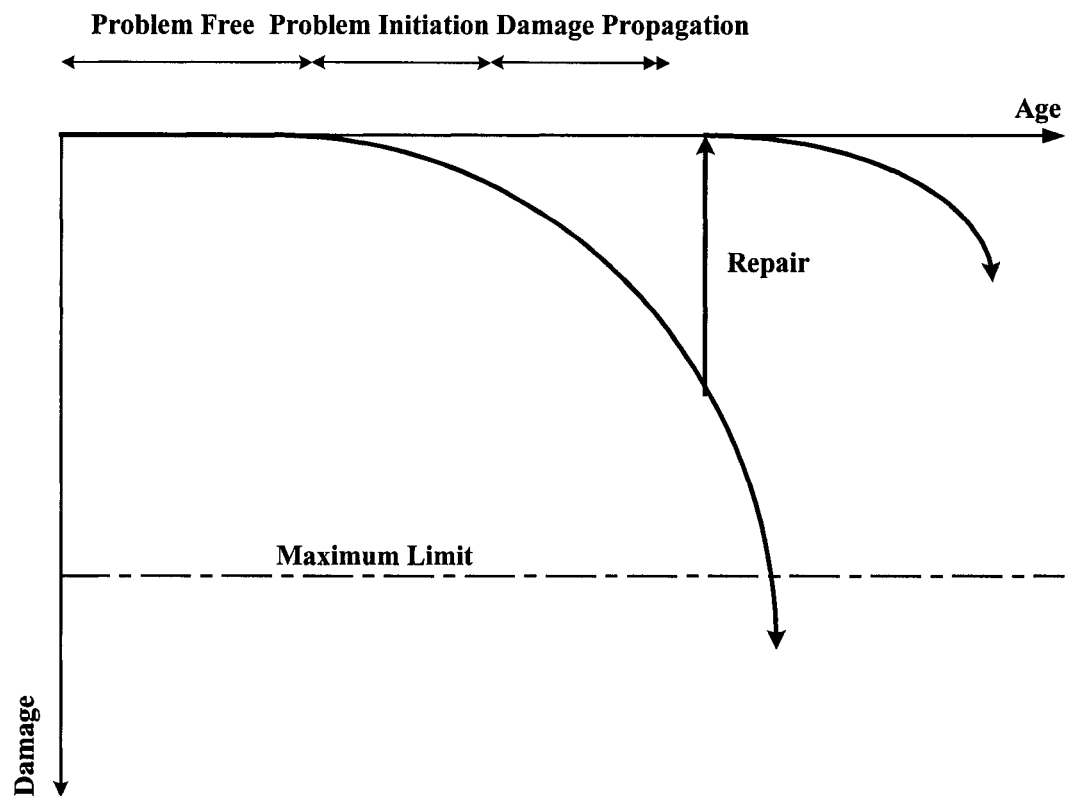


Figure 1.2: Anatomy of the Life Cycle of a Concrete Structure

third largest deficit in the country [5]. In U.K the cost of such repair is estimated to be in excess of 500 million pounds annually [6], whereas in Australia it is estimated to cost in excess of AUS \$ 200 million per year [7]. In the Arabian Gulf region, the potentially aggressive environment has resulted in premature deterioration requiring extensive repairs [8-13]. It is estimated that repair and maintenance of concrete structures in Saudi Arabia would run into billions of Saudi Riyals in the coming few decades [14].

The rapid growth in restoration has undoubtedly greatly influenced the market for the products used in the maintenance and repair of deteriorated concrete structures, which has literally been inundated by new products. However this explosion of new products has not only considerably complicated the selection of most suitable materials for the specific work but has also helped the circulation of products which are unsuitable for the job due to lack of norms indicating performance requirements of these materials. The commercially available repair materials fall into two main categories [6]:

- Cementitious and modified cementitious repair mortars and micro-concrete
- Resin based repair mortars and pure resins

The later category is used principally in crack injections, thin repairs and under chemical exposure situations.

Depending on the nature of application a repair system should meet the following requirements [15]:

- Arrest the deterioration of concrete
- Form an impermeable barrier to prevent ingress of deleterious or aggressive species (Oxygen, Carbon Dioxide, moisture and aggressive chloride and sulfate ions)
- Create an environment that restores passivity of the reinforcement

- Restore the integrity of the structure
- Provide an aesthetically acceptable finish

To achieve these requirements the primary focus in the development of repair products has been on the production of materials with high compressive strength, which has resulted in the development of unprecedented high early compressive strength repair materials. Despite of this achievement the repaired structures in many projects have shown early signs of distress and failure in the form of extensive cracking and/or delamination from the substrate [16]. In the Eastern province of Saudi Arabia some structures have been repaired thrice over a span of three years thus defeating the prime objective of restoration through costly repairs.

### **1.3 Moisture transport and durability of cementitious materials**

The single most important factor, which plays a dominant role in problem initiation, incubation and damage propagation period, is the movement of moisture in concrete. In a cementitious material saturated by liquid water, which is suddenly subjected to an ambient environment of lower relative humidity, an initial thermodynamic imbalance occurs between the external vapor concentration and that within the specimen. To restore thermodynamic equilibrium, the sample exchanges water vapor with the exterior through surface convection, resulting in diffusion of moisture from the core of concrete towards its exterior boundaries. The moisture diffusion process continues until a hygral equilibrium state is reached.

Cementitious materials are affected by moisture and moisture variations in a number of ways. A change in moisture condition can cause cracking of the material, which can reduce serviceability of the structure. Shrinkage strains develop, as moisture is lost to environment. In case of drying shrinkage it develops near the drying surface much quicker than in the center of the element. This occurs initially at a high rate but slows down with time as the material ages.

The prediction of spatial distribution and time history of moisture content in a structural or non-structural concrete element is of paramount importance. It is needed for the determination of shrinkage, creep, thermal dilatation, strength, durability, rate of hydration, thermal conductivity, fire resistance, radiation shielding and in the design of pre-stressed concrete pressure vessels for nuclear reactors [17].

The penetration of moisture into building structures can cause damage by the action of chemical contaminant agents transported by water, by the action of micro-organisms growing in the humid environment or by the mechanical action of freezing and thawing [Figure 1.3]. On the other hand, most of this moisture leaves the porous system by drying, which causes shrinkage and carbonation [Figure 1.4, 1.5], in cementitious materials [18].



Figure 1.3: Freeze Thaw Action in Concrete due to Moisture Penetration



Figure 1.4: Drying Shrinkage Cracks in Concrete due to Moisture Loss

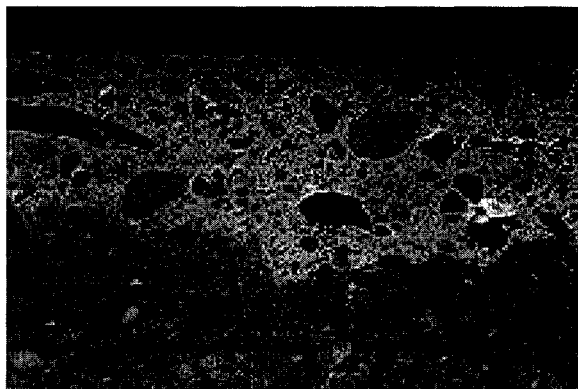


Figure 1.5: Carbonation in Concrete due to Moisture Loss

#### **1.4 Parameters affecting Moisture transport in cementitious materials**

The material parameters, which have a significant influence on the moisture diffusion process, are the co-efficient of moisture diffusivity ( $D$ ) and the convective surface transfer coefficient ( $h_f$ ). Moisture diffusivity is a material property and can be defined as the flux of moisture flowing through the material when there exists a unit moisture gradient, in the absence of bulk motion [19]. Diffusion of moisture from concrete and repair is a key physical process, which has a significant influence on durability and integrity of concrete members.

Water cement ratio plays a significant role in concrete after hydration. The contacts between C-S-H particles are dependant on water films that are physically adsorbed at the surfaces of these particles. Mechanisms like shrinkage and creep are very much affected by the movement of C-S-H particles caused by hygral gradients. In the Arabian Gulf region condensed silica fume is now being extensively used in concrete, it reacts with CH phase in the cement paste to produce secondary C-S-H having larger volume. This affects the porosity of the system and ultimately the moisture diffusivity of the material.

Moisture diffusivity is hence the key physical parameter that is required for computation of moisture transport in cementitious materials. The transport coefficient is largely material specific, i.e. depends exclusively on material porosity, pore structure and moisture content. It is known that in the diffusion of gas through a catalyst, the diffusion paths are tortuous, irregularly shaped channels; accordingly, the flux becomes less than it would be in a uniform pore of the same length and mean radius. The effective coefficient

of diffusivity in linear diffusion problems can be expressed in terms of a tortuosity parameter ( $\tau$ ), a factor that describes the relationship between the actual path lengths relative to the nominal length of the porous media [20]. In lieu of measuring the tortuosity, diffusivity may be established as a regressed function of the water/cement ratio for cementitious materials. However, inasmuch as the diffusion of moisture through concrete is now known to be a non-linear problem, the influence of moisture concentration level on the diffusivity has also to be considered [21].

External influences like ambient temperature, humidity and wind speed are also believed to have an influence on the moisture diffusivity coefficient and the convective surface transfer coefficient [22]. Water transport processes are often accompanied by temperature variation. From the thermodynamic theory, it should be expected that the transport properties increase with the temperature. According to the Hirschfelder equation [23], for diffusion of a gas through a binary gas mixture, the diffusivity varies approximately in the ratio of absolute temperatures to the power 1.5. Jooss and Reinhardt [24], have recently noted the application of this to concrete moisture diffusivity.

## 1.5 Need for Research

The need for this research exists both from a basic and applied research point of view. The deterioration and serviceability of concrete structures (new & repaired) are directly related to the durability of concrete and repair materials, which in certain aspects depends on the moisture transport in these cementitious materials, as described earlier.

Owing to the hot & arid climate of Saudi Arabia, there is a need to study the effect of temperature on coefficient of moisture diffusivity ( $D$ ) and the effect of wind speed on convective transfer coefficient ( $h_f$ ) for both concrete and repair materials. Also the discussion in section 1.4 obviates the importance of investigating the effect of water-cement ratio on  $D$  of concrete.

This research will provide a basis for expressing  $D$  as a function of water-cement ratio, moisture concentration and temperature for concrete, and will enable to express  $h_f$  in terms of wind speed. This can supply basic expressions for use in transport of aggressive species through concrete, the modeling of which relates to the core issues of concrete durability.

Further the results of this research would be useful in context of concreting under hot weather conditions. Cracking of fresh concrete (prevalent in arid environments) is inevitably linked to rate of water evaporation from concrete surface and this research would allow a rational basis for developing a model to predict evaporative losses under varying environmental conditions.

## 1.6 Aims and Objectives of Research

The primary objective of this research is to investigate the influence of temperature on coefficient of moisture diffusivity ( $D$ ) and wind speed on convective transfer coefficient ( $h_f$ ), for the selected concrete mixes and repair materials. In addition the role of water-cement ratio in influencing  $D$  of concrete will also be established.

A combined experimental-numerical approach will be adopted to identify the impact of above stated parameters. The research program includes the following aspects:

- Experimental investigation of evolution of moisture loss and free shrinkage strain, in concrete of varying water-cement ratio and repair materials, under different temperatures and wind speeds.
- Experimental investigation of compressive strength evolution and water permeability of the concrete mixes.
- Determination of coefficient of moisture diffusivity ( $D$ ) and convective transfer coefficient ( $h_f$ ), using the experimental moisture loss data in an existing finite element model [25], simulating the exposure conditions of the experimental specimen.
- Development of regression models, relating  $D$  of concrete to moisture loss, shrinkage strain, compressive strength & water permeability, and expressing  $h_f$  in terms of wind speed.

## 1.7 Research Methodology

The accomplishment of this research involved the following four phases. A general overview of research methodology and the phases involved is shown in Figure 1.6.

The **first phase** included a comprehensive literature survey and data collection in the following areas:

- Moisture transport and drying shrinkage in cementitious materials.
- Available techniques for computing moisture diffusivity of cementitious materials.
- Selection of repair materials.
- Water permeability of concrete.

The **second phase** involved fabrication, upgrading and calibration of the equipment and molds:

- Two environmental chambers already available, equipped with humidity and temperature control were upgraded in terms of wind speed, required as per testing conditions for the moisture loss and shrinkage tests on concrete and repair materials. The temperature and humidity units were also repaired or replaced and all the equipment was properly calibrated.
- Molds were manufactured for casting specimens to be used in the different tests.

In the **third phase** mix design and proportioning of the ingredients of concrete were carried out, according to ACI 211.1-91. Three different water-cement ratios 0.45, 0.5 & 0.6 were selected to allow generation of enough data to ascertain the influence of w/c ratio on coefficient of moisture diffusivity. This phase also involved carrying out moisture

loss and drying shrinkage tests on the specimens of selected concrete mixes & repair materials. All these tests were carried out for a period of two to three months in environmental chambers, under selected exposure conditions, dictated by the prevailing summer environment in the Eastern province of Saudi Arabia. Testing was also done for determining certain mechanical properties of the selected concrete mixes:

- Compressive strength evolution.
- Water permeability.

The **fourth and final phase** involved the analysis of experimental data and the use of a numerical model based on non-linear finite element method, developed earlier [19, 25, 26, 27]. The model was used for simulation of moisture diffusion in concrete & repair materials, under subjected environmental conditions, and hence computing the corresponding values of coefficient of moisture diffusivity ( $D$ ) and convective transfer coefficient ( $h_f$ ). Regression models were then developed utilizing these results, to serve as guidelines for researchers and engineers.

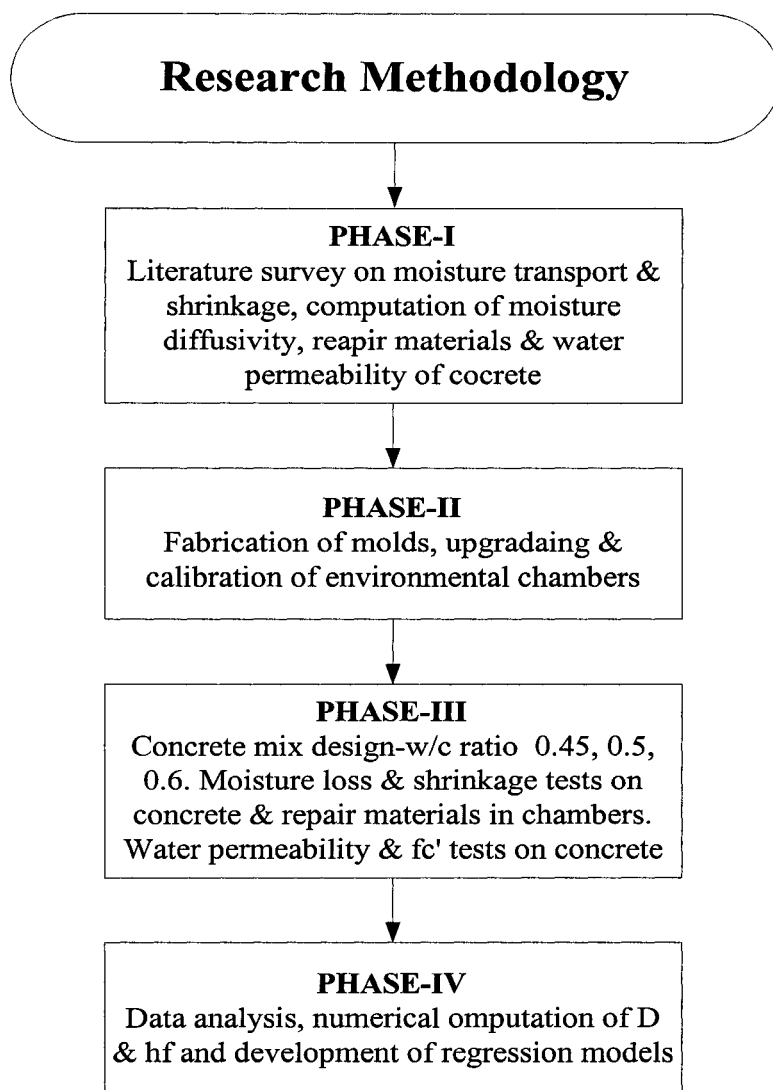


Figure 1.6: Phases of the Research

## CHAPTER 2

### LITERATURE REVIEW

#### 2.1 Types of Moisture Transport in Cementitious Materials

Typical moisture transport processes important in porous cementitious materials include diffusion, viscous saturated flow and capillary transport.

**Viscous Saturated Flow** is driven by a difference in water pressure. The flow depends both on the geometry of the porous material and on properties of the fluid itself. The saturated flow ( $g$ ) is often described by Darcy's law, which expressed in the 3-D pressure field becomes:

$$g = -\frac{k_p}{\eta} \nabla p \quad (2.1)$$

where  $k_p$  is the permeability of the material and  $\eta$  is the dynamic viscosity of water. For a one-dimensional case, Darcy's law becomes:

$$g = -\frac{k_p}{\eta} \frac{dP}{dx} \quad (2.2)$$

**Capillary Transport** occurs due to surface tension between water and air, which is caused by the attraction forces acting on the molecules of the liquid. The magnitude of the attraction decreases strongly with the increasing distance between the molecules. This distance is considerably larger in a gas than in a liquid, therefore, liquid molecules at the surface are more attracted towards the interior liquid than towards a surrounding gas. The liquid will therefore tend to form a relatively tough skin or film on its surface and minimize the surface area by striving to form a spherical drop. Energy is needed to transport a molecule from the bulk to the surface, which is numerically the surface tension [28]. The simplest model of capillary transport is to approximate the wetted region as a fully saturated rectangular wetting front or a moving boundary. For many applications this model is accurate enough and can be used more or less directly.

$$x = B\sqrt{t} \qquad B = \sqrt{\frac{r_o \sigma}{2\eta} \cos \theta} \qquad (2.3)$$

Where  $x$  is the penetration depth of the suggested sharp wetting front,  $t$  is the time,  $r_o$  is the pore radius,  $\eta$  is the dynamic viscosity,  $\sigma$  is the surface tension,  $\theta$  is the contact angle between the edge of the molecule meniscus and solid material and  $B$  is the penetration coefficient to be determined experimentally [29].

**Diffusion** at isothermal conditions is driven by a difference in vapor pressure, i.e. the water molecules are moving towards a lower vapor pressure or in other words under a concentration gradient. Sherwood in a series of papers in 1930's used linear mathematical

theory of diffusion, generally referred as Fick's second law to predict the drying of solids.

The diffusion equation in a linear diffusion theory is of the form:

$$\frac{\partial C}{\partial t} = D \frac{\partial^2 C}{\partial x^2} \quad (2.4)$$

Where C represents vaguely defined moisture content and D represents an experimentally determined coefficient

Carlson [30] first used the diffusion equation to predict shrinkage in concrete members. He found that only first half of the moisture loss from prisms dried at room temperature and 50 % relative humidity could be approximated by the linear diffusion theory, the final moisture being lost with ever increasing difficulty. Pickett [31] also used the linear diffusion theory to predict moisture loss in unrestrained un-reinforced concrete members. He also observed that with the progress of drying the remaining moisture is lost with ever-increasing difficulty and much slower than a linear diffusion theory would predict. He treated diffusion coefficient as a function of time, which preserves the linearity of the problem and admits analytical solution to predict shrinkage in concrete elements. Van Arsdell in 1944 investigated the effect of variable diffusivity on the drying rates predicted by the diffusion theory in the area of chemical engineering. The dependence of diffusivity on moisture content renders the problem non-linear. The diffusion equation modified to the form

$$\frac{\partial C}{\partial t} = \frac{\partial}{\partial x} \left( D \frac{\partial C}{\partial x} \right) \quad (2.5)$$

was used by Van Arsdel to solve numerically for moisture loss to yield similar results to those found in laboratory.

Philajaavara [32] first considered the dependence of diffusivity on moisture content in numerical analysis of drying of slabs. He used various hypothetical forms of dependence of diffusivity on moisture content. Bazant and Najjar [17] presented a comprehensive computer analysis of experimental drying data and mathematical formulation for non-linear diffusion analysis. They considered moisture diffusion in terms of relative humidity rather than moisture content. They postulated that diffusivity and other material parameters are strongly dependent on pore humidity, temperature and degree of hydration of concrete. Bazant contended that due to porosity becoming non-uniform with time, the usage of evaporable water content ( $w_e$ ) as a basic variable in diffusion equation involves error, since Fick's law in terms of  $w_e$  cannot be applied to obtain diffusion equation governing drying process when hydration proceeds. Bazant used the following equation for predicting moisture loss in concrete

$$\frac{\partial h}{\partial t} = \text{div}(D(h)\text{grad}(h)) + \frac{\partial H_s}{\partial t} + K \frac{\partial T}{\partial t} \quad (2.6)$$

where,  $h$  is the pore humidity,  $\frac{\partial H_s}{\partial t}$  is the change in  $h$  due to self-desiccation i.e. loss of free water due to hydration,  $\frac{\partial T}{\partial t}$  is the change in temperature due to hydration. Bazant

formulation based on pore humidity and non-linear diffusion equation has been used in several studies for predicting moisture loss and shrinkage in concrete. Johansson [33], Garbozyskwi and Shah [34] and Alvaredo [35] are some examples.

Sakata [22, 36], Penev and Kawamura [37], and Asad et al. [26-27, 38-39] used non-linear moisture diffusion theory in terms of moisture content, rather than pore humidity. Granger, Torrenti and Acker [40] have analyzed the two classical hypothesis, treating moisture diffusion equation in terms of relative humidity and moisture content. They have shown that in many cases, the good linearity of the de-sorption isotherm between 50% and 100% relative humidity allows for both types of models.

## **2.2 Microstructure & Transport Properties of Cementitious Materials**

### **2.2.1 Introduction**

In cement-based materials, the presence and transport of moisture in macro and micro arterial network of pores is of paramount importance in several phenomena including drying shrinkage. Concrete is a composite material whose microstructure is random over a wide range of length scales. At the largest scale, concrete can be considered to be a mortar rock composite, where the randomness in the structure is on the order of centimeters the size of a typical coarse aggregate. Mortar can be considered as a hydrated cement paste-sand composite, with random structure on the order of millimeters. Hydrated cement paste can further be considered as a random composite material made up of un-reacted cement, CSH Calcium Silicate Hydrate gel, CH Calcium Hydroxide or Portlandite, capillary pores and other chemical phases. The randomness of the hydrated

cement paste microstructure is on the order of micrometers. Finally CSH is itself a complex material, with random structure as seen by neutron scattering, on the order of nanometers [41]. This range of random structure, from nanometers (CSH) to centimeters (concrete) covers seven orders of magnitude in size.

Two very simple ideas control how the spatial geometry of the microstructure of cementitious materials affects transport properties. These ideas can be expressed in terms of the Tube theory:

- Large diameter tubes have higher transport rates than the small diameter tubes.
- Tubes that are blocked have zero transport rates.

These ideas phrased more rigorously as pore size and connectivity, provide the theoretical framework necessary for describing how the transport properties depend on pore structure. Cementitious mortars have a broad distribution of pores from some tenths of angstrom to several microns. The distribution, random connectivity and tortuosity of these pores play an important role in phenomena like vapor adsorption and de-sorption and moisture transfer in cementitious materials [42].

### **2.2.2 Microstructure and Diffusivity of Hydrated Cement Paste**

It is important to begin with hydrated cement paste since it is the matrix material that along with sand and rock inclusions forms the concrete composite. In a pure hydrated cement paste (hcp), irregularly shaped cement particles exist in aqueous suspension, which undergoes random growth due to hydration reaction. Un-hydrated cement consists of a fine powder whose main constituents are:

- Tri-calcium silicate  $C_3S$
- Di-calcium silicate  $C_2S$
- Tri-calcium aluminate  $C_3A$
- Tetra-calcium alumino ferrite  $C_4AF$
- Calcium sulfate added to prevent flash set of cement

Hydrated Cement paste can be thought of as consisting of four phases:

- Un-reacted cement
- Surface products like CSH
- Pore products like CH
- Capillary pore space

Surface products grow out from the un-reacted cement particles and contain continuous gel pores, while pore products are generally crystalline and fully dense, with no connected pores. The capillary pores are the left over space between solid phases [Figure 2.1, 2.2].

The connectivity of different phases and particularly the pore phases change with time. Immediately after mixing, the solid phases are discontinuous and so the freshly mixed paste is a viscous liquid. The solid phase is then built up through random growth of reaction products, and at some point becomes continuous across the sample mainly due to the formation of CSH surface products [43].

Water in the hydrated cement paste can be bound both physically and chemically. In contact with moist air, water molecules are bound physically by adsorption and capillary condensation, to the surfaces of the pore system by Vander Waal forces, until equilibrium with the humidity of the ambient air is reached. There is never a static condition, as some water molecules leave the pore surface, other become attached.

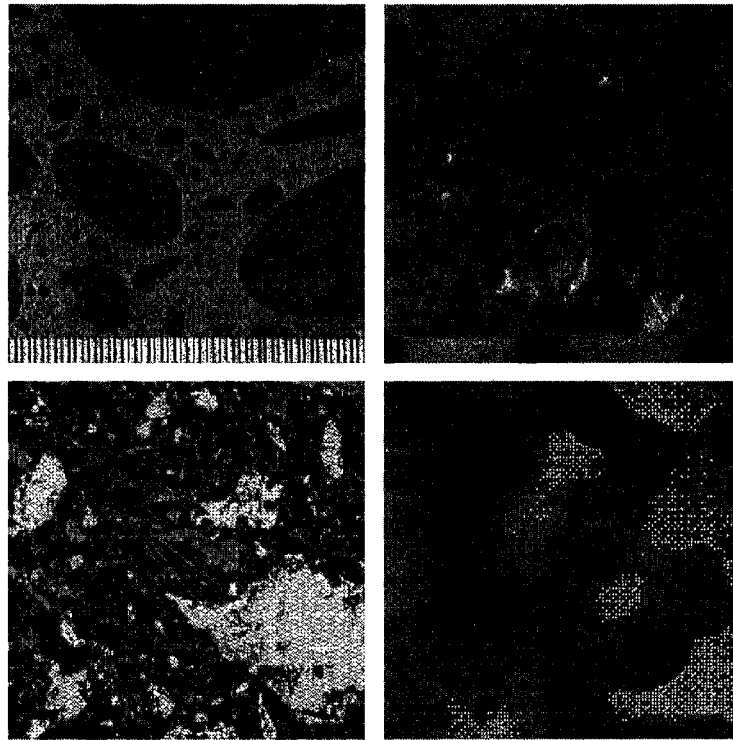


Figure 2.1: Electron Microscope Image of Concrete (top left), Mortar (top right),  
Hydrated Cement Paste (bottom left) & CSH (bottom right)

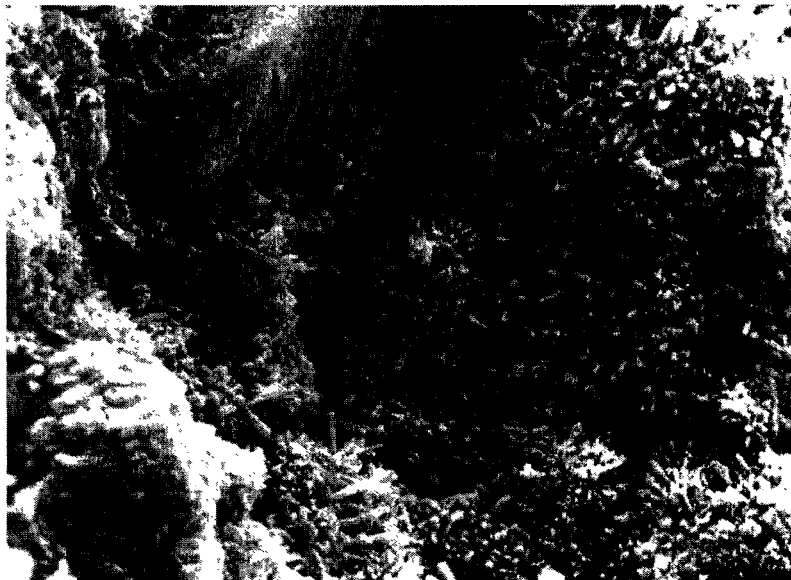


Figure 2.2: High Resolution Electron Microscope Image of Hydrated Cement Paste

At equilibrium number of molecules leaving is same as number becoming bound to the surface. Chemically bound water exists within the cement gel and is not lost until the gel is heated well above 105°C. Also classified as evaporable or non-evaporable, normally physically bound water is taken as evaporable and vice versa [29].

A percolation threshold that is more important for transport processes is the point at which capillary pore space loses continuity. Such a percolation threshold can exist, because as the hydration products are formed, pieces of the capillary pore space will be trapped and cut off from the main pore network, thus reducing the fraction of the pores that form a connected pathway for transport. As this process continues, the capillary pore space can lose all long range connectivity, so that fast transport of water or ions through the relatively large capillary pore system would end, and slow transport would then be regulated by the smaller CSH gel pores [42]. Results from computer simulation modeling of hydrated cement paste microstructure by Garboczi & Bentz [44] provide evidence for such a percolation threshold.

Early in the hydration, capillary pore space is fully percolated and these pores are much larger than the CSH gel pores and so dominate the moisture transport. During hydration, capillary porosity and capillary pore size decreases due to consumption of water during hydration, producing hydration products that fill in the capillary pore space. As the capillary porosity reduces the capillary pores become smaller and only partially connected, so for porosities near but above the percolation threshold, pure capillary pore paths have only slightly more influence on flow than hybrid paths that are made up of isolated capillary pockets linked by CSH gel pores. The capillary pores are still somewhat bigger than the gel pores but their connectivity is becoming small. Below the critical

capillary porosity all the flow should now go through CSH gel pores, but flow will be dominated by paths that contain some isolated capillary pore regions and are not just made up of pure CSH gel pores. If this were not true, then after a certain point, diffusivity would begin going up with increasing hydration, since more CSH and thus more gel pores being formed [42].

The transport properties of hydrated cement paste would thus depend on the hydration time, particle size distribution, original water-cement ratio & the type and quantity of admixtures. When polymers are mixed in powdered form to a cementitious product, normally in repair materials, the polymer particles are uniformly dispersed in the system. The porosity, pore volume, pore distribution and pore shape in polymer modified cementitious material are different from those of the unmodified. It results in a lower number of pores with a radius greater than 200nm but significantly more with a radius of 25nm or less [45,46]. The polymer modification results in two processes in the hydrated cement paste:

- Cement hydration
- Polymer film formation

As the water evaporates from a polymer system, the polymer spheres approach each other and eventually touch and fuse into a continuous film. With the loss of water due to evaporation and cement hydration, polymer particles get gradually confined in capillary pores. With the progress of cement hydration, capillary water is reduced and polymer particles coalesce to form a continuous closed packed layer on the surfaces of the cement gel particles.

Many of the new generation cementitious repair products also contain condensed silica fume, which has very small particles and high silica content, with a specific surface area of 20,000 m<sup>2</sup>/kg. The silica fume reacts with the CH phase in the hydrated cement paste to produce secondary CSH, having larger volume than original CH and silica fume combined. It tends to reduce the capillary porosity of the hcp due to two effects, 'Pore size refinement', since it produces more volume of CSH replacing the pore volume and 'Grain size refinement', since it replaces part of larger grained cement [47].

### **2.2.3 Microstructure and Diffusivity of Mortar & Concrete**

Mortar and concrete are normally considered as composite materials with the fine and coarse aggregates as inclusions and hydrated cement paste as the matrix. The transport properties of aggregate are measurable and usually constant in time. The aggregates are dispersed in the cement paste matrix in a manner that does not provide a continuous porous path for the transport of moisture. Aggregate pores act only as a buffer zone, which can either store or release moisture to the surrounding cement paste matrix. However the Interfacial Transition Zone (ITZ), between the cement paste and aggregates, coarse or fine, plays a critical role in determining the bulk transport properties [Figure 2.3, 2.4].

The characteristic features seen in the interfacial zone are higher capillary porosity and higher CH volume fractions than in the bulk and generally bigger pores. These features are typically seen in the hydrated cement paste volume that is within 50 µm [48].

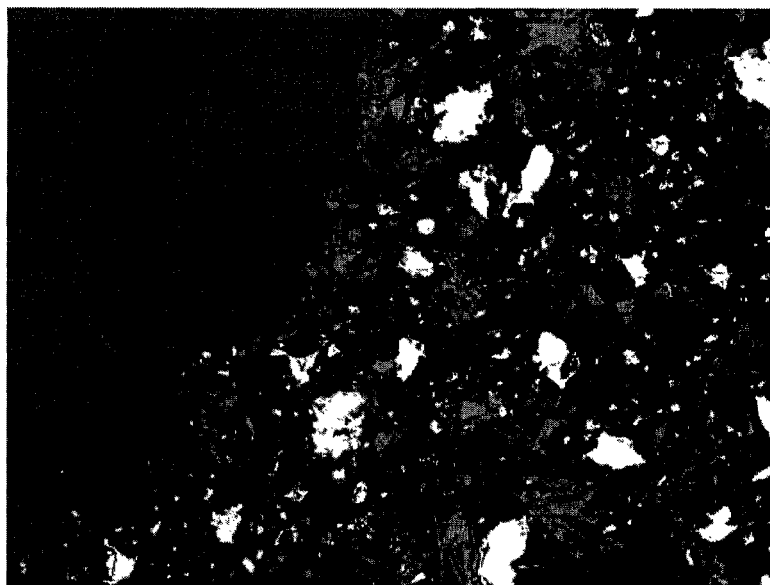


Figure 2.3: SEI of Interfacial Transition Zone between Coarse Aggregate and Hydrated Cement Paste

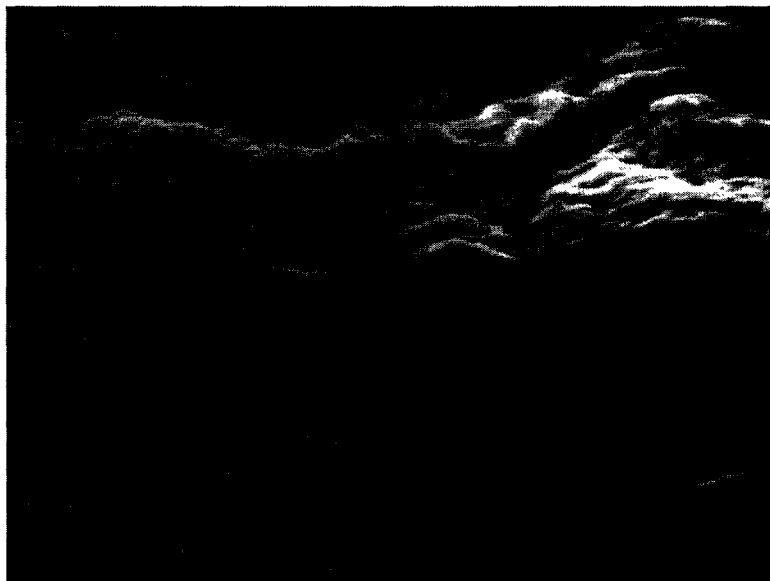


Figure 2.4: SEI of Interfacial Transition Zone b/w Hydrated Cement Paste and Sand Grain

The two major causes of ITZ microstructure are the ‘particle-packing effect’ and ‘one-sided growth effect’ [49]. The particle packing effect arises from the fact that particles cannot pack together as well near a flat edge as in free space. Since the typical aggregate is many times larger than the typical cement particle, even for the fine aggregate, locally the aggregate edge appears flat to the surrounding cement particles. This inefficient packing causes less cement and higher porosity to be present initially near the aggregate surface and so even after hydration this condition persists. On the average there is a reactive growth coming into capillary pore space from all directions since the cement particles are originally located randomly and isotropically. But near an aggregate surface reactive growth is coming from the cement paste side only and not from the aggregate side, this explains the one-sided growth effect.

Mineral admixtures like silica fume and fly ash also affect the ITZ properties. Two main variables of importance for mineral admixtures are particle size and reactivity with the CH phase. The particle size of mineral admixture controls the width of packing effect at aggregate edge, with admixtures having smaller particle size allowing better packing. The reactivity controls amount of CH consumed and converted to CSH [50].

The effective transport properties of concrete can increase greatly as more aggregate is added past a critical amount [51]. The only possible micro-structural explanation of this behavior besides extensive micro cracking is the effect of transport of fluids or ions through interfacial zone. However, if the interfacial zones do not percolate, then their effect on transport will only be negligible, as any transport path through concrete would have to go through the bulk cement paste.

Bentz, Garboczi, Snyder, Stutzman and Winslow [52-55] studied interfacial zone percolation in concrete using the ‘hard-core / soft shell’ model [56] and mercury intrusion data. The inner region of the ITZ was found to be of more importance since its transport properties were higher than the outer region because of the larger pore size and porosity. The ITZ was found fully percolated for aggregate volume fractions above 50%. Most concretes have aggregate volume fractions well above 50%, so they concluded that ITZ in usual Portland cement concrete are percolated and will have an effect on its transport properties.

### **2.3 Mechanism of Moisture Transport in Cementitious Materials**

Moisture transport involves a complex interaction between different transport processes. It can be basically classified as:

- Moisture transport at the boundaries of the system.
- Moisture transport within the domain of the system.

The physics of boundary layer moisture transport is in itself quite involved. A simplified condition considers the transport in the form of a constant flux boundary condition [57]. Moisture transport within the domain of a cementitious material at microscopic and macroscopic level is discussed in the following sections.

### 2.3.1 Moisture Transport at Microscopic Level

The number of physical processes involved in the transport of water or water vapor in cementitious materials varies according to the moisture content of the material. In a typical pore of a cementitious material, moisture predominantly exists in the form of an adsorbed phase on the walls of the pore and a condensed phase in the capillary pore. The adsorption of moisture on the pore walls results from the interaction between the gas and a solid surface. The process continues until a thermodynamic equilibrium is reached.

The thickness of the adsorbed water film increases with relative humidity, varying from about  $1 \text{ \AA}$  to about  $13 \text{ \AA}$  at 100 % relative humidity. Adsorbed water is fixed to the pore surfaces by van der Waals' forces, with the intensity depending on distance to the surface, the first layer being most firmly bound [58].

Condensation of moisture in a capillary pore occurs when the effective pore radius is lower than the threshold pore radius as obtained from Kelvin-Laplace equation:

$$\frac{-2\sigma \cos \beta}{R_{pk}} = v \frac{RT}{M} \ln RH \quad (2.7)$$

where	$\sigma$ = surface tension (N/m)	$R$ = gas constant (J/mole-K)
	$v$ = density ( $\text{kg/m}^3$ )	$T$ = temperature ( $^{\circ}\text{K}$ )
	$R_{pk}$ = pore radius ( $\mu\text{m}$ )	$RH$ = relative humidity
	$M$ = molecular mass	

In cement based materials the Kelvin-Laplace equation implies that condensation occurs in all pores smaller than  $1\text{ }\mu\text{m}$  as soon as the relative humidity reaches 99.99 %. Since a cement paste has a larger number of pores smaller than  $1\text{ }\mu\text{m}$ , the capillary condensation plays a major role in such materials [58].

From Kelvin-Laplace equation, it is also apparent that in small capillaries the liquid may be in equilibrium at relative humidity much less than 100 %. Figure 2.5 shows the relationship between the relative vapor pressure and the water filled capillary pore radius, which would be in equilibrium with it [59]. It can be seen that water filled capillary radius of 2 nm would be in equilibrium with a relative vapor pressure, or relative humidity, of 0.58. If relative humidity were increased to 0.78 then the capillaries with radius up to 4 nm would gradually fill. Conversely, if R.H were reduced to say 0.6, all capillaries with radius greater than 2 nm would be empty. This mechanism provided an explanation for the de-sorption isotherms [Figure 2.6].

### **2.3.2 Moisture Transport at Macroscopic Level**

When a cementitious product saturated by liquid water is subjected to an environment having lower relative humidity, an initial thermodynamic imbalance occurs between the exterior vapor concentration and that within the specimen. The specimen exchanges water vapor with the exterior, to restore equilibrium. For water to remain in (isothermal) equilibrium within the specimen the water pressure also decreases and this causes it to evaporate [60].

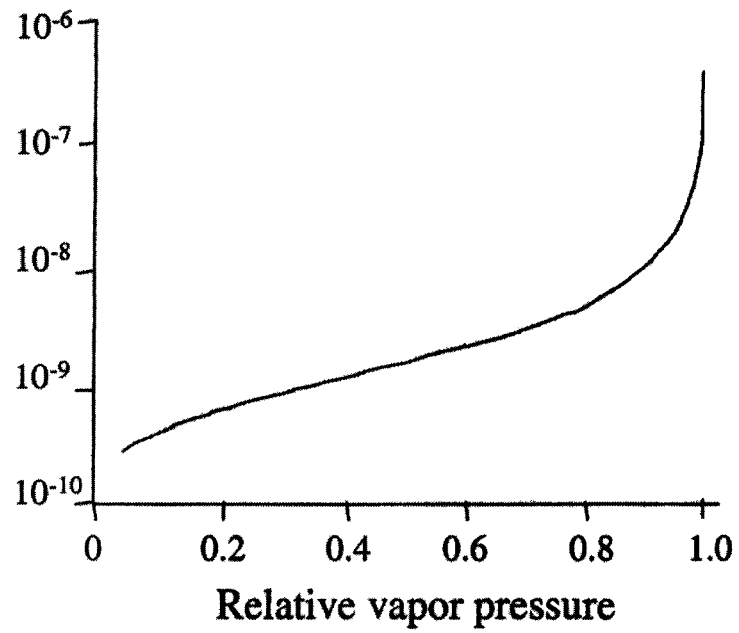


Figure 2.5: Equilibrium Vapor Pressure for Capillary Pores

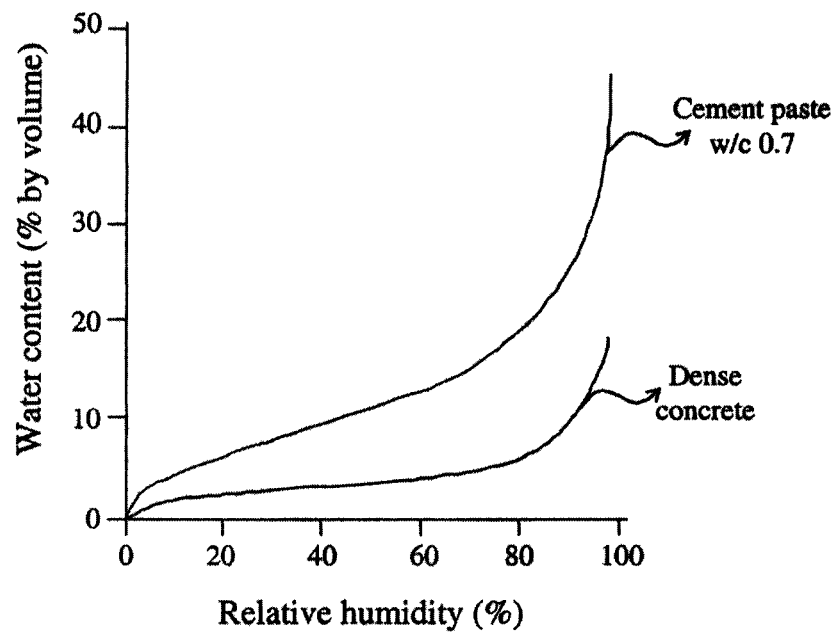


Figure 2.6: De-sorption Isotherms in Cement Paste & Dense Concrete

The moisture transport is characterized by three phases [35] as shown in figure 2.7. In the first phase moisture transport is limited by evaporation at the boundaries of the element and the rate of moisture movement in this region is almost constant. This continues as long as solid surface is sufficiently wet to simulate free water, by moisture flow to the surface from the domain. When the rate of moisture transport from the domain to the surface decreases due to depletion of free water, the rate of moisture flow decreases linearly as indicated by BC. The surface starts to dry out, as the moisture supply from the domain can no longer keep pace with evaporation from the surface. This phase ends as the moisture content at the surface comes in equilibrium with the ambient relative humidity. The phase III of moisture transport is characterized by a rate of moisture transport asymptotically tending to zero. In this phase moisture transport is characterized by sub-surface evaporation in which the plane of vaporization recedes further into the body. This phase ends when the entire element reaches hygral equilibrium with the environment. Nilsson [61] has shown that phase I is virtually absent in cementitious materials, except for very immature concrete with high water-cement ratio and cured under water. Boundary conditions are expressed quite accurately by assuming that the concrete surface is immediately in moisture equilibrium with the ambient air.

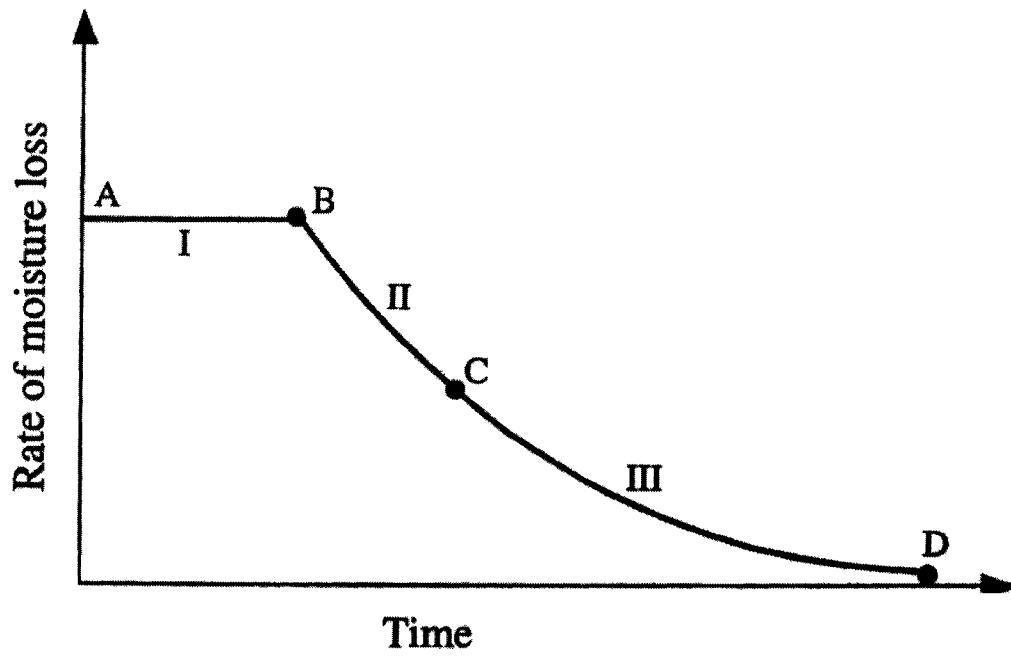


Figure 2.7: Three Phases of Moisture Transport at Macroscopic Level

## 2.4 Moisture Diffusivity & Surface Transfer Coefficient

Moisture diffusivity is the key physical parameter required for the computation of moisture transport in cementitious materials using the non-linear diffusion equation. It is a term defined at macroscopic level in which the several modes of moisture transport are lumped together. The computational models for moisture diffusion in cementitious materials require an empirical diffusivity law for computations of time history of moisture content over the spatial domain of the element [25].

Surface moisture transfer coefficient  $h_f$ , expressed in units of cm/day, represents the speed of surface evaporation by its control over the moisture gradient or moisture flow at the drying surfaces. In diffusion process it enters into mathematical formulation through the boundary conditions. This coefficient may be a surface as well as material property, which may have its own functional form and be independent of other material parameters. In general it may depend on many factors like environmental humidity, temperature and wind speed at the convective surface [62].

Bazant and Najjar [63] have determined that diffusivity decreases sharply, about 20 times, when the moisture content decreases from 90 % to 60 %, whereas it is found to be approximately constant below 60 % pore humidity.

Lowe, Hughes and Walker [64] observed that samples which had been cured for 200 days exhibited the same drying curves as the samples cured for 28 days, concluding that continuing hydration of the cement paste during drying does not cause a change in diffusion coefficient.

Bazant et al. [65] determined the overall effects of cracks on diffusivity of concrete. These cracks serve as conduits for water vapor and enhance the moisture transmission. They found that crack width of 0.1 mm spaced at 70 mm shows a diffusivity increase of about 2.25 times.

Wittmann et al. [66] have shown that diffusivity of concrete decreases as the water-cement ratio decreases. Initially, at 100 % relative humidity, diffusivity of concrete varies from 0.5 cm<sup>2</sup>/day to about 0.3 cm<sup>2</sup>/day as the water-cement ratio changes from 0.6 to 0.4. Below 60 % relative humidity the difference is lower. Persson [67] also carried out studies on the effect of water cement ratio on diffusivity of concrete at various ages. He observed that at early ages diffusivity increases as the water-cement ratio increases but for mature concrete it is substantially low.

Penev and Kawamura [37] studied the diffusivity of soil cement mixtures and lean concrete. They found that diffusion coefficients of lean concrete and soil cement mixtures are much higher than those in usual concrete, attributed to the difference in their pore size distributions. It was found that lean concretes have higher coefficients than soil cement mixtures.

Akita et al. [68] found that at a constant water-cement ratio, diffusivity at relative humidity of 100 % tends to be large when the unit water mass is small or the volumetric aggregate ratio is large. Also the influence of surface factor on water content or decrease in mass is small, except in the initial stage of drying and is derived from the diffusion coefficient of water vapor in air under suitable assumptions.

Iding and Bresler [69] assumed a surface transfer coefficient dependent on the diffusivity of the material. An expression  $h_f = 1.67 D$  was used for the analysis of

shrinkage in concrete. However, in general a constant mean value of  $h_f$  is assumed in moisture diffusion analysis by several researchers.

Sakata [36] found that diffusion coefficient is dependent on moisture content in concrete. It was found almost constant,  $0.05 \text{ cm}^2/\text{day}$ , in the range of low moisture content, below 80 %, while at high moisture content or in the early period of drying, it increased. Surface factor was found to have a close relationship with water-cement ratio of concrete. Moisture diffusion was found to be high in the neighborhood of the drying surface, but extremely small in the concrete interior.

Rahman [25] conducted drying tests under controlled environmental conditions to determine the diffusivity and convective transfer coefficient for repair materials. He found diffusion coefficient for repair materials to be high at initial stages, the values however showed a rapid decrease as the moisture content reduced from 99-90 %. Diffusivity almost became zero below moisture content of 50 percent. The mean diffusivity of superior performing repair materials was found to be in the range of  $0.05\text{-}0.06 \text{ cm}^2/\text{day}$ , whereas, the mean diffusivity of the repair materials that cracked in a patch repair environment was of the order of  $0.2 \text{ cm}^2/\text{day}$ . It was also noted that diffusivity of repair materials increased with the increase in temperature. He stated that a mean value diffusivity criterion could be established as less than or equal to  $0.05 \text{ cm}^2/\text{day}$  for the repair materials.

## 2.5 Effect of Temperature & Wind on Moisture Transport

Quenard and Sallee [58] found that at high relative humidity moisture diffusivity decreases when the temperature increases, they attributed this to variation of moisture properties at high temperature. At low relative humidity the effect of temperature up to 60 degree centigrade was observed to be negligible.

A recent publication by Jooss and Reinhardt [24] has appeared in which the authors have discussed the influence of temperature on permeability and moisture diffusivity of concrete. They performed several tests on high performance concrete, copolymer sate concrete and self-compacting concrete & found that diffusivity increases by 10-21 % from 20 to 50 °C and by 8-21 % from 50 to 80 °C. However, in this research, diffusivity is measured using DIN 52615 which results in a constant value. It is now well known that the modeling of stresses and damage associated with the restrained shrinkage of concrete cannot be established using constant values for the coefficient of diffusivity [19, 25, 70, 71]. The simulation of this problem can only be achieved by treating moisture diffusivity as a function of moisture concentration, which renders the boundary value problem non-linear. One feasible approach for this is to calibrate an assumed form for the coefficient of diffusivity in terms of unknown parameters of known functions of moisture concentration level, water-cement ratio and temperature, using data from experiments and numerical results from a finite element driven program [25].

Nilsson [61] indicated that the diffusion coefficient decreases slightly with the aggregate to cement ratio and with the modulus of fineness. He also investigated the effect of wind on the drying process. Specimen kept in a wind tunnel at a wind speed of 5

m/sec and under normal conditions showed a very little difference in weight loss, shrinkage and creep. He concluded that rate of moisture evaporation at the surface, essentially depends on moisture content and not much influenced by wind. However, it is expected that the moisture evaporation should increase with the increase in wind speed to which the specimen is exposed, because it will result in forced convection at the boundary. This effect may be captured in numerical computations using a higher value of convective transfer coefficient ( $h_f$ ).

## **2.6 Review of Methods for Measuring Moisture Profiles / Diffusivity**

In general moisture diffusivity cannot be measured. Moisture profiles are generated experimentally, measured at various times after start of moisture redistribution, i.e. moisture uptake or moisture loss and then analyzed/fitted using mathematical or numerical techniques to compute the values of moisture diffusivity and convective transfer coefficient. However DIN dry & wet cup methods [2.6.1] can be used for measuring moisture diffusivity, but these are not considered valid since they result in a constant value of diffusivity. Various methods available in literature for measuring moisture profiles are as follows:

1. Slice-dry-weigh [2.6.2]
2. Electrical methods [2.6.3]
3. Gamma ray attenuation [2.6.4]
4. Neutron radiography [2.6.5]
5. Nuclear magnetic resonance, NMR [2.6.6]

6. Computer tomography [2.6.7]
7. Microwave beam [2.6.8]
8. Thermal conductivity [2.6.9]
9. Thermal imaging [2.6.10]
10. Capillary water uptake [2.6.11]
11. Moisture loss / drying [2.6.12]

### **2.6.1 DIN Dry & Wet Cup Method**

These tests are given by the German standard, DIN 52615. In the dry cup method, the coefficient of moisture diffusivity and vapor resistance are determined between 0 % and 50 % relative humidity. The actual measuring device consists of a small cup, on which the concrete samples are attached, the desiccator and the climatic chamber. The cups have a diameter of 100 mm, a height of approximately 10 mm and made of either aluminium or stainless steel. The desiccator has an internal diameter of 300 mm. By installing several floors, the desiccator can be used to full capacity.

To ensure a uniform moisture distribution, a ventilator is attached to the upper tubes, which also assures an air velocity of 0.02-0.3 m/s. To simulate temperatures above 50 °C the desiccator is placed in a climatic chamber with temperature tolerance of  $\pm 1$  °C. Test specimen is 100 mm in diameter and approximately 20-25 mm thick. Salt solutions like silica gel, phosphorous pent-oxide, sodium dichromate, and sodium bromide are used for constant humidity.

Humidity is lower in the cup as compared to the desiccator and moisture diffuses through the specimen into the cup. The arrangement consisting of the cup, specimen and sealing is weighed at regular intervals and from these weight changes, moisture difference and specimen thickness the coefficient of moisture diffusivity is calculated, according to the specified procedure.

Wet cup method is similar in construction to the dry cup method but the diffusion coefficient and water vapor resistance are determined between 50 % and 93-100 % relative humidity. The wet cup method is opposite to dry cup method in the sense that the moisture in the cup is higher than in the desiccator and the moisture flows from the cup into the desiccator. All the other procedure is same as in case of the dry cup method.

Jooss & Reinhardt [24] used the dry and wet cup methods for measuring the moisture diffusivity of high performance concrete and self-compacting concrete etc. and found that on materials with little or no super hygroscopic range, i.e. with pore radii smaller than 50 nm, cup method (dry + wet) alone is sufficient enough to measure the moisture diffusivity. This is due to the fact that these materials are already water saturated, at equilibrium with approximately 98 % relative humidity. Examples of such materials are concrete with low water cement ratio and granite etc. Hedenblad [72, 73] reported the moisture permeability and Kirchhoff's flow potential values for a large quantity of different building materials, as measured by the cup method in hygroscopic range at isothermal conditions.

On materials with a coarse porous system e.g. some natural sand stones, bricks and aerated autoclaved concrete, the cup method measurements should be supplemented by

some other methods like measurements from water retention curves. Such measurements are described and reported by Krus [74] and Kiebel et al. [75].

### **2.6.2 Slice-Dry-Weigh Method**

In this method the specimen is rapidly sliced into discs that are weighed, dried and weighed again. Water in the disc evaporates during drying and the water content in mass by mass can be calculated from the weight loss. The drying procedure consists of using an oven at 105°C. Materials that cannot resist heat are dried in an exsiccator with some drying agent like silica gel or sulfuric acid, but the procedure becomes time consuming.

Akita et al. [68] used this method to generate moisture profiles for the analysis of moisture transfer in concretes with varying mix proportions. Prisms of size 10x10x40 cm were used, notched in preparation for splitting and subjected to one and six face drying. The method was found to have certain disadvantages as it only gives average moisture content for each slice, different specimens are used each time and a large number of specimens are required due to the destructive nature.

The method is time consuming and slicing may be difficult for some materials, since a saw cannot be used because of the heat generated or water added during sawing. Thus the specimen is sliced, by splitting, but in this way it is difficult to get the crack perfectly parallel to the surface exposed to moisture. An error in measuring the x-coordinate of the disc is thus easily obtained. It might also be difficult to split the specimen into discs thin enough to evaluate a very steep waterfront and practically impossible to get number of specimens high enough if they have to be taken from an

existing structure. This method is suitable when water and non-volatile fluids are used for the absorption experiment. It is one of the most accurate methods because the actual amount of water in the specimen is measured.

### **2.6.3 Electrical Methods**

Two non-destructive electrical methods are available, one is based on measuring the variation of electrical conductivity (resistance), and the other is based on measuring the variation of electrical capacitance. For most materials the electrical conductivity increases with increasing moisture content and vice versa, and capacitance increases with the moisture content due to high dielectric constant of water [76]. Both of these methods, especially the resistance method, are inexpensive.

The conductivity or actually the electrical resistance is measured between two electrodes in direct contact with the material. The water content is evaluated from the resistance measured using a calibration curve valid for the actual material. The calibration curve is obtained with rather time consuming and extensive calibration tests. The conductivity is influenced by factors like water content, salts, temperature and density. According to Wormald et al. [77], the resistivity of concrete with the same water content may vary up to 40 % with change in the salt concentration of the pore water. The use of this method is thus limited when any of the above-mentioned factors is varying. A conductivity measurement made on aerated autoclaved concrete with accuracy on moisture content of  $\pm 10$  % is presented by Sandin [78]. One possible way of avoiding the effect of salts is to measure the conductivity in a special sensor, e.g. a piece of wood that

is embedded in the material to be studied. The sensor can be protected from salts in the material. After a certain time it will adopt the same moisture state as the material. A calibration curve for the sensor is required, however. This type of sensor can only be used when slow changes in the moisture state are to be measured. That is because it will take a relatively long time for the sensor to adopt the same moisture state as the material.

The capacitance method uses the tested material as dielectric. According to Krus [74], the dielectric constant of water is 10-40 times larger than that of a dry building material when the frequency is 1 GHz. In that way the change of the capacitance is a measure of the water content in the material being used as the dielectric. Salts in the pore water and the density differences less influence the capacitance method than the conductivity method. It however requires a more complicated laboratory set up. According to Wormald [77], the accuracy of capacitance method applied to concrete is  $\pm 0.25$  % of moisture content mass, per moisture mass in the range 0-6.5 %.

#### 2.6.4 Gamma Ray Attenuation

This is a non-destructive method. If two different gamma ray sources are used, both the water content and density can be measured. The gamma rays (photons) interact with the orbital electrons in the material and are absorbed or scattered. The intensity of a narrow beam of gamma rays passing through a material can be expressed by the following equation [79, 80]:

$$I = I_0 e^{-\mu \rho x} \quad (2.8)$$

Where

$I$  is the gamma ray intensity after passing through the material [counts/sec]

$I_0$  is the initial gamma ray intensity [counts/sec]

$\mu$  is the mass absorption coefficient of the material [ $\text{m}^2/\text{kg}$ ]

$\rho$  is the density of the material [ $\text{kg}/\text{m}^3$ ]

$x$  is the thickness of the material sample [m]

In order to perform a measurement of the moisture profile, a gamma ray source and a detector are needed. The source can be buried in the material with the detector on the surface, or, more commonly, the specimen can be placed between the source and the detector. The gamma ray equipment must be calibrated against the specific material in question. The equipment is rather expensive. Gamma rays however should not be used if the material structure changes in time, e.g. during the hydration process of young concrete. The reason is that hydration reduces the moisture content by transforming free water into chemically combined water and during this process density of concrete also increases. According to Adamson et al. [76], the accuracy of gamma ray method applied to concrete is  $\pm 0.5$  % of moisture content mass, per unit mass. Another disadvantage of the gamma ray method is that special safety arrangements must be taken due to the radioactivity. Examples of results and laboratory setups are shown in Wormald et al. [77], Nielsen [80] and Quenard et al. [81].

### 2.6.5 Neutron Radiography

This is also a non-destructive method using radiation similar to gamma ray attenuation method. In contrast to gamma rays, neutrons interact mainly with the hydrogen nuclei. The attenuation of a neutron beam, caused by scattering and absorption of the neutrons, will therefore be directly related to the total water content in the material. The intensity of a neutron beam passing through a specimen is described by an expression similar to equation 2.8, Pel [82]:

$$I = I_o e^{-x(\mu_{mat} + \mu_w \varepsilon)} \quad (2.9)$$

Where

$I$  is the intensity of a neutron beam after passing the material [counts/sec]

$I_o$  is the initial intensity of the neutron beam [counts/sec]

$\mu_{mat}$  is the macroscopic attenuation coefficient of the specific material [ $m^{-1}$ ]

$\mu_w$  is the macroscopic attenuation coefficient of water [ $m^{-1}$ ]

$x$  is the thickness of the material sample [m]

$\varepsilon$  is the water content volume by volume of the material [ $m^3/m^3$ ]

The coefficients  $\mu_{mat}$  and  $\mu_w$  are determined independently by measuring the neutron transmission through pore water and through the dry material. During the test, specimen is placed between the neutron source and the detector. The neutron beam can be produced by a combination of boron and cadmium and can be detected by a helium

proportional detector [82]. When running a neutron radiography test safety arrangements must be taken and specially trained personnel are necessary.

Results from measurements with neutron transmission radiography on different materials and experimental arrangements are given in Pleinert et al. [18], Pel [82], Adan [83], Justnes et al. [84] and Dawei et al. [85].

### **2.6.6 Nuclear Magnetic Resonance (NMR)**

This is also a non-destructive method. The accuracy of the water content measurement is approximately 0.5 to 0.1 % by volume according to Kiebel [86]. NMR has a spatial resolution of better than 1 mm according to Kopinga et al. [87]. With NMR a distinction can also be made among free, physically bound and chemically bound water. Thus it is very well suited for measuring transient water movements in building materials. A primary disadvantage is the high cost of the equipment.

In an NMR measurement the number of hydrogen nuclei are counted. A magnetic movement is associated with the intrinsic spin of the material's hydrogen nuclei. In this experiment an external permanent magnetic field is applied, when the electromagnetic field is applied perpendicular to the constant magnetic field, some energy is absorbed, which is proportional to the number of hydrogen nuclei in the measurement volume.

According to Kopinga et al. [87], NMR offers better sensitivity than gamma ray attenuation and neutron radiography. Unlike the results from gamma ray method, NMR results are directly related to the amount of hydrogen nuclei. In de Freitas et al. [88], a comparison between gamma ray attenuation and NMR however revealed no significant

difference in accuracy. An advantage of NMR as compared to gamma ray attenuation and neutron radiography is that no radioactivity is involved during the experiment. Examples of results from NMR are given in Krus [74], Pel [82], Kiebel et al. [86], Kopinga et al. [87] and Brocken et al. [89].

### **2.6.7 Computer Tomography**

The principle of computer tomography is to measure the intensity loss of a narrow beam of X-rays passing through the specimen. The absorption is a measure of the density of the specific material in question. The magnitude of absorption is measured with a CT value. The scale is calibrated against distilled water. By definition water has a CT value of 0. The absorption or CT value in air is  $-1000$ , which is taken as no absorption (100 % less). The absorption of X-rays in concrete is 145-150 % greater than in water. The CT value of concrete consequently is 1450-1500 [90]. The difference in the CT value between air and water is an indicator for measuring the water content in the material.

### **2.6.8 Microwave Beam**

Non-destructive measurement of the moisture profile can also be carried out with a microwave beam. Microwave attenuation is strongly influenced by the dielectric constant of the material [76]. The dielectric constant of water is 10-40 times higher than that of a dry material.

During the measurement the specimen is placed between a transmitter and a receiver, and the attenuation of the beam caused by oscillation of the water molecules is

measured. The magnitude of attenuation corresponds to the water content of the tested material. The equipment needs to be calibrated for the specific material. If the power of the beam is too high, temperature of water in the material will strongly increase during the test. Moisture migration caused by the temperature gradient might therefore occur. This measuring technique and some results are described in detail in Volkwein [91, 92] and Witting et al. [93].

### **2.6.9 Thermal Conductivity**

The thermal conductivity of a material increases with increasing moisture content. If the relation between the moisture content and thermal conductivity is known for a certain material, the moisture content can be measured with this method.

The principle of this method is to generate a known amount of heat locally in the material and then measure the temperature versus time curve at a certain distance from the heat source. This temperature curve is a measure of the thermal conductivity. Therefore, if the relation between the moisture content and thermal conductivity is known, the moisture content can be calculated. The heat source will however generate a temperature gradient, which will influence the moisture flux and hence acts as a source of error. According to Vos [94] it is possible to measure the moisture content with a precision of  $\pm 1$  vol. %.

### 2.6.10 Thermal Imaging

This is a simple method to determine the moisture distribution or the distribution of volatile fluids. The principle is based on decreasing temperature when liquids evaporate. The method is destructive and one sample is used every time the moisture profile is measured. When the profiles are to be measured the specimen is split into two halves, perpendicular to the exposed surface. The temperature of the split surface is measured with an infrared camera. From the temperature distribution the moisture profile is evaluated. According to Sosoro et al. [95], the moisture profile in a specimen with a constant cross section over the depth can be calculated by:

$$\varepsilon(x) = \frac{(T_o - T_s(x))^2}{\frac{S}{V_{fl}} \cdot \int_0^l (T_o - T_s(x))^2 dx} \quad (2.10)$$

Where

- $\varepsilon$  is the water content volume, per volume [ $\text{m}^3/\text{m}^3$ ]
- $T_o$  is the temperature of the surrounding air [K]
- $T_s$  is the surface temperature [K]
- $x$  is the coordinate in the direction of water transport [m]
- $S$  is the surface area exposed to fluid [ $\text{m}^2$ ]
- $V_{fl}$  is the total absorbed test fluid [ $\text{m}^3$ ]
- $l$  is the specimen length [m]

Another method is to calibrate the measured temperature of the split surface against the temperature of the split surfaces of well-conditioned specimens. The calibration is performed on specimens of the specific material with different and known moisture contents. The measuring and conditioning procedure must take place in a climate room with constant relative humidity and temperature, and the image must be taken at the same time after splitting the specimen. This conditioning procedure would be very time consuming, but the accuracy of the measured water content would probably be higher than the water content obtained with equation 2.10. Sosoro et al. [95] and Sosoro [96] gave profiles of different liquids and laboratory arrangements.

### **2.6.11 Capillary Water Uptake**

During this test the specimen absorbs de-ionized water from a reservoir. The specimen is connected to the reservoir through a nozzle and a liquid supply system. Both the nozzle and supply system are made of glass. A balance records the loss of weight of the water reservoir. In more sophisticated versions the weight data is transmitted on to a computer automatically at fixed intervals of time. In order to prevent evaporation from the water reservoir the balance is placed in a small chamber with approximately 100 % relative humidity. Evacuating the air through a valve on the nozzle starts the test. In this way, the entire specimen end is wetted. The nozzle is designed in such a way that the whole specimen surface is wetted within a few seconds.

From this test the sorption coefficient 'A' is calculated, as slope of the graph between the amounts of water absorbed per unit surface area versus square root of time.

Several methods are available in literature for calculating the coefficient of moisture diffusivity from the sorption coefficient, e.g. Kunzel [97] & Johannesson [98].

### **2.6.12 Moisture Loss / Drying**

Drying tests are conducted on thin specimens of various sizes. Since diffusivity is independent of the size and shape of the specimen, different kinds of specimen have been reported in the literature. Rahman [25] used specimen of sizes 200x200x40 mm up to 200x200x300 mm for one-dimensional drying tests on selected repair materials, at controlled temperatures, relative humidity and wind speeds. He also carried out two-dimensional drying tests on specimens of sizes 25x25x285 mm and 40x40x300 mm. Sakata [36] conducted 1-D drying tests on concrete specimens of sizes 40x40x10 cm.

The specimens are sealed using silicon sealant and aluminium tapes on different faces as per requirement, i.e. 1-D or 2-D moisture loss test. After this the specimens are dried in environmental chambers under controlled temperature, humidity and wind speed for a particular amount of time, normally several months & weights of the specimens are recorded at regular intervals, thus giving the moisture loss & in this way moisture profiles are generated. This test can be performed under varying environmental conditions; gives best results since moisture is measured directly on the specimens and is also very easy to perform, hence it was adopted in this research.

## 2.7 Review of Methods used for Computing Moisture Diffusivity

Non-linear or linear regression analysis of moisture loss versus square root of time data obtained from drying (moisture loss) test was used traditionally for the computation of moisture diffusivity. Mills [99] reported a diffusion coefficient dependent upon thickness of concrete, slope of the moisture loss versus square root of time curve and the mass of the evaporable water. Various methods reported in literature for the determination of coefficient of moisture diffusivity for cementitious mortars and concrete, from the measured moisture profiles, can be categorized as follows:

1. Boltzmann-Matano method [2.7.1]
2. Profile / gradient method [2.7.2]
3. Difference method [2.7.3]
4. Double integration method [2.7.4]
5. Numerical methods [2.7.5]

### 2.7.1 Boltzmann-Matano Method

Sakata [36] first used Boltzmann-Matano method for the analytical solution for diffusion coefficient as a function of moisture content. In this method the time and space dependent moisture concentration  $w(x, t)$  is expressed in terms of a single variable  $U = x / \sqrt{t}$  (Boltzmann variable), and the non-linear moisture diffusion equation is transformed into an ordinary differential equation. The determination of moisture dependent diffusivity coefficient requires a regressed relationship between the moisture

content  $w$  and the variable  $U$ , which is obtained using the moisture profiles measured across the depth of the specimen [Figure 2.8]. The equation is as follows:

$$D_w(w_2) = -\frac{1}{2 \cdot \frac{\partial w}{\partial U}} \cdot \int_{w_{in}}^{w_2} U dw \quad (2.11)$$

Where

$w$  is the moisture content [ $\text{kg/m}^3$ ]

$U$  is the Boltzmann variable [ $\text{m/s}^{1/2}$ ]

$D_w$  is the moisture dependent diffusivity coefficient

Asad et al. [26-27, 38-39], Penev and Kawamura [37], Akita et al. [68], and Perrin et al. [100] have used this approach for computing the moisture diffusivity coefficient for repair materials, soil-cement mixtures & lean concrete and ordinary concrete respectively. Diaw et al. [101] validated this method for the moisture transfer inside terracotta & showed that for a medium strictly satisfying the diffusion equation, Boltzmann-Matano method gives quite good results with the exception of some inaccuracies at extreme values of moisture contents. Drchalova et al. [102] showed similar results for their studies on moisture transport in autoclaved aerated concrete and face bricks.

However this method also has a few drawbacks. It requires the relationship between Boltzmann variable  $U$  and the measured moisture content, which is obtained approximately in this method by fitting experimental data from drying tests. Also the requirement that initial and boundary conditions should be expressed in terms of Boltzmann variable is hard to satisfy when drying occurs in concrete structures of finite

thickness, such as concrete pavements or repair layer in the repair system [103]. Moreover, verification of this approach by using the diffusivity law so obtained, in a finite element based drying model and comparison of measured and computed solutions has scarcely been documented.

### 2.7.2 Profile / Gradient Method

This method is based on using two moisture profiles measured at different times, calculating the moisture flux and applying the Fick's law in 1-D [104]. Moisture diffusivity is expressed as a function of an average moisture profile curve between the two measured profiles [Figure 2.8].

$$D_w = -\frac{1}{dt} \cdot \frac{\int_{x=x_o}^{x=l} (w_{t+dt}(x) - w_t(x)) dx}{\frac{\partial w_o}{\partial x_o}} \quad (2.12)$$

Where x is the depth of the specimen.

### 2.7.3 Difference Method

Cerny et al. [105], originally developed this method for determination of thermal conductivity. For an application to calculating moisture diffusivity, a similar treatment has been used [102]. The equation for coefficient of diffusivity is given as:

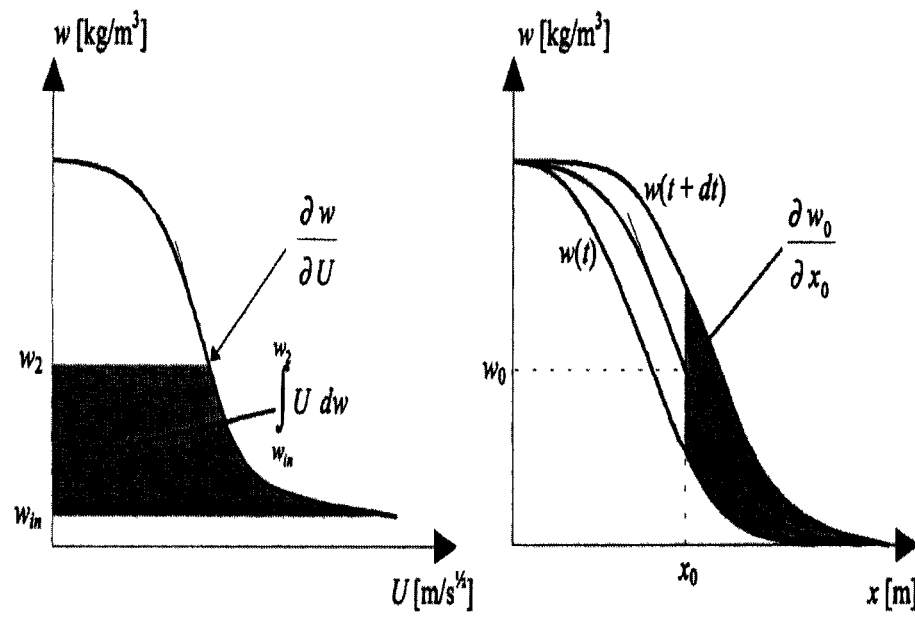


Figure 2.8: Principle of Boltzmann-Matano Method (left),  
Profile / Gradient Method (Right)

$$D_w(x - \Delta x / 2, t + \Delta t / 2) = D_w(x + \Delta x / 2, t + \Delta t / 2) \cdot \frac{A}{C} - \frac{B}{C} \quad (2.13)$$

$$A = w(x + \Delta x, t) - w(x, t) + w(x + \Delta x, t + \Delta t) - u(x, t + \Delta t) \quad (2.14)$$

$$B = \frac{(\Delta x)^2}{2 \cdot \Delta t} (w(x, t + \Delta t) - w(x, t)) \quad (2.15)$$

$$C = w(x, t) - w(x - \Delta x, t) + w(x, t + \Delta t) - w(x - \Delta x, t + \Delta t) \quad (2.16)$$

where  $\Delta x$  is the space interval and  $\Delta t$  is the time interval.

Equation 2.13 is a recursive relation for determining moisture diffusivity in dependence on moisture. Its application requires the knowledge of at least one value of moisture diffusivity e.g. for  $w$  approaching to zero.

#### 2.7.4 Double Integration Method

This method employs several moisture profiles for determining the coefficient of diffusivity [106, 107]. The resulting formula is as under:

$$D_w = \frac{\int_o^{x_o(v, \tau)} w(\xi, \tau) d\xi - \int_o^{x_o(v, o)} w(\xi, o) d\xi - v[x_o(v, \tau) - x_o(v, o)] - Q(\tau)}{\int_o^\tau \frac{\partial w(x_o(v, t), t)}{\partial x} dt} \quad (2.17)$$

Where  $v$  is a chosen constant value of moisture content,

$$Q(\tau) = \int_0^l (w(x, \tau) - w_2) dx \quad (2.18)$$

$l$  is the length of the sample and  $w_2$  is the initial moisture content.

### 2.7.5 Numerical Methods

Several numerical methods are also reported in literature for computation of moisture diffusivity of cementitious materials. Wittman et al. [66] used finite difference combined with non-linear least squares fit method to obtain the best fit diffusion coefficient by comparing with the measured experimental moisture profiles during the moisture loss test. Xin, Zollinger and Allen [103] used inverse diffusion analysis to determine diffusion coefficient of hardening concrete. A least squares minimization was used for ensuring best agreement between calculated and measured humidity profiles, using probe type sensors at each measured point and at each time level to calculate diffusivity. Diffusivity was not only considered as a function of pore humidity but also the spatial and temporal variations were accounted for in this approach. Rahman [25] developed a 2-D non-linear finite element model combined with non-linear least squares fit method for the computation of diffusivity law parameters for repair materials. The parameters were obtained by comparing the computed moisture profiles with the measured profiles obtained during the moisture loss test.

## 2.8 Types of Repair Materials

Repair materials are widely used in many applications, such as:

- Overlays for new bridge decks
- Repair of old bridge decks
- Highway and airport pavements
- Parking garages
- Pavement toppings
- Patching of damaged concrete in structures

For repair, rehabilitation and strengthening of concrete structures, a wide array of repair and strengthening systems are currently available. These systems can be classified into the following major groups [108]:

- Cement based repair materials
- Resin based repair materials [epoxy & polyester, acrylic & polyurethane]
- Crack injections [polyurethane, resins & micro-cement]
- Corrosion protection systems [corrosion inhibitors & cathodic protections]
- Protective systems [polymer based]
- External structural strengthening [steel & carbon fibers]

Further classification of cement based repair materials is given in [Figure 2.9]:

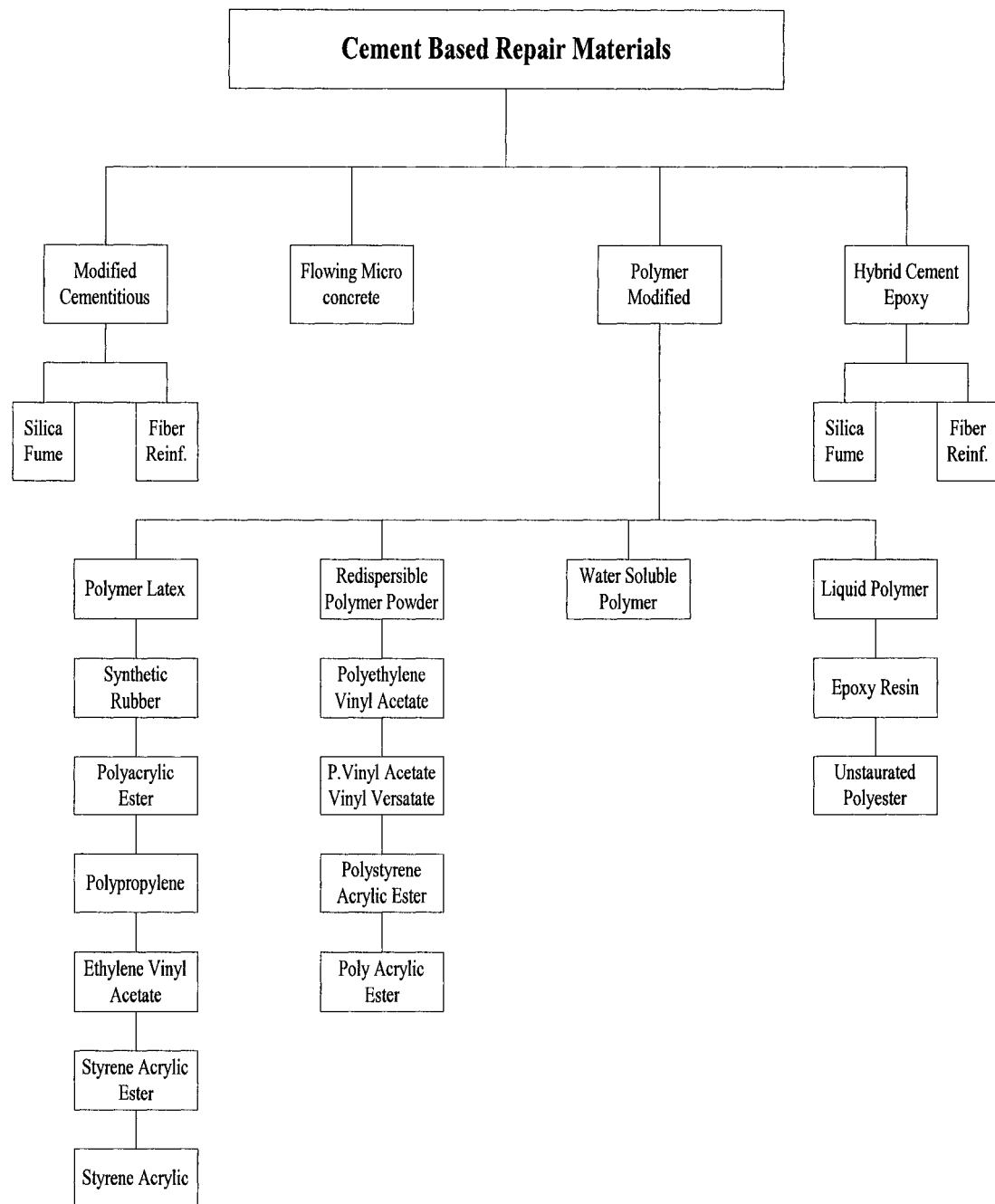


Figure 2.9: Classification of Cement Based Repair Materials

Flowing micro-concrete class of cementitious repair materials is now being used extensively. It flows freely and can penetrate deep into congested reinforcement. It is self-compacting in nature and eliminates the presence of honeycombing and voids in concrete. It also undergoes significant gaseous expansion in plastic state, which compensates for shrinkage in the plastic and hardened states. Its high strength and low permeability provides maximum protection against chlorides and carbon dioxide. Also because of the low alkali content, the risk of alkali-silica reaction gets minimized. Because of these properties it becomes very suitable for the reinstatement of large structural sections of concrete as well as for many smaller locations where difficulties of access make hand or trowel applied mortars impracticable.

In this research only the flowing micro-concrete class repair materials were considered because of their wide applicability in patch repair of concrete, thin overlays, jacketing of structural elements and compatibility with the concrete substrate.

## **2.9 Properties of Repair Materials**

The key material parameters, which need to be considered in evaluating a repair material, include the following [109-111]:

### **Structural Properties**

- Tensile strength
- Flexural strength
- Elastic modulus in compression, tension and flexure
- Creep

- Compressive strength
- Ductility and toughness
- Strain capacity
- Abrasion and skid resistance

**Physical Properties**

- Shrinkage and swelling
- Coefficient of thermal expansion
- Adhesion in tension and shear
- Diffusivity

**Barrier Properties**

- Resistance to chloride ingress
- Resistance to carbonation
- Water absorption
- Permeability to water, air, gases and chemicals
- Resistance to seawater and sulfates

Investigation of structural and barrier properties is beyond the scope of this research and focus is only on the moisture diffusivity of selected micro-concretes.

## 2.10 Shrinkage of Concrete

Concrete experiences volume changes throughout its service life. The total in-service volume change is the resultant of applied loads, shrinkage, creep, and thermal movements [112]. Shrinkage is defined as the time dependent strain measured in an unloaded and unrestrained specimen at constant temperature. As the concrete cures and dries, tensile stresses are created due to hydration and loss of moisture. These tensile stresses cause the concrete to shrink. When the shrinkage of concrete is restrained from within itself, i.e. aggregate, or from outer sources, i.e. reinforcing bars and member supports etc., the tensile stresses exceed tensile strength of concrete and this leads to cracking of concrete. This enables the aggressive species to diffuse or permeate through concrete easily, causing reinforcement corrosion, cracking, spalling and de-lamination of concrete cover.

In concrete the loss of water occurs from its fresh state to later ages, and on this basis shrinkage of concrete is divided into the following types, namely, plastic shrinkage, autogenous shrinkage or chemical shrinkage, carbonation shrinkage, thermal shrinkage and drying shrinkage.

Plastic shrinkage is due to the moisture loss from concrete before it has set, due to evaporation from the surface. This type of shrinkage normally occurs within five to six hours of casting. The magnitude of plastic shrinkage depends on the amount of water lost, which is influenced by temperature, ambient relative humidity and wind speed. If the amount of water lost exceeds the amount of water brought to the surface by bleeding, surface cracking can occur.

Autogenous or chemical shrinkage is associated with the loss of water from the capillary pores due to the hydration of cement [113]. This process of removal of water is known as self-desiccation. In practice this shrinkage occurs in the interior of the concrete mass and is restrained by rigid skeleton of already hydrated cement paste and aggregates, and hence it is of much smaller magnitude. Autogenous shrinkage tends to increase at high temperatures, higher cement content, finer cement particles and low water cement ratios.

Carbonation shrinkage is caused by the chemical reaction of various cement hydration products with carbon dioxide present in the air and is usually limited to the concrete surface only. Thermal shrinkage is the volume contraction of concrete due to the dissipation of heat, generated during the hydration of cement. Also concrete cured continuously under water from the time of placing exhibits a net increase in volume known as swelling. This is due to the absorption of water by the cement gel.

Drying shrinkage is the volumetric change in concrete due to withdrawal of water during drying. Capillary depression, variations in surface tension and disjoining pressures, and movement of the interlayer C-S-H water, are all associated with the movement and loss of water during drying of concrete [114, 115]. Neville [116] discussed that the change in volume of concrete due to drying shrinkage is not equal to the volume of water lost. The loss of free water occurs first with little to no shrinkage. As the drying process continues, adsorbed water held by hydrostatic tension in small capillaries ( $<50$  nm), is removed. This induces tensile stresses, which cause the concrete to shrink.

Drying shrinkage is further split into two parts, reversible and irreversible drying shrinkage, where reversible drying shrinkage is the part, which is reproducible during

alternate wet and dry cycles and vice versa. For a typical concrete the irreversible amount may be up to 30 % of the total drying shrinkage. This is attributed to the formation of extra bonds within the gel matrix during drying when closer contact between the gel particles is established.

Values of 28 days drying shrinkage strains have been measured for water-cement ratio of 0.45 and found to vary from  $+13 \times 10^{-6}$  to  $-410 \times 10^{-6}$  depending on the curing regime used [117]. Sakata [36] reported that drying shrinkage strain of concrete differs according to depth from the drying surface, being larger in the concrete exterior. It is furthermore closely related to moisture loss and especially in the neighborhood of the drying surface a straight line can express the relation.

Various models have been reported in literature for predicting shrinkage in concrete elements. The five most popular are as follows:

- American Concrete Institute-ACI 209 code model, to predict ultimate shrinkage strain in concrete.
- Bazant B3 model, to predict ultimate shrinkage strain, using water content of concrete, cross section shape, relative humidity and concrete age as factors [118].
- Euro-International Concrete Committee-CEB 90 code model, to predict drying shrinkage of concrete, employing cement type, relative humidity and compressive strength as factors [119, 120].
- Gardner/Lockman model, to predict ultimate shrinkage strain, using relative humidity, age of concrete, time of drying and cement type as factors [121].

- Sakata model, to predict ultimate shrinkage strain using water content of concrete, relative humidity, volume to surface area ratio of the concrete element and drying time as parameters [122].

## **2.11 Factors Affecting Drying Shrinkage of Concrete**

Since drying shrinkage is related to the moisture loss from concrete, it is influenced by external factors that affect drying and also internal factors related to concrete and its constituents [Figure 2.10]. Following are the different factors reported in literature:

### **2.11.1 Ambient Conditions**

Air temperature, relative humidity and wind speed affect loss of moisture from the surface of concrete. ACI [123] discusses how the combination of these factors affects the evaporation rate. Higher drying shrinkage is to be expected with the increase in ambient temperature, decrease in relative humidity, increase in air movement or wind speed around concrete and with the increase in the length of time for which concrete is exposed to drying conditions [124]. Torrenti et al. [125] found that thermal expansion coefficient of concrete has a direct relation to the shrinkage values of concrete & variations in relative humidity have a major influence on the thermal expansion coefficient than ambient temperature.

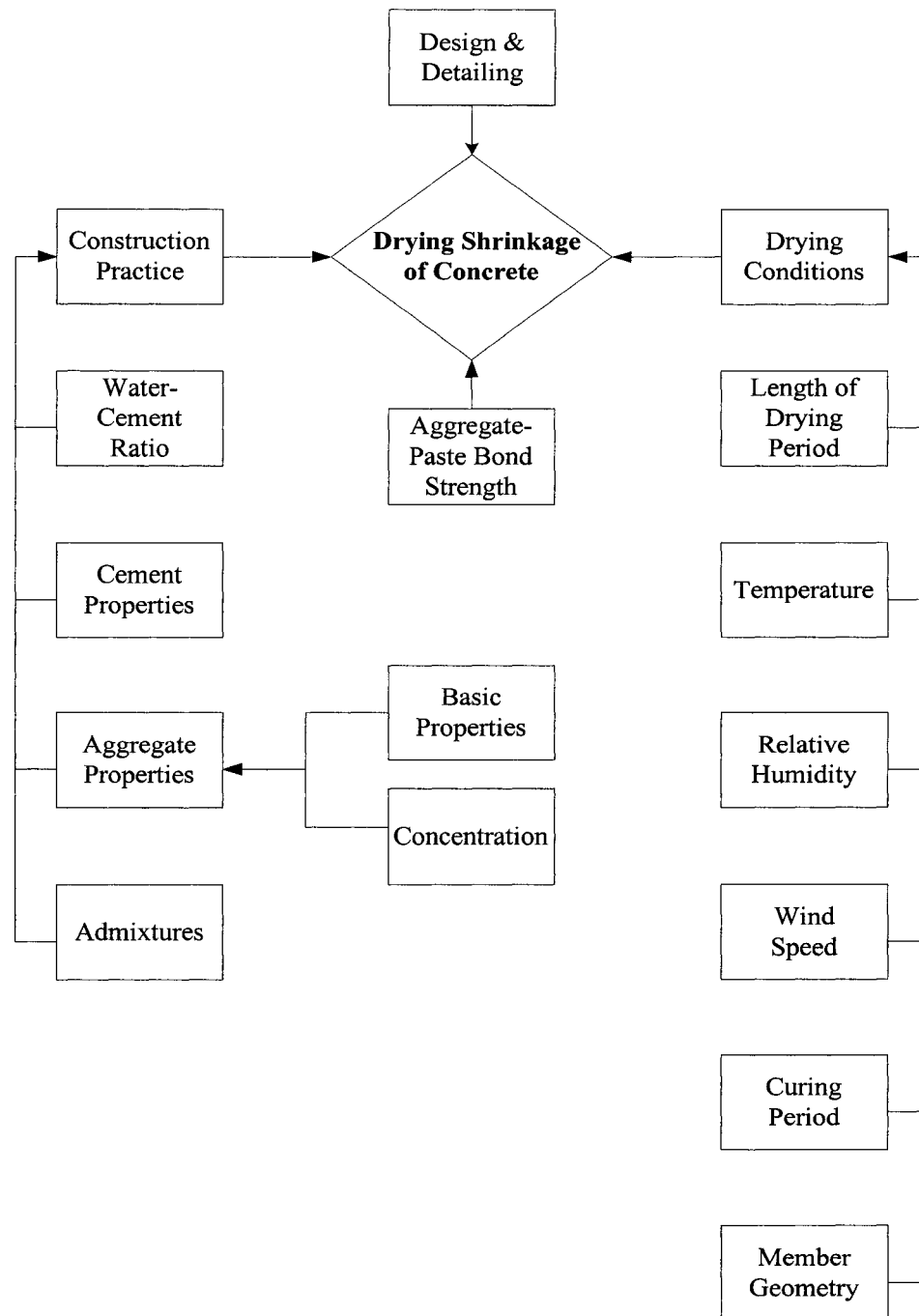


Figure 2.10: Factors Affecting Drying Shrinkage of Concrete

### **2.11.2 Curing of Concrete**

The longer the curing time, the lesser is the drying shrinkage. Al-sayed [126] examined the effects of different curing methods on drying shrinkage of concrete. He found that burlap, polyethylene and air curing, all result in high shrinkage rates. However, watering the concrete four to five times a day during curing reduces the rate of drying shrinkage.

### **2.11.3 Member Geometry**

Large, thick concrete members dry out slowly as compared to the small ones. As a result, for the same drying period and conditions, drying shrinkage of large sized members is lower than the small sized which can dry out to their cores more quickly [124]. Al-Mudaiheem & Hansen [127] also observed similar behavior.

### **2.11.4 Cement Content, Type & Fineness**

Higher cement contents are found to result in higher drying shrinkage strains, keeping the other mix variables constant [128]. Chemical composition of cement is now believed not to affect the drying shrinkage of concrete, except that cements deficient in gypsum exhibit an increase in shrinkage strains. Shrinkage of concrete made with high alumina cement is of the same magnitude as that of ordinary Portland cement, but it takes place in a much shorter time. Fineness of cement is a factor only in so far as particles are coarser than 75  $\mu\text{m}$ , since they hydrate comparatively less and have a restraining effect similar to aggregates [116].

### **2.11.5 Water-Cement Ratio & Water Content**

Drying shrinkage of concrete increases with increasing the water content. Concrete with higher water content and higher water-cement ratio has a lower strength, lower modulus of elasticity, and more amount of water to be lost during drying, and hence has a greater tendency to shrinkage [129].

### **2.11.6 Aggregates**

Aggregates have a restraining effect on the shrinkage of concrete. However, this depends on the type of aggregate, water demand of aggregate, aggregate stiffness, volumetric concentration and aggregate-paste interaction [130]. Aggregates should have low water absorption, high modulus of elasticity and should be free from contaminants such as clay, coal, wood or organic matter for producing concrete with low shrinkage. Other aggregate properties such as grading, maximum size, shape and texture have an indirect effect on drying shrinkage in terms of the changes they cause to concrete mix design.

### **2.11.7 Admixtures**

The most commonly used mineral admixtures in concrete are silica fume and fly ash. Most of these admixtures increase the water demand of concrete, which is associated with higher drying shrinkage, however studies have shown that it is not always the case. Mixes with fly ash exhibit higher drying shrinkage than those with silica fume or blast furnace slag [130].

Chemical admixtures like shrinkage reducing admixtures (SRA) and high range water reducers (HRWR) are presently being used on a limited basis. SRA lowers the surface tension of pore water solution in the cement paste, thus decreasing the shrinkage stresses. HRWR produces a concrete of higher workability with low water cement ratio and in this way has an indirect effect on the drying shrinkage of concrete [130].

#### **2.11.8 Construction Practice**

Concrete placing and compaction are also important factors in reducing the magnitude of drying shrinkage. Adding further water on site during placing of concrete to restore slump or ease the finishing will increase the drying shrinkage. Proper compaction is required to produce dense concrete with reduced or discontinuous capillaries, resulting in lower moisture loss and reduced drying shrinkage [124].

## 2.12 Water Permeability of Concrete

The lack of durability of concrete structures is often linked to the ingress of deleterious agents from the surrounding environment. There are three fluids principally relevant to durability, which can enter concrete, water-pure or carrying aggressive ions, carbon dioxide and oxygen [116]. The permeation of moisture and air can result in the corrosion of re-bars ultimately leading to cracking and spalling of concrete cover and can also affect the thermal insulation properties of concrete. Permeability of concrete is also of interest in relation to liquid retaining and some other structures with respect to water tightness, and development of hydrostatic pressure in the interior of the concrete mass.

Permeability of concrete is defined as the ease with which fluids, both liquids and gases, can enter and move through concrete. It refers to flow under a pressure differential. However, it is important to differentiate between permeability and porosity of concrete. Porosity is a measure of the proportion of the total volume of concrete occupied by pores. If the porosity is high and the pores are interconnected, they contribute to the transport of fluids through concrete so that its permeability is also high, but on the other hand if these pores are discontinuous, permeability of concrete is low, though porosity is the same [116]. Figure 2.11 further illustrates this concept.

Permeability of concrete primarily depends on the structure of the hydrated cement paste, more explicitly on the nature of the pore system within the bulk hydrated cement paste, and also on the interfacial zone between aggregate and cement paste. Aggregates also contain pores but these are usually discontinuous, and moreover the cement paste envelops aggregates so that the pores in aggregates do not contribute to the

permeability of concrete. The pores relevant to permeability are those with a diameter of at least 120 or 160 nm and have to be continuous. Whereas the pores, which contain adsorbed water or have a narrow entrance are ineffective with respect to permeability of concrete. In short permeability of concrete is not only a simple function of porosity but it also depends on the size, distribution, shape, tortuosity and continuity of pores.

It has been confirmed from mechanical tests that low permeability values are related with high compressive strength values to indicate a reliable concrete or mortar [131]. Meziani et al. [132] showed that permeability of concrete is very sensitive to changes in porosity and micro cracking. Helene et al. [133] found that water permeability of concrete is lower than its gas permeability & attributed this to re-hydration, dissolution and migration of fine elements, and water adsorption in thinnest pores. Larbi [134] found that despite the higher porosity of interfacial zone, hydrated cement paste controls the permeability of concrete, since it is the only continuous phase in concrete. Roy [135] reported that permeability of hardened cement paste is not lower than that of the concrete with a similar cement paste. However, any movement of fluids has to follow a path made longer and more tortuous by the presence of aggregate, which also reduces the effective area of flow. Reinhardt et al. [136] found that water permeability values of concrete tested by either DIN 1048 or ISO 7031 method are not much different. They also found that organic liquids, e.g. diesel, penetrate into a dense partly dried concrete after 72 hours by almost the same amount, as does water in a wet concrete.

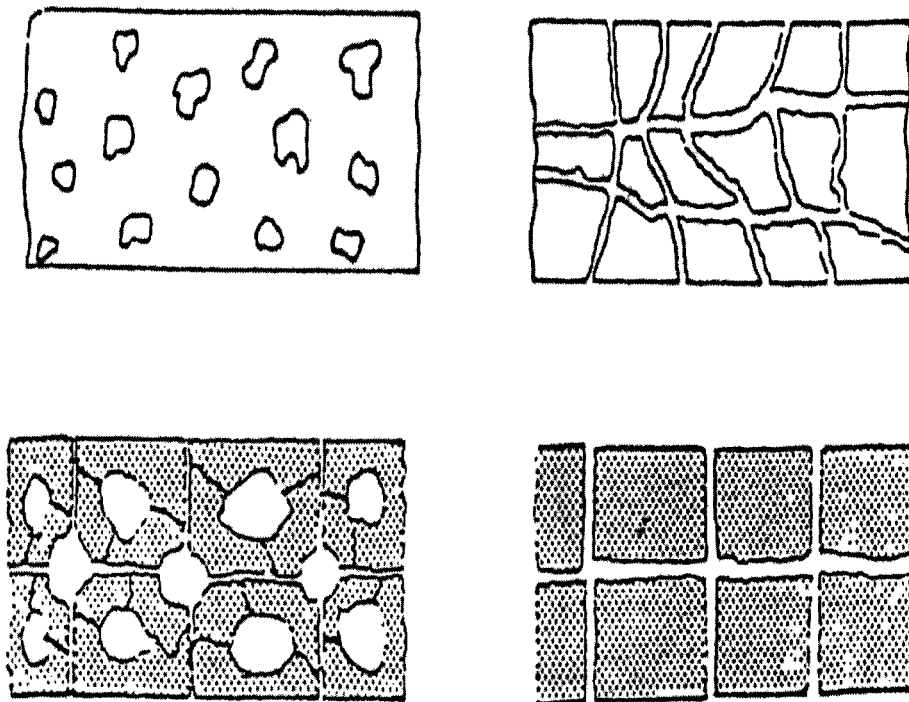


Figure 2.11: Illustration of Permeability and Porosity. Porous-Impermeable (Top Left),  
Porous-Permeable (Top Right), Highly Porous-Less Permeable (Bottom Left),  
Less Porous-Highly Permeable material (Bottom Right)

## **2.13 Factors Affecting Water Permeability of Concrete**

Following are the different factors reported in literature that affect the water permeability of concrete:

### **2.13.1 Water-Cement Ratio**

The most important parameter that influences water permeability of concrete is the water-cement ratio. As the water-cement ratio is increased, the cement paste and concrete become more permeable. Water in excess of what is required for hydration of cement, tends to create zones of low-density porous paste in the matrix, especially at or near the interfacial zone [137].

### **2.13.2 Degree of Hydration**

In a fresh concrete the flow of water is controlled by the size, shape and concentration of original cement particles. With the progress of hydration permeability decreases rapidly, because the gross volume of gel including the gel pores becomes approximately twice the volume of un-hydrated cement, so that the gel gradually fills some of the original water filled space [116].

### **2.13.3 Properties of Cement**

For the same water-cement ratio, coarse cement tends to produce a hardened cement paste with higher porosity than fine cement. The compound composition of

cement affects permeability in so far as it influences the rate of hydration, but the ultimate porosity and permeability remain un-affected.

#### **2.13.4 Curing Time**

If the surface of concrete dries out more during curing i.e. if the dry curing period is too long, a shortage of water is created at the surface and the hydration reactions cannot complete satisfactorily, thus leaving higher pore volumes at the concrete surface and making it more permeable. Another reason may be that during drying, shrinkage may rupture some of the gel between the capillaries and thus opens new passages to water [136].

#### **2.13.5 Temperature**

Hydration reaction is exothermic, which in combination with the high ambient temperature can cause the concrete to dry out too quickly and prevent full completion of the hydration reactions. Also it may induce thermal cracking and cause water inside the hydrating cement to boil, thus creating bubbles. This increases the permeability of concrete. Reinhardt et al. [24] have shown that permeability increases by 13-62 % for different concrete mixes with the temperature rising from 20 to 50 °C and by 3-55 % with an additional increase to 80 °C.

### **2.13.6 Aggregate Properties**

Porosity and pore size is largest in the interfacial zone between cement-paste and aggregate. As the maximum aggregate size is increased micro cracking in this zone becomes severe, thus increasing the water permeability [138]. A well-graded aggregate reduces the permeability of concrete since the fine aggregate fills in the voids between the coarser particles. If the aggregate has very low permeability, its presence reduces the effective area over which the flow can take place. Further flow path has to circumvent the aggregate particles & the effective path may become so long that a significant reduction in permeability occurs.

### **2.13.7 Mineral Admixtures**

The use of mineral admixtures in concrete, e.g. fly ash, silica fume and blast furnace slag, is associated with the phenomena of pore size refinement and grain size refinement. Also due to slower hydration, the heat of hydration and thermal cracking is minimized [139]. Owing to these processes the permeability of concrete reduces significantly.

## CHAPTER 3

# EXPERIMENTAL PROGRAM FOR THE RESEARCH

### 3.1 Scope of the Experimental Work

The experimental work involved testing of selected concrete mixes and repair materials, for moisture transport properties under varying exposure conditions and certain physical properties helpful in understanding and predicting this behavior. It consisted of the following components:

- **Drying tests** conducted on specimens of various sizes with unidirectional moisture movement, for computing moisture diffusivity of the selected repair materials and concrete mixes. These tests were carried out in environmental chambers with controlled temperature & wind speed, to see the effect of these variables on moisture transport.
- **Shrinkage tests** conducted on prismatic specimens of various sizes for concrete mixes and repair materials, along with the respective diffusivity/drying test specimens. Shrinkage strains were measured by means of embedded strain gauges and recorded by a data logger throughout the exposure period.
- **Compressive strength evolution tests** conducted on cylinders for each concrete mix.

- **Water permeability tests** conducted on cube specimens for each concrete mix.

## **3.2 Selected Repair Materials**

Two commercially available cement based repair materials of the flowing micro-concrete category were selected for this research, from different vendors, owing to their best performance and wide applicability in structural repairs in Saudi Arabia [71]. A brief description of each of them is provided in the following discussion:

### **3.2.1 Fluid Micro-Concrete (FMC1)**

This is a single component free flowing low alkali micro-concrete. It is supplied as a ready to use blend of dry powders, which requires only the site addition of clean water to produce a free flowing, shrinkage compensated micro-concrete. The material is based on Portland cement, graded aggregates and additives, which impart controlled expansion in both the plastic and hardened states while minimizing the water demand. The low alkali content minimizes the risk of alkali-silica reaction. It has exceptional bond to concrete substrates without independent primer and is suitable for placement by pumping. The self-compacting nature eliminates honeycombing and the high strength and low permeability provides maximum protection against chlorides and carbon dioxide. It is supplied in 30 kg bags and requires 4 liters of water per bag of the mix. The major properties as provided by the manufacturer are as under:

Test Method	Typical Result
Compressive Strength (BS 1881)	30 N/mm <sup>2</sup> at 3 days 45 N/mm <sup>2</sup> at 7 days 60 N/mm <sup>2</sup> at 28 days
Water Absorption (BS 1881)	0.0125 ml/m <sup>2</sup> /sec at 10 min 0.0013 ml/m <sup>2</sup> /sec at 2 hrs
Modulus of Elasticity (BS 1881)	33 GPa at 28 days
Coefficient of Thermal Expansion	10 to 12 x 10 <sup>-6</sup> / °C
Bond Strength (BS 6319)	66 N/mm <sup>2</sup> at 28 days

### 3.2.2 Flowing Precision Concrete (FMC2)

This is a high strength precision concrete requiring only the on-site addition of water to provide a free flowing concrete free from segregation and bleeding. It is a pre-packaged blend of Portland cement, carefully graded natural aggregate, specially selected sands, fillers, shrinkage control agents and fluidifiers. Utilization of low water cement ratio ensures minimum permeability and high durability. It is self-compacting in nature and the unique formulation provides dual expansion system in plastic and hardened states. The specified amount of water to obtain the desired consistency should not exceed 3.5 liters per 25 kg bag. Some typical properties as provided by the manufacturer are as under:

Test Method	Typical Result
Wet Density	2300 kg/m <sup>3</sup>
Compressive Strength (BS 1881)	65 N/mm <sup>2</sup> at 28 days
Flexural Strength (BS 1881)	5 N/mm <sup>2</sup> at 28 days
Modulus of Elasticity (BS 1881)	30 GPa
Water Permeability (DIN 1048)	Nil

### 3.3 Concrete Mix Design

Concrete mix design was carried out following the ACI 211.1-91 [140] specified procedure for selection of mix proportions of concrete. In order to see the effect of water cement ratio (w/c) on moisture diffusivity of concrete, mix design was done for three water cement ratios 0.45, 0.5 and 0.6, keeping the cement content (Type-I) constant at 420 Kg/m<sup>3</sup>. Minimum water cement ratio of 0.45 was selected so as to avoid the use of super plasticizers and hence non-uniformity among the mixes. The maximum aggregate size was selected as 3/8" depending on the minimum thickness of the diffusivity specimens being used. Aggregate grading was selected according to ASTM C 33 standard specifications for coarse aggregates as under:

$$3/8'' = 45\% \qquad 3/16'' = 45\% \qquad 3/32'' = 10\%$$

Aggregate was sieved following ASTM C-136 procedure, properly washed to remove any dust or fines and then dried at room temperature for several weeks before use.

The following parameter values were assumed for mix design based upon previous research on the local constituent material:

Specific Gravity of Cement = 3.15

Unit Weight of Coarse Aggregate (C.A) = 1600 kg/m<sup>3</sup>

Specific Gravity of C.A = 2.6

Fineness modulus of sand (F.A) = 2.6

Specific Gravity of F.A = 2.5

Table 3.1: Concrete Mix Design

<b>W/C</b>	<b>WATER Kg/m<sup>3</sup></b>	<b>CEMENT Kg/m<sup>3</sup></b>	<b>C.A Kg/m<sup>3</sup></b>	<b>F.A Kg/m<sup>3</sup></b>
0.45	189	420	770.4	945
0.5	210.5	420	770.4	1003
0.6	252	420	770.4	788

### 3.4 Shape and Size of Test Specimens

Various types of prismatic specimens were used in this research. Some of them were selected according to the standard ASTM or DIN specifications, while some non-standard specimens were also used in order to minimize the variation in sizes. Geometry and total number of the specimens used in various tests is described in Table 3.2.

Table 3.2: Description of Test Specimens

TEST	SPECIMEN SIZE	TOTAL No.
Drying (concrete)	100x100xB (B = 25,50,75,100 mm)	144
Drying (repair)	100x100xB (B = 10,20,30,40,50,60,75 mm)	126
Shrinkage (concrete)	75x75x300 mm prisms ASTM C 531	36
Shrinkage (repair)	25x25x285 mm prisms ASTM C 157	18
Compressive strength	75x150 mm cylinders ASTM C 39	84
Water permeability	150x150x150 mm cubes DIN 1048	09

### 3.5 Moulds for Specimens

All the specimens were cast in metallic or wooden moulds. Wooden cylindrical moulds for compressive strength test and metallic cube moulds for water permeability test were already available in the laboratory. Moulds for shrinkage and drying tests on repair materials were also available. However for concrete, wooden shrinkage moulds and aluminium diffusivity moulds with partitions for casting several specimens in multiples were fabricated at the KFUPM workshop [Figure 3.1].

### 3.6 Manufacturing of Specimens

Manufacturing of the specimens was carried out in different phases as governed by the selected exposure regimes and availability of the environmental chambers.



Figure 3.1: Moulds for Drying & Shrinkage Tests on Concrete

All the specimens required for different tests on a particular mix/material were cast together to have uniformity of the mix. The moulds were always screwed tight, properly cleaned and oiled before used for casting. For each test sufficiently large number of test specimens were prepared to ensure credibility of the results.

### **3.6.1 Mixing Procedures**

Mixing of concrete was carried out in a standard rotary drum mixer. The required quantities of water, cement, sand and aggregates were measured and put into separate containers before mixing. The mixer was thoroughly washed and cleaned before use. Coarse aggregates and sand were then put into the mixer and mixed for some time for proper blending. Cement was then added into the mixer and mixed for uniform distribution. Water was then added into the mixer in two steps and the mixer operated for about 3-5 minutes each to ensure proper mixing and blending of the ingredients in order to have a uniform mix. The mix was then put in a hand pushed trolley for placing into the moulds.

Mixing of repair mortars was carried out using a forced action mixer. The forced action mixer was enacted using a spiral paddle attached to a drill machine. A heavy-duty drill machine of speed up to 500 rpm was used for this purpose. The amount of clean water specified by the manufacturer was placed in a suitable sized plastic drum, which was washed and cleaned before use. A full bag of the repair material was then added with the spiral paddle rotating. Mixing was carried out for 2-5 minutes depending on the manufacturer's recommendations, until a smooth and even consistency was obtained and

the mortar became homogenous and lump free. Restrictions by the manufacturer on mixing time, reworking of the mortar and adding additional water to get workability were strictly adhered to.

### **3.6.2 Placing of Concrete & Repair Mortars**

Concrete was placed into the moulds in three layers, properly vibrating each layer for 5-10 seconds. Strain gauges were placed in the shrinkage moulds during placing operation, approximately embedding in the center of the specimen. The top surface was firmly finished by steel floats & all the exposed surfaces were then covered with Pyrex glass plates and/or polythene sheets until de-molding.

Repair mortars were placed into the moulds for moisture diffusivity and shrinkage immediately after mixing. Care was taken not to exceed the manufacturers stipulated maximum working time of 30 minutes, by increasing the manpower. The mortars were then poured into moulds by small holding cans without vibration. Strain gauges were placed into the shrinkage moulds, well embedded into the mortar approximately in the center, after some time to allow the mortars to set a bit. The mortars were then given a final finish with a steel float and the moulds were properly covered with pyrex glass plates and polythene sheets. A light pressure was applied at the top by means of some metal plates to prevent unrestricted expansion at the exposed surfaces, as per manufacturer recommendations.

### **3.6.3 Curing Regimes for the Test Specimens**

Diffusivity and shrinkage test specimens for the repair mortars were kept in the moulds for 24 hours after placing. After that the specimens were de-molded, covered around with wet burlap, wrapped with polythene sheets and kept at room temperature of  $23\pm 2^{\circ}\text{C}$  for a period of 7 days. Afterwards the specimens were transferred into the environmental chambers for testing.

Similar procedure was adopted for the shrinkage and diffusivity specimens of concrete. However, the water permeability and compressive strength specimens were cured initially in the same manner up to 7 days. Afterwards the permeability specimens were air cured at room temperature of  $23\pm 2^{\circ}\text{C}$  and relative humidity of  $65\pm 5\%$  up to 28 days, before testing, while the compressive strength specimens were also cured in a similar manner until the times of testing.

All the specimens were marked for identification, according to a system of nomenclature developed for these materials and/or experiments, before putting them for curing.

## **3.7 Test Procedure for Compressive Strength**

Compressive strength tests were carried out on specimens of the three concrete mixes of water cement ratios 0.45, 0.5 and 0.6, on 75x150 mm cylinders according to ASTM C-39 standard specifications. Before testing the cylinders, rough end surfaces were capped with sulfur to ensure uniform distribution of load on the entire specimen. Tests were conducted in a hydraulic machine with a load capacity of 3000 KN [Figure 3.2].



Figure 3.2:Arrangement for Compressive Strength Test

Loading rate was kept at 3.3 KN/sec for all the tests & the load value was taken from the load cell built in the equipment. Tests were conducted at the specimen age of 3, 7, 28, 60 and 105 days after casting to see the evolution of compressive strength. Four cylinders were tested at each age for each mix and the average strength was taken. If the strength value differed from the mean value by more than 15%, it was rejected and average of the remaining readings was taken and recorded as the compressive strength at that age.

### **3.8 Test Procedure for Water Permeability**

Basic procedure of such a test is to apply water under pressure to one surface of the specimen for a specific time and then split the specimen perpendicular to the injected face and determine visually the depth of penetration. The arrangement of the test cell is shown in Figure 3.3.

The test was carried out according to German Standard DIN 1048 on concrete specimens of size 150x150x150 mm, at an age of 28 days. The test cell assembly used had the provision for testing six cubes at a time [Figure 3.4]. Three specimens were used for each mix and the average depth of water penetration was taken.

Once the specimens were assembled in the test cells, a water pressure of 100 KPa (1 bar) was applied for the first 48 hours, followed by pressures of 300 KPa (3 bar) and 700 KPa (7bar) for 24 hours each. Water pressure was applied by means of an arrangement consisting of a water tank connected to an air compressor through a valve, to adjust the pressure [Figure 3.5].

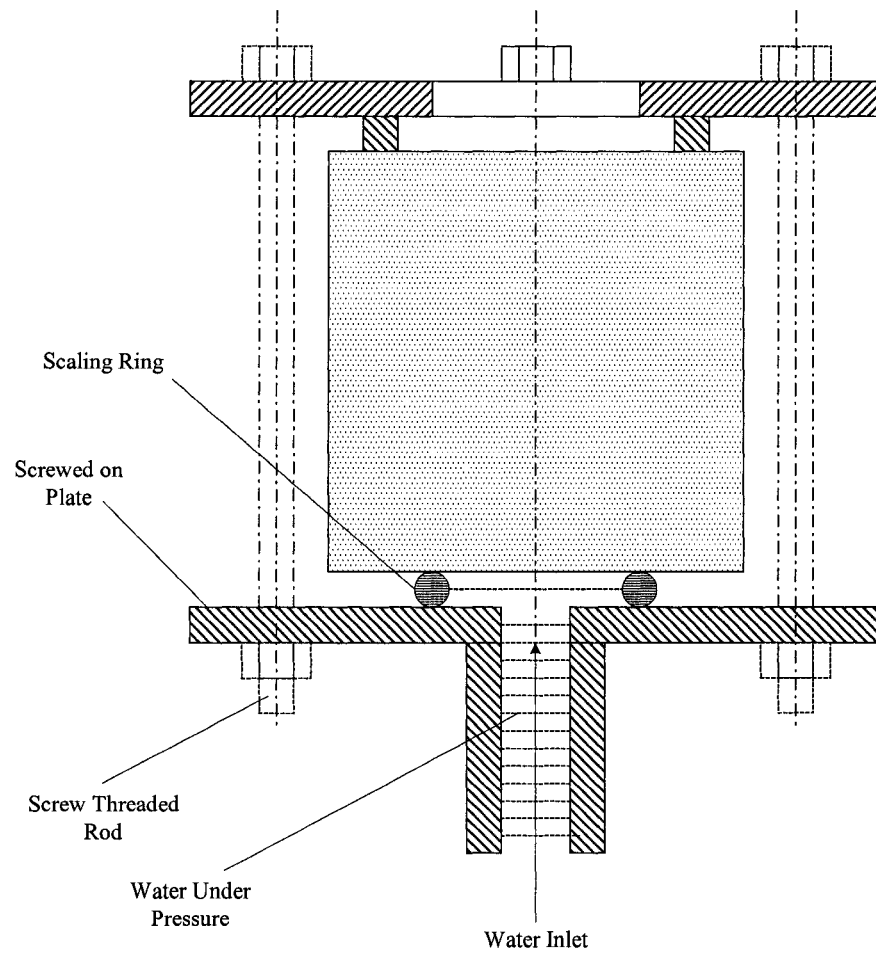


Figure 3.3: Sketch of the Test Cell for Water Permeability by DIN 1048

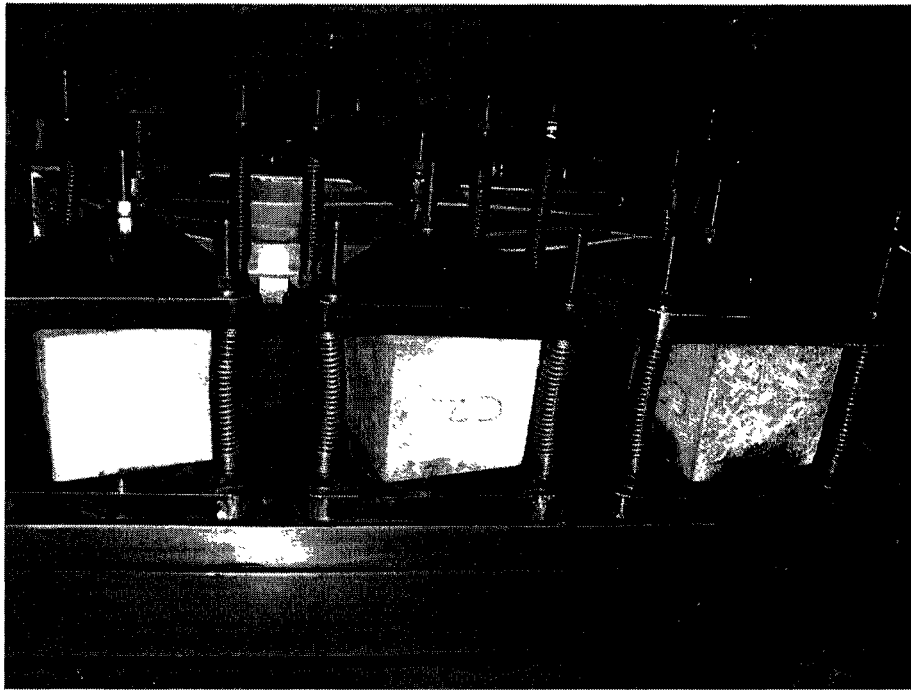


Figure 3.4: Water Permeability Specimens in the Test Cells Assembly

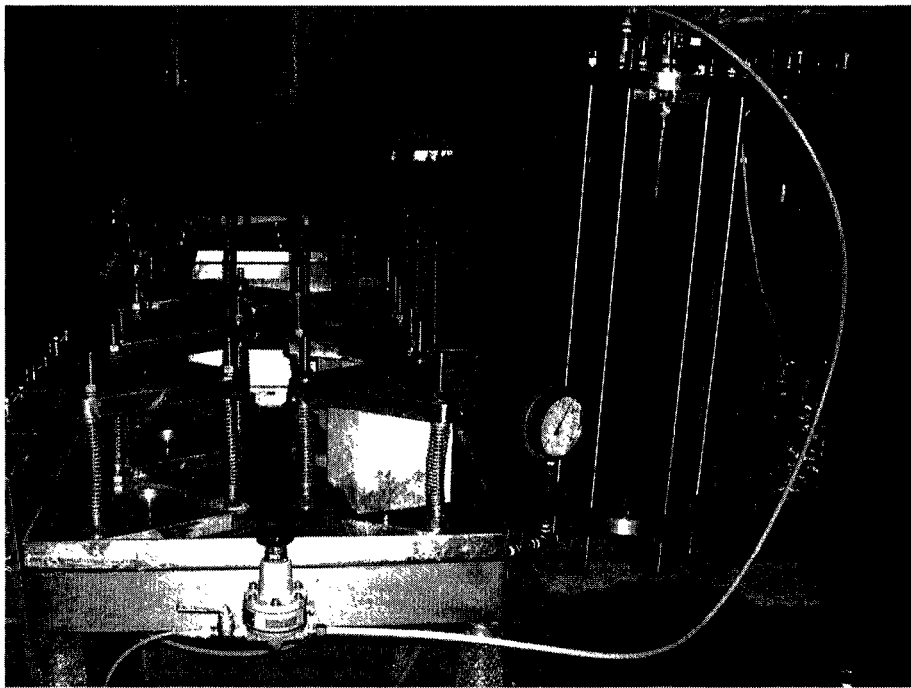


Figure 3.5: Water Tank, Valve & Pressure Meter Arrangement for Permeability Test

The specimens were then removed from the cells, surface dried and split in half perpendicular to the injected surface [Figure 3.6]. The maximum depth of penetration of water was then measured on the two halves of the split specimen [Figure 3.7] by means of a Vernier Caliper and average taken. This gives an idea of water permeability of concrete in terms of depth of penetration.

### **3.9 Procedure for Drying Tests**

Drying tests were carried out on a series of sealed specimens, allowing only unidirectional moisture diffusion for computing moisture diffusivity of the selected concrete mixes & repair mortars under varying exposure temperature and wind speed.

#### **3.9.1 Specimen Preparation**

Specimens after removal from curing tanks at 7 days were placed under wet burlap, after cleaning the edges, to prevent any loss of moisture. After that four faces of the specimens along thickness were coated with high temperature silicone followed by one layer of good quality self-adhesive aluminium tapes to seal them completely against any moisture movement. Sealing of a single specimen was completed within 2-3 minutes and all the specimens were again kept under wet burlap. Each specimen was then weighed and transferred into the respective environmental chamber for drying test to proceed [Figure 3.8, 3.9].

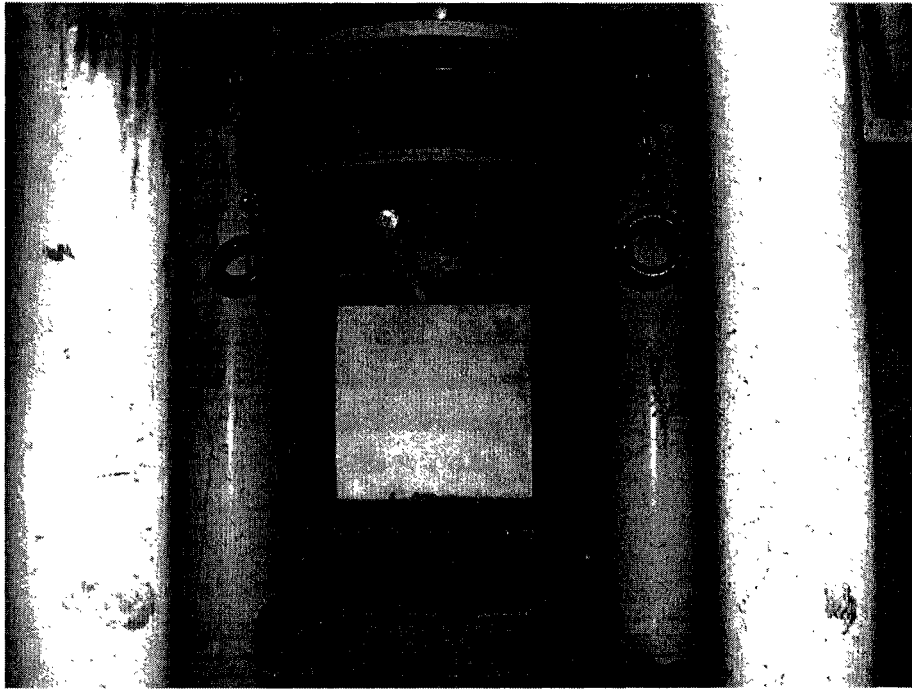


Figure 3.6: Splitting Arrangement for Water Permeability Specimens

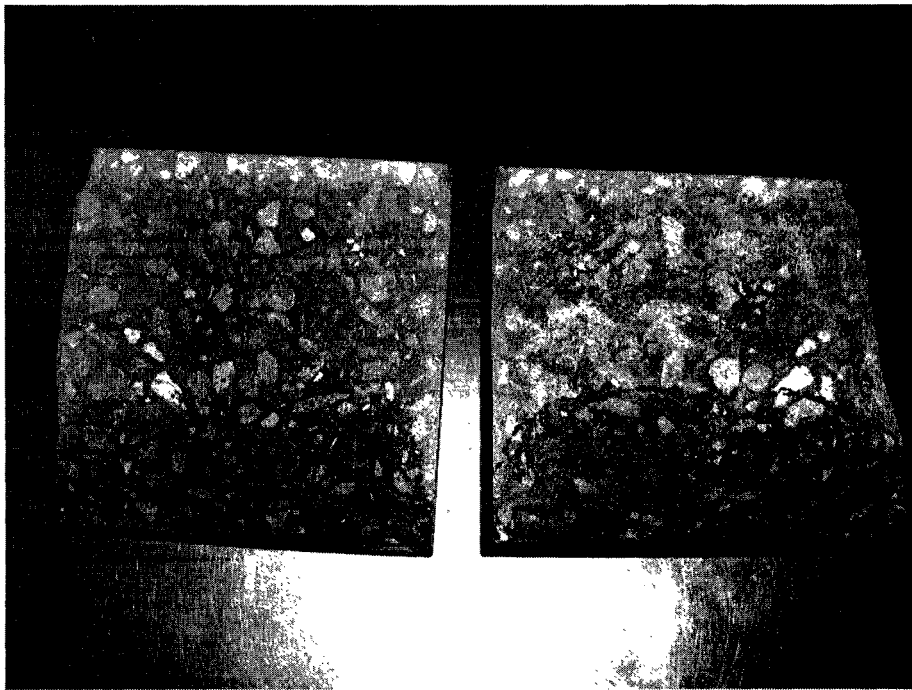


Figure 3.7: Split Permeability Specimen showing Depth of Water Penetration

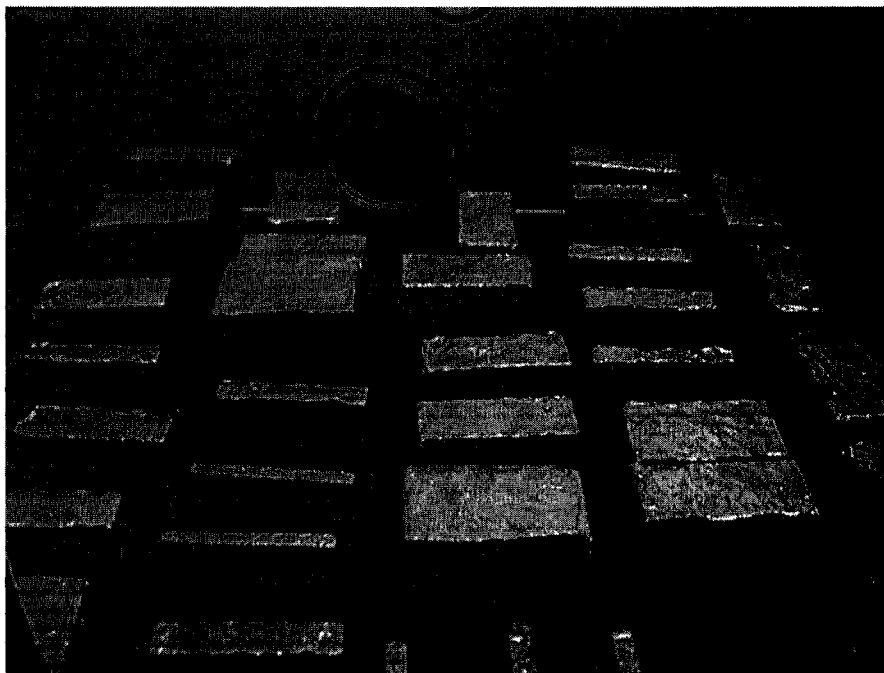


Figure 3.8: Sealed Diffusivity Specimens of Repair in Pyrex Chamber

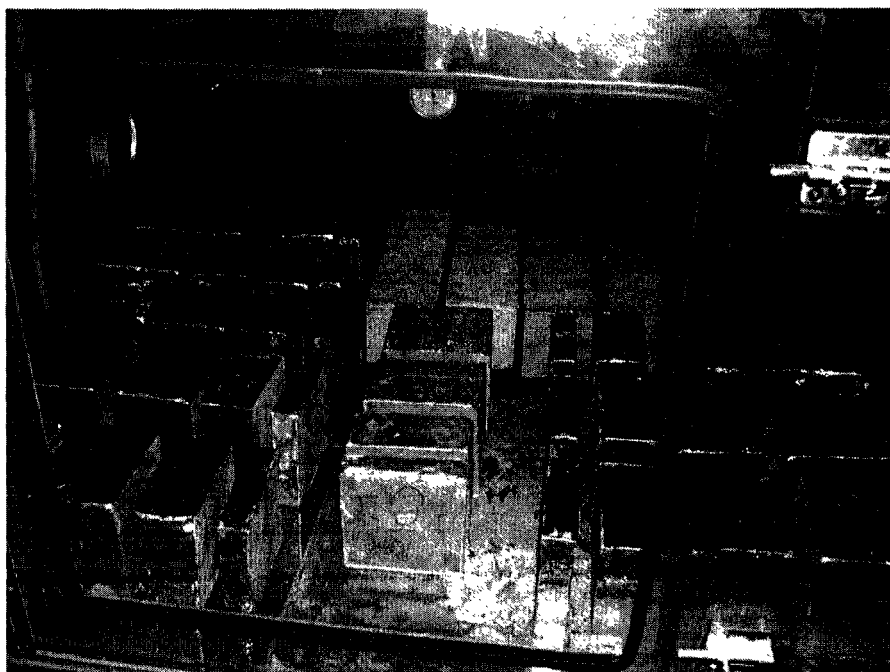


Figure 3.9: Sealed Diffusivity Specimens of Concrete in Pyrex Chamber

### 3.9.2 Environmental Chambers

Two environmental chambers were already available in the laboratories equipped with temperature and humidity controls. One of the chambers was made of pyrex glass with all the controls mounted onto the chamber itself. Temperature was controlled in this chamber, within  $\pm 2^{\circ}\text{C}$ , by means of a fan heater with a built in thermostat placed in a separate compartment of the chamber and measured by means of a wall mounted electronic digital thermometer with its probe within the main chamber area. Humidity was generated in the chamber by means of a room humidifier with distilled water filled in manually, placed in the separate compartment and controlled within  $\pm 4\%$  by an automatic humidity control with built in sensor, attached to the walls of the main chamber. Humidity was measured by means of a wall mounted humidity meter. A fan fixed to the compartment wall was used to transfer the humidity fumes and hot wind from fan heater into the main chamber. An access window was used for transferring specimens into and out of the chamber. This chamber did not have any provision for wind control and its appliances were also very old [Figure 3.10].

The other chamber made of steel had the controls built in a separate unit and a wind source in terms of a solitary fan fixed to the chamber ceiling with little wind speed range up to 10-15 Km/hr [Figure 3.11, 3.12]. Temperature was automatically controlled in this chamber from the separate unit and displayed on a digital wall mounted thermometer with its sensor placed inside the chamber. Temperature variation was maintained at  $\pm 1^{\circ}\text{C}$ . Humidity was automatically controlled by means of humidity unit attached to the back of the chamber and working on the principle of blowing water vapors through a circulation

system and measured by a humidity meter fixed inside the chamber. Distilled water was automatically taken from an overhead tank for this purpose. However, this overhead tank was filled manually from a water reservoir on the ground by means of an electric motor. Humidity variation in this chamber was within  $\pm 2$  %. An access door was located at the front of the chamber for transferring the specimens.

Both of these chambers were used in their existing form for testing the repair materials. However, they were upgraded and re-calibrated for testing concrete specimens, because of the high wind speed requirement. In the steel chamber a new set up for generating very high wind speeds up to 30 Km/hr was made and installed on the chamber roof. It consisted of an electric motor, a shaft taken into the chamber and a fan blade attached to the shaft bottom. The shaft is rotated through a pulley and belt system, it rotates the fan blade which generates wind inside the chamber. Wind speed could be controlled either by changing the pulley system (diameter of pulleys) or using the regulator attached. Motor was kept cool during operation by means of a small fan built into the assembly [Figure 3.13, 3.14].

Pyrex chamber was completely overhauled. A fan was fixed to its ceiling so as to generate wind speeds up to 15 Km/hr and controlled by means of a regulator fixed outside onto the chamber wall. The old fan heater was removed and a new rod heater was installed in the main chamber below this fan, with its thermostat fixed on the chamber roof. The humidifier was replaced with a new one and a new humidity control unit was also installed, with all the operating system up graded [Figure 3.15].

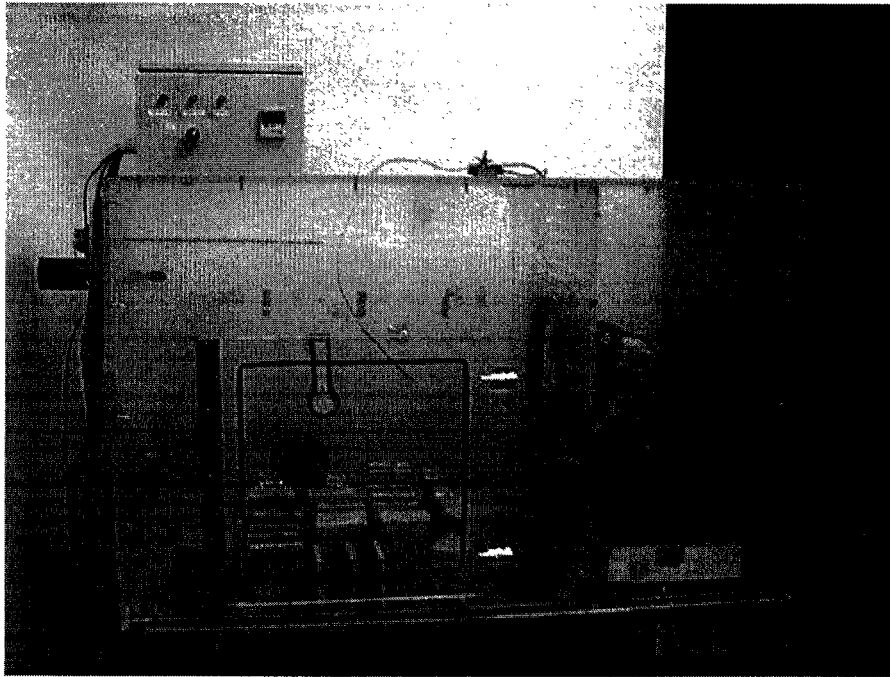


Figure 3.10: Pyrex Glass Environmental Chamber in its Old Form



Figure 3.11: Outside view of the Steel Environmental Chamber & Control Unit (Old)

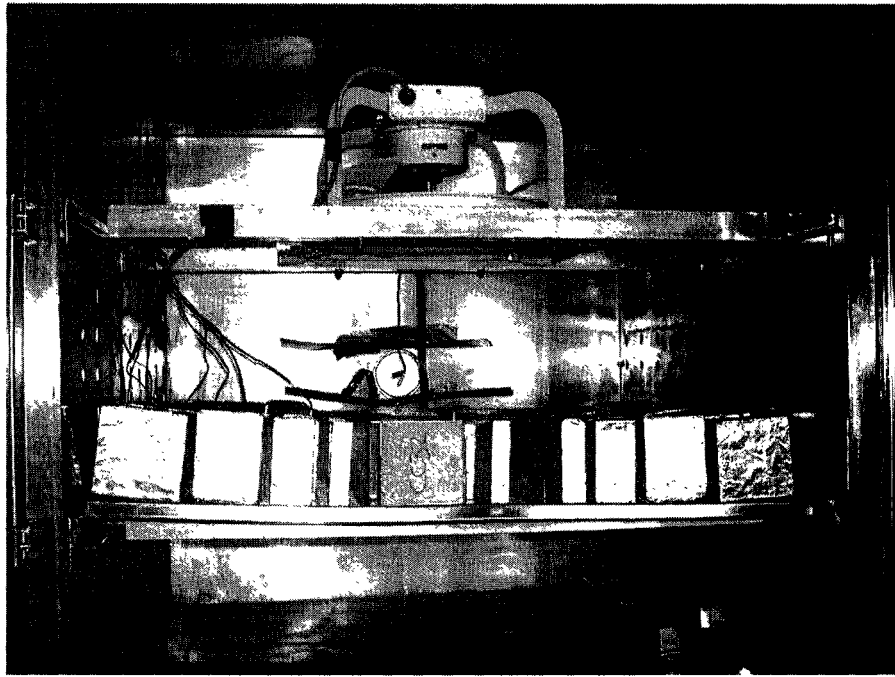


Figure 3.12: Inside view of Old Steel Chamber with Diffusivity Specimens

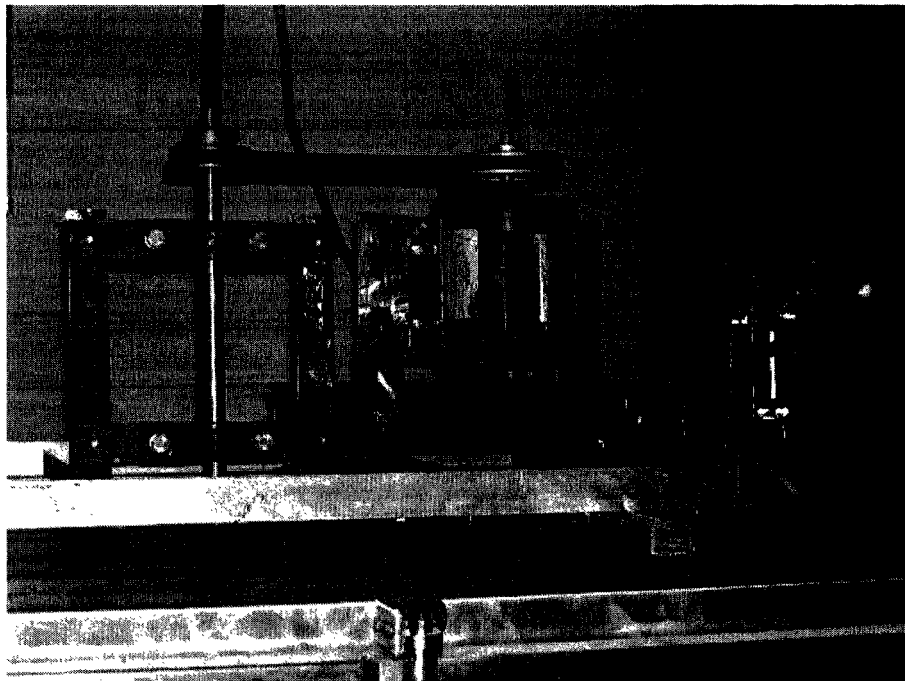


Figure 3.13: Set Up for Generating Very High Wind Speeds in Steel Chamber

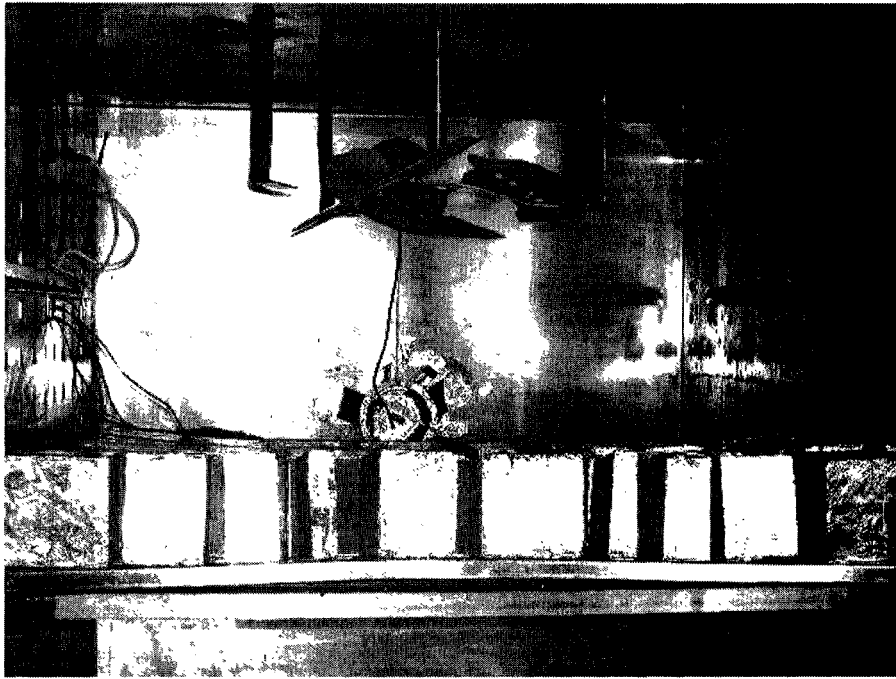


Figure 3.14: Inside View of Up Graded Steel Chamber With Shaft & Fan Blade

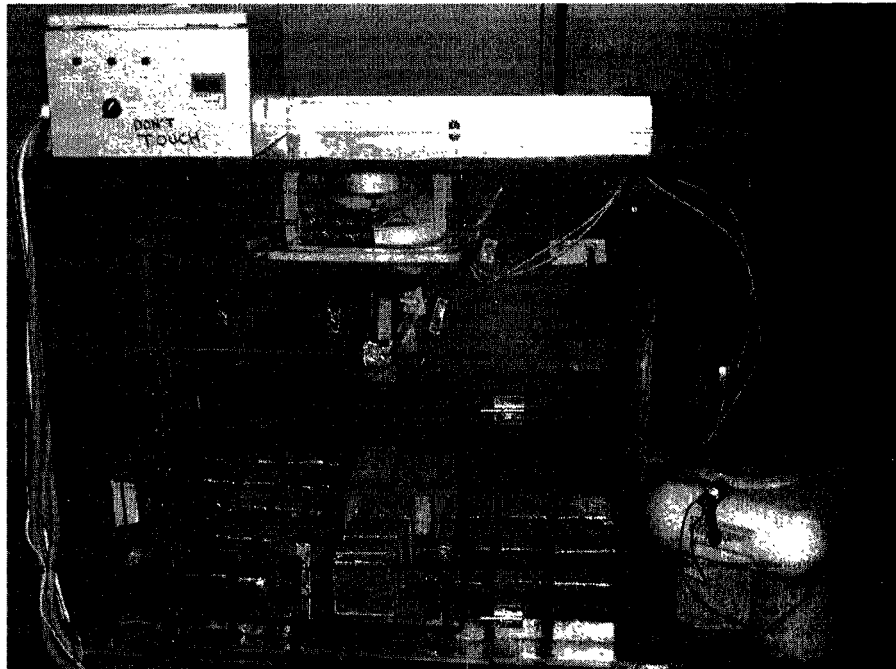


Figure 3.15: Up Graded Pyrex Glass Chamber with Diffusivity & Shrinkage Specimens

### **3.9.3 Weight Loss Measurements**

Specimen weights were taken at regular intervals after placing them in the environmental chambers. In the starting phase readings were taken number of times a day, which was later on reduced to few times a week. The interval of taking readings was governed by the change in weights of the specimens or the amount of moisture being lost, in order to have sufficient data to generate the moisture loss curves properly. Weights were taken using electronic digital weighing balance with an accuracy of 0.01 grams and the same balance was used for all specimens. A glass plate was put on the top of the balance while taking weights in order to avoid any thermal disturbance from the specimen affecting the readings. The weighing operation was completed in a short time and specimens were taken out only in small numbers at a time to preclude the effects of altered environment on the specimens.

### **3.9.4 Testing Regimes**

Drying tests were carried out in two parts. In the first part, tests were performed on the two selected repair mortars FMC1 and FMC2. Testing regime for each of these materials is given in Table 3.3. Each of these tests was continued for a period of 8-12 weeks in the environmental chambers. For the first two regimes, tests were carried out in the pyrex glass chamber operated at different times, whereas for the third regime, steel chamber was used. The exposure conditions were selected so as to generate enough data to investigate the effect of varying wind speed and temperature on moisture transport in these repair mortars, in addition to the comparison among the individual materials at a

particular testing regime. Also several sizes of specimens for the same material at a particular testing regime were used to increase reliability of the results and validate the non-dependence of moisture diffusivity on specimen size.

Table 3.3: Drying Test Regime for FMC1 & FMC2

Relative Humidity (%)	Temperature ( $^{\circ}\text{C}$ )	Wind Speed (km/hr)
60	30	Nil
50	50	Nil
50	50	12

In the second part, tests were carried out on the three concrete mixes of water cement ratio 0.45, 0.5 and 0.6. For each w/c ratio, the testing regime is given in Table 3.4. For all these tests **ambient humidity** was maintained at a constant value of **40%**. Temperatures and wind speeds were selected to be representative of the climatic conditions of the Eastern Province of Saudi Arabia, and enabled to investigate the effect of varying temperature and wind speed on moisture transport in concrete, in addition to the influence of w/c ratio. Testing under this part was further divided into two phases, based upon the exposure temperatures. In each phase both the chambers were operated simultaneously, with the steel chamber reserved for testing under the high wind speed and vice versa. Each chamber was operated for a period of 8-12 weeks to generate enough data for the moisture loss curves to be generated. In this way each chamber was operated only twice for this part of the testing, which minimized the overall time of testing.

Table 3.4: Drying Test Regime for Each Concrete Mix

Serial No.	Temperature ( $^{\circ}\text{C}$ )	Wind Speed (km/hr)
1	35	6
2	35	22
3	50	6
4	50	22

### 3.9.5 Moisture Content Determination

After the completion of a particular drying test, all the specimens were weighed and then placed in an oven to determine the evaporable moisture content, by drying the specimens at  $105 \pm 5^{\circ}\text{C}$ , to draw the moisture loss (%) curves. Specimens were kept in oven until the moisture loss did not exceed 0.1% of their weight over the previously measured weight 24 hours before. Since the specimens were sealed on four sides the above mentioned condition was achieved only after 10-15 days of drying.

### 3.10 Shrinkage Test Procedure

Shrinkage strains were recorded in repair and concrete specimens right after transferring them into the environmental chambers, along with the respective diffusivity/drying test specimens. This would enable to relate shrinkage of concrete to its moisture diffusivity. For repair specimens, embedded TML strain gauges of type PMLS-45 with a gauge length of 40 mm were used, whereas for concrete, embedded TML strain gauges of type PML-60 with a gauge length of 60 mm were used.

To record shrinkage strains, all the gauges were connected to a data logger and extension box. A computer connected to the data logger then recorded the readings automatically. The complete set up is shown in Figure 3.17. Normally at least two specimens were connected for each case to have a check on the readings and also to indicate and overcome malfunctioning of any of the gauges. Strains were recorded at intervals of  $\frac{1}{2}$  hour, 1 hour, 2 hours, 4 hours and ultimately 6 hours until the end of the testing period. This was done to generate enough data to plot the shrinkage strain evolution curves.

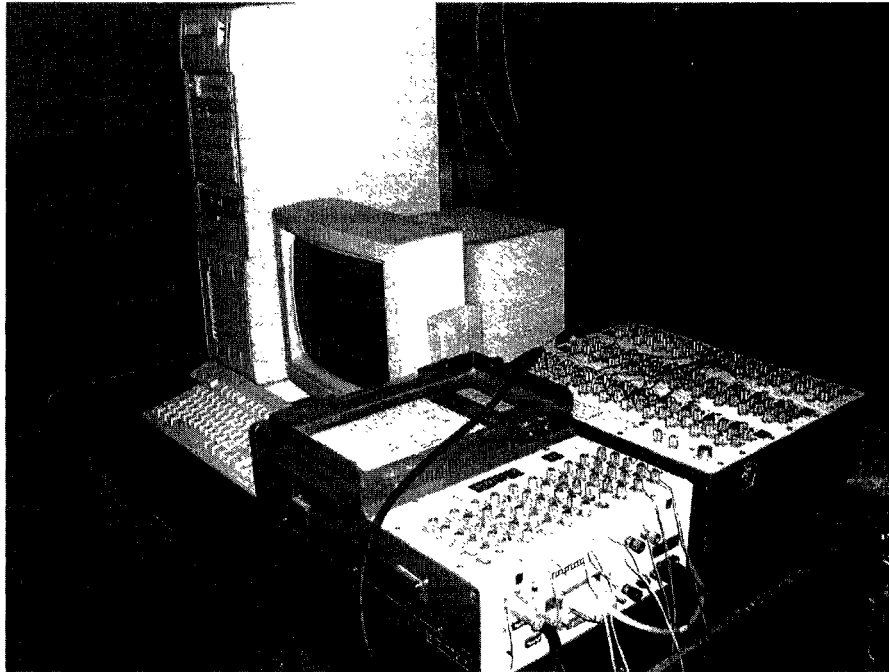


Figure 3.16: Shrinkage Specimens Connected to Data Logger & Computer

## **CHAPTER 4**

# **ANALYSIS AND DISCUSSION OF RESULTS**

### **4.1 Properties of Concrete**

As discussed in chapter 3, the knowledge of certain properties of concrete is important to understand, explain and predict its moisture transport behavior. In this context concrete mixes were tested for the evolution of compressive strength and water permeability.

#### **4.1.1 Evolution of Compressive Strength**

Table 4.1 gives the values of cylinder compressive strength for the three concrete mixes of water-cement ratio 0.45, 0.5 and 0.6, obtained up to an age of 105 days.

Figure 4.1 shows the evolution of compressive strength for each mix, i.e. strength gain with age, and also the comparison of strengths among the mixes at a particular age. It can be seen that with the decrease in water-cement ratio of concrete, the compressive strength increases. For example at 28 days, strength of the mix with w/c 0.45 is 24 % higher than that of w/c 0.5 and 97 % higher than that of w/c 0.6. In fact water-cement ratio determines the porosity of the hardened cement paste at any stage of hydration. The higher the water-cement ratio, the higher is the porosity or volume of voids and the lower

is the compressive strength, which in turn is a function of the volume of voids, all the other mix parameters being same.

Also it can be seen that the compressive strength of each mix increased with the age. The evolution of compressive strength shows that mixes achieved 55-65 % of the 28-day strength at 3 days and 70-80 % of the 28-day strength at 7 days. Only 10-20 % increase in strength was observed after 28 days up to an age of 105 days. This follows the progress of hydration of cement with the age. At 28 days most of the hydration products have been formed so after that the rate of strength gain becomes slower.

The evolution of concrete compressive strength can be predicted using ACI strength evolution equation [141], which is given as

$$f_c'(t) = \frac{t}{(a + bt)} \quad (4.1)$$

The regression coefficients 'a' (days/MPa) and 'b' (1/MPa) for these mixes are however different. The values of these regression coefficients and coefficient of determination  $R^2$  are given in Table 4.2. The regression coefficients have higher values for the higher water-cement ratios to make the compressive strength values smaller. In all the cases  $R^2$  values are higher than 98 %.

Table 4.1: Compressive Strength of Concrete

WATER CEMENT RATIO	COMPRESSIVE STRENGTH (MPa)					
	0 DAYS	3 DAYS	7 DAYS	28 DAYS	60 DAYS	105 DAYS
0.45	0	28.77	33.31	42.33	45.52	47.38
0.5	0	19.37	23.47	34.52	36.76	40.13
0.6	0	12.87	15.56	21.14	23.14	25.76

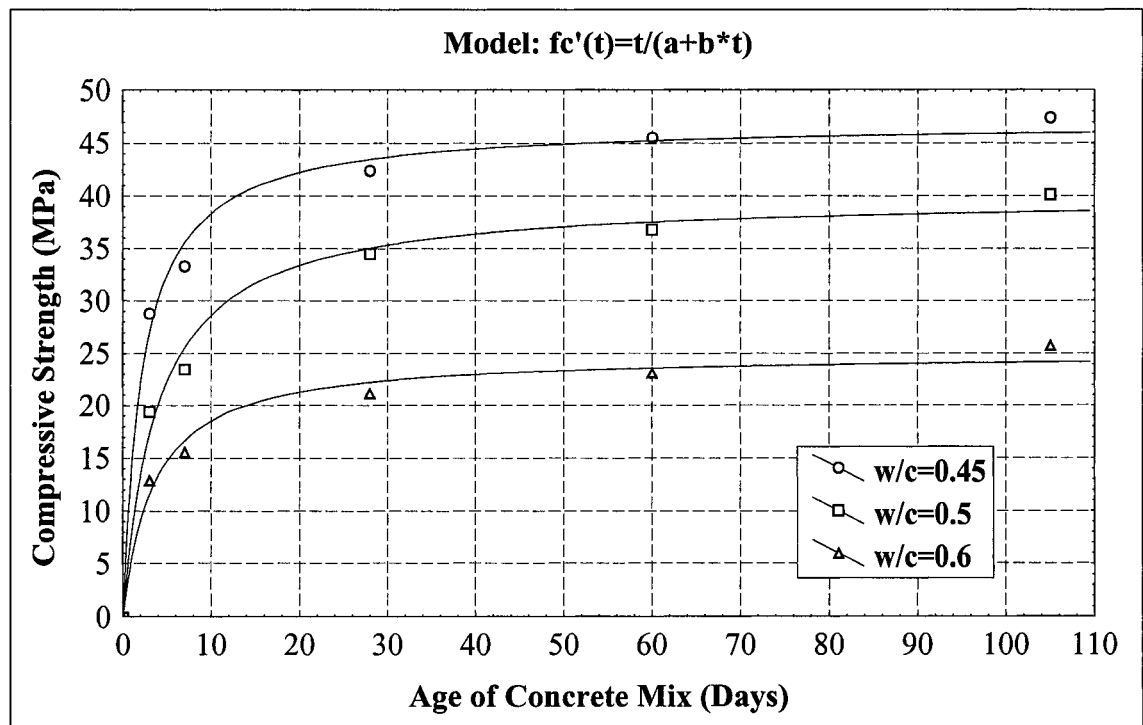


Figure 4.1: Evolution of Compressive Strength of Concrete

Table 4.2: Regression Coefficients for ACI Compressive Strength Evolution Equation

WATER CEMENT RATIO	a	b	R <sup>2</sup>
0.45	0.04749	0.021319	99.228 %
0.5	0.09888	0.025018	98.904 %
0.6	0.13963	0.040030	98.434 %

#### 4.1.2 Water Permeability

As mentioned in section 3.8, water permeability of concrete was measured following DIN 1048 standard specifications, in terms of depth of penetration of waterfront.

Figure 4.2 shows comparison among the mixes for water penetration depth 'e'. It can be seen that at higher water cement ratio, the penetration depth is higher. Thus the mix with water-cement ratio of 0.6 gives an average value of 60 mm, which is 54 % higher than that with water-cement ratio 0.5 and 75 % higher than that with water-cement ratio of 0.45. This is attributed to the fact that at higher water-cement ratio the hydrated cement paste tends to become more porous and water in excess of what is required for hydration of cement tends to create zones of low-density porous paste in the matrix, especially at or near the interfacial zone.

Figure 4.3 shows the regressed relationship between concrete compressive strength at 28 days and water permeability in terms of water penetration depth. The  $R^2$  value is above 97 %. This relationship can be used to predict water permeability of an ordinary concrete mix, given its compressive strength at 28 days. Hence it enables to avoid the sophisticated lab set up required for this test.

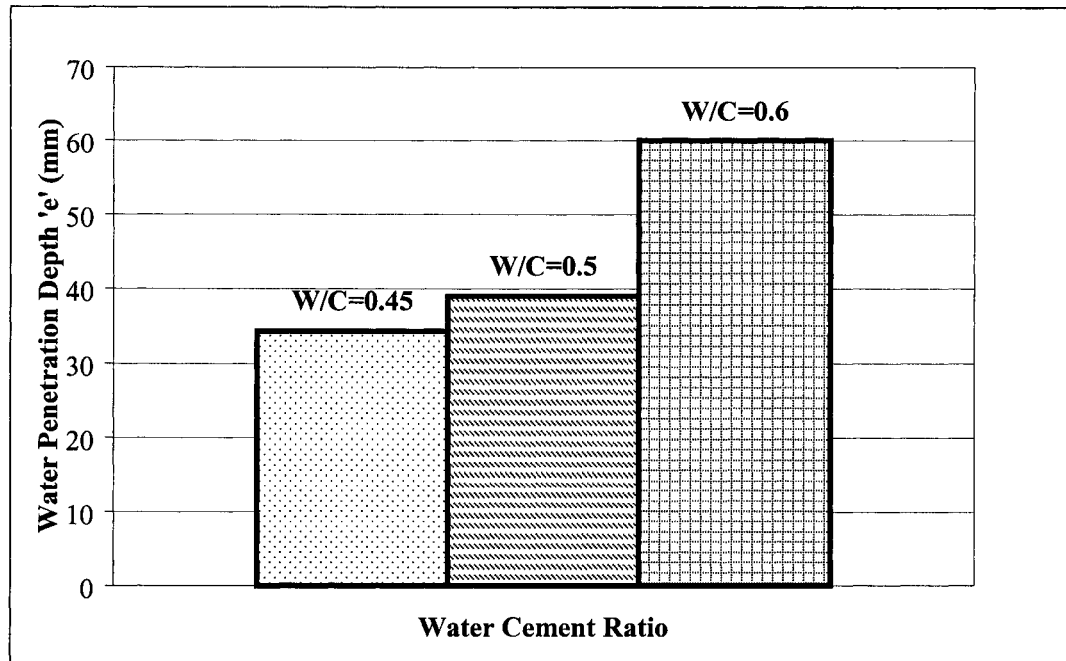


Figure 4.2: Comparison of Water Permeability of Concrete Mixes

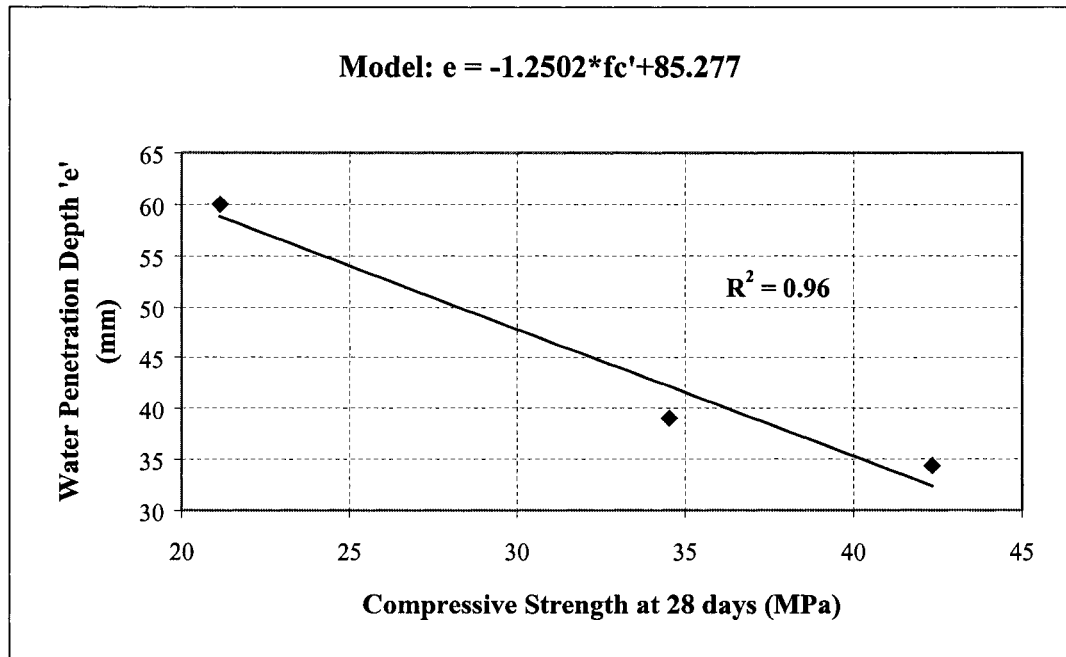


Figure 4.3: Relationship b/w Concrete Compressive Strength at 28 days and Water Penetration Depth

## **4.2 Drying tests for Moisture Diffusivity**

Drying tests were carried out on sealed specimens of selected concrete mixes and repair materials allowing unidirectional movement of moisture, under specified exposure conditions in the environmental chambers, to generate moisture profiles in terms of moisture loss in percentage for numerical computation of corresponding values of coefficient of moisture diffusivity ( $D$ ) and convective transfer coefficient ( $h_f$ ). Results of these tests are presented and discussed in the following sections.

### **4.2.1 Moisture Loss in Concrete**

Drying tests were conducted on concrete mixes, water-cement ratio 0.45, 0.5 and 0.6, specimen size of 100x100xB ( $B = 25, 50, 75, 100$  mm), under varying temperature & wind speed as given in Table 3.4. Effect of these factors on moisture loss in concrete is described in the following sub-sections.

#### **4.2.1.1 Effect of Water-Cement Ratio**

Under this section the results within each testing regime/chamber setup are covered. At an ambient temperature of  $50^{\circ}\text{C}$  and wind speed of  $6\text{ km/hr}$ , Figure 4.4 shows the effect of water-cement ratio on moisture loss in percentage for the specimen thickness of 25 mm. It can be seen that during the first 1-2 days moisture loss is almost similar for all the mixes but diverged later on. Moisture loss stopped after about 40 days of exposure in all the cases, being shown by the flattened curves. Specimens of mix with

water-cement ratio of 0.45 lost about 60 %, whereas 0.5 lost 62 % and 0.6 lost 64 % of the evaporable moisture in total.

Figure 4.5 shows similar comparison for 50 mm specimen. Moisture loss became constant after about 80 days of exposure in this case. Specimens of mix with water-cement ratio of 0.45 lost about 58 % of the evaporable moisture, while 0.5 lost 61 % and 0.6 lost 63 % in total.

Figure 4.6 shows the comparison for 75 mm specimen under similar conditions. It can be seen that during the first 2-3 days the curves are almost merged together, however, they diverge later on. Moisture loss in specimens of water-cement ratio of 0.45 is 41 % at 28 days of exposure while in 0.5 it is 44 % and in 0.6 it is about 46 %. Figure 4.7 shows similar comparison for specimen thickness of 100 mm. Specimens with water-cement ratio of 0.45 lost 35 %, 0.5 also lost 35 % and 0.6 lost 38 % of the total evaporable moisture at 28 days. The moisture loss did not stop in this case and would have required much higher time of exposure to do so, owing to the very high specimen thickness, increased moisture content and longer path for diffusion.

In all of the above cases it is evident that moisture loss increases with the increase in water-cement ratio. This can be attributed to the fact that at higher water-cement ratio porosity of the hydrated cement paste and interfacial zone increases and tortuosity of the diffusion paths tends to decrease, which enables the moisture to diffuse easily.

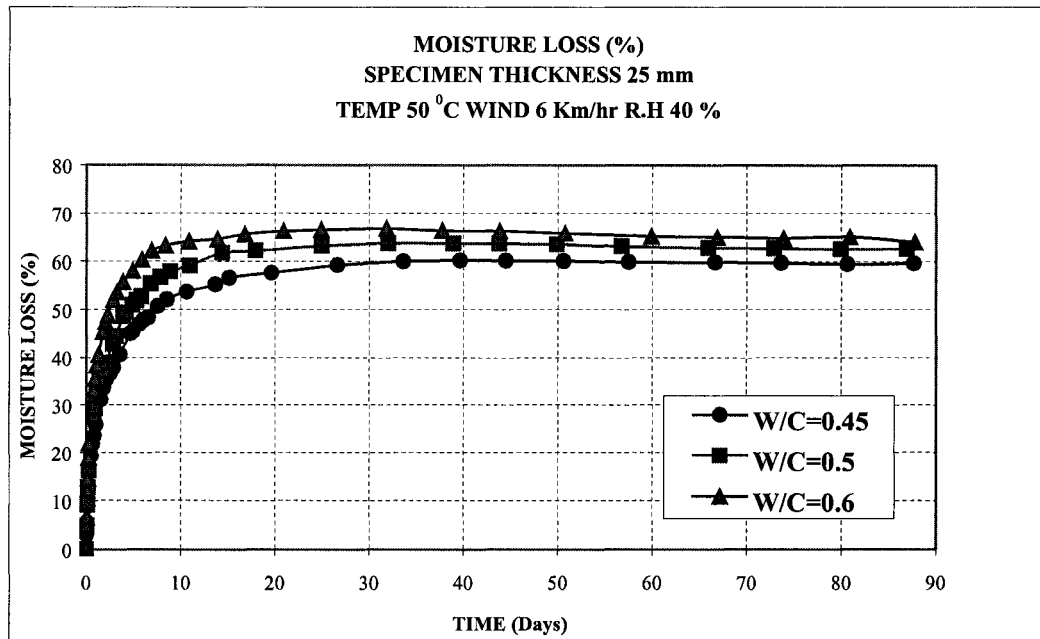


Figure 4.4: Effect of W/C Ratio on Moisture Loss (%) for 25 mm Specimen  
 at 50 °C and 6 km/hr Wind

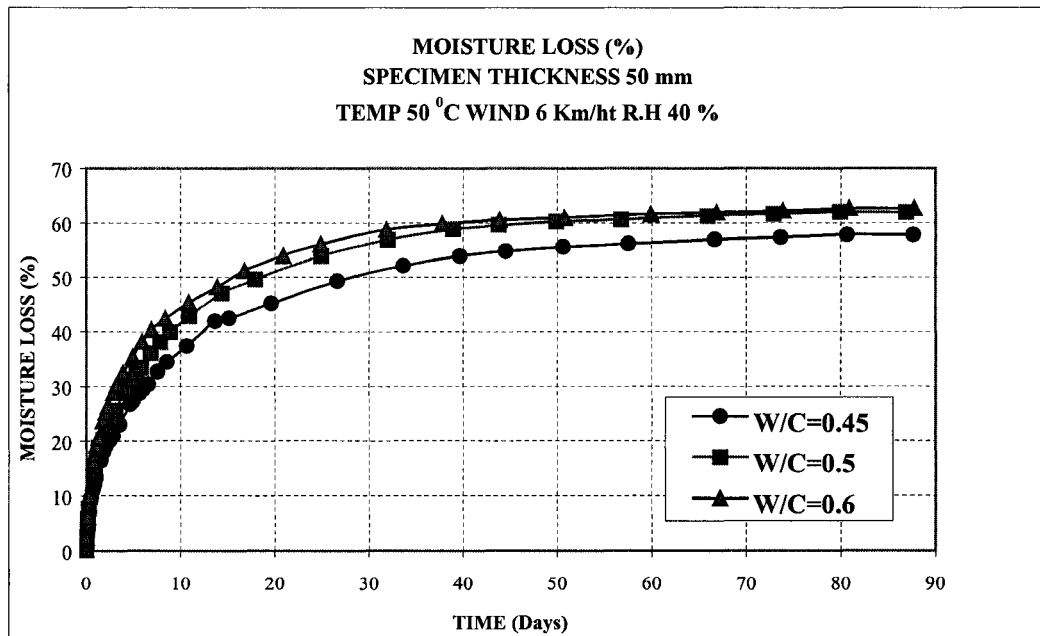


Figure 4.5: Effect of W/C Ratio on Moisture Loss (%) for 50 mm Specimen  
 at 50 °C and 6 km/hr Wind

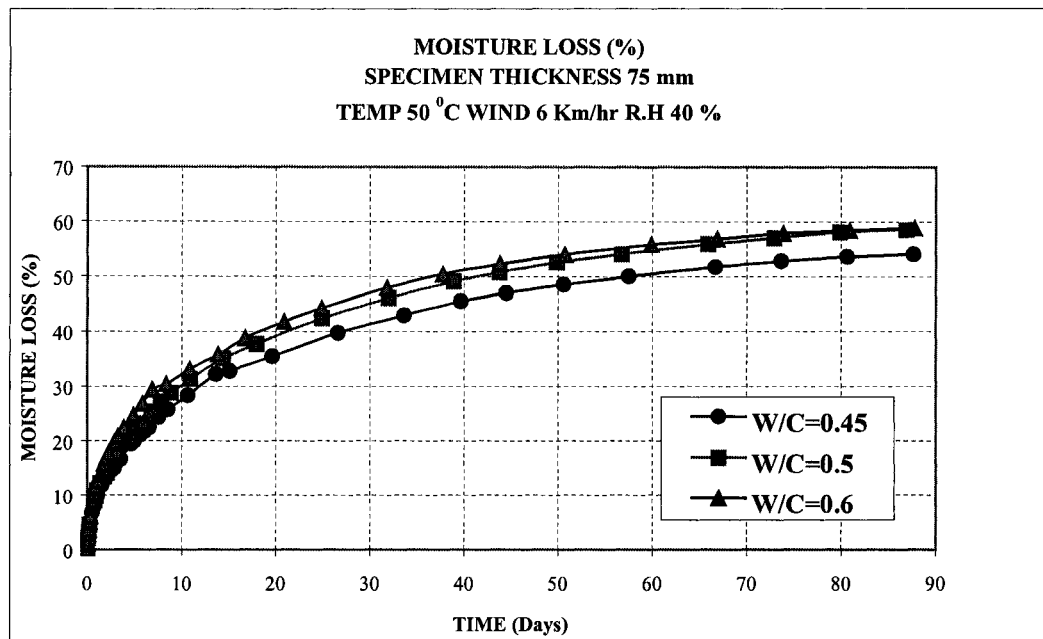


Figure 4.6: Effect of W/C Ratio on Moisture Loss (%) for 75 mm Specimen  
 at 50 °C and 6 km/hr Wind

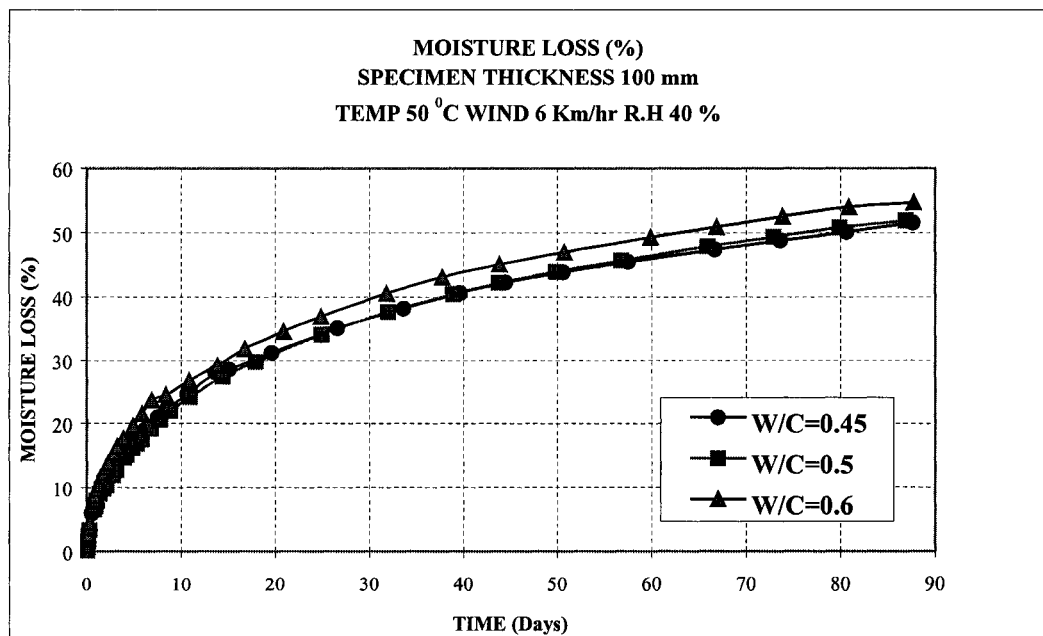


Figure 4.7: Effect of W/C Ratio on Moisture Loss (%) for 100 mm Specimen  
 at 50 °C and 6 km/hr Wind

At an ambient temperature of  $50^{\circ}\text{C}$  and wind speed of **22 km/hr**, Figure 4.8 shows the effect of water-cement ratio on moisture loss in percentage for the specimen thickness of 25 mm. After about 50 days of exposure the curves flatten out indicating that specimens have lost all of their evaporable moisture by that time. Specimens of the mix with water-cement ratio of 0.45 lost 65 %, while that of 0.5 lost 66 % and that of 0.6 lost 69 % of the evaporable moisture in total.

Figure 4.9 shows similar comparison for 50 mm thick specimens. In this case, moisture loss stopped after about 70 days of exposure. Specimens of water-cement ratio of 0.45 lost 63 % of the total evaporable moisture, whereas that of 0.5 lost 65 % and that of 0.6 lost 68 %.

Figure 4.10 shows comparison for moisture loss in percentage under similar exposure conditions, for the 75 mm thick specimens. 45 % of the total evaporable moisture was lost by specimens of water-cement ratio of 0.45 after 28 days of exposure, whereas, 46 % and 51 % respectively by the 0.5 and 0.6 mix specimens. Figure 4.11 shows similar comparison for the specimen thickness of 100 mm. Specimen with water-cement ratio of 0.45 lost about 37 % of the total evaporable moisture, while that of 0.5 lost 38 % and that of 0.6 lost 41 %.

Again the important thing to be noted was the increase in moisture loss with the increase in water-cement ratio, for all the cases. In some of the above-mentioned cases moisture loss is observed to be slightly higher than 60 %, which is theoretically not possible when the chamber humidity is 40 %. This can be attributed to the fact that humidity was measured only at one particular point within the chamber throughout the test and there may be some slight variations at other points.

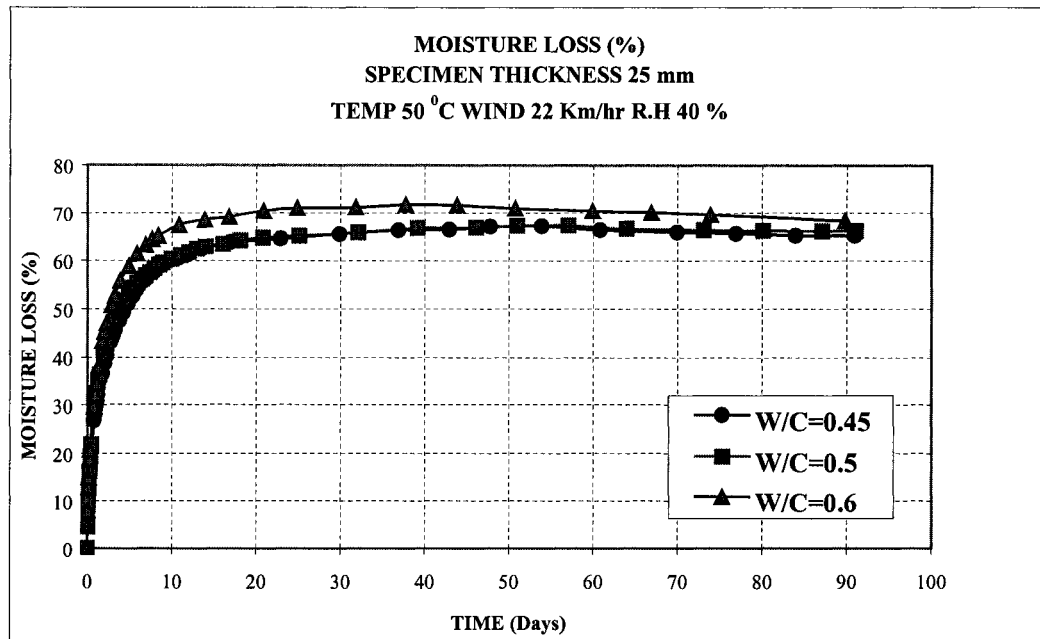


Figure 4.8: Effect of W/C Ratio on Moisture Loss (%) for 25 mm Specimen  
 at 50 °C and 22 km/hr Wind

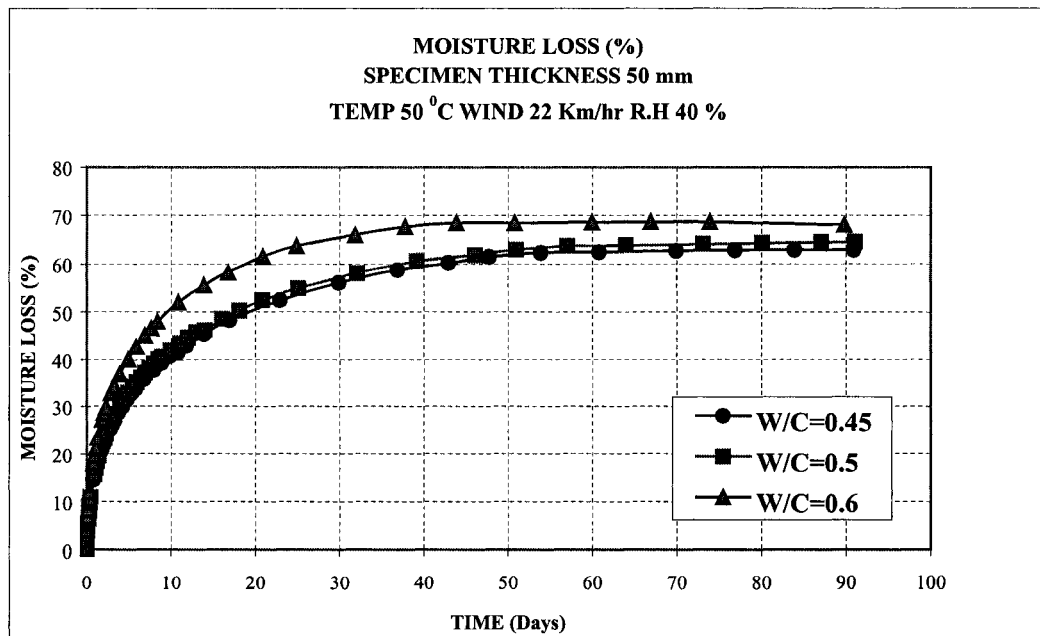


Figure 4.9: Effect of W/C Ratio on Moisture Loss (%) for 50 mm Specimen  
 at 50 °C and 22 km/hr Wind

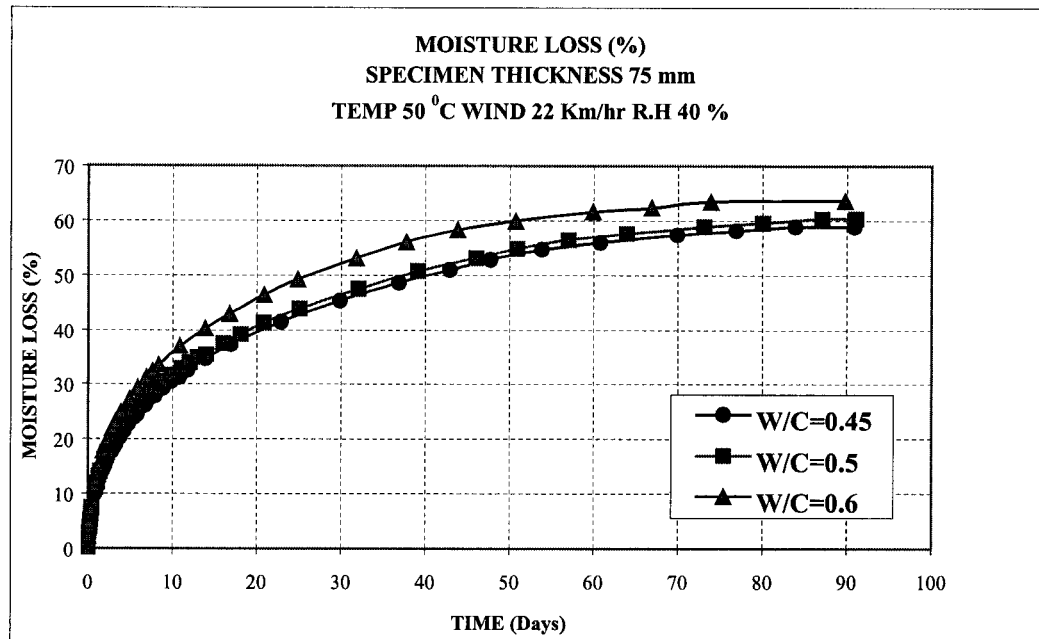


Figure 4.10: Effect of W/C Ratio on Moisture Loss (%) for 75 mm Specimen  
 at 50 °C and 22 km/hr Wind

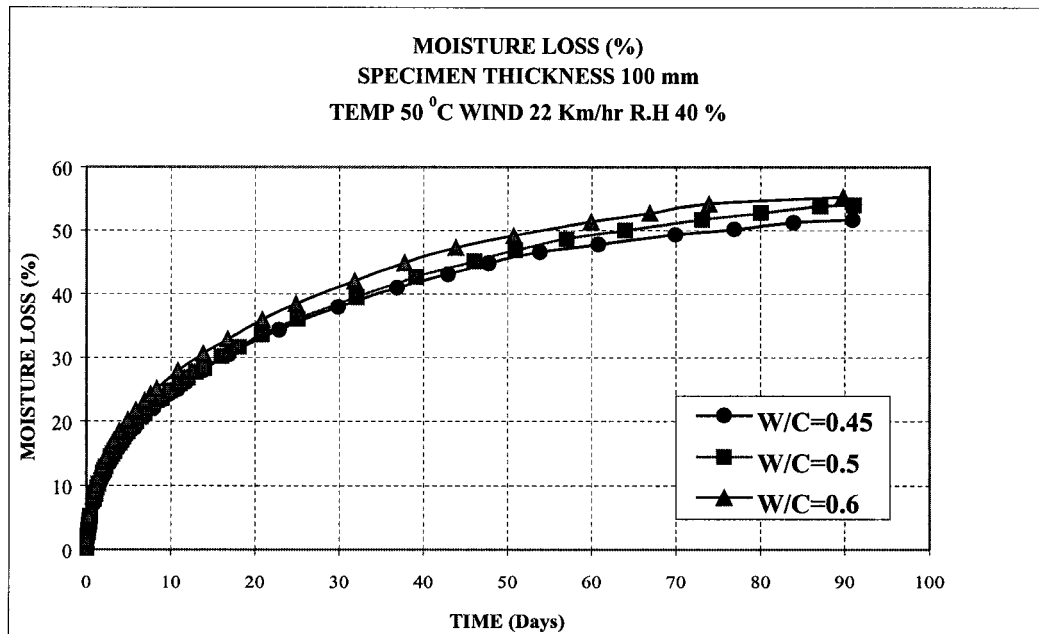


Figure 4.11: Effect of W/C Ratio on Moisture Loss (%) for 100 mm Specimen  
 at 50 °C and 22 km/hr Wind

At an ambient temperature of  $35^{\circ}\text{C}$  and wind speed of **6 km/hr**, Figure 4.12 shows the effect of water-cement ratio on moisture loss in percentage for specimen thickness of 25 mm. Specimens of the mix with water-cement ratio of 0.45 lost 43 % of the total evaporable moisture while that of 0.5 lost 51 % and that of 0.6 lost about 52 % at the end of the test.

Figure 4.13 shows similar comparison for 50 mm thick specimens. It can be seen that the moisture loss was still continuing even towards the end of the test and it would have required a higher time of exposure to drive out the whole evaporable moisture under these conditions. In this case specimens of water-cement ratio 0.45 lost 35 %, whereas that of 0.5 lost 43 % and that of 0.6 lost 50 % of evaporable moisture.

Figure 4.14 shows the comparison under similar exposure conditions, for 75 mm thick specimens. 23 % of the total evaporable moisture was lost by the specimens of water-cement ratio 0.45 after 28 days of exposure, whereas, 28 % and 33 % respectively by the specimens of 0.5 and 0.6 w/c ratio. Figure 4.15 shows similar comparison for the specimen thickness of 100 mm. Moisture loss in specimens with water-cement ratio of 0.45 was about 17 %, while in that of 0.5 it was 23 % and it was found to be 27 % in that of 0.6.

Next we discuss the effect of water-cement ratio on moisture loss in percentage at an ambient temperature of  $35^{\circ}\text{C}$  and wind speed of **22 km/hr**. Figure 4.16 shows the moisture loss curves for specimen thickness of 25 mm. At the end of the test, specimens of the mix with water-cement ratio of 0.45 had lost 54 % of the total evaporable moisture while that of 0.5 lost 61 % and that of 0.6 about 67 %.

Figure 4.17 shows similar comparison for 50 mm thick specimens. In this case the specimens of w/c ratio of 0.45 lost 44 % of moisture, whereas that of 0.5 lost 54 % and that of 0.6 lost 59 %.

Figure 4.18 shows the comparison for specimen thickness of 75 mm. 28 % of the total evaporable moisture was lost by the specimens of water-cement ratio 0.45 after 28 days of exposure, whereas, 35 % and 37 % respectively by that of 0.5 and 0.6 mix. Figure 4.19 shows similar comparison for the specimen thickness of 100 mm. Moisture loss in specimens with water-cement ratio of 0.45 was found to be 23 %, while in that of 0.5 it was 27 % and in that of 0.6 about 31 %.

Again in all of these cases the acceleration of moisture loss with the increase in water-cement ratio of concrete is evident, the reasons been discussed earlier.

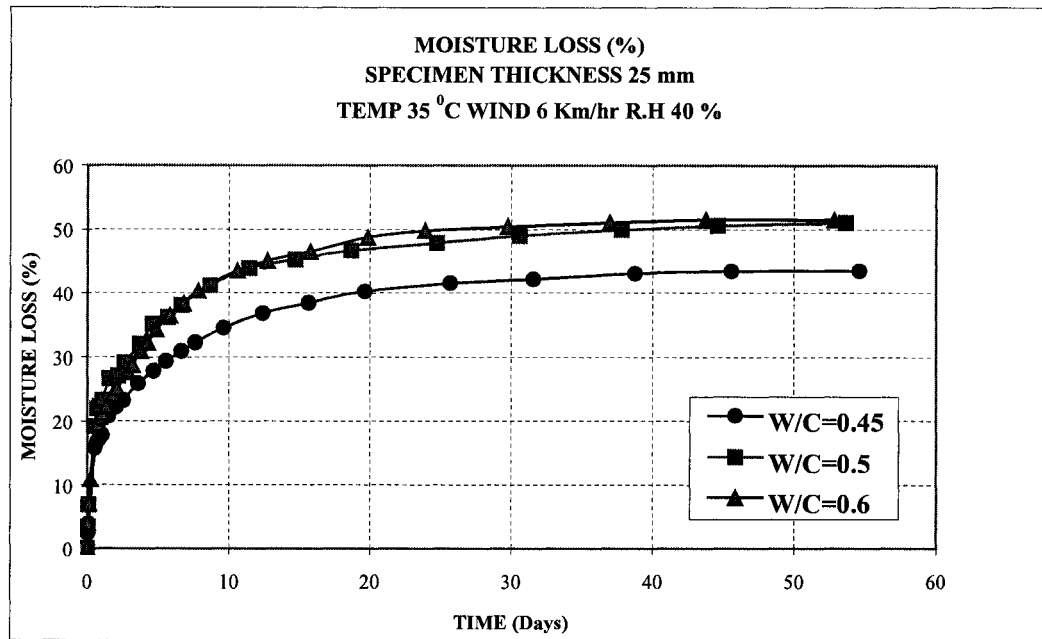


Figure 4.12: Effect of W/C Ratio on Moisture Loss (%) for 25 mm Specimen  
 at 35 °C and 6 km/hr Wind

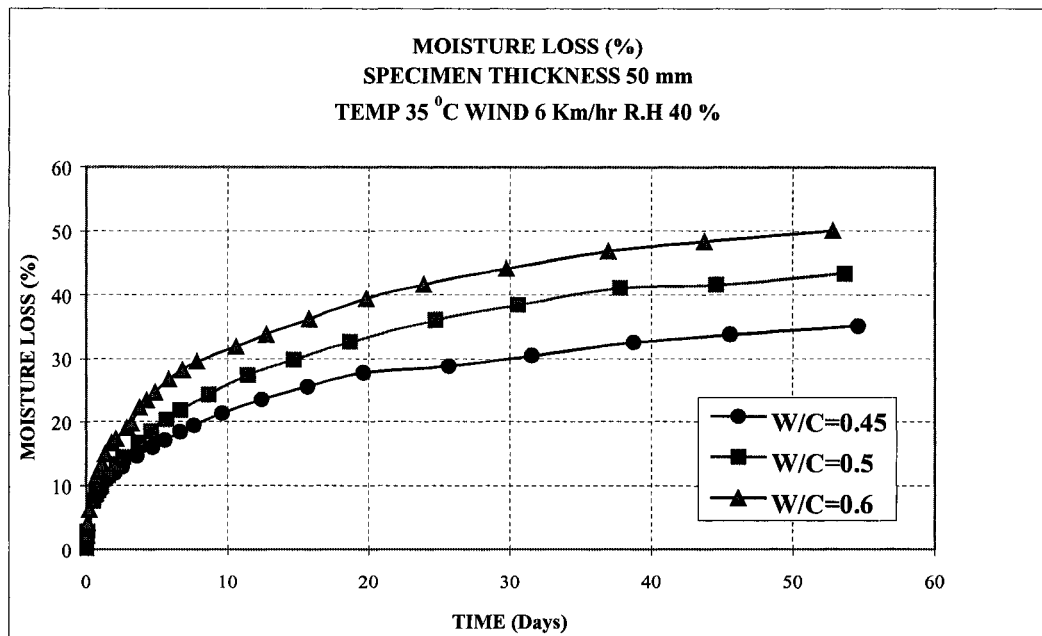


Figure 4.13: Effect of W/C Ratio on Moisture Loss (%) for 50 mm Specimen  
 at 35 °C and 6 km/hr Wind

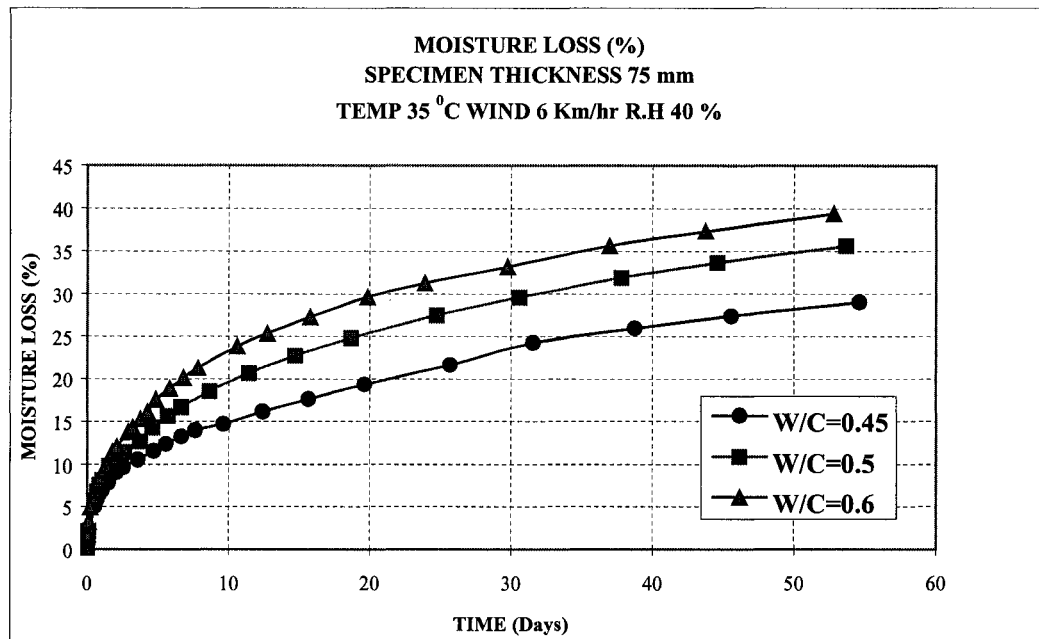


Figure 4.14: Effect of W/C Ratio on Moisture Loss (%) for 75 mm Specimen  
 at 35 °C and 6 km/hr Wind

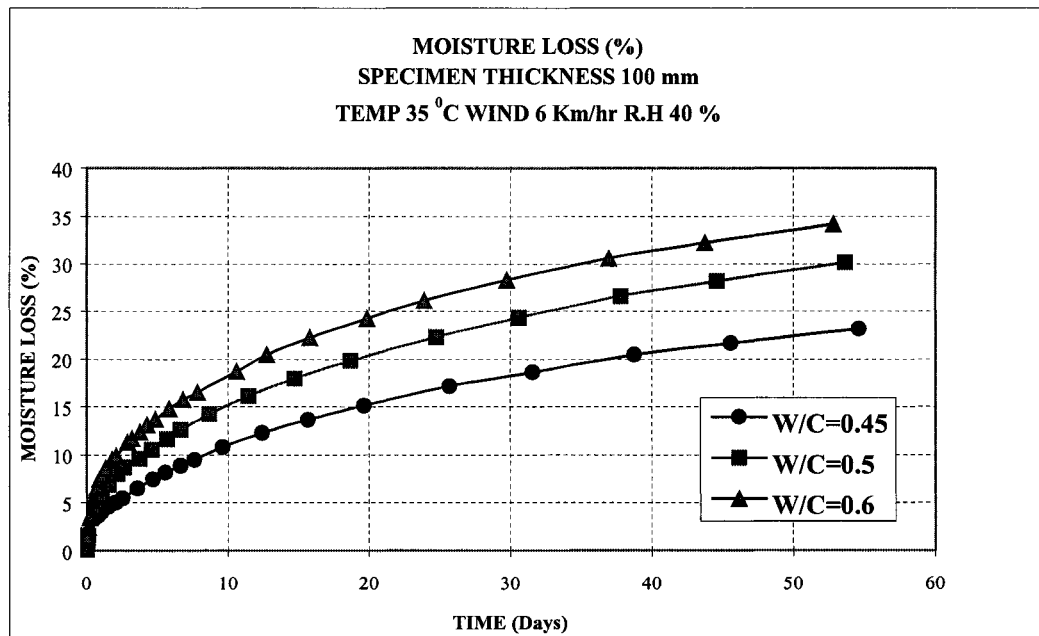


Figure 4.15: Effect of W/C Ratio on Moisture Loss (%) for 100 mm Specimen  
 at 35 °C and 6 km/hr Wind

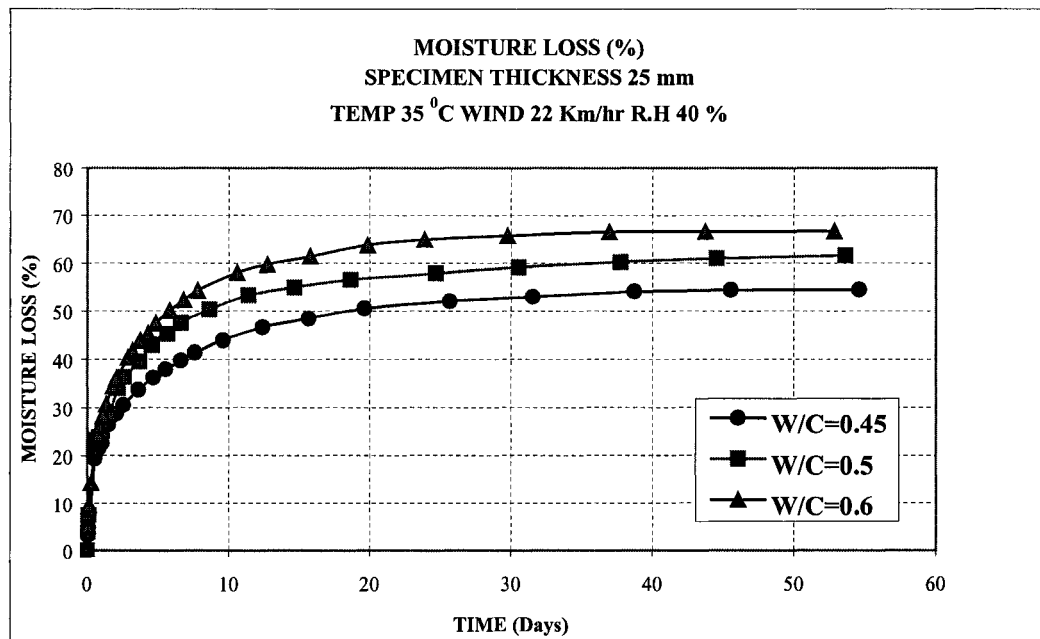


Figure 4.16: Effect of W/C Ratio on Moisture Loss (%) for 25 mm Specimen  
 at 35 °C and 22 km/hr Wind

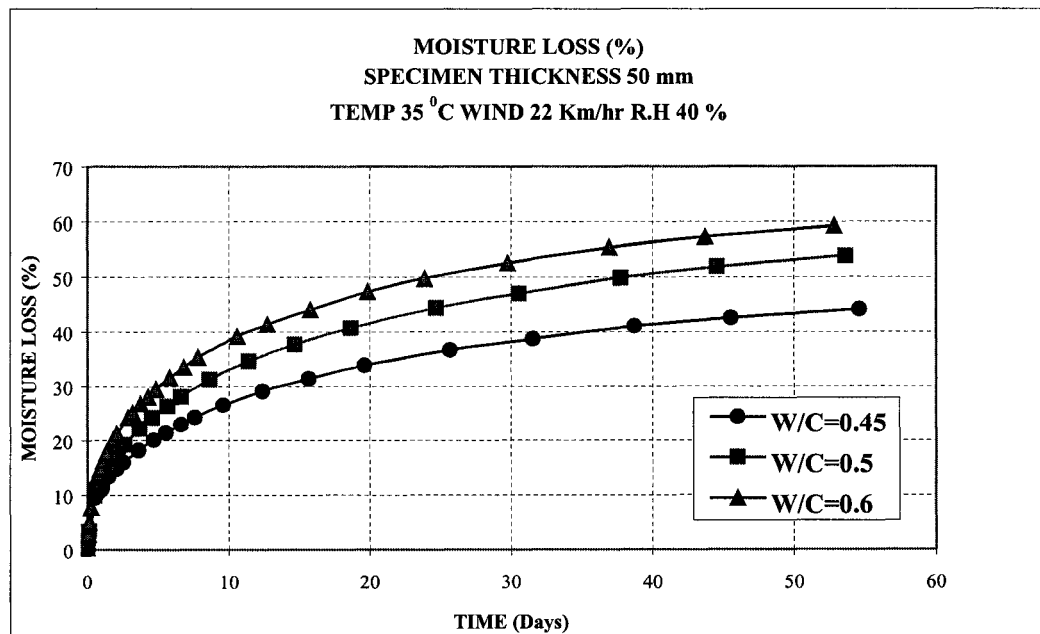


Figure 4.17: Effect of W/C Ratio on Moisture Loss (%) for 50 mm Specimen  
 at 35 °C and 22 km/hr Wind

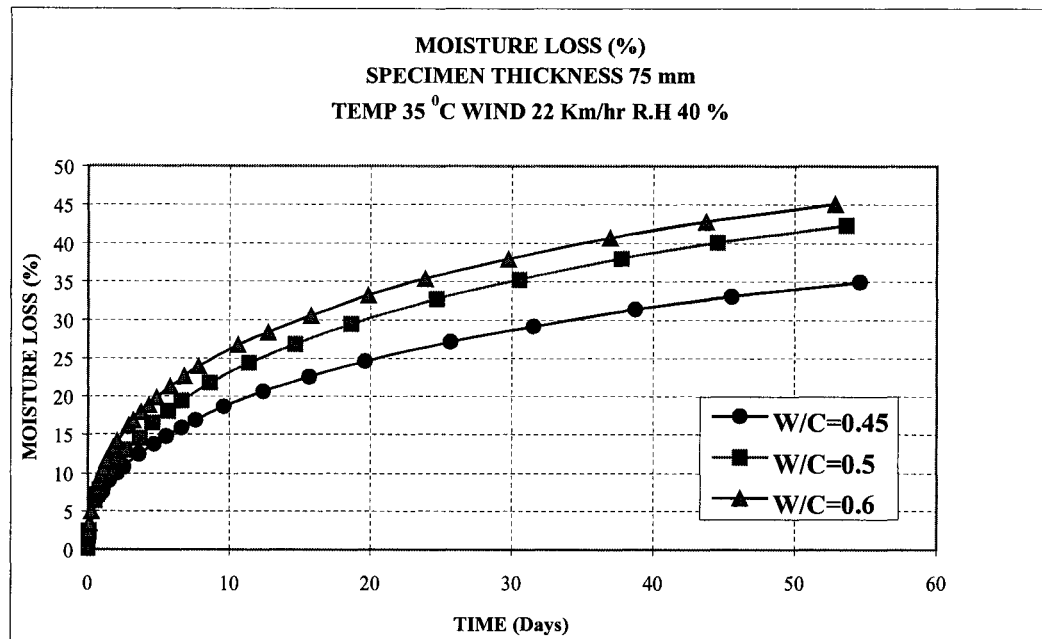


Figure 4.18: Effect of W/C Ratio on Moisture Loss (%) for 75 mm Specimen  
 at 35 °C and 22 km/hr Wind

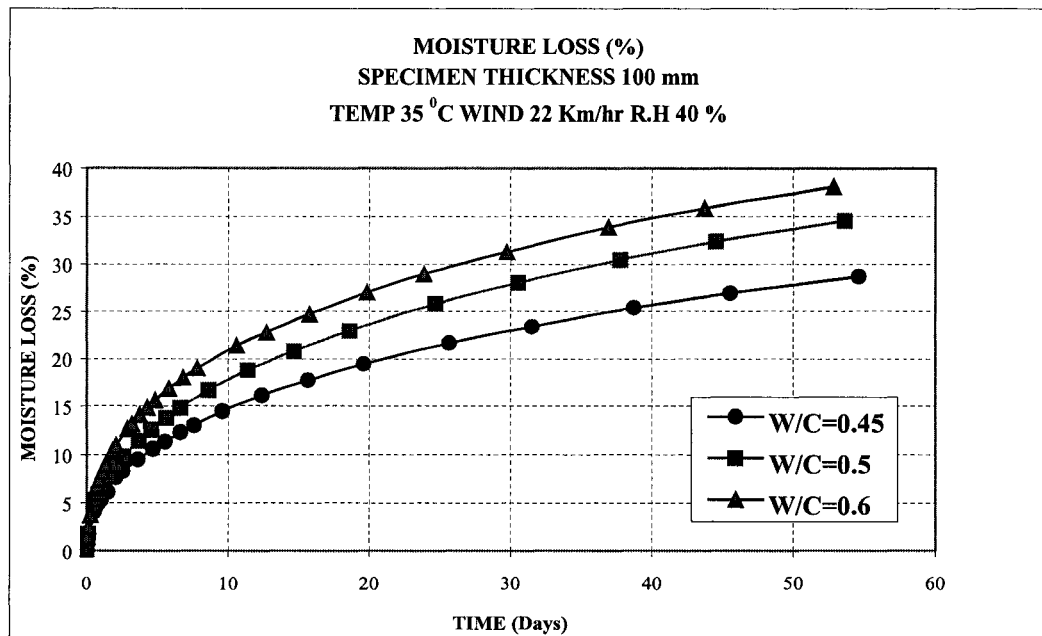


Figure 4.19: Effect of W/C Ratio on Moisture Loss (%) for 100 mm Specimen  
 at 35 °C and 22 km/hr Wind

#### 4.2.1.2 Effect of Wind Speed

To ascertain the influence of wind speed on convective transfer coefficient ( $h_f$ ) for concrete, drying tests were carried out at two wind speeds, 6 km/hr & 22 km/hr, in the environmental chambers.

Effect of wind speed on moisture loss evolution is discussed in the following paragraphs. First we consider the effect at an ambient **temperature of 50 °C**.

For the **w/c = 0.45**, Figure 4.20 shows the effect of wind speed on moisture loss in percentage for specimen thickness of 25 mm. At 20 days, for instance, specimen under low wind lost about 58 % of the evaporable moisture, whereas the specimen under high wind lost 65 %.

Figure 4.21 shows the effect for 75 mm specimens under similar conditions. At low wind speed 36 %, while under high wind 40 % of the total evaporable moisture was lost, after 20 days of exposure.

Next we discuss the effect of wind speed on moisture loss in % for specimens of **w/c = 0.5**. Figure 4.22 shows the comparison for 25 mm thick specimens. At 20 days the specimens under high wind speed of 22 km/hr lost 65 % of evaporable moisture while those under low wind speed of 6 km/hr lost 62 %. Figure 4.23 shows the comparison for 75 mm specimens. The specimens exposed to high wind speed achieved 3 % higher moisture loss than the others, at 20 days of exposure.

The effect of wind speed on moisture loss for specimens with **w/c = 0.6** is discussed next. Figure 4.24 shows the comparison for specimen thickness of 25 mm. It can be seen that at 20 days the specimens exposed to high wind speed lost 6 % more of

the evaporable moisture. Figure 4.25 shows similar trend for 75 mm specimen, with the moisture loss being higher at high wind speed. In this case 53 % of moisture was lost at 20 days under high wind speed and 47 % for the other case.

In each case the initial slope of the moisture loss curve can be observed to be steeper at high wind speed. Also it is evident from these graphs that moisture loss gets accelerated with the increase in wind speed. Similar trend was observed in specimens of other thickness in each case. This is due to the fact that evaporation or convective transfer of the moisture, which is coming to the specimen surface through diffusion, increases with the increase in wind speed to which the specimen is exposed.

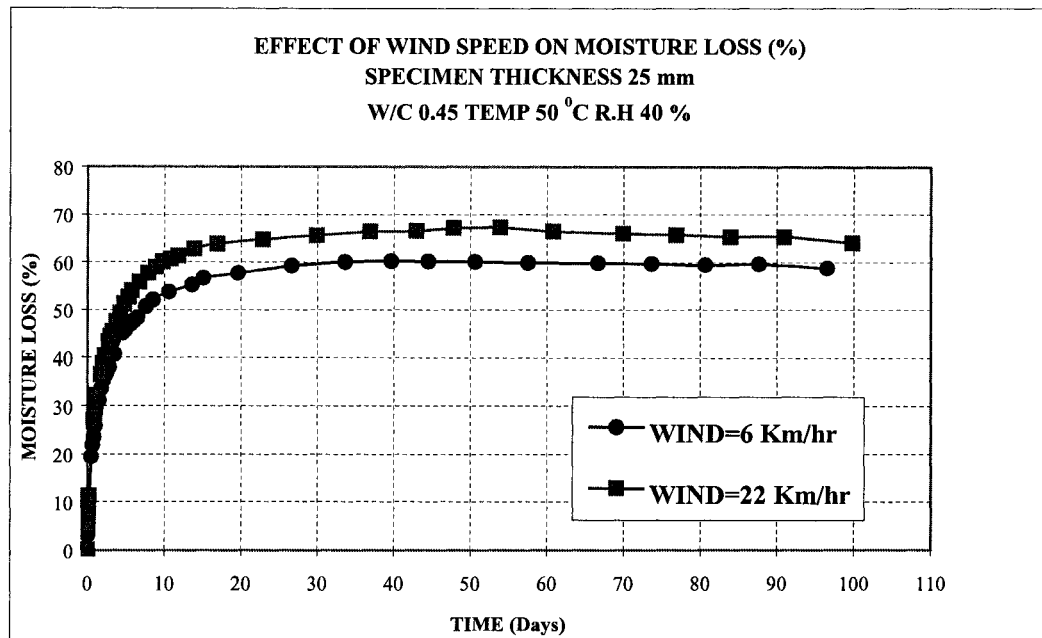


Figure 4.20: Effect of Wind Speed on Moisture Loss (%) for 25 mm Specimens  
 for W/C Ratio 0.45 at 50 °C

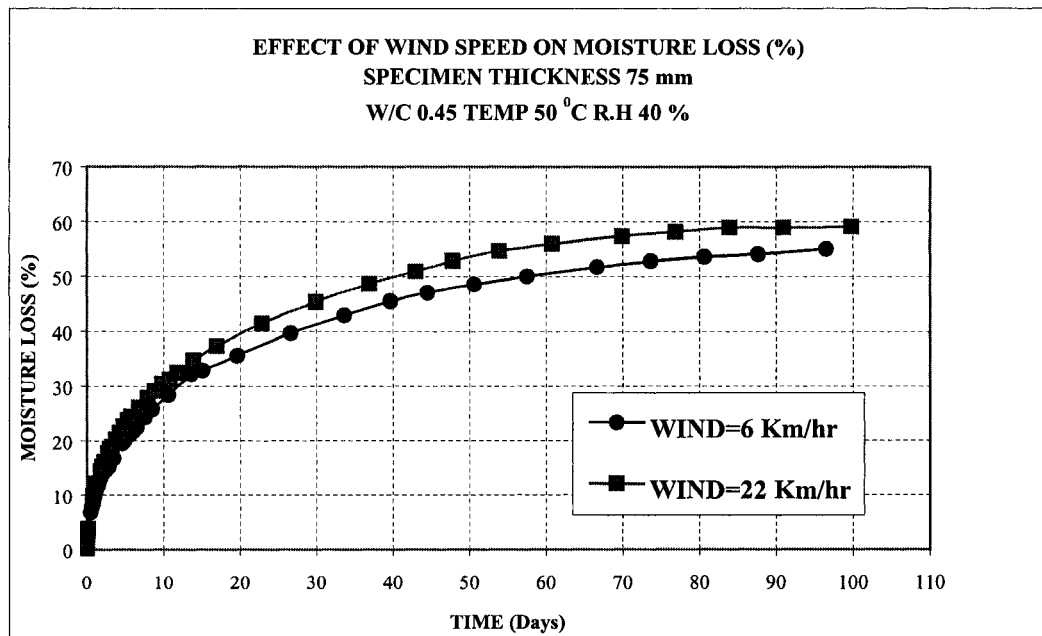


Figure 4.21: Effect of Wind Speed on Moisture Loss (%) for 75 mm Specimens  
 for W/C Ratio 0.45 at 50 °C

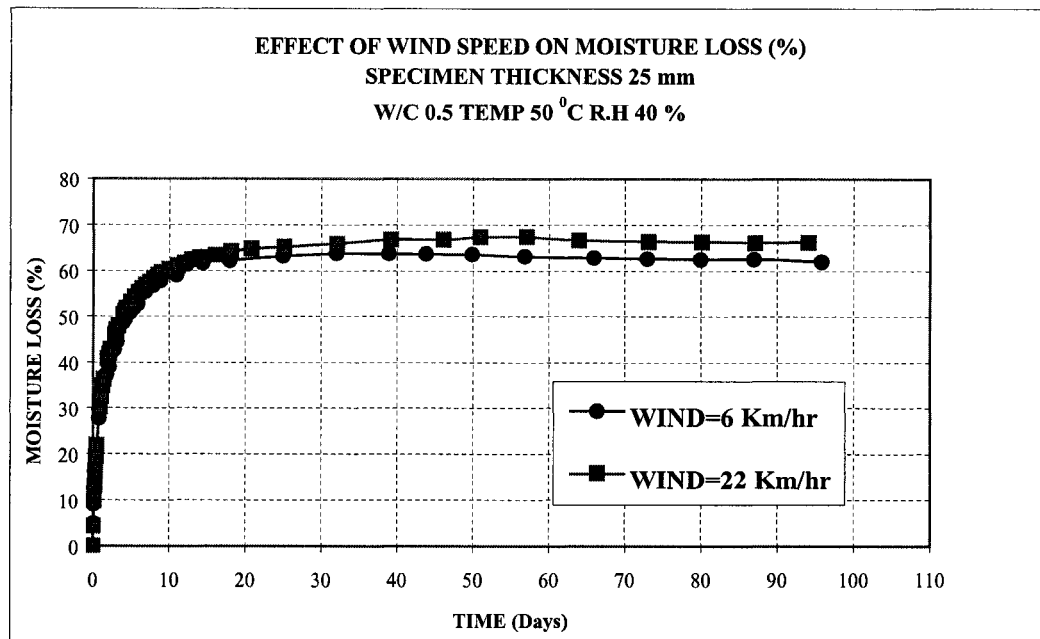


Figure 4.22: Effect of Wind Speed on Moisture Loss (%) for 25 mm Specimens  
for W/C Ratio 0.5 at 50 °C

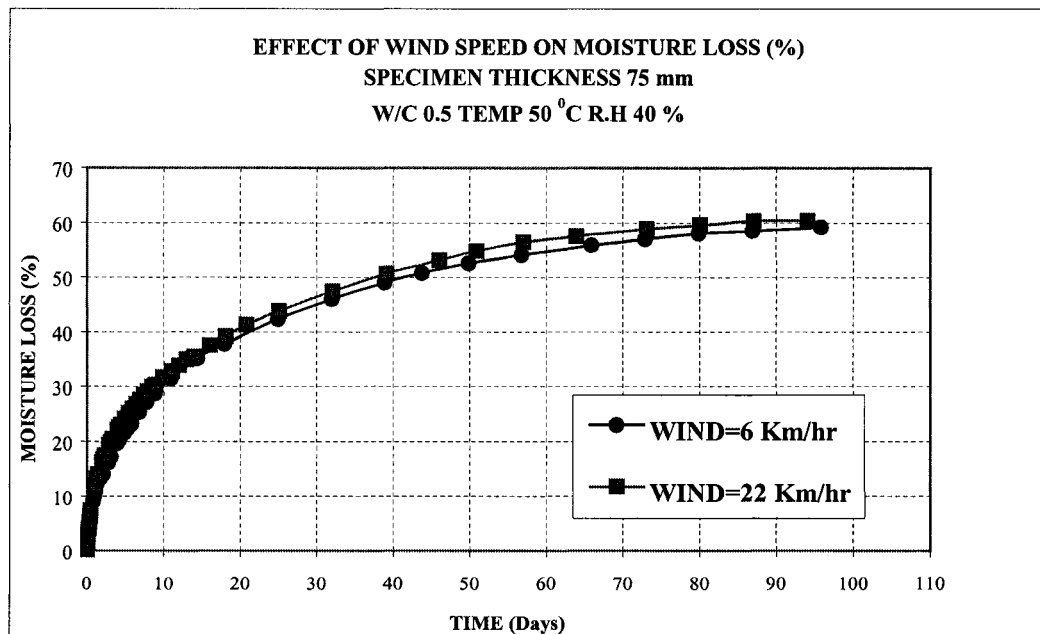


Figure 4.23: Effect of Wind Speed on Moisture Loss (%) for 75 mm Specimens  
for W/C Ratio 0.5 at 50 °C

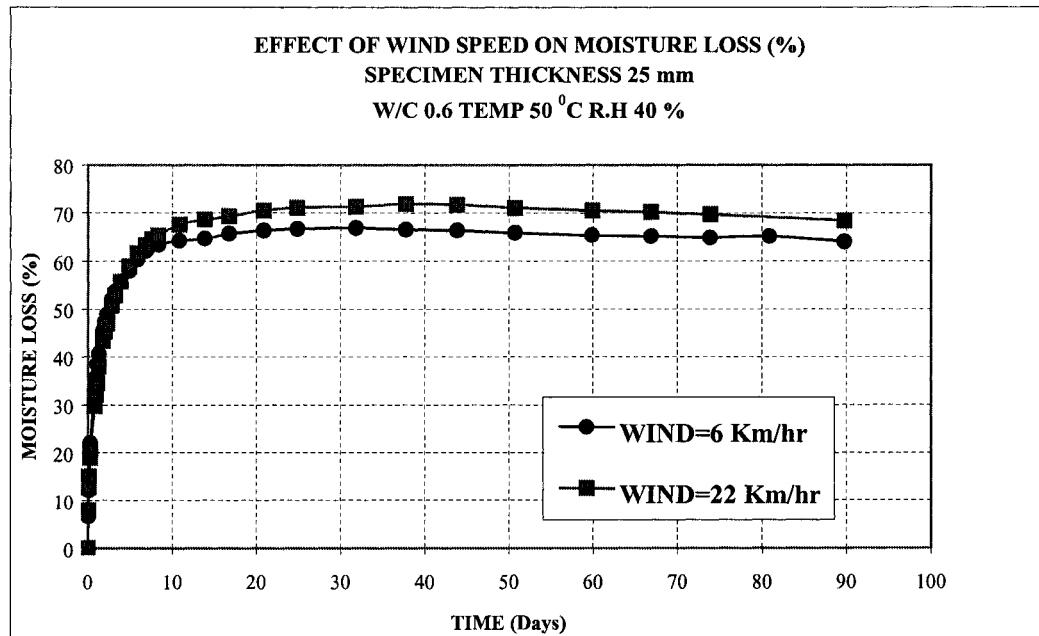


Figure 4.24: Effect of Wind Speed on Moisture Loss (%) for 25 mm Specimens  
for W/C Ratio 0.6 at 50 °C

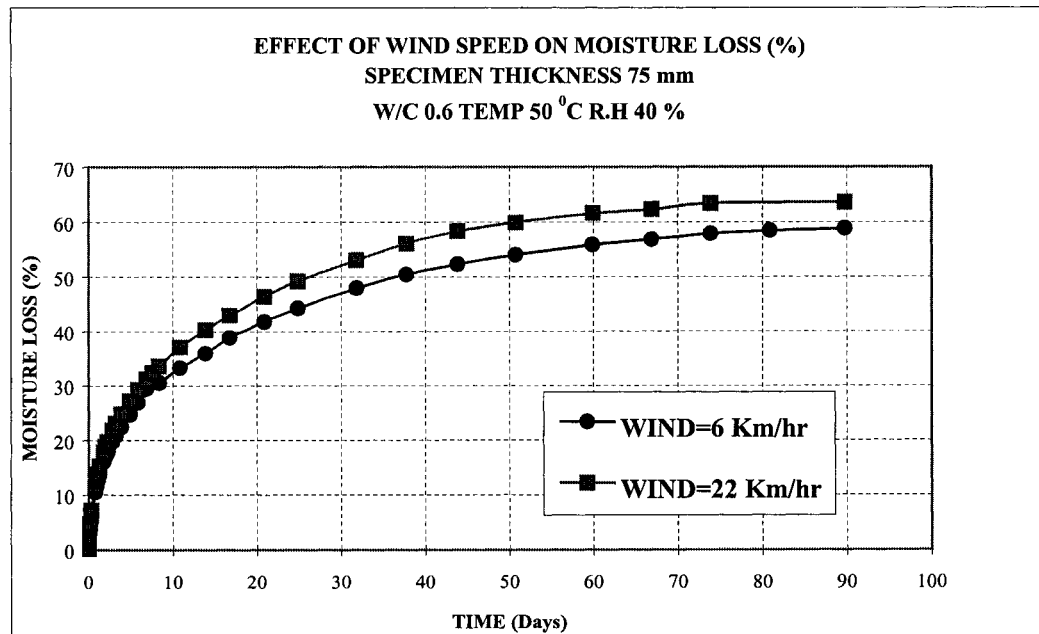


Figure 4.25: Effect of Wind Speed on Moisture Loss (%) for 75 mm Specimens  
for W/C Ratio 0.6 at 50 °C

Next we consider the effect of wind speed on moisture loss in percentage at an ambient **temperature of 35 °C**. Comparison graphs were plotted for each mix for each specimen size, with each case showing similar trend, however, results for only two sizes are presented and discussed here as before.

For  $w/c = 0.45$ , Figure 4.26 shows the effect for specimens of 25 mm thickness. At 20 days of exposure specimens under low wind lost 40 % of the evaporable moisture, whereas the specimens under high wind lost 50 %. Figure 4.27 shows the effect for 75 mm specimens under similar conditions. At low wind speed 20 % of the evaporable moisture was lost while under high wind the loss was found to be 25 %.

For the effect on  $w/c = 0.5$ , Figure 4.28 shows the comparison for 25 mm thick specimens. At 20 days the specimens at high wind of 22 km/hr lost 57 % of evaporable moisture while those at low wind of 6 km/hr showed only 47 % loss. Figure 4.29 shows similar comparison for 75 mm specimens. The specimens exposed to high wind speed achieved 5 % higher moisture loss than the ones under low wind.

In the end we discuss the effect for specimens with  $w/c = 0.6$ . Figure 4.30 shows the comparison for specimen thickness of 25 mm. It can be seen that at 20 days the specimens exposed to high wind lost 15 % more of the evaporable moisture. Figure 4.31 shows similar trend for 75 mm specimens, with the moisture loss again being higher at high wind speed. In this case 33 % of moisture was lost at 20 days under high wind speed and 30 % under the low wind case.

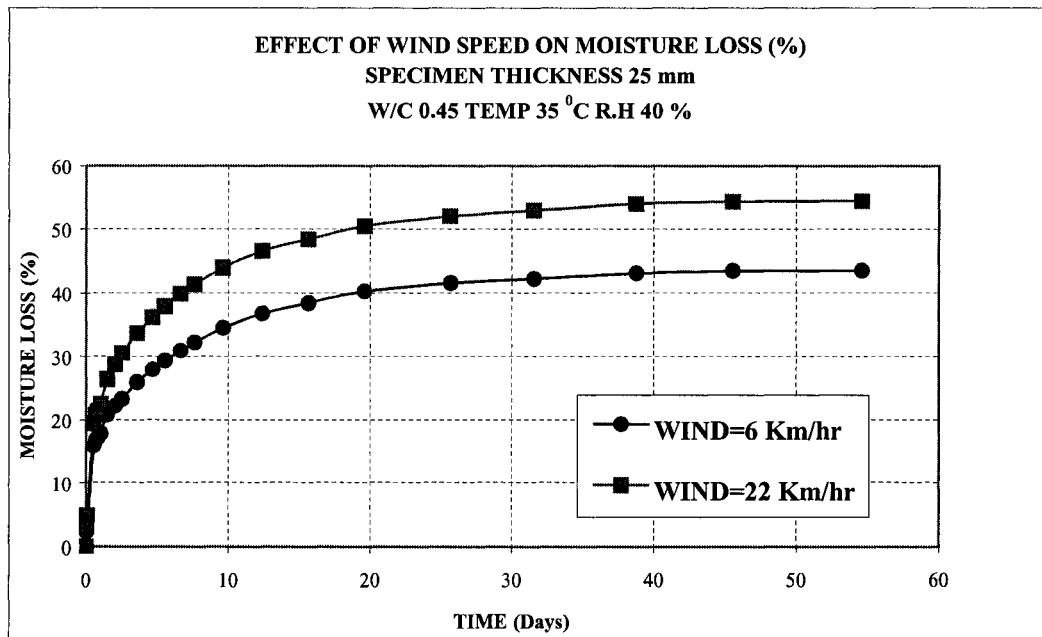


Figure 4.26: Effect of Wind Speed on Moisture Loss (%) for 25 mm Specimens  
for W/C Ratio 0.45 at 35 °C

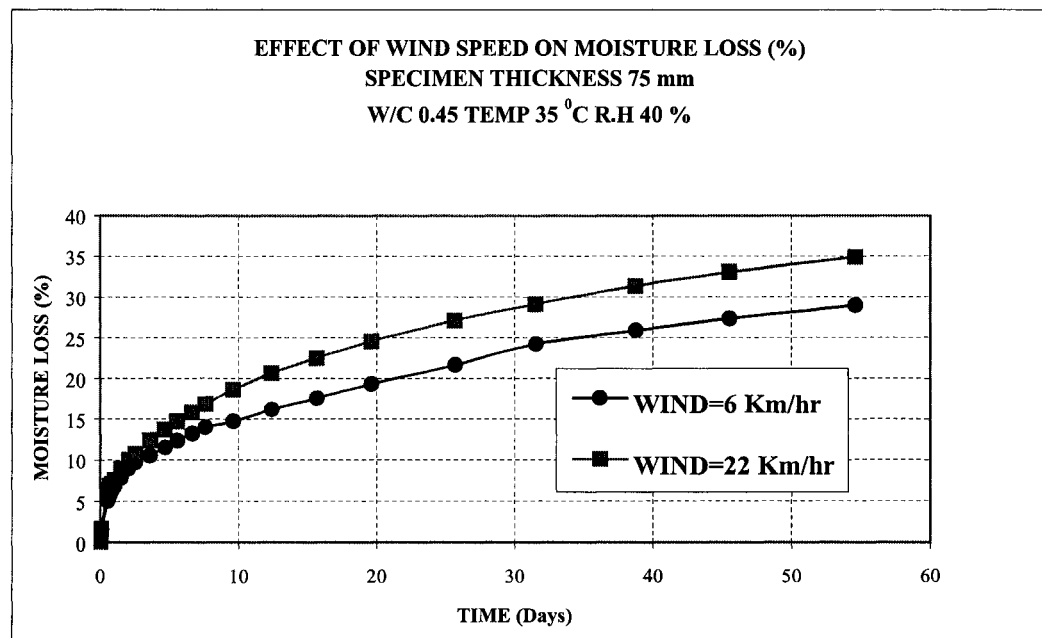


Figure 4.27: Effect of Wind Speed on Moisture Loss (%) for 75 mm Specimens  
for W/C Ratio 0.45 at 35 °C

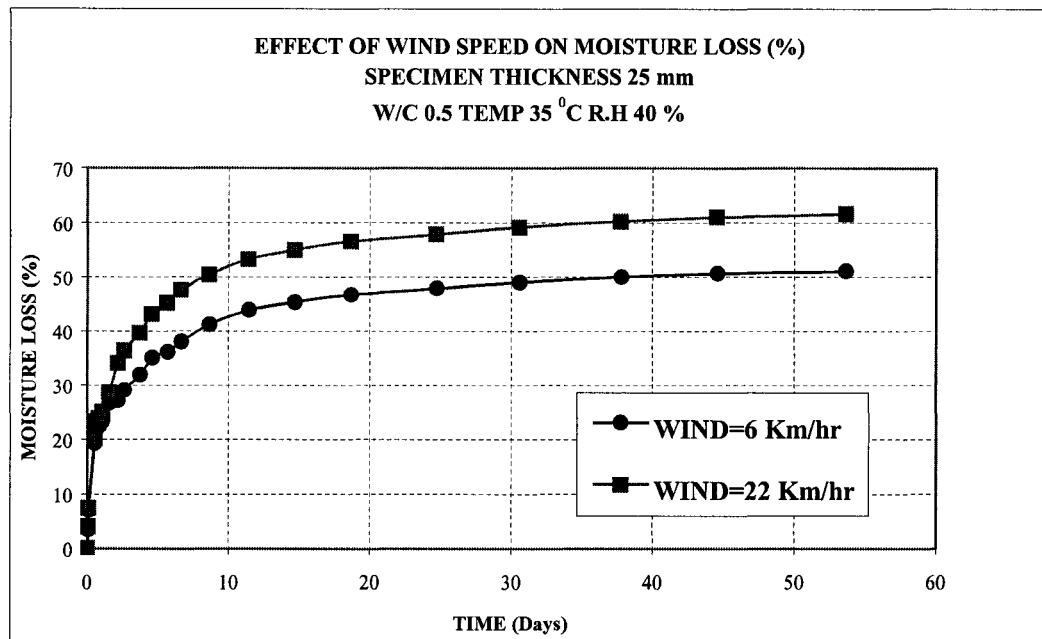


Figure 4.28: Effect of Wind Speed on Moisture Loss (%) for 25 mm Specimens  
for W/C Ratio 0.5 at 35 °C

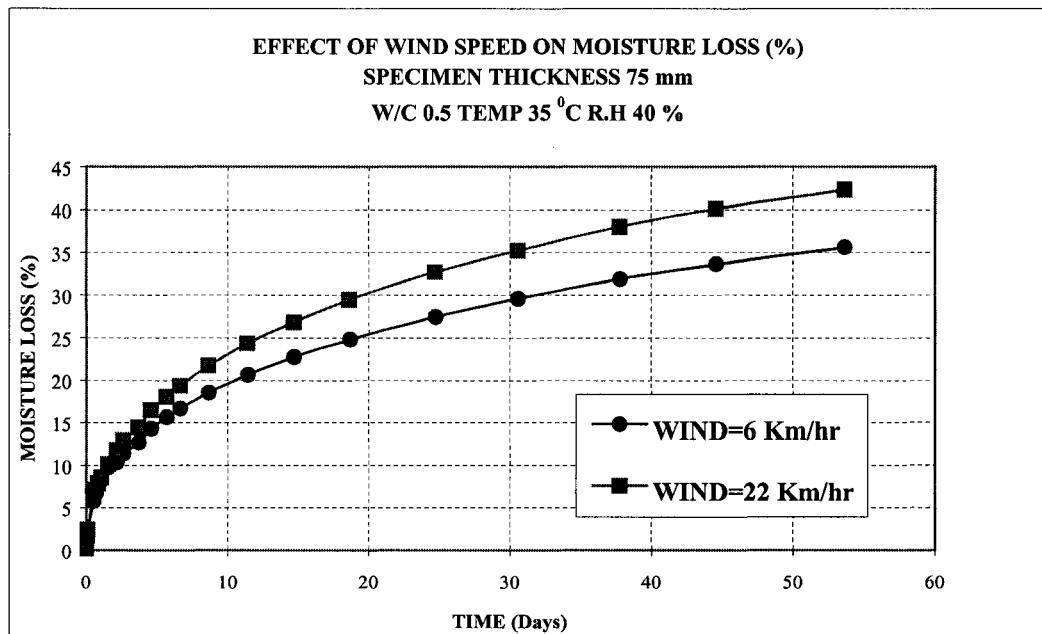


Figure 4.29: Effect of Wind Speed on Moisture Loss (%) for 75 mm Specimens  
for W/C Ratio 0.5 at 35 °C

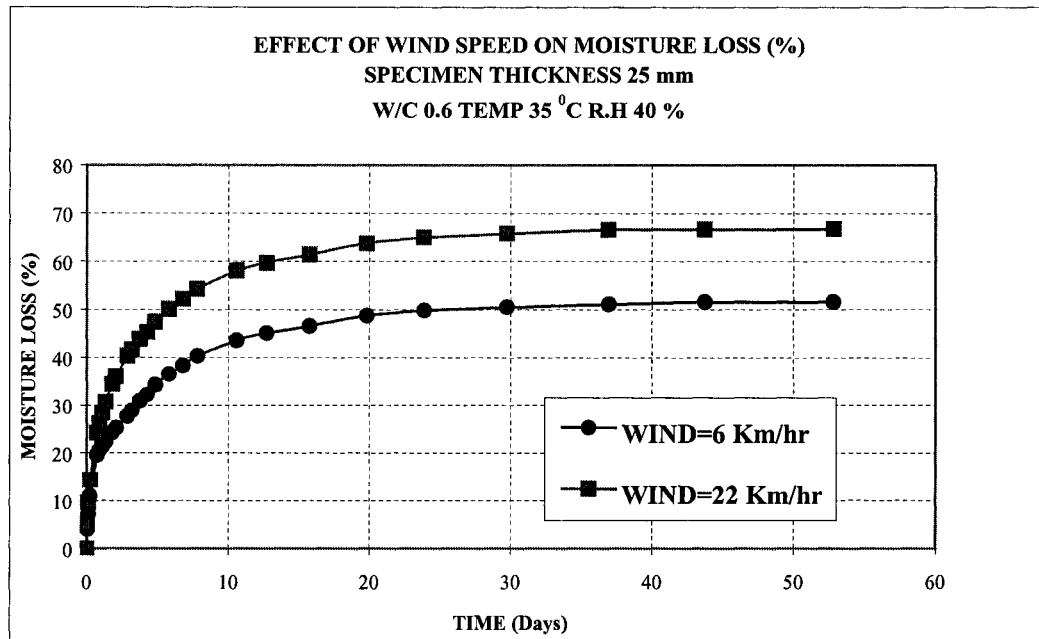


Figure 4.30: Effect of Wind Speed on Moisture Loss (%) for 25 mm Specimens  
for W/C Ratio 0.6 at 35 °C

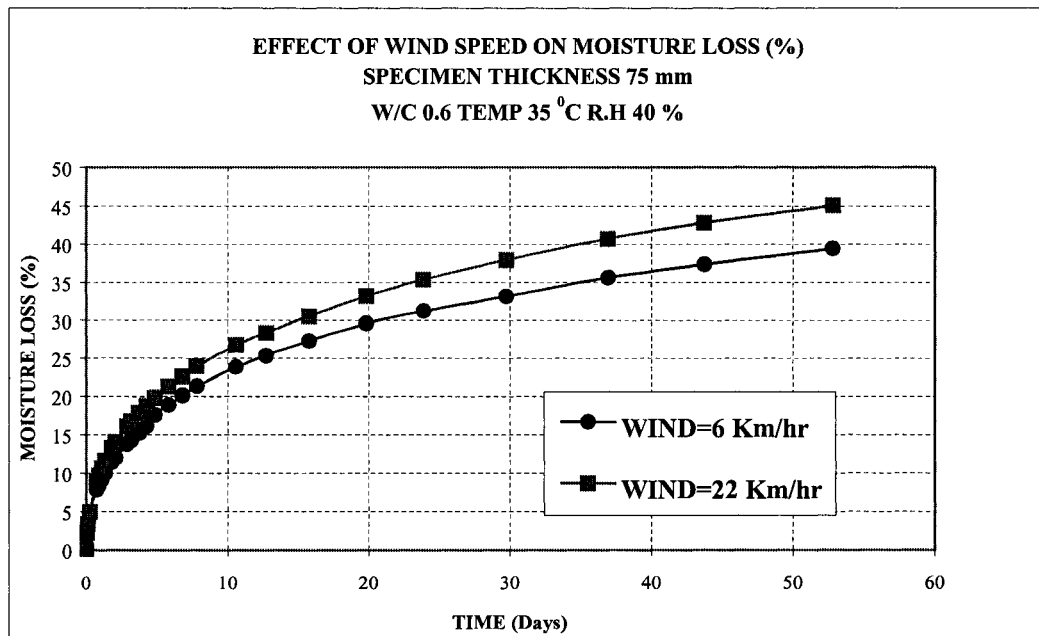


Figure 4.31: Effect of Wind Speed on Moisture Loss (%) for 75 mm Specimens  
for W/C Ratio 0.6 at 35 °C

#### 4.2.1.3 Effect of Temperature

To investigate the effect of temperature on coefficient of moisture diffusivity ( $D$ ) of concrete, the mixes were exposed to two sets of exposure temperatures in the environmental chambers. Diffusivity specimens were hence subjected to drying at 35 °C and 50 °C at a constant average relative humidity of 40 %. Moisture loss (%) curves were then generated from these experimental results and will be compared in the following discussion.

First we consider the effect of temperature on moisture loss in percentage at a **wind speed of 6 km/hr**. For water-cement ratio 0.45, Figures 4.32 & 4.33 show the effect for specimens of 50 & 100 mm thickness respectively. With the increase in ambient temperature from 35-50 °C a 15-20 % increase in moisture loss is evident. For instance at an exposure time of 50 days the moisture loss is 35~55 % and 23~43 % for the two specimen sizes. Figures 4.34 & 4.35 show similar comparison for w/c ratio 0.5. In this case the increase in moisture loss is approximately 10-18 %, with 42~60 % and 29~44 % moisture loss at 50 days for the two sizes respectively. Comparison plots for w/c ratio 0.6 are presented in Figures 4.36 & 4.37, which show moisture loss acceleration by about 10-13 %. At 50 days of exposure the moisture loss is found to be 49~62 % and 34~47 % for the two specimen sizes.

Next we consider the temperature effect on moisture loss (%) under an exposure **wind speed of 22 km/hr**. For w/c ratio 0.45, Figure 4.38 shows the comparison for a specimen thickness of 50 mm. At 50 days of exposure the moisture loss is 44 % at 35 °C and 62 % at 50 °C. Figure 4.39 shows a moisture loss increase by approximately 10-18 %

for specimen thickness of 100 mm. Similarly comparison for w/c ratio 0.5 is reported in Figures 4.40 & 4.41. At 50 days of exposure moisture loss of 53~63 % and 33~47 % is shown by the specimens of 50 & 100 mm thickness respectively. Figures 4.42 & 4.43 show an acceleration of moisture loss by approximately 10-13 % for the specimens with w/c ratio 0.6. In this case the moisture loss at 50 days of exposure is found to be 58~68 % and 37~49 % for the two specimen sizes respectively.

It should be noted here that the comparison graphs were plotted for all specimen sizes under each wind speed, but here results for only two sizes are reported to give a general picture of the observed trend.

From the above discussion it becomes evident that the moisture loss in concrete increases significantly with the increase in exposure temperature, which is attributed to the increase in energy of water vapor molecules and expansion of pores at higher temperature. Also hydration is not 100 percent complete by 7 days of curing and it continues after that though at a much slower rate. This means that in our case a small part of hydration would have occurred when the specimens were inside the environmental chambers and at higher temperature it would result in slightly higher porosity of the system and thus higher moisture loss.

It is interesting to note that the effect of temperature on moisture loss is much more pronounced/significant as compared to that of varying wind speed or water-cement ratio. Similar trend should be reflected by the average moisture diffusivity values also.

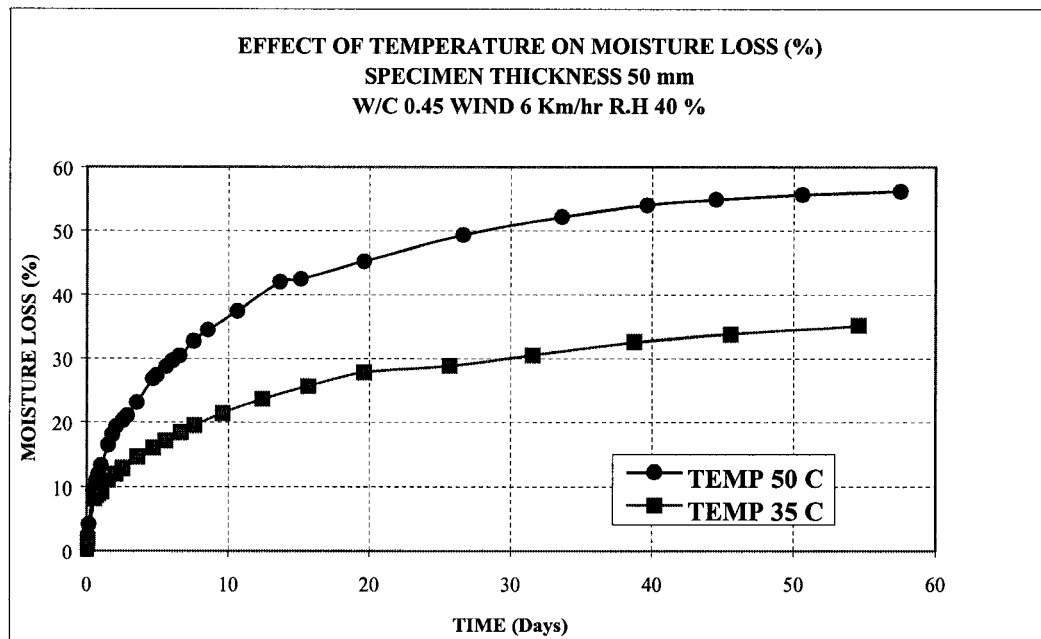


Figure 4.32: Effect of Temperature on Moisture Loss (%) at Wind Speed 6 km/hr

W/C Ratio 0.45 Specimen Thickness 50 mm

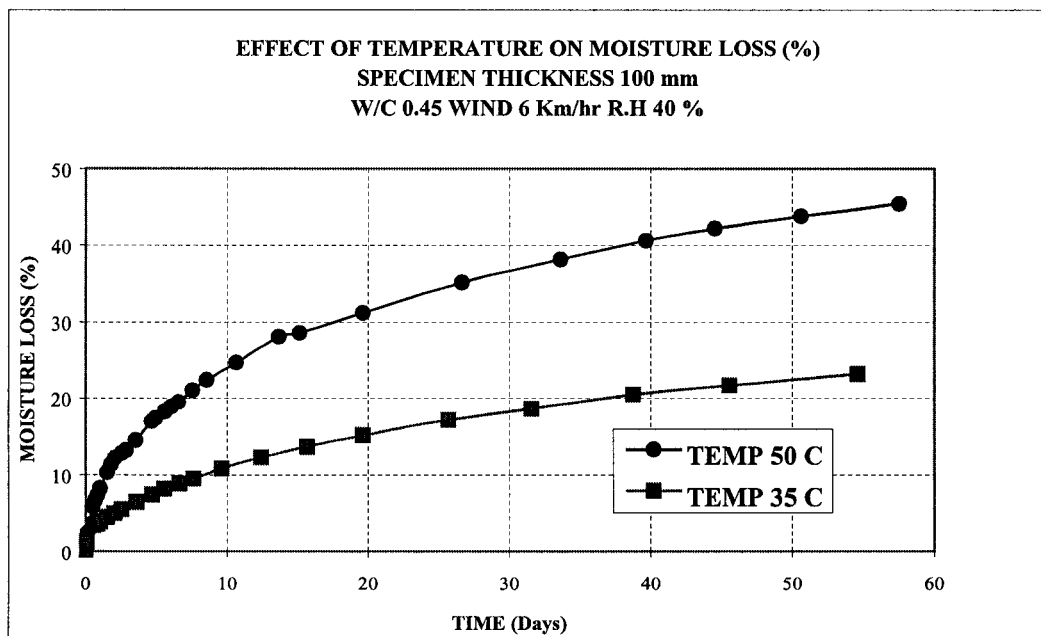


Figure 4.33: Effect of Temperature on Moisture Loss (%) at Wind Speed 6 km/hr

W/C Ratio 0.45 Specimen Thickness 100 mm

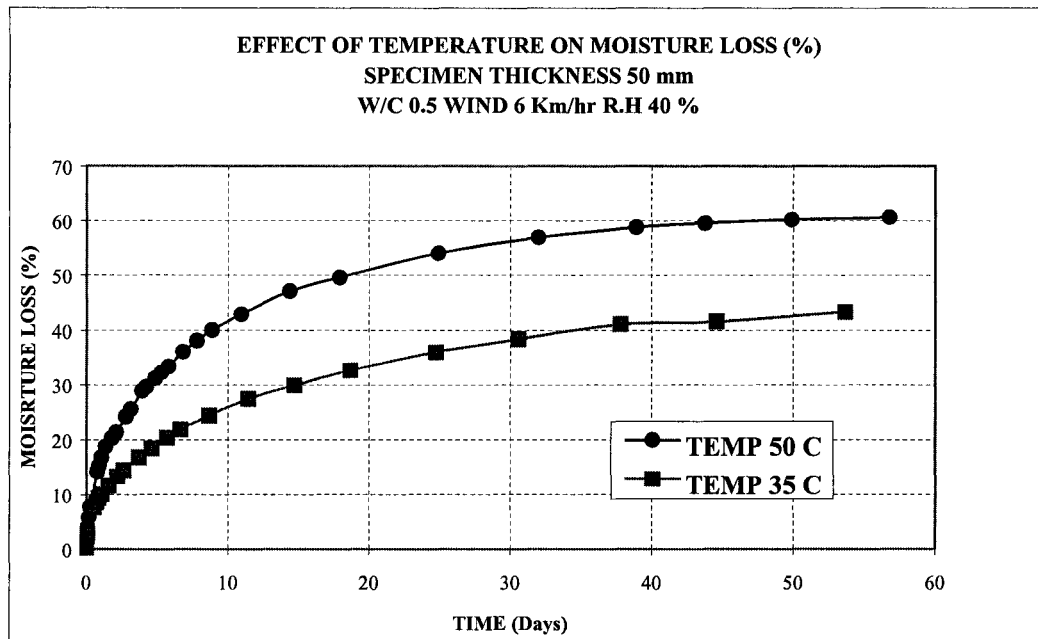


Figure 4.34: Effect of Temperature on Moisture Loss (%) at Wind Speed 6 km/hr

W/C Ratio 0.5 Specimen Thickness 50 mm

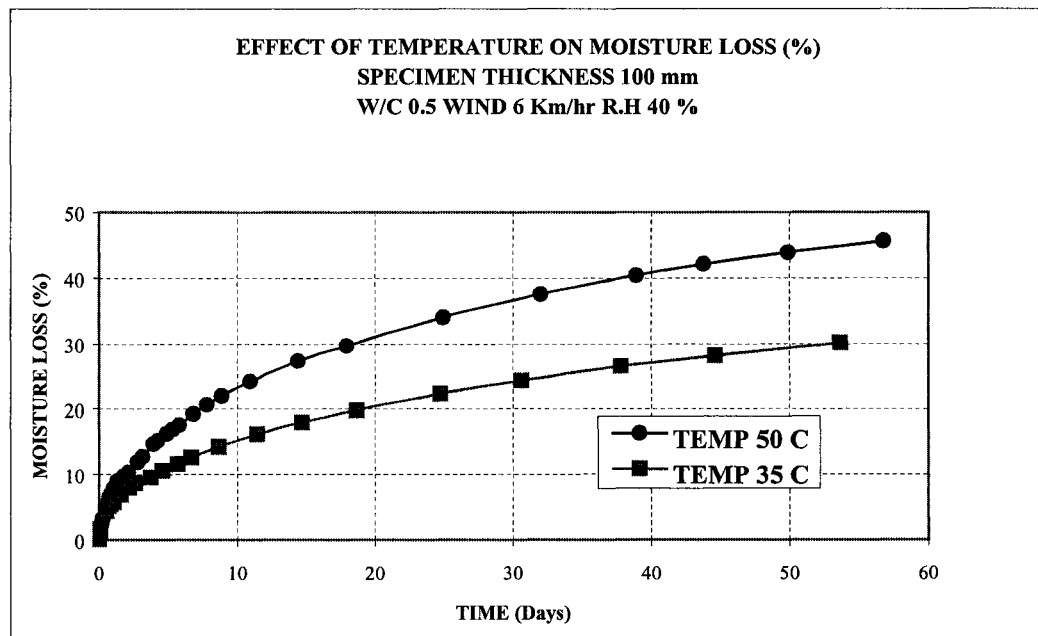


Figure 4.35: Effect of Temperature on Moisture Loss (%) at Wind Speed 6 km/hr

W/C Ratio 0.5 Specimen Thickness 100 mm

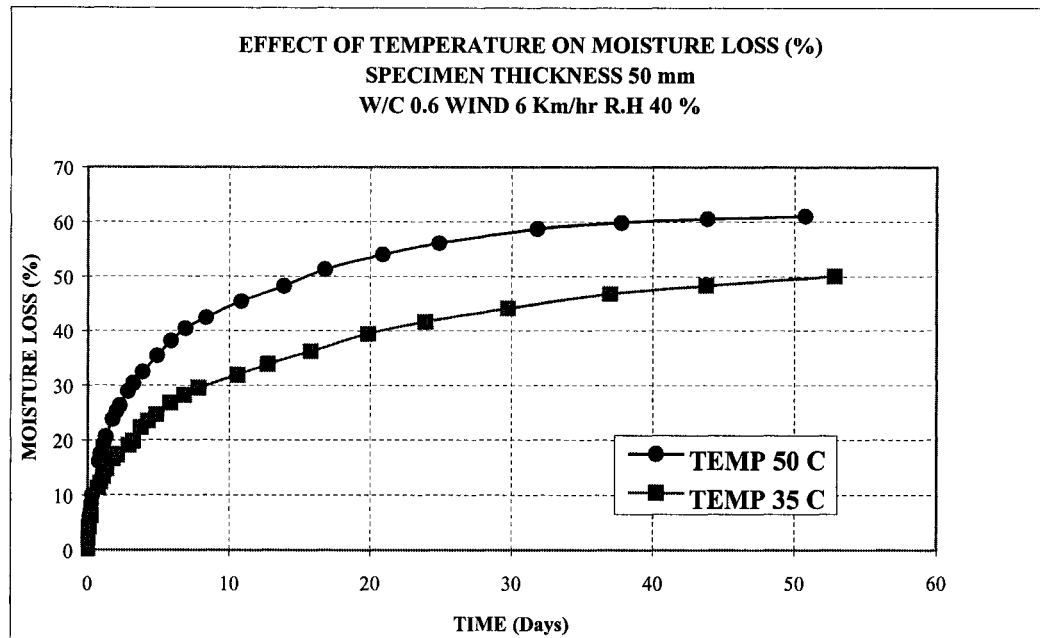


Figure 4.36: Effect of Temperature on Moisture Loss (%) at Wind Speed 6 km/hr

W/C Ratio 0.6 Specimen Thickness 50 mm

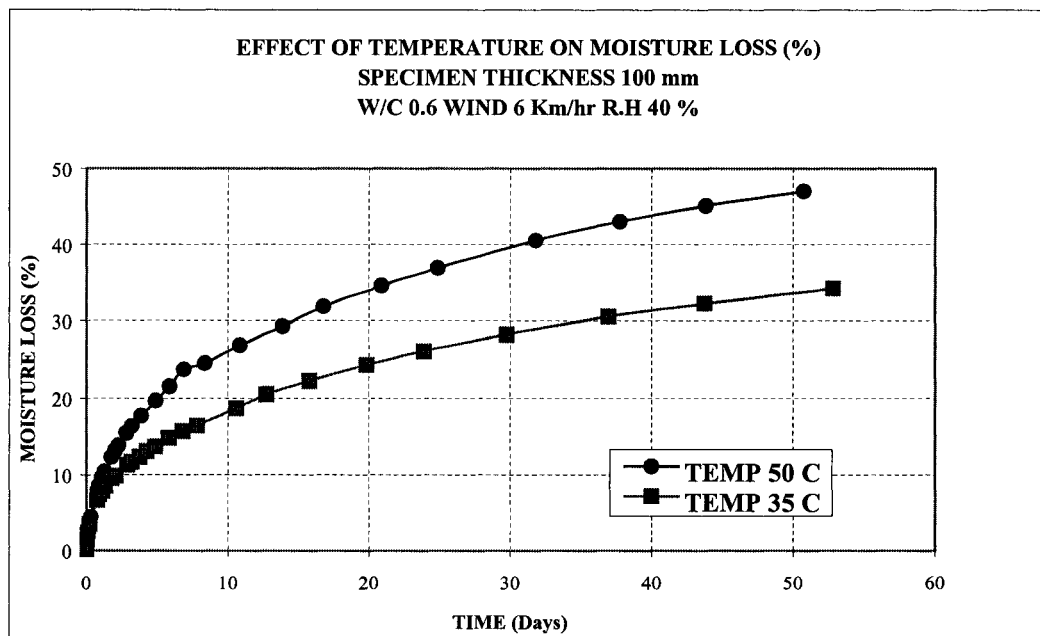


Figure 4.37: Effect of Temperature on Moisture Loss (%) at Wind Speed 6 km/hr

W/C Ratio 0.6 Specimen Thickness 100 mm

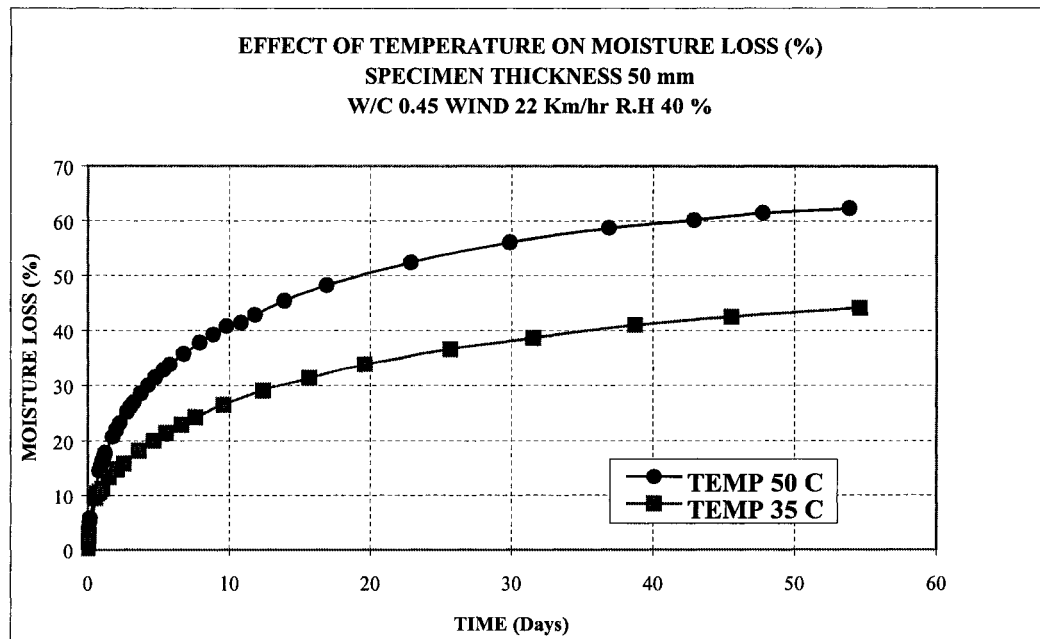


Figure 4.38: Effect of Temperature on Moisture Loss (%) at Wind Speed 22 km/hr

W/C Ratio 0.45 Specimen Thickness 50 mm

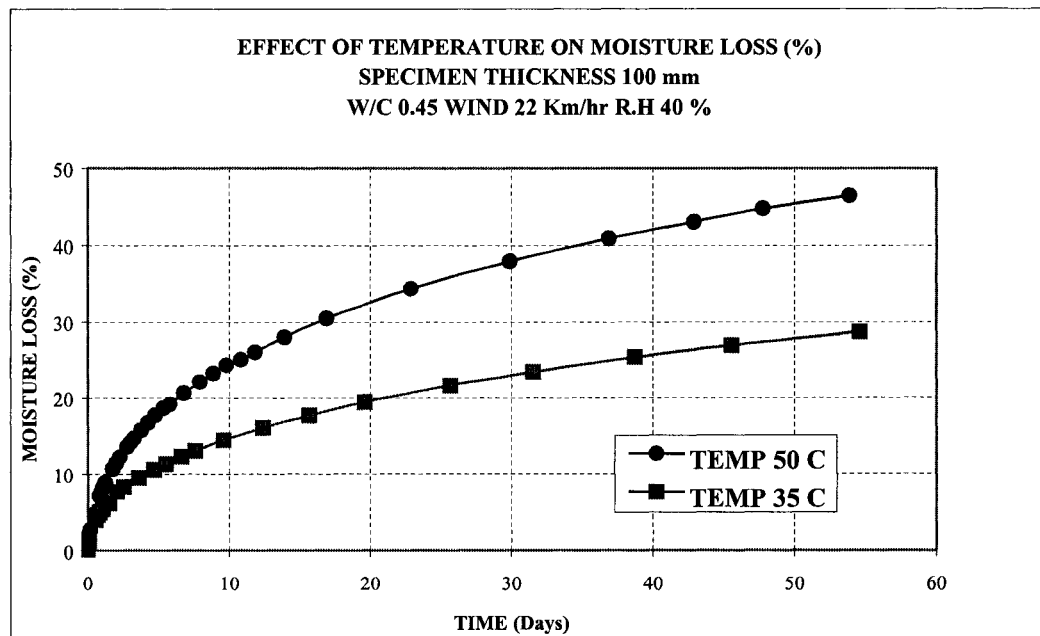


Figure 4.39: Effect of Temperature on Moisture Loss (%) at Wind Speed 22 km/hr

W/C Ratio 0.45 Specimen Thickness 100 mm

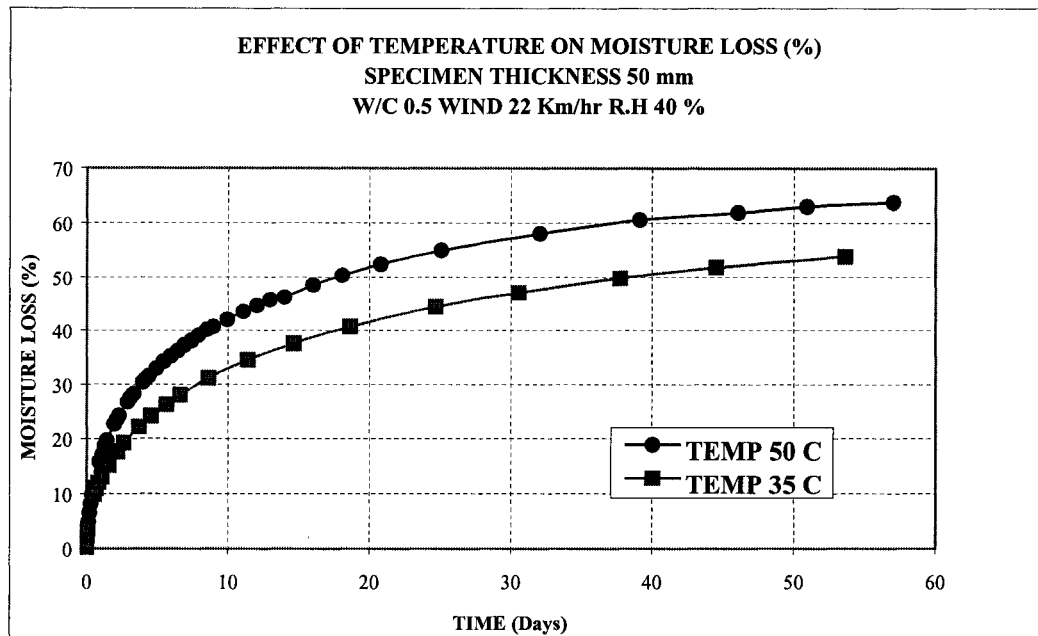


Figure 4.40: Effect of Temperature on Moisture Loss (%) at Wind Speed 22 km/hr

W/C Ratio 0.5 Specimen Thickness 50 mm

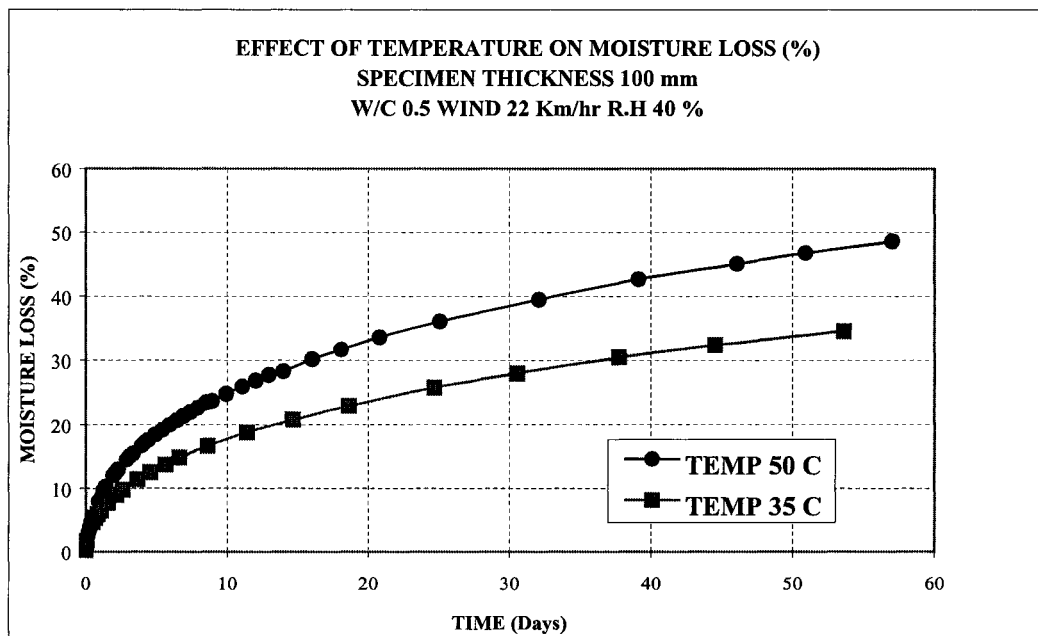


Figure 4.41: Effect of Temperature on Moisture Loss (%) at Wind Speed 22 km/hr

W/C Ratio 0.5 Specimen Thickness 100 mm

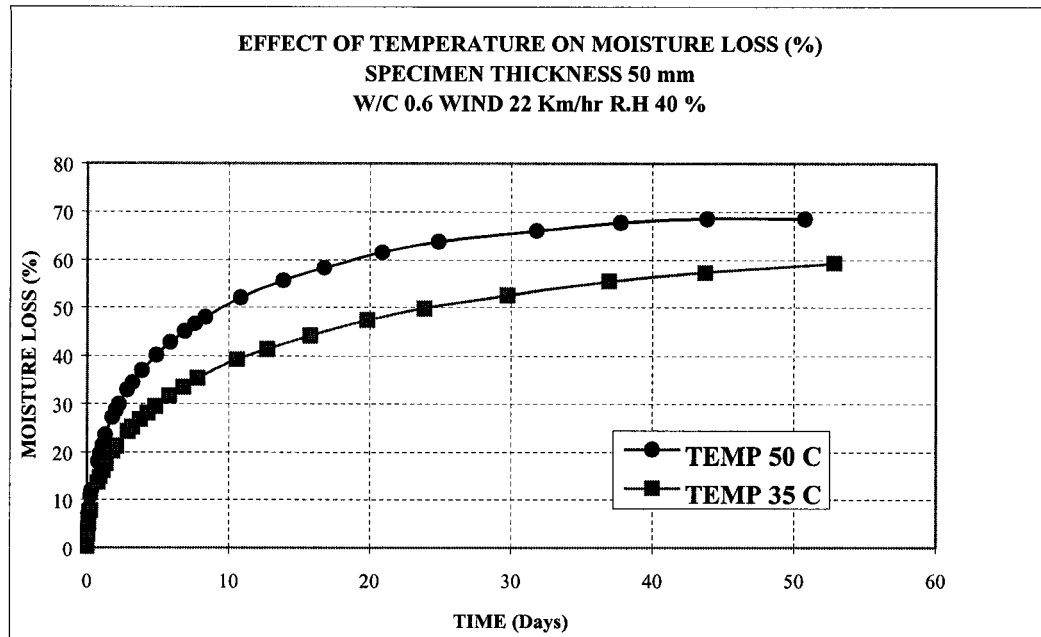


Figure 4.42: Effect of Temperature on Moisture Loss (%) at Wind Speed 22 km/hr

W/C Ratio 0.6 Specimen Thickness 50 mm

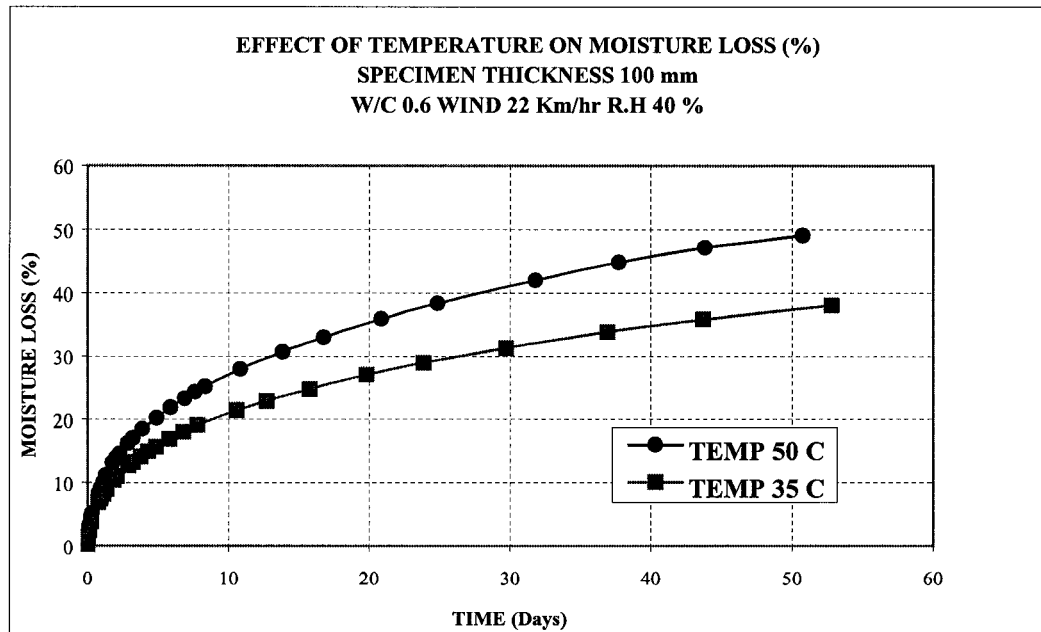


Figure 4.43: Effect of Temperature on Moisture Loss (%) at Wind Speed 22 km/hr

W/C Ratio 0.6 Specimen Thickness 100 mm

#### 4.2.2 Moisture Loss in Repair Materials

Drying tests were carried out on the selected repair materials FMC1 & FMC2 in the environmental chambers, under specified exposure regimes as given in Table 3.3. From the results, moisture loss (%) curves were generated to compute values of  $D$  &  $h_f$  under varying temperature and wind speed respectively.

At an average ambient temperature of  $30^{\circ}\text{C}$  and relative humidity of  $60\%$ , Figure 4.44 & 4.45 show the evolution of moisture loss in grams & percentage for FMC2 for each specimen size. It can be noticed that at any exposure time, moisture loss (%) is higher for the specimen with smaller thickness, which is due to the shorter path for moisture diffusion to the surface.

At an ambient temperature of  $50^{\circ}\text{C}$  and average relative humidity of  $50\%$ , Figure 4.46 shows the moisture loss evolution (%) curves for FMC1. The moisture loss curves for 20 & 30 mm specimens became flat after 50 days of exposure, showing that the specimens cannot lose any further moisture under the given exposure conditions. Figure 4.47 gives the moisture loss curves for FMC2 under similar conditions. It can be seen that specimens of 10 mm thickness reached equilibrium stage for moisture loss in just 20 days of exposure.

Figures 4.48 & 4.49 show the moisture loss in percentage for FMC1 and FMC2 at an ambient temperature of  $50^{\circ}\text{C}$ , relative humidity of  $50\%$  and an average wind speed of **12 km/hr**. It can be noticed that for some cases the moisture loss is higher than  $50\%$ , the possible reason already been discussed in section 4.2.1.1.

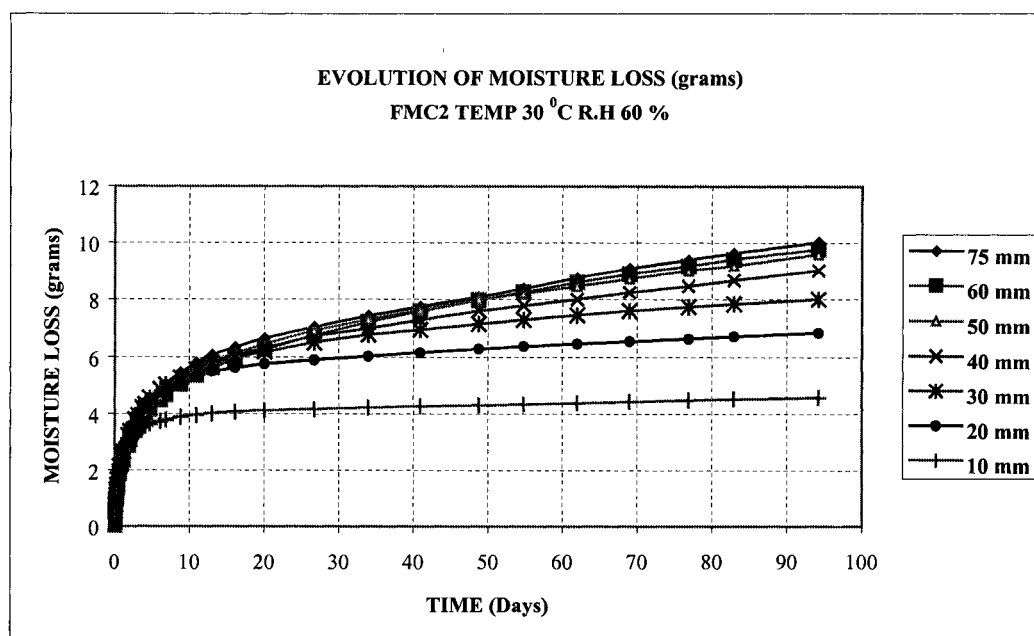


Figure 4.44: Evolution of Moisture Loss (grams) for FMC2  
at 30 °C & 60 % R.H

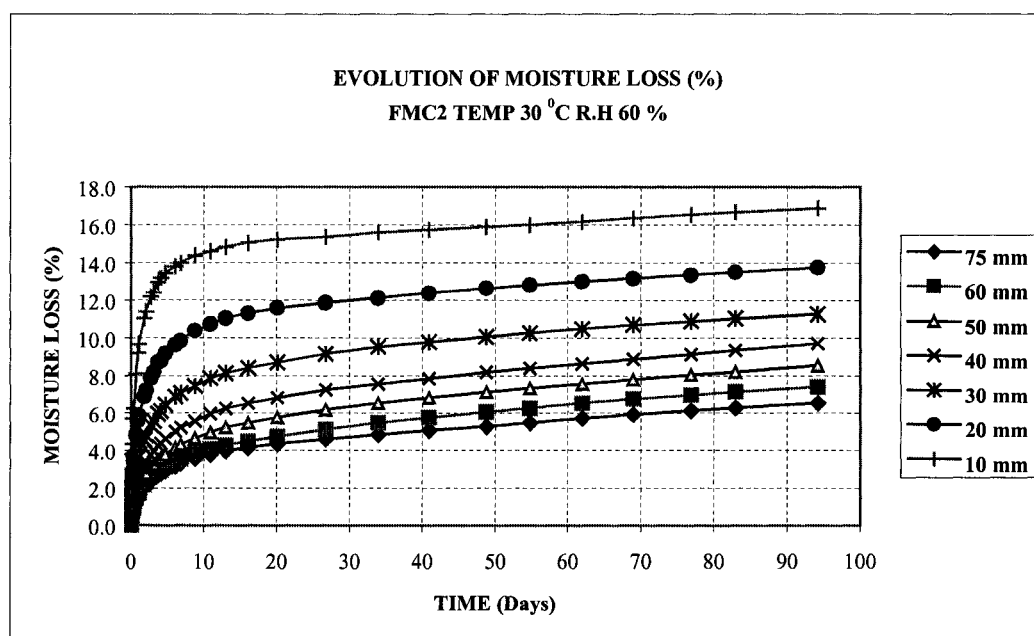


Figure 4.45: Evolution of Moisture Loss (%) for FMC2  
at 30 °C & 60 % R.H

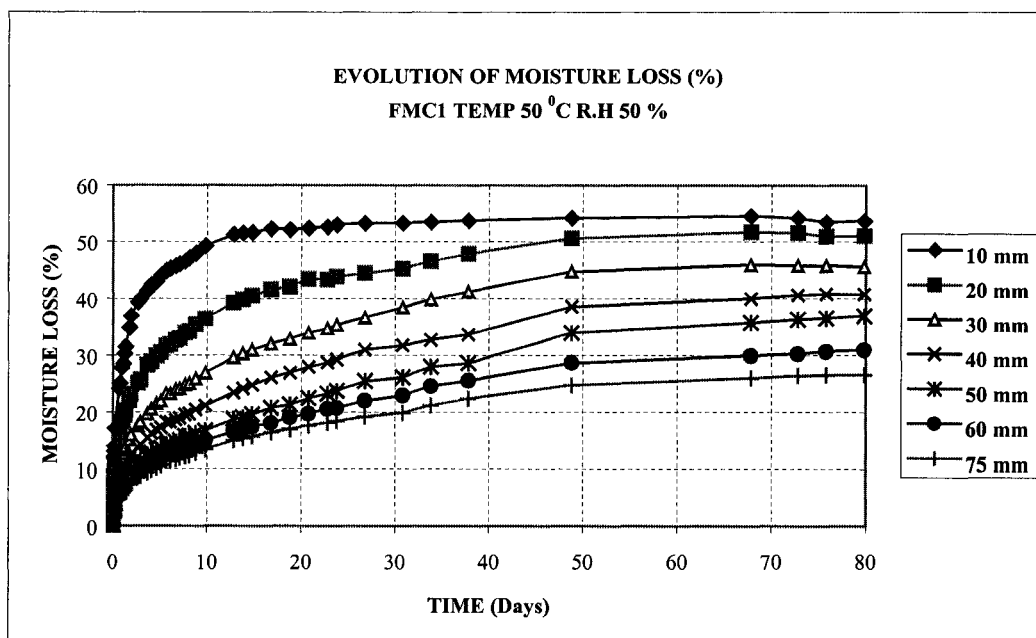


Figure 4.46: Evolution of Moisture Loss (%) for FMC1  
at 50 °C & 50 % R.H

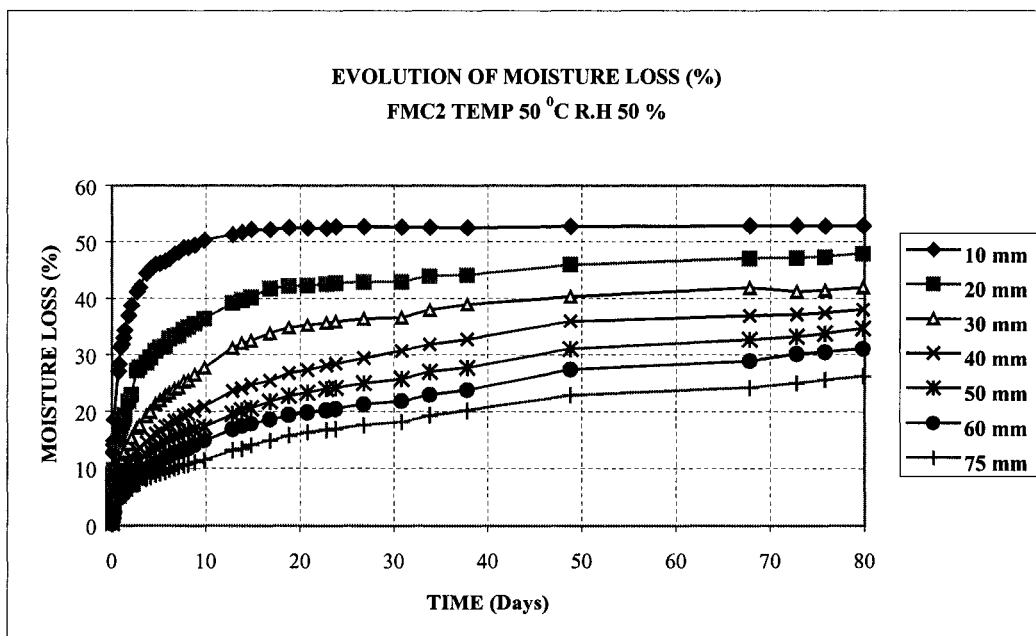


Figure 4.47: Evolution of Moisture Loss (%) for FMC2  
at 50 °C & 50 % R.H

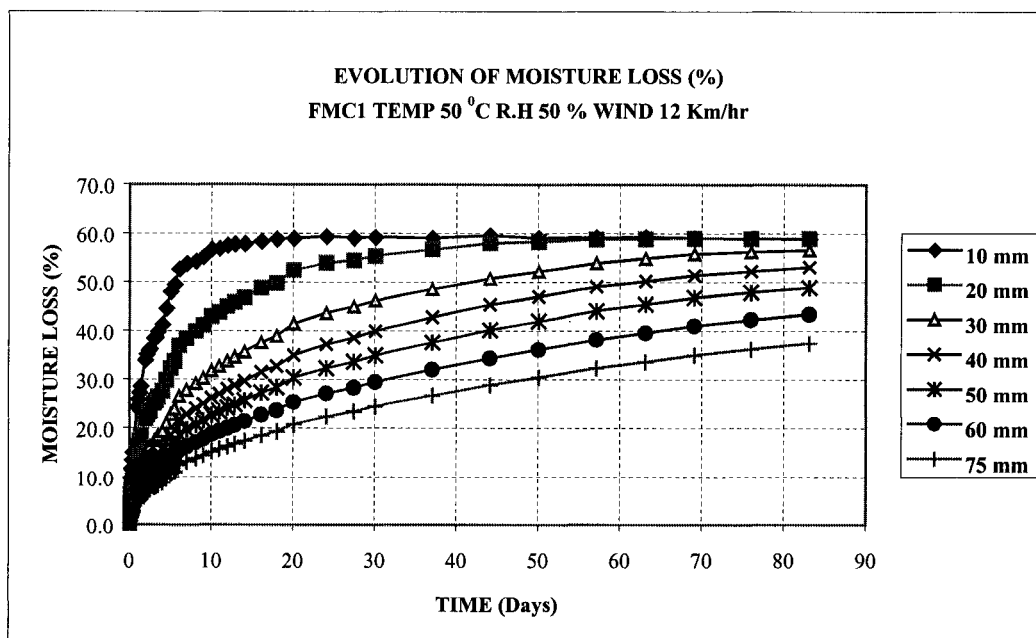


Figure 4.48: Evolution of Moisture Loss (%) for FMC1  
at 50 °C, 50 % R.H & 12 km/hr wind

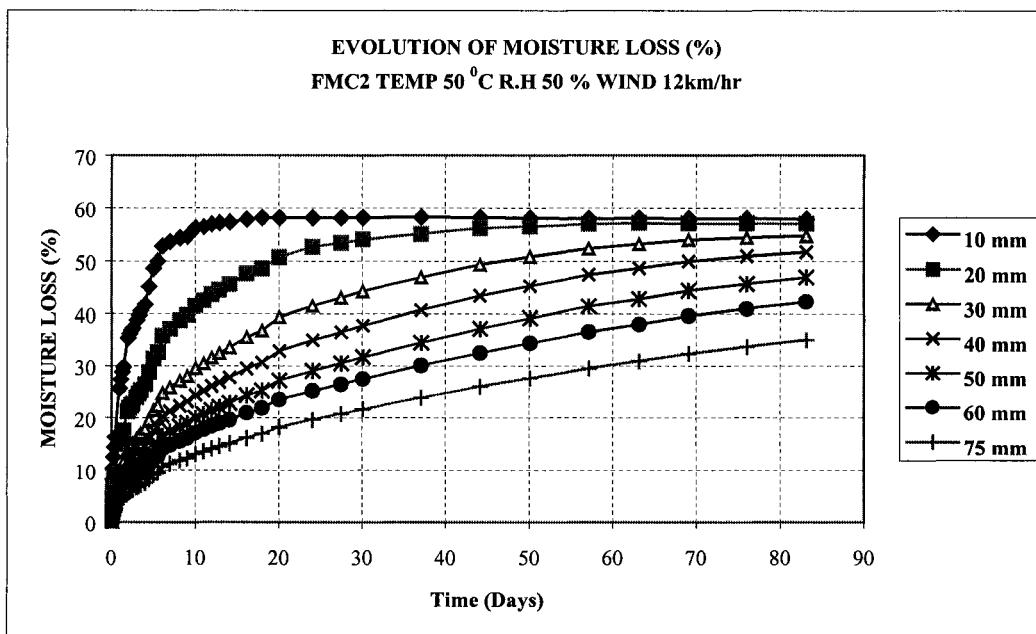


Figure 4.49: Evolution of Moisture Loss (%) for FMC2  
at 50 °C, 50 % R.H & 12 km/hr wind

In all of the above-mentioned cases, corresponding moisture loss was found to be slightly higher in FMC1 as compared to FMC2. This can be attributed to the higher moisture diffusivity of FMC1, which will be confirmed later on.

#### **4.2.2.1 Influence of Wind**

In order to see the effect of wind on convective transfer coefficient ( $h_f$ ), drying tests were carried out on both FMC1 & FMC2 under a no wind condition and an average wind speed of 12 km/hr, at ambient temperature of 50 °C and relative humidity of 50 %.

For FMC1, Figures 4.50 & 4.51 show the effect of wind on moisture loss (%) for specimen thickness of 40 & 50 mm respectively. An increase in the rate of moisture loss and increased initial slope of the curve is evident under windy conditions. For instance at an exposure time of 20 days for the 40 mm specimens, moisture loss is found to be 28 % and 35 % under the two exposures, respectively.

Figures 4.52 & 4.53 give a similar comparison for FMC2. It can be seen that during the first 2-3 days of exposure the difference in moisture loss is not that evident but the curves keep on diverging from each other thereafter. At an exposure period of 20 days for the 40mm specimen, moisture loss is found to be about 27 & 33 % respectively.

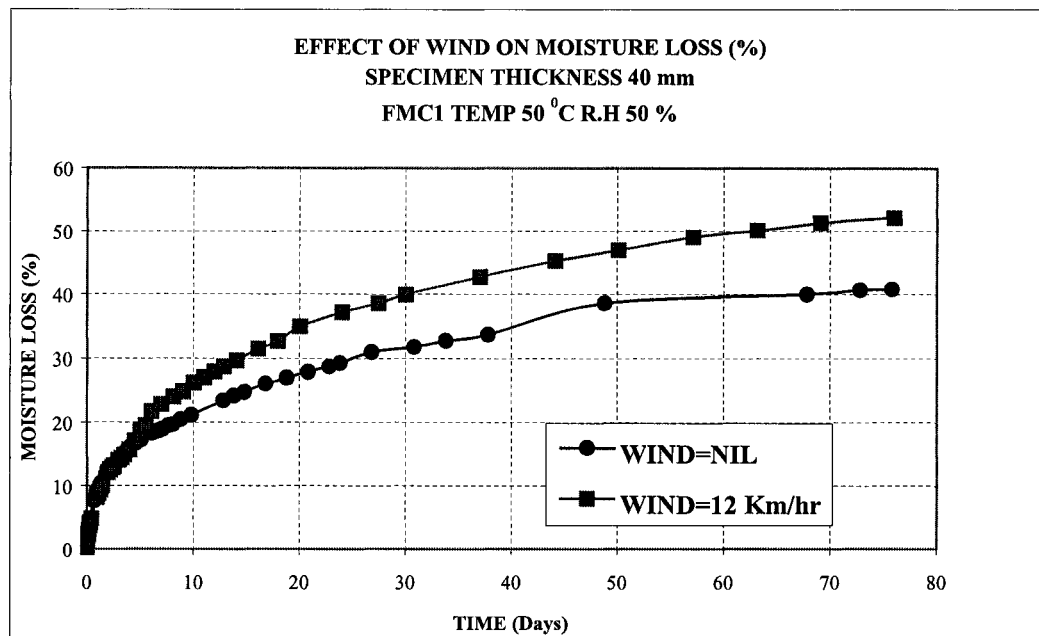


Figure 4.50: Effect of Wind on Moisture Loss (%) for FMC1,  
Specimen Thickness-40 mm

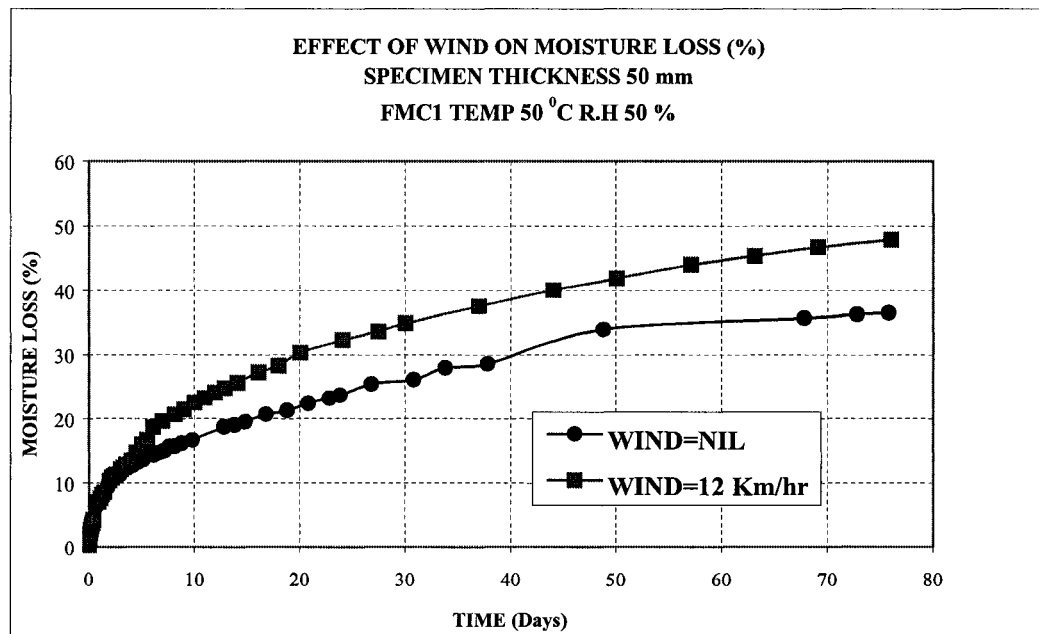


Figure 4.51: Effect of Wind on Moisture Loss (%) for FMC1,  
Specimen Thickness-50 mm

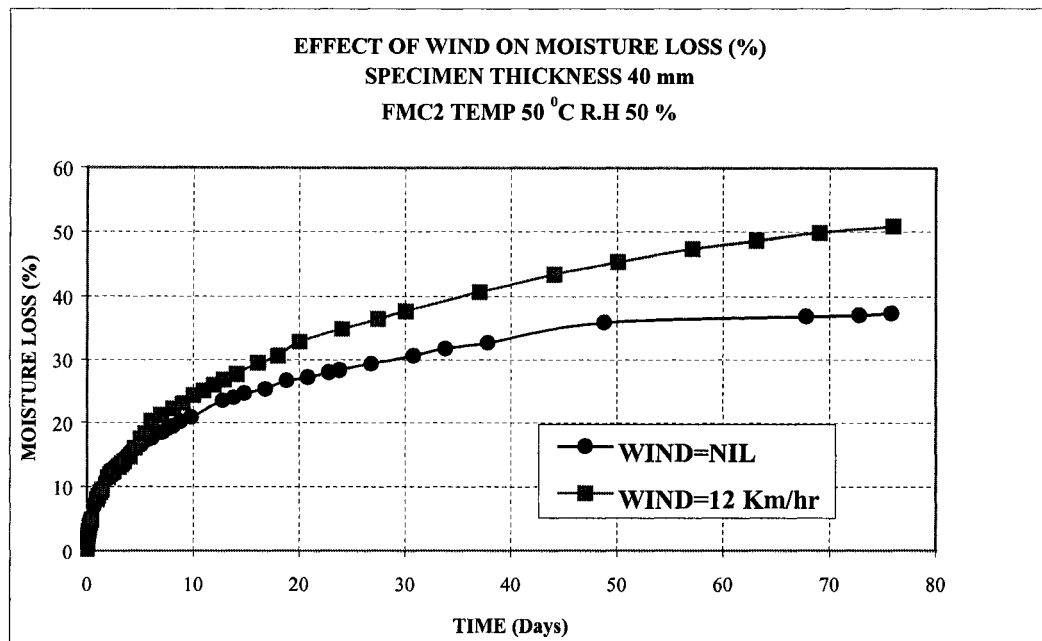


Figure 4.52: Effect of Wind on Moisture Loss (%) for FMC2,  
 Specimen Thickness-40 mm

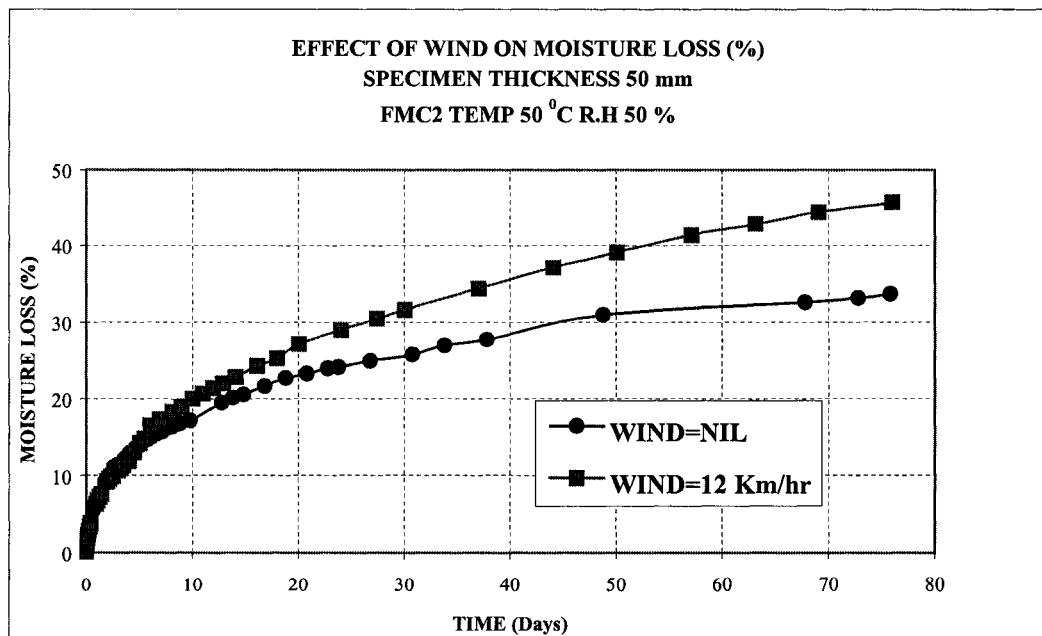


Figure 4.53: Effect of Wind on Moisture Loss (%) for FMC2,  
 Specimen Thickness-50 mm

#### **4.2.2.2 Influence of Temperature and Relative Humidity**

Drying tests were carried out on both FMC1 & FMC2 at ambient temperatures of 30 °C and 50 °C to study the effect of temperature on coefficient of moisture diffusivity (D). The effect of increase in temperature & reduction in ambient humidity on moisture loss (%) for FMC2 is presented in the following discussion

Comparison for 30 & 40 mm specimens is shown in Figures 4.54 & 4.55. At higher temperature & lower R.H the specimens lost about 41 % & 38 % of the evaporable moisture in total, whereas at lower temperature and higher R.H they lost only 11 % & 9 % respectively.

At a relative humidity of 60 % & 50 %, a maximum of 40 % & 50 % of the total evaporable moisture can be driven out of the specimen, respectively. This means that moisture loss should be higher at lower R.H values. Also there is an increase in moisture loss with the increase in temperature, as discussed in section 4.2.1.3. Since both these factors were combined here hence a significantly higher amount of moisture loss was observed.

It should be noted that comparison graphs were plotted for all specimen sizes, however to give a general idea of the behavior, results for only two have been presented in the above sections.

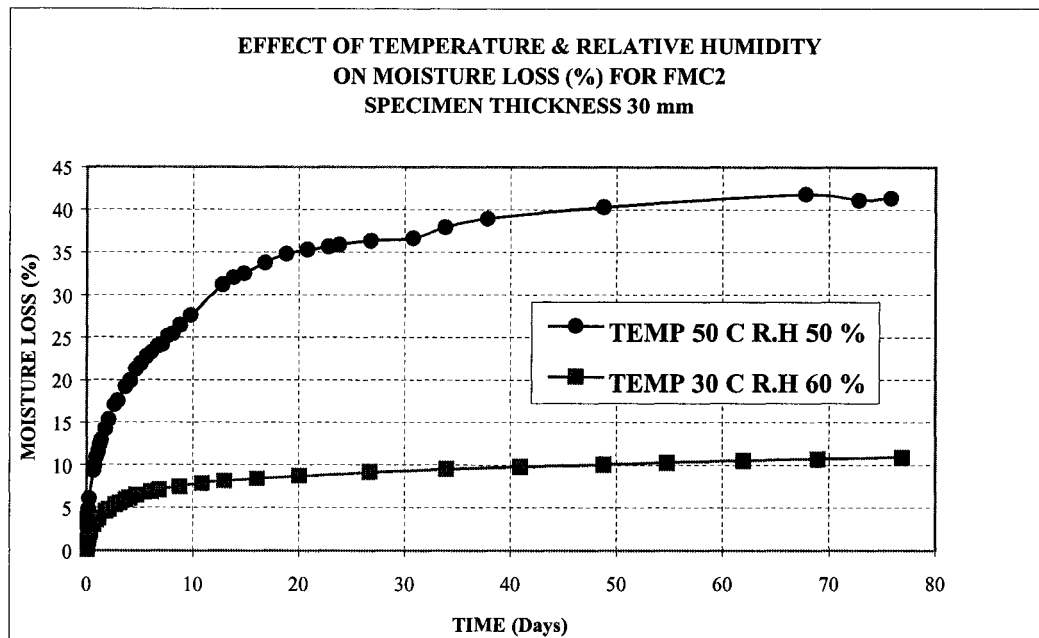


Figure 4.54: Effect of Temperature & Relative Humidity on Moisture Loss (%)  
for FMC2, Specimen Thickness-30 mm

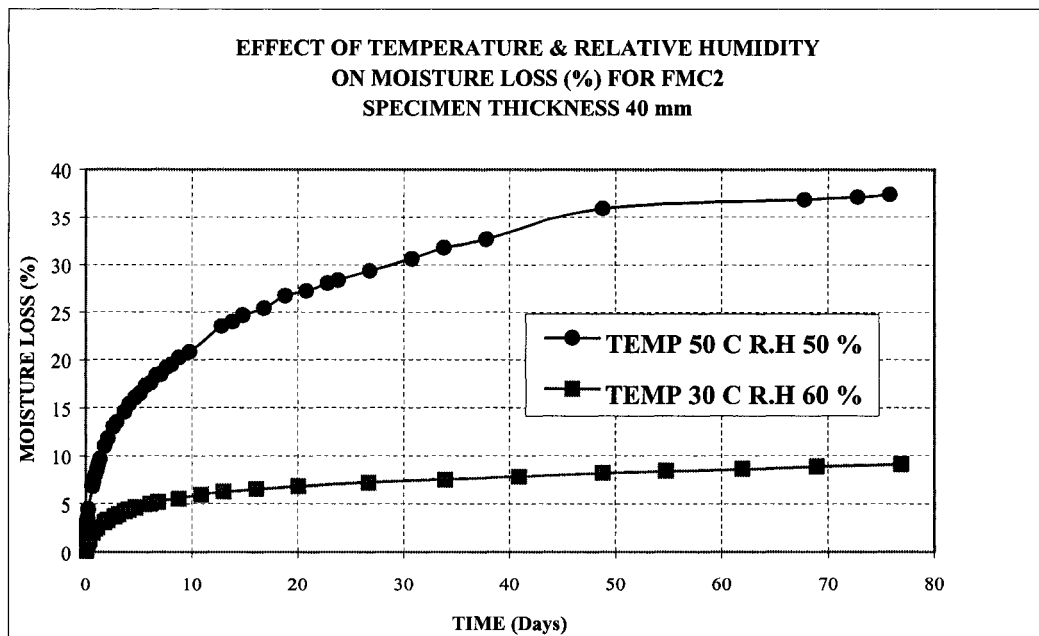


Figure 4.55: Effect of Temperature & Relative Humidity on Moisture Loss (%)  
for FMC2, Specimen Thickness 40 mm

### 4.3 Drying Shrinkage

An experimental investigation of drying shrinkage was undertaken for the concrete mixes and selected repair materials on specimens placed in the environmental chambers along with respective diffusivity specimens. Detailed results are presented and discussed in the following sections.

#### 4.3.1 Shrinkage Strains in Concrete

Figure 4.56 shows the development of shrinkage strain in specimens of each mix under a chamber temperature of **50 °C**, relative humidity of **40 %** and wind speed of **6 km/hr**. It can be seen clearly that the specimens with higher water-cement ratio attained higher shrinkage strains at each stage of drying. Similar trend was observed in terms of moisture loss also, as discussed in section 4.2.1.1. At 50 days of exposure shrinkage strain in the specimen with w/c ratio 0.45 is  $420 \times 10^{-6}$ ,  $0.5-450 \times 10^{-6}$  and  $0.6-480 \times 10^{-6}$ . Soroka [129] also reported a greater tendency to shrinkage in concrete with higher water-cement ratio or higher water content.

Figure 4.57 shows the shrinkage plots under similar exposure conditions but a wind speed of **22 km/hr** with behavior similar to that discussed above. Specimens of w/c ratio 0.45 achieved shrinkage strain of  $465 \times 10^{-6}$ ,  $0.5-520 \times 10^{-6}$  and  $0.6-560 \times 10^{-6}$  at 50 days of exposure.

Figure 4.58 and 4.59 show the shrinkage strain evolution curves for each mix under exposure temperature of **35 °C**, relative humidity of **40 %** and wind speeds of **6 km/hr** and **22 km/hr** respectively. It can be seen that after 45-48 days of exposure

specimens with w/c ratio 0.45 attained shrinkage strain of  $355 \times 10^{-6}$  &  $395 \times 10^{-6}$ , 0.5 attained  $385 \times 10^{-6}$  &  $440 \times 10^{-6}$ , while those of 0.6 achieved  $410 \times 10^{-6}$  &  $475 \times 10^{-6}$ , respectively under each exposure.

It can be observed from the above discussion that under high wind speed and high temperature, rate of development of shrinkage strain increases, which is because of the higher rate of moisture loss. This trend is similar to that mentioned in a recent publication of cement and concrete association of Australia [124], which reports that higher drying shrinkage is to be expected with the increase in ambient temperature, decrease in relative humidity, increase in air movement/wind speed around concrete and with the increase in the length of time for which concrete is exposed to drying conditions.

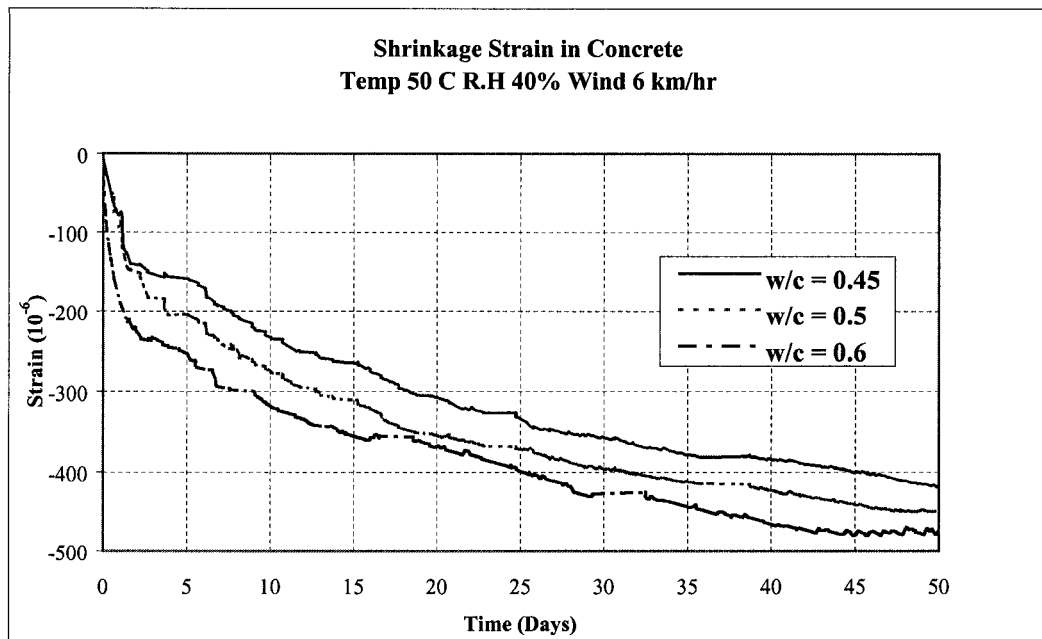


Figure 4.56: Shrinkage strain in Concrete at 50  $^{\circ}$ C, 40 % R.H & 6 km/hr Wind

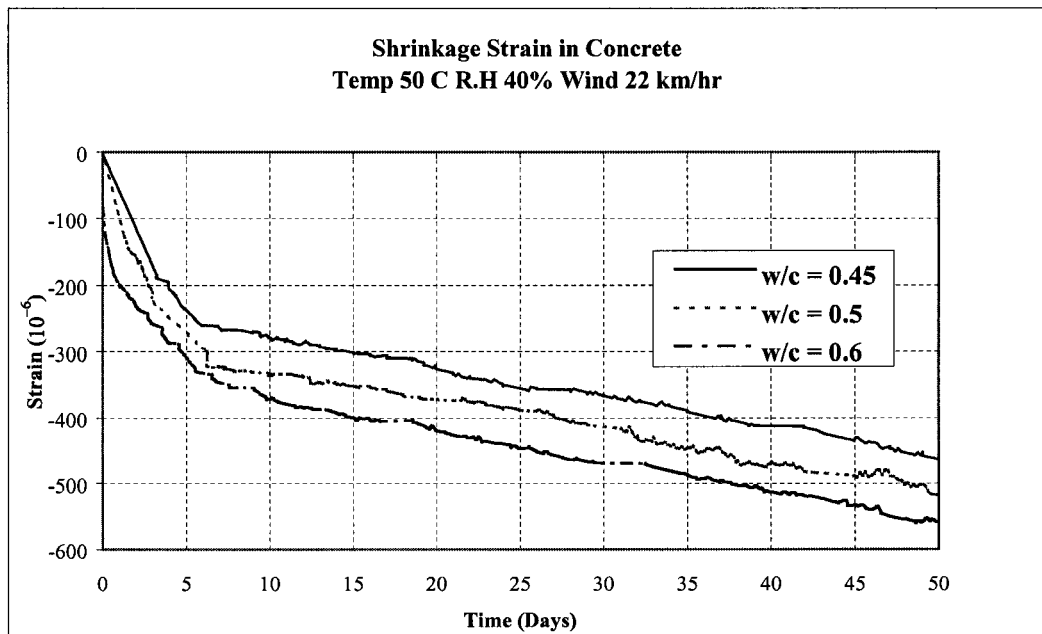


Figure 4.57: Shrinkage strain in Concrete at 50  $^{\circ}$ C, 40 % R.H & 22 km/hr Wind

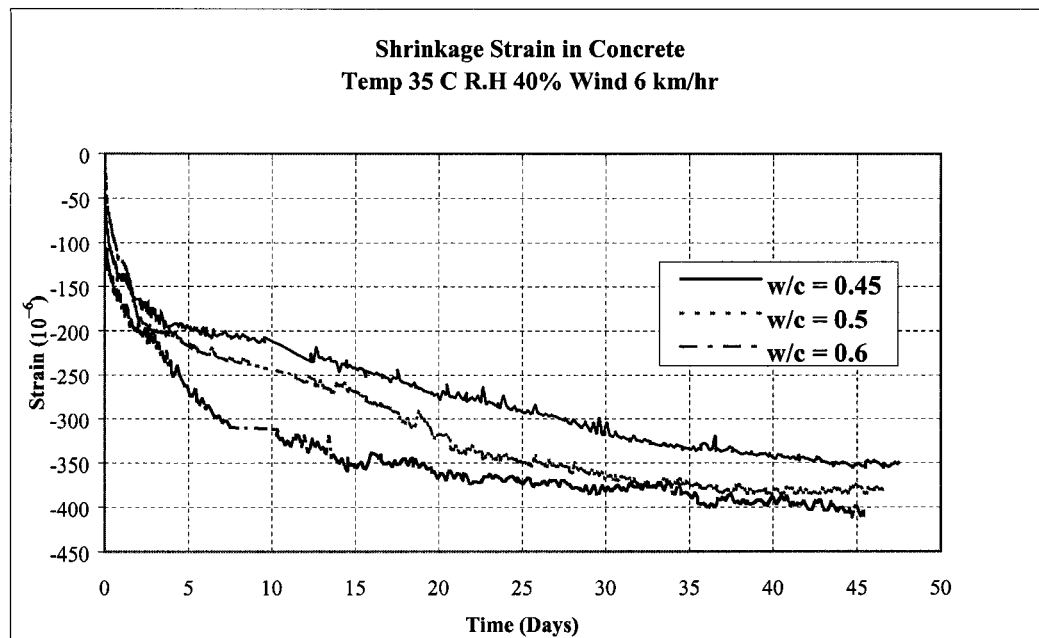


Figure 4.58: Shrinkage strain in Concrete at 35  $^{\circ}$ C, 40 % R.H & 6 km/hr Wind

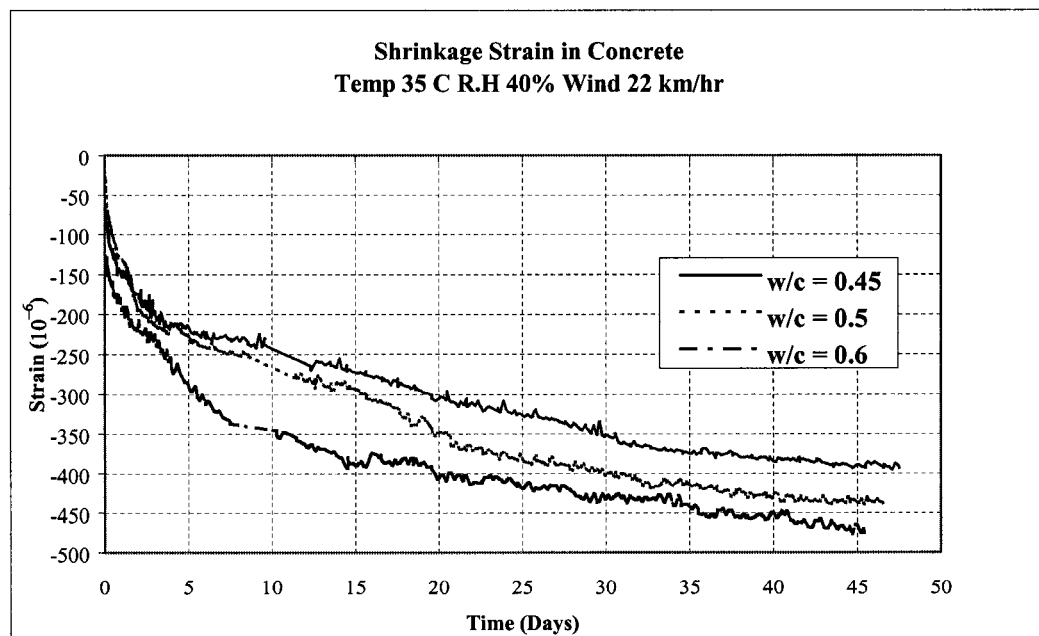


Figure 4.59: Shrinkage strain in Concrete at 35  $^{\circ}$ C, 40 % R.H & 22 km/hr Wind

### 4.3.2 Shrinkage Strain in Repair Materials

Shrinkage tests were conducted on specimens of FMC1 and FMC2 under an exposure temperature of  $50^{\circ}\text{C}$  and relative humidity of 50 % only, to compare both the repair materials and the repair materials and concrete in terms of their corresponding shrinkage strain values.

Figure 4.60 shows that FMC1 attained shrinkage strain of  $800 \times 10^{-6}$ , whereas, FMC2 achieved  $750 \times 10^{-6}$  after 45 days of exposure. Thus FMC1 has slightly higher shrinkage, which is due to a higher rate of moisture loss as observed in section 4.2.2.

The average shrinkage strain in concrete at 50 days of exposure, under roughly similar exposure conditions, is about 60 % of that in repair materials. This can be attributed to the to the bigger specimen size and the restraining effect in concrete coming from the coarse aggregates, as reported by Al-Mudaiheem & Hansen [127]& Mokarem [130].

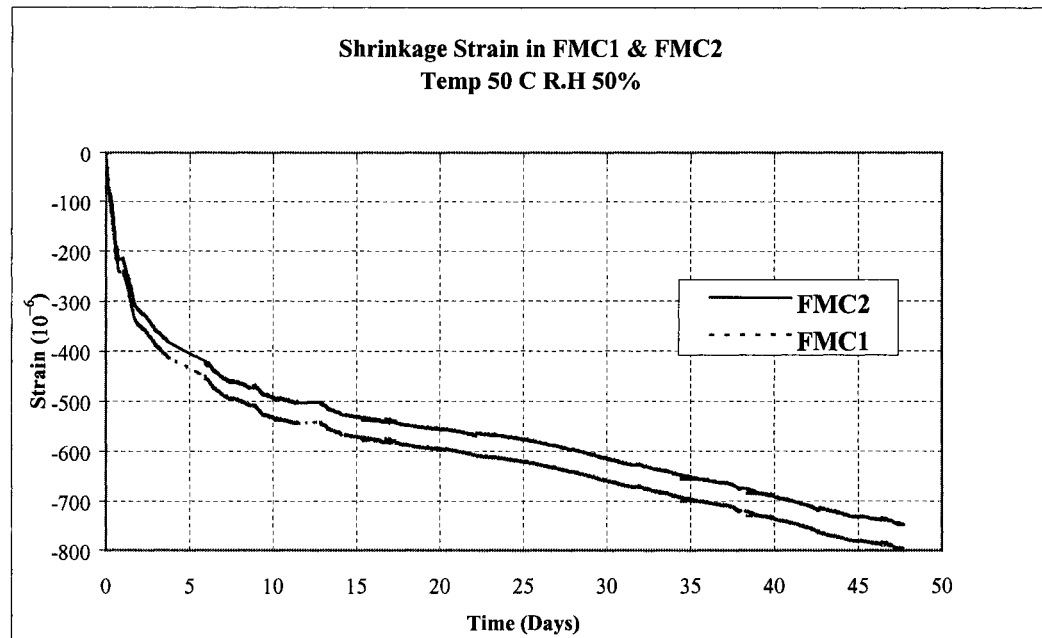


Figure 4.60: Shrinkage strain in FMC1 & FMC2 at 50 °C & 50 % R.H

## CHAPTER 5

# NUMERICAL COMPUTATION OF MOISTURE DIFFUSIVITY

### 5.1 Introduction

Different methods available for the computation of moisture diffusivity were described in section 2.7. Procedure adopted for the computation of moisture diffusivity in this study is based on the work of Rahman [25]. A combined experimental-numerical approach is used utilizing results from the drying tests and running a non-linear 2-D finite element model, **DIANA-2D (Diffusion Analysis)**, developed by him. He used a phenomenological approach in which various transport mechanisms were lumped together by defining the “diffusivity” of the material at macroscopic level. Diffusivity hence became the rate of vapor and liquid transport in the domain of the system without distinction of the different flow mechanisms, which were considered in an integral form. Hence diffusivity was considered to be dependent on moisture concentration in spatial domain of the system, which rendered the boundary value problem non-linear.

The governing non-linear differential equation for moisture diffusion in the domain of a generalized 3-D solid in terms of the moisture content in the solid can be written as:

$$\frac{\partial C(x_k, t)}{\partial t} = \frac{\partial}{\partial x_i} \left[ D(C) \frac{\partial C(x_k, t)}{\partial x_i} \right] \quad (5.1)$$

Where

$$k = 1, 2, 3 \quad i = 1, 2, 3$$

$C = C(x_i, t)$  is the moisture content varying in domain and with time

$D(C)$  is the isotropic moisture diffusivity coefficient being function of  $C$

Moisture diffusion at the boundary/surface of the solid is considered in the form of a convective boundary condition and can be written as:

$$D(C) \frac{\partial C(x_i, t)}{\partial x_i} n_i = h_f (C_e - C_s) \quad (5.2)$$

Where

$\frac{\partial C}{\partial x_i} n_i$  is the moisture gradient at the drying surface with a unit normal 'n'

$h_f$  is the surface factor or convective transfer coefficient

$C_s$  is the moisture content at the solid surface

$C_e$  is the moisture content/relative humidity of the ambience

## 5.2 Description of DIANA-2D

The program DIANA-2D (written in FORTRAN) is used to compute the moisture content history in a cementitious material due to moisture diffusion in the system. Owing to the dependence of diffusivity on moisture concentration and hence the non-linear nature of the problem, explicit analytical solution is not possible and such a model becomes necessary for the solution of the moisture diffusion equation.

### 5.2.1 Governing Finite Element Equations

The matrix differential equation governing moisture diffusion in any typical 2-D element in a finite element system and used in DIANA-2D is as follows:

$$[M_D]^e \{C\}^e + [V]^e \left\{ \dot{C} \right\}^e + [M_s]^s \{C\}^s = \{F\}^e \quad (5.3)$$

Where

$[M_D]^e$	Element moisture diffusivity matrix
$[V]^e$	Moisture velocity matrix
$\{F\}^e$	Moisture loading vector
$\{C\}^e$	Nodal moisture content
$\left\{ \dot{C} \right\}^e$	Nodal moisture content differentiated with respect to time
$[M_s]^s$	Moisture diffusivity matrix contribution from surface diffusion

$\{C\}^s$  Nodal moisture content of diffusing surface nodes

For 'N' denoting the element nodal shape functions,  $\Omega$  representing the domain of the element and  $\Gamma$  showing the boundary of the element

$$[M_D]^e = \int_{\Omega_e} D(C) \left[ \frac{\partial N^T}{\partial x} \frac{\partial N}{\partial x} \right] d\Omega_e \quad (5.4)$$

$$[V]^e = \int_{\Omega_e} N^T N d\Omega_e \quad (5.5)$$

$$[M_s]^s = h_f \int_{\Gamma} N^T N d\Gamma \quad (5.6)$$

$$\{F\}^e = h_f C_e \int_{\Gamma} N d\Gamma \quad (5.7)$$

The  $[M_s]^s$  matrix is added at appropriate locations to the  $[M_D]^e$  matrix to obtain the total element moisture diffusivity matrix  $[M]^e$ . Equation 5.3 thus takes the final form:

$$[M]^e \{C\}^e + [V]^e \left\{ \dot{C} \right\}^e = \{F\}^e \quad (5.8)$$

DIANA-2D solves equation 5.8 over the finite element domain to obtain nodal moisture content as a function of time. The transient nature of this equation is accounted for in the model by a step-by-step time integration scheme.

Weighted residual FEM in time domain is used to obtain the recurrence relationship for solving the transient moisture diffusion equation. To solve for unknown moisture content at any time  $t_{i+1}$ , in the finite element domain, the following relationship was obtained:

$$[A]\{C_{i+1}\} = [P]\{C_i\} + \{F^*\} \quad (5.9)$$

Where

$$[A] = [V] + [M]\theta\Delta t_i \quad (5.10)$$

$$[P] = [V] - (1 - \theta)[M]\Delta t_i \quad (5.11)$$

$$\{F^*\} = \theta\{F_{i+1}\}\Delta t_i + (1 - \theta)\{F_i\}\Delta t_i \quad (5.12)$$

Where  $\theta$  is the controlling parameter, with its value depending on the type of finite difference scheme used for these time computations.

### 5.2.2 Functional Form of Diffusivity

Different investigators have used different mathematical forms for the dependence of coefficient of moisture diffusivity ( $D$ ) on moisture content ( $C$ ). Bazant and Najjar [17] proposed an S-shaped curve for diffusivity coefficient as a function of pore humidity ( $h$ ):

$$D(h) = D_1 \left[ \alpha + \frac{1 - \alpha}{1 + \left( \frac{1 - h}{1 - h_c} \right)^n} \right] \quad (5.13)$$

Where

$D_1$ ,  $\alpha$ ,  $h_c$  and  $n$  are the parameters of the model

Philajavaara and Vaisanen [32] proposed a power function for diffusivity coefficient:

$$D(C) = p_1 + p_2 (C)^{p_3} \quad (5.14)$$

Where  $p_1$ ,  $p_2$  and  $p_3$  are the regression coefficients.

Mensi et al. [142] used exponential form of diffusivity relationship:

$$D(C) = P_1 \exp(P_2 C) \quad (5.15)$$

Penev and Kawamura [37] proposed hyperbolic expressions for diffusivity:

$$D = D_0 + a \left( \frac{C}{1-C} \right)^b \quad (5.16)$$

Where ‘a’ & ‘b’ are regression parameters and  $D_0$  is the diffusivity at oven dry conditions ( $C = 0\%$ ).

Pleinert et al. [18] proposed a polynomial form for diffusivity:

$$D(C) = p_1 + p_2 C + p_3 C^2 + p_4 C^3 \quad (5.17)$$

Where  $p_1$ ,  $p_2$ ,  $p_3$  and  $p_4$  are the regression parameters.

Rahman [25] however observed that the moisture loss ~ time curves for repair materials are steep at early ages, which correspond to the loss of water from large capillary pores and later the rate of moisture loss becomes extremely slow characterizing a low diffusivity of the materials. He incorporated the following functional form for diffusivity into **DIANA-2D**:

$$D(C) = b_0 \tan(b_1 C^n) \quad (5.18)$$

Where  $b_0$ ,  $b_1$  and  $n$  are diffusivity parameters evaluated for best fit.

### 5.2.3 Role of Convective Transfer Coefficient

Solution of the non-linear diffusion equation also requires the specification of initial and boundary conditions. Rahman [25] assumed the initial condition as the initial saturated state with a uniform moisture content  $C_0$  specified over the entire domain and specified a convective boundary condition at the edges of the 2-D element, in terms of the convective transfer coefficient ( $h_f$ ). He then carried out 2-D finite element computation for repair mortars, using DIANA-2D, with the assumed diffusivity law and associated parameters to ascertain the effect of  $h_f$  on moisture loss and found that it affects the initial slope of the moisture loss ~ time curves. Figure 5.1 shows the qualitative effect of varying  $h_f$  on the moisture loss evolution curves.

### 5.2.4 Procedure for Computation of Diffusivity

A half model of cross section of the experimental specimen is always considered for DIANA-2D [Figure 5.2]. Geometry of the specimen model, initial and boundary conditions, experimental moisture loss data & preliminary estimated values of the diffusivity law parameters are incorporated in the input file used for running DIANA-2D. It computes moisture loss over the entire domain of the specimen followed by the computation of mean moisture loss at specified time intervals. Based on the method of least squares it then uses the following equation to compute a residual or functional error:

$$Error = \sum_{t=0}^{ntime} [W_{ex}(t) - W_{fe}(t)]^2 \quad (5.19)$$

Where

$W_{ex}(t)$  is the mean experimental moisture loss at any time

$W_{fe}(t)$  is the mean moisture loss computed from the finite element run

Varying the assumed parameter values, iterative runs of the program are then carried out and values of the parameters for which the error is below a certain specified tolerance give the best fit. Parameter values hence selected are then used to carry out analysis on specimens of other thickness and hence tuned for goodness of fits. The effect of different exposure conditions is captured into the model by employing different values of diffusivity law parameters and convective transfer coefficient.

The step-by-step computational strategy used in DIANA-2D for moisture content determination at any time interval is presented in the Figure 5.3. Figure 5.4 shows flowchart of the subroutines and steps followed in DIANA-2D.

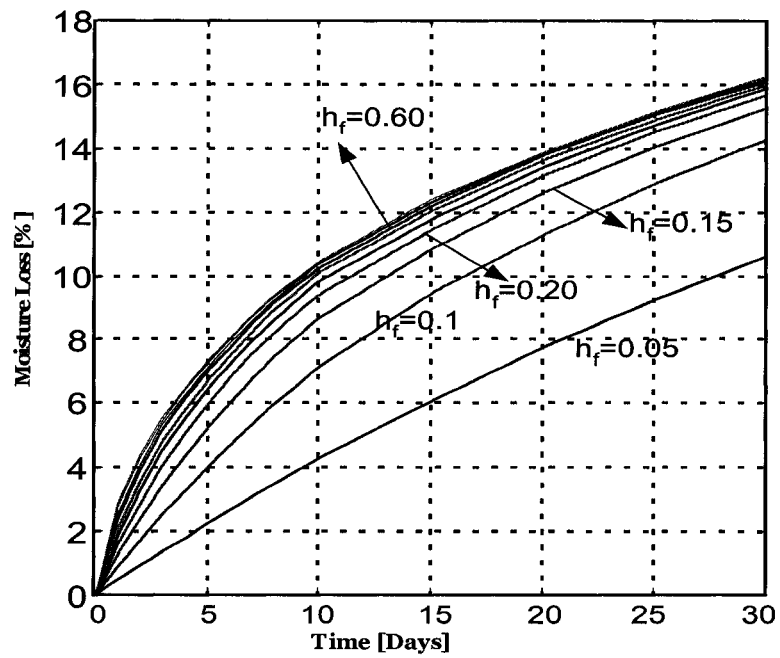


Figure 5.1: Influence of Convective Transfer Coefficient on Moisture Loss

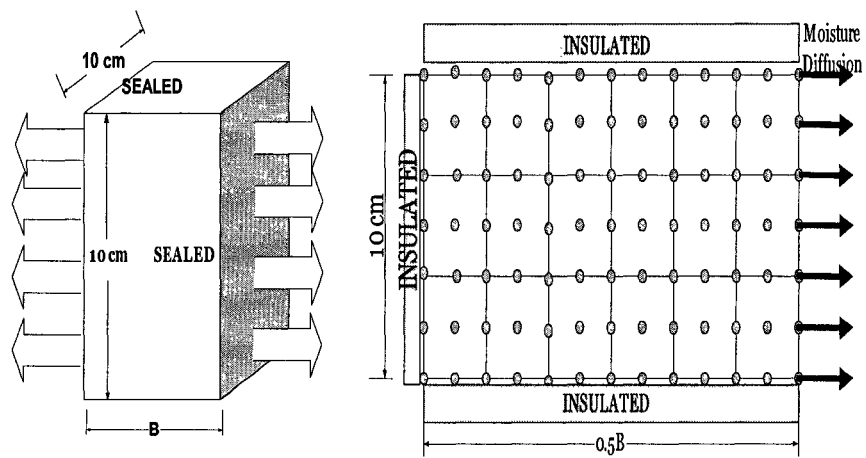


Figure 5.2: Finite Element Discretization of Diffusivity Specimen for DIANA-2D

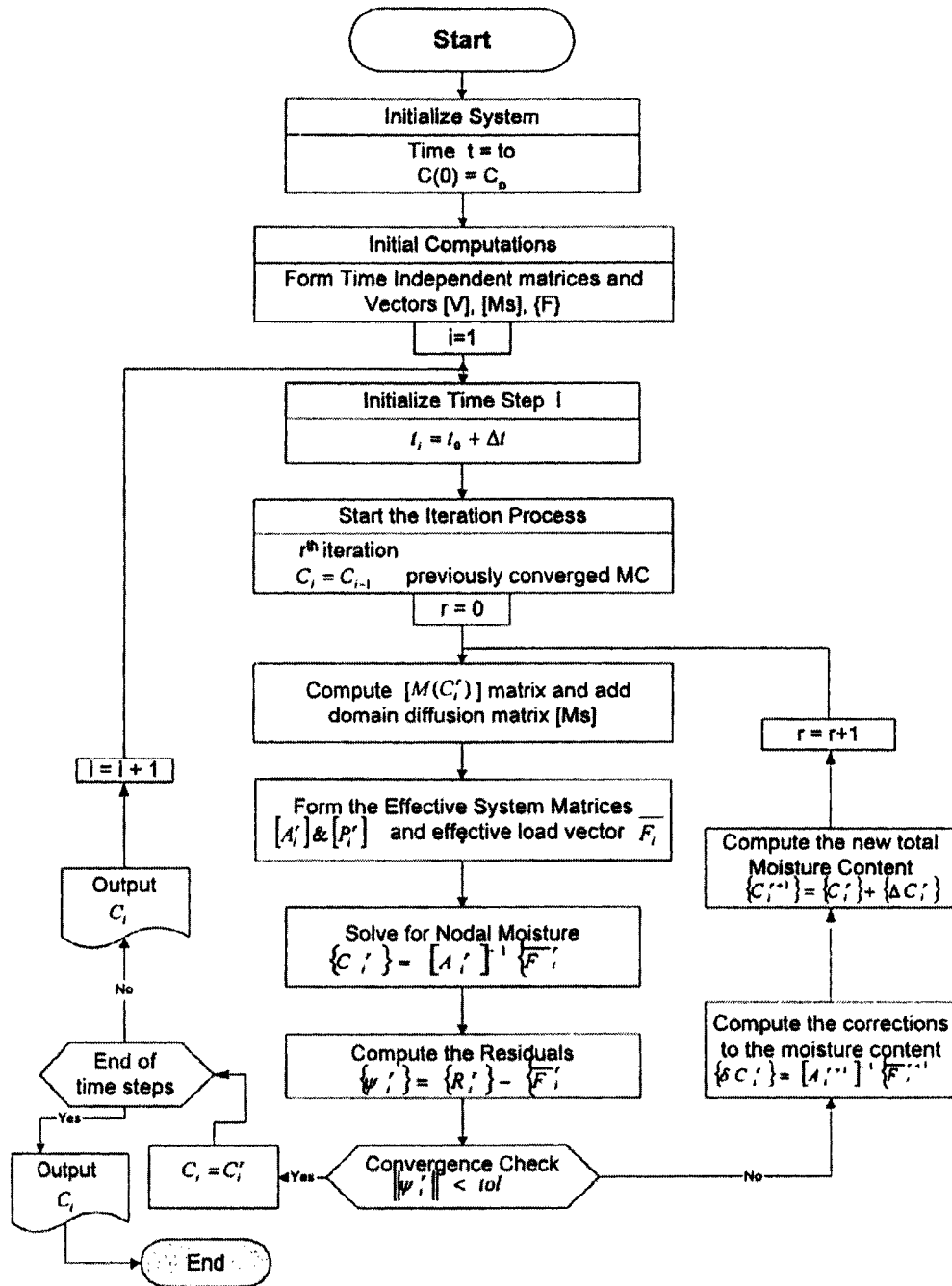


Figure 5.3: Flow Chart for Time Step Computations of Moisture Content in DIANA-2D

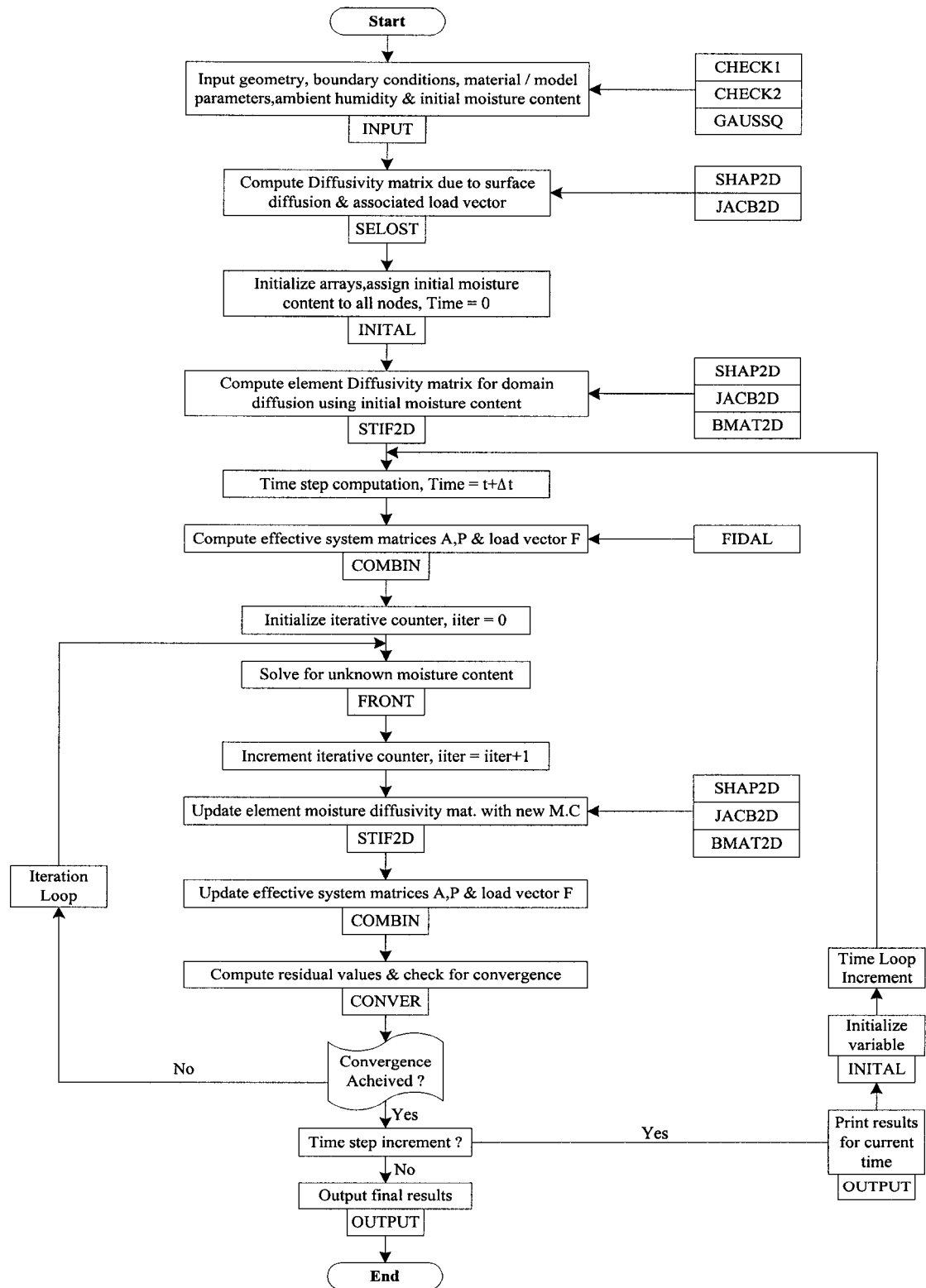


Figure 5.4: Basic Flow Chart of Finite Element Program DIANA-2D

### 5.3 Best Fit Diffusivity Law Parameters for Concrete

Numerical computation of diffusivity law parameters ( $b_0$ ,  $b_1$  &  $n$ ) of Eqn. 5.18 and convective transfer coefficient  $h_f$ , were carried out for the specimens of each concrete mix under each exposure regime using DIANA-2D, following the procedure described in section 5.2.4. For each case iterative runs were first carried out for the 100x100x75 mm specimen to ascertain values of  $b_0$ ,  $b_1$ ,  $n$  &  $h_f$  which best fit the experimental data for moisture loss (%) versus time. Later the computed parameter values were verified by running the model for specimens of other thickness and fine-tuned.

It should be noted here that for each different run of the model, a new input file has to be prepared. A sample input file is given in appendix A.

#### 5.3.1 Parameters at 50 °C & 6 km/hr Wind

For water-cement ratio 0.45 and specimen size of 100x100x75 mm, Figure 5.5 shows that for the selected parameter values, computed mean moisture loss gives a good fit with the experimental mean moisture loss data. Same parameter values were then used in the model when checking for other specimens with varying thickness of 25, 50 and 100 mm. The resulting good fits for each thickness confirmed these parameter values, given in Table 5.1. Fit for specimen thickness of 100 mm is shown in Figure 5.6.

Similar procedure was followed for the specimens of water-cement ratio 0.5. Figure 5.7 & 5.8 show the fits for 75 & 100 mm specimens. Selected parameter values give a very good fit with the experimental moisture loss data.

Next DIANA-2D was used to find the diffusivity parameters for specimens of water-cement ratio 0.6. Comparison of the computed and experimental results is presented in Figures 5.9 & 5.10. Again excellent fits were obtained for the selected parameters. The parameter values, as given in table 5.1.

### **5.3.2 Parameters at 50 °C & 22 km/hr Wind**

Diffusivity parameters for specimens of each mix under this exposure regime were also determined in a similar fashion. Figures 5.11 & 5.12 show the comparison of computed and experimental moisture loss for specimens of 75 & 100 mm thickness respectively, for the w/c ratio 0.45.

Next the diffusivity parameters were obtained for specimens of w/c ratio 0.5. Figures 5.13 & 5.14 show good agreement between the computed and experimental mean moisture loss data. Results for w/c 0.6 are presented in Figures 5.15 & 5.16. Selected parameter values for all of these cases are also reported in Table 5.1.

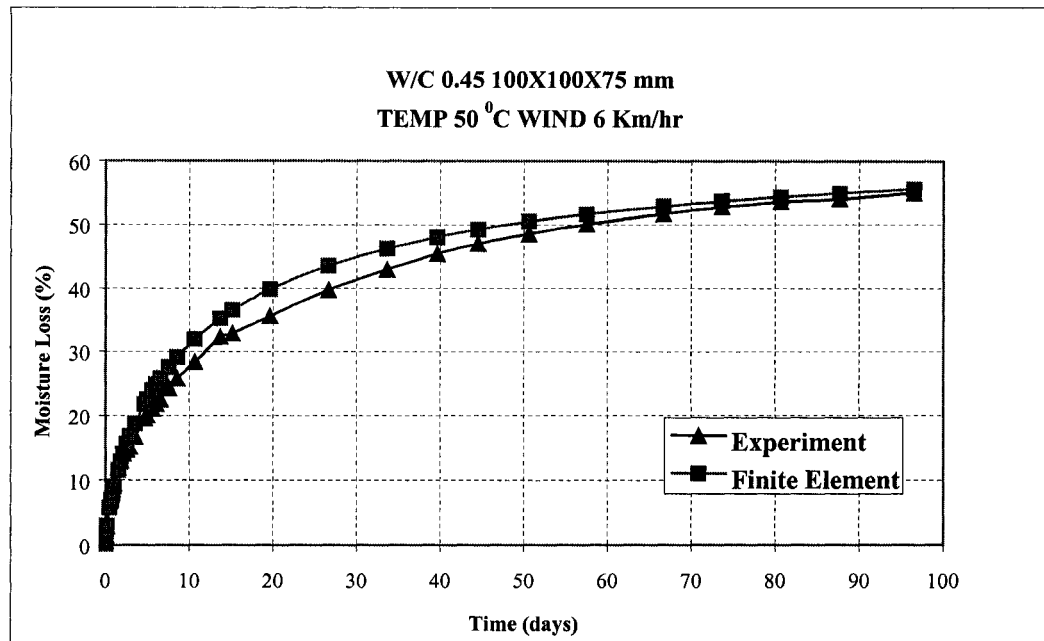


Figure 5.5: Computed & Experimental Mean Moisture Loss (%) for  
W/C 0.45 - 100x100x75 mm Specimen at 50 °C & 6 km/hr Wind

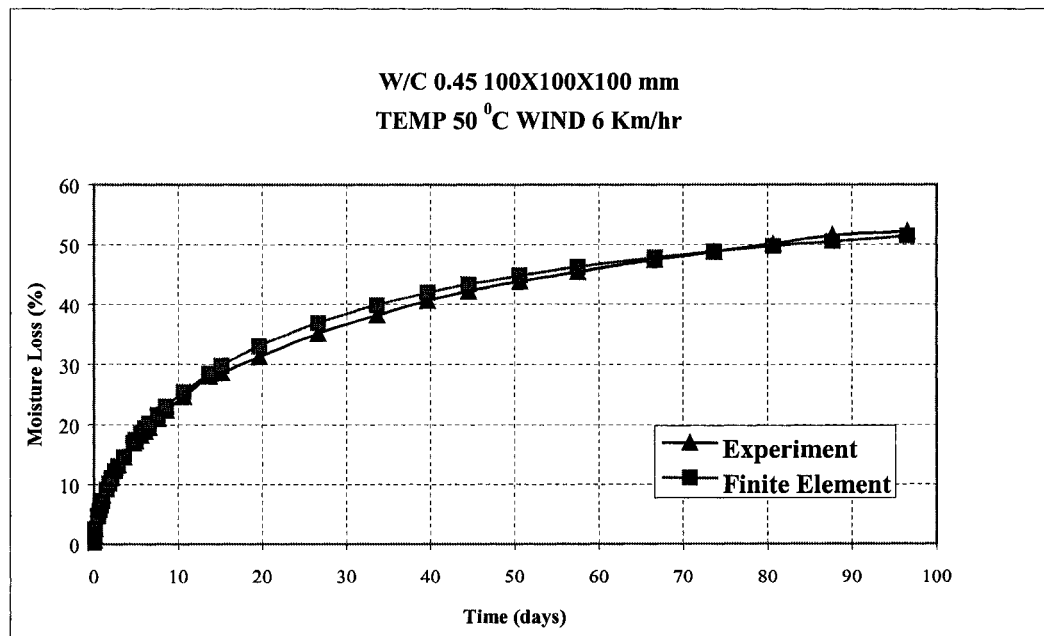


Figure 5.6: Computed & Experimental Mean Moisture Loss (%) for  
W/C 0.45 - 100x100x100 mm Specimen at 50 °C & 6 km/hr Wind

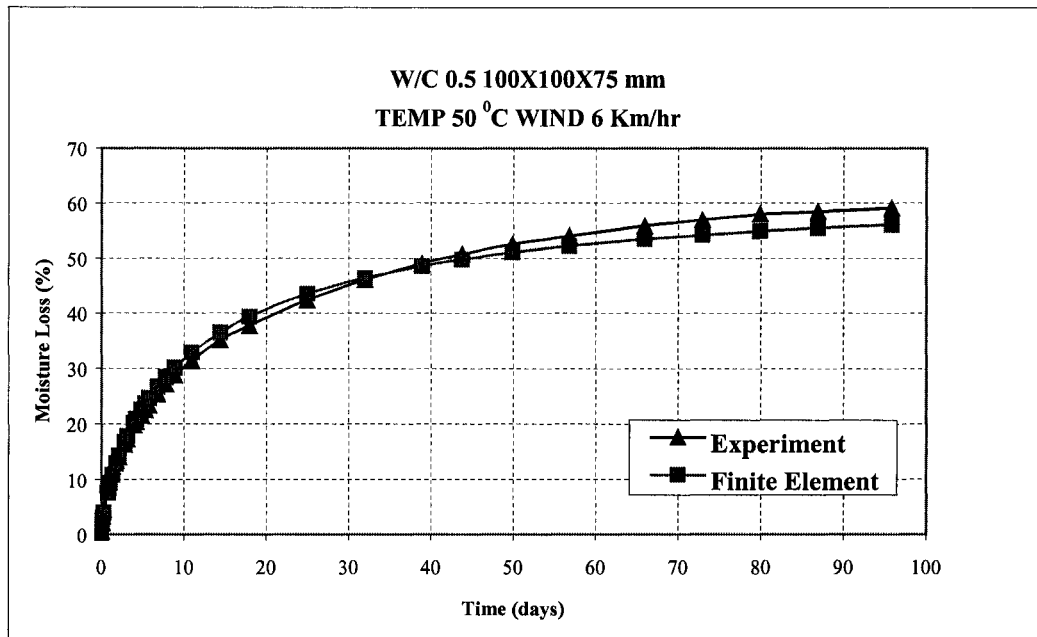


Figure 5.7: Computed & Experimental Mean Moisture Loss (%) for  
W/C 0.5 - 100x100x75 mm Specimen at 50 °C & 6 km/hr Wind

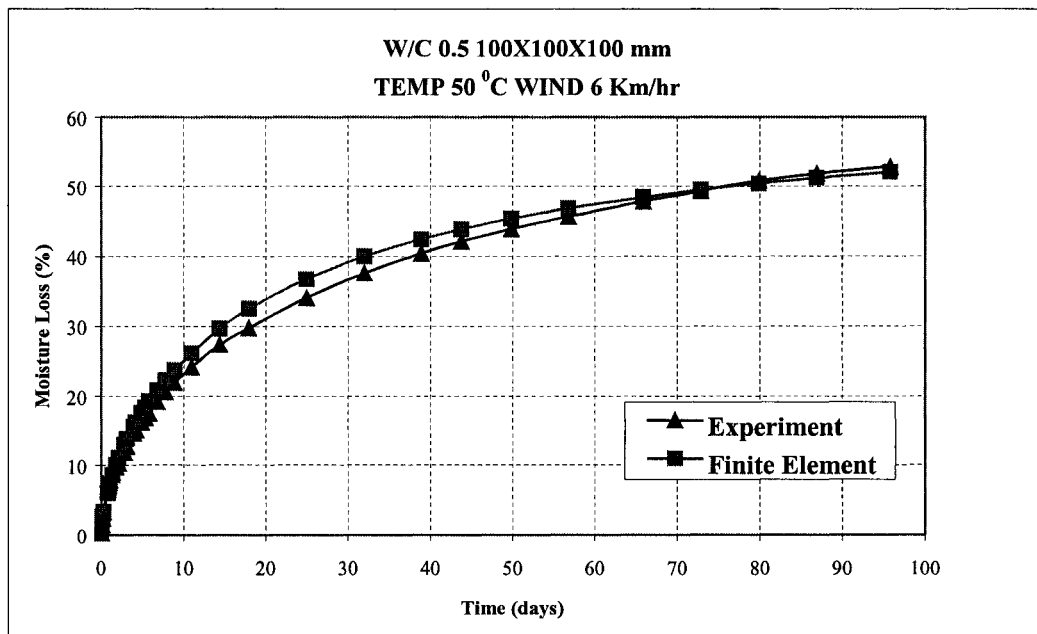


Figure 5.8: Computed & Experimental Mean Moisture Loss (%) for  
W/C 0.5 - 100x100x100 mm Specimen at 50 °C & 6 km/hr Wind

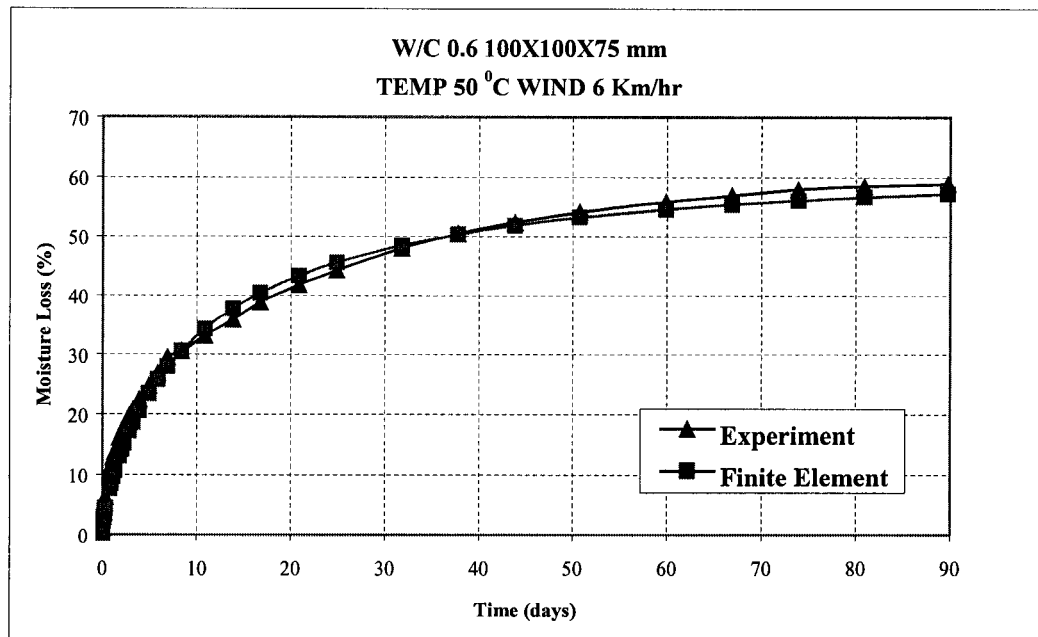


Figure 5.9: Computed & Experimental Mean Moisture Loss (%) for  
W/C 0.6 - 100x100x75 mm Specimen at 50 °C & 6 km/hr Wind

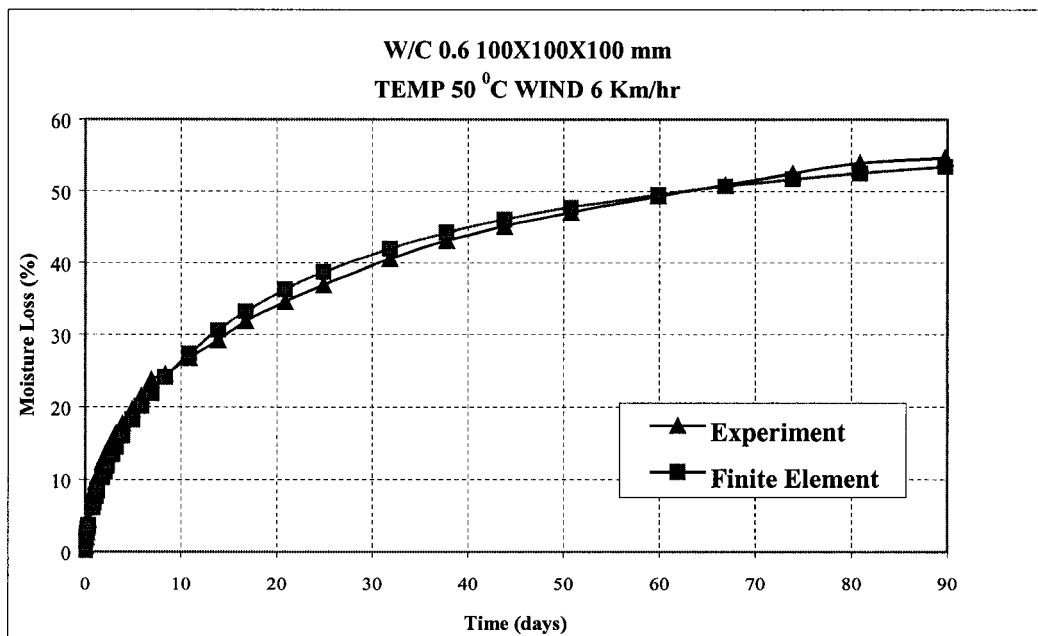


Figure 5.10: Computed & Experimental Mean Moisture Loss (%) for  
W/C 0.6 - 100x100x100 mm Specimen at 50 °C & 6 km/hr Wind

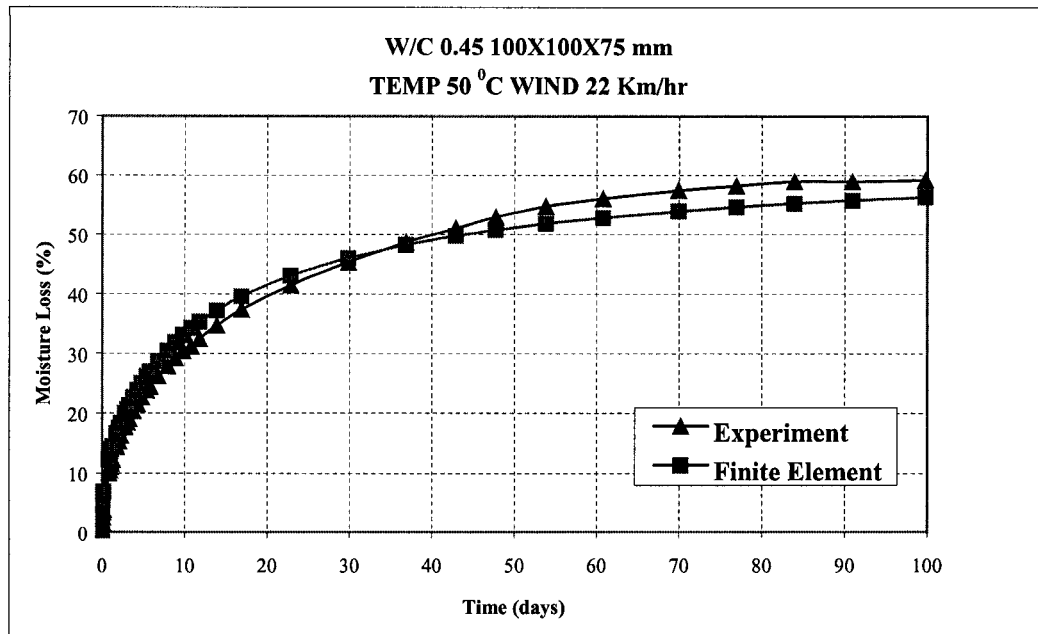


Figure 5.11: Computed & Experimental Mean Moisture Loss (%) for  
W/C 0.45 - 100x100x75 mm Specimen at 50 °C & 22 km/hr Wind

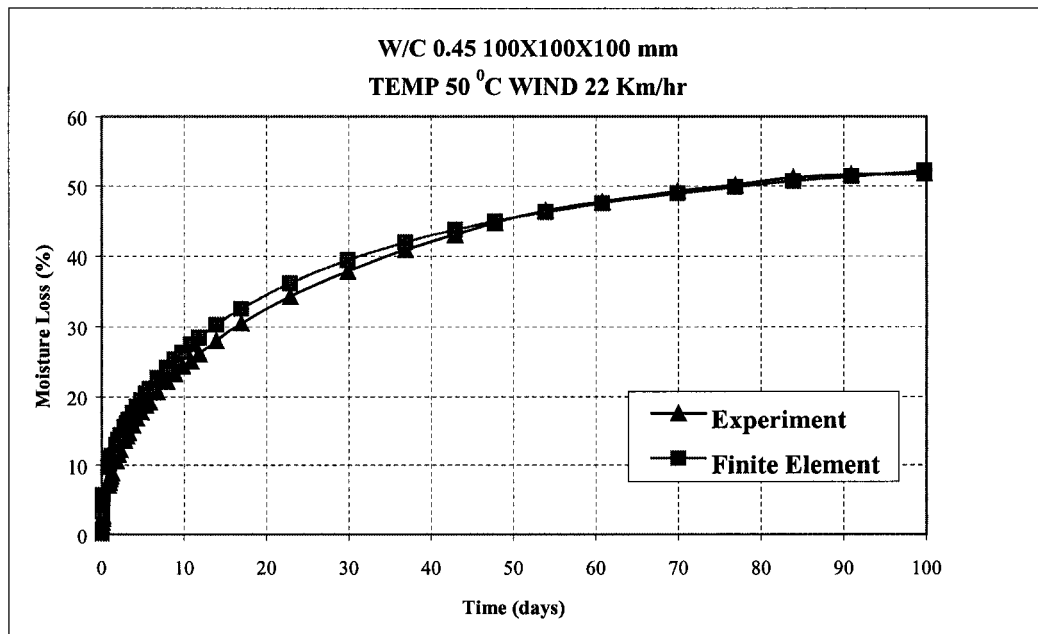


Figure 5.12: Computed & Experimental Mean Moisture Loss (%) for  
W/C 0.45 - 100x100x100 mm Specimen at 50 °C & 22 km/hr Wind

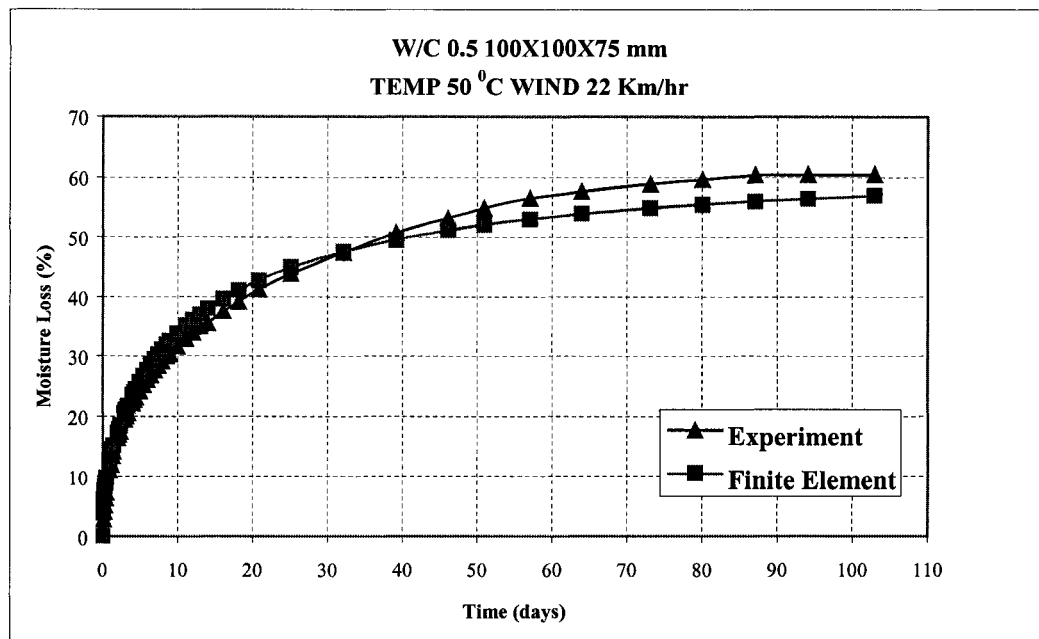


Figure 5.13: Computed & Experimental Mean Moisture Loss (%) for  
W/C 0.5 - 100x100x75 mm Specimen at 50 °C & 22 km/hr Wind

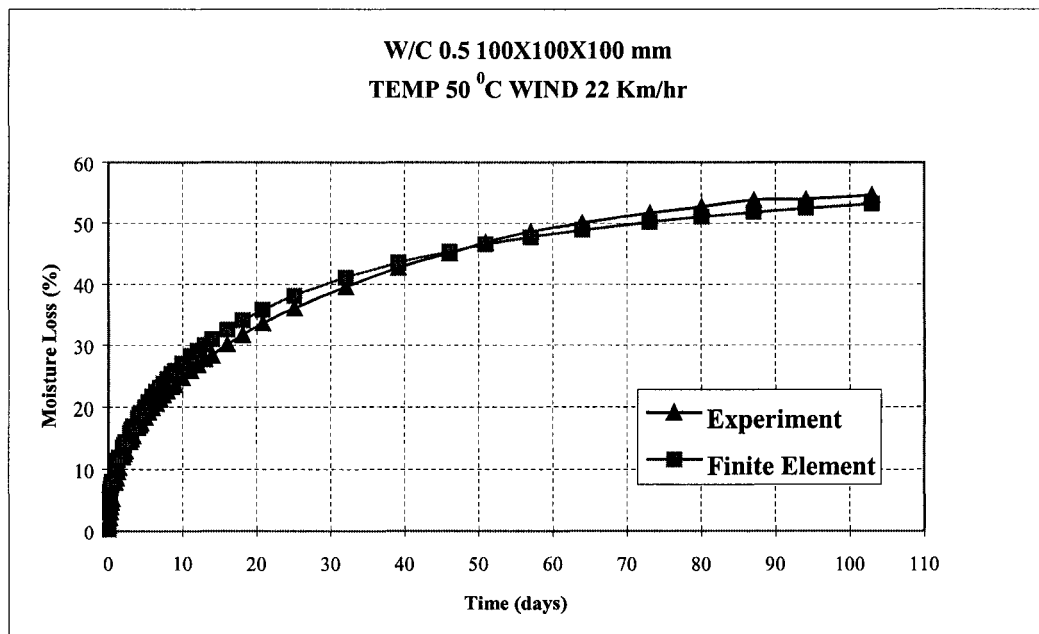


Figure 5.14: Computed & Experimental Mean Moisture Loss (%) for  
W/C 0.5 - 100x100x100 mm Specimen at 50 °C & 22 km/hr Wind

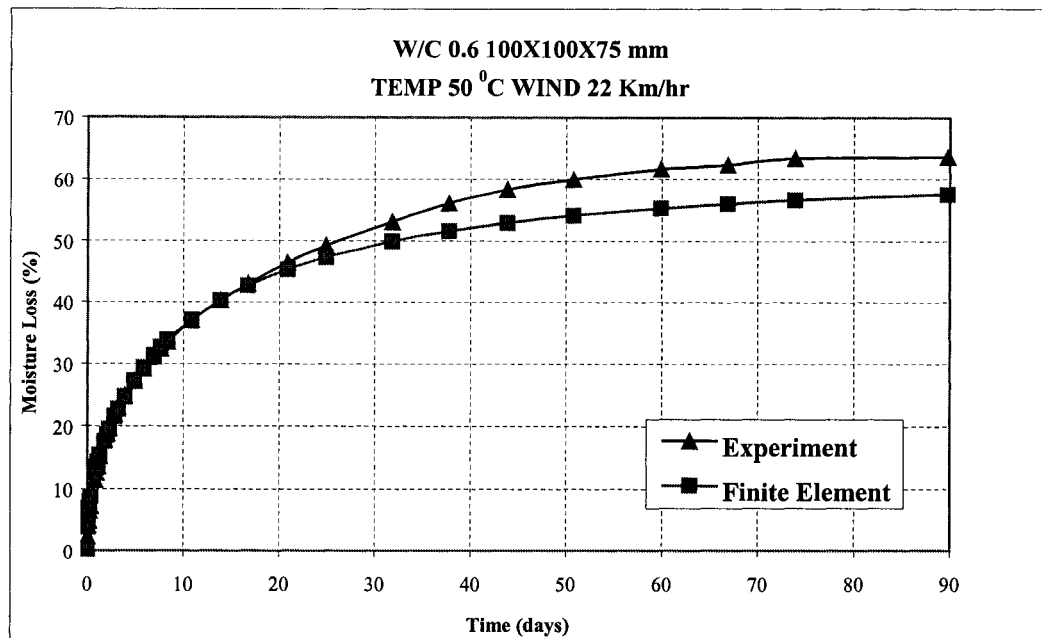


Figure 5.15: Computed & Experimental Mean Moisture Loss (%) for  
W/C 0.6 - 100x100x75 mm Specimen at 50 °C & 22 km/hr Wind

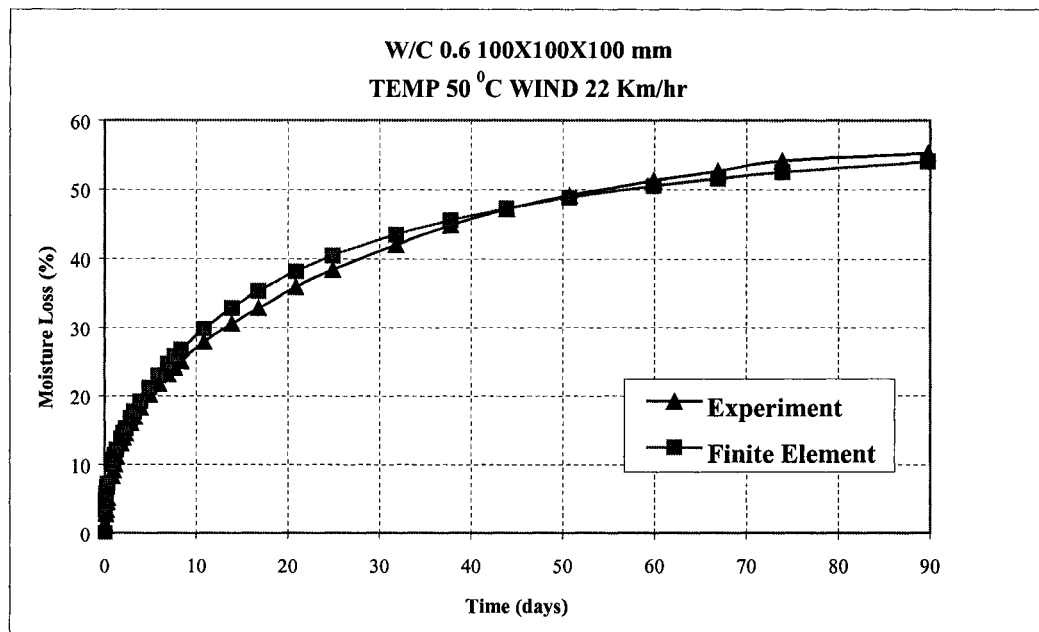


Figure 5.16: Computed & Experimental Mean Moisture Loss (%) for  
W/C 0.6 - 100x100x100 mm Specimen at 50 °C & 22 km/hr Wind

### **5.3.3 Parameters at 35 °C & 6 km/hr Wind**

For the selected parameter values, comparison plots of mean experimental and computed moisture loss for each mix under this exposure, for specimens of 75 & 100 mm thickness, are given in Figures 5.17-5.22 & the parameter values are reported in Table 5.1.

### **5.3.4 Parameters at 35 °C & 22 km/hr Wind**

Similar procedure was followed again to determine the best-fit values of  $b_0$ ,  $b_1$ ,  $n$  &  $h_f$ , for specimens of each mix under this exposure set up. Figures 5.23-5.28 show the comparison of computed and experimental moisture loss for specimens of 75 & 100 mm thickness.

It should be noted here that moisture loss curve fitting was done for all specimen sizes, however representative results for only two are presented here. From the above discussion it becomes evident that for the selected parameter values, DIANA-2D gave excellent match with the experimental moisture loss data for concrete specimens of different water-cement ratios having 1-D moisture diffusion under different exposures.

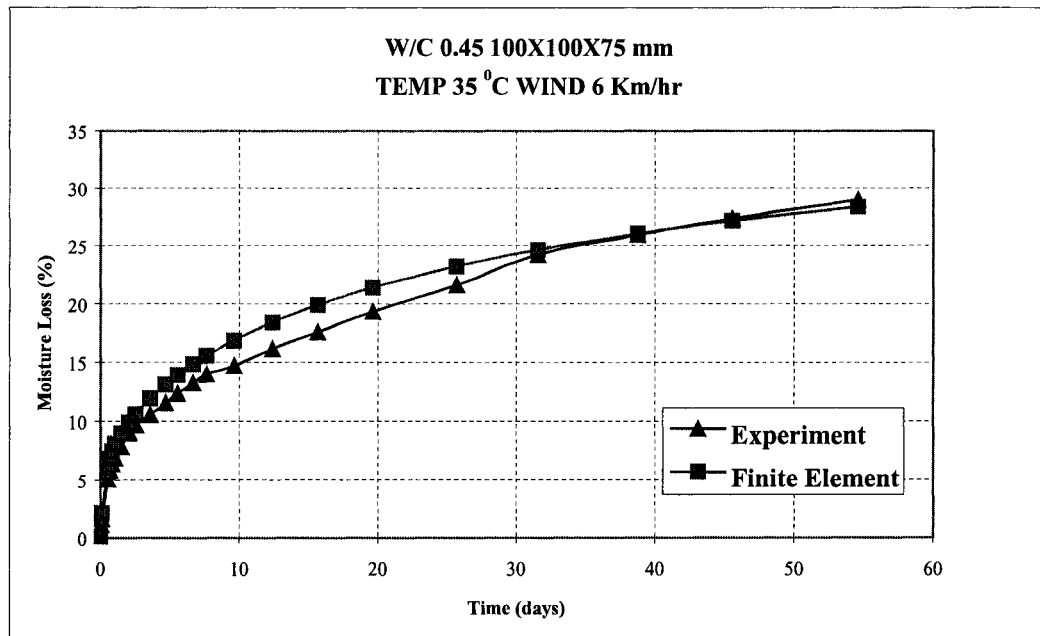


Figure 5.17: Computed & Experimental Mean Moisture Loss (%) for  
W/C 0.45 - 100x100x75 mm Specimen at 35 °C & 6 km/hr Wind

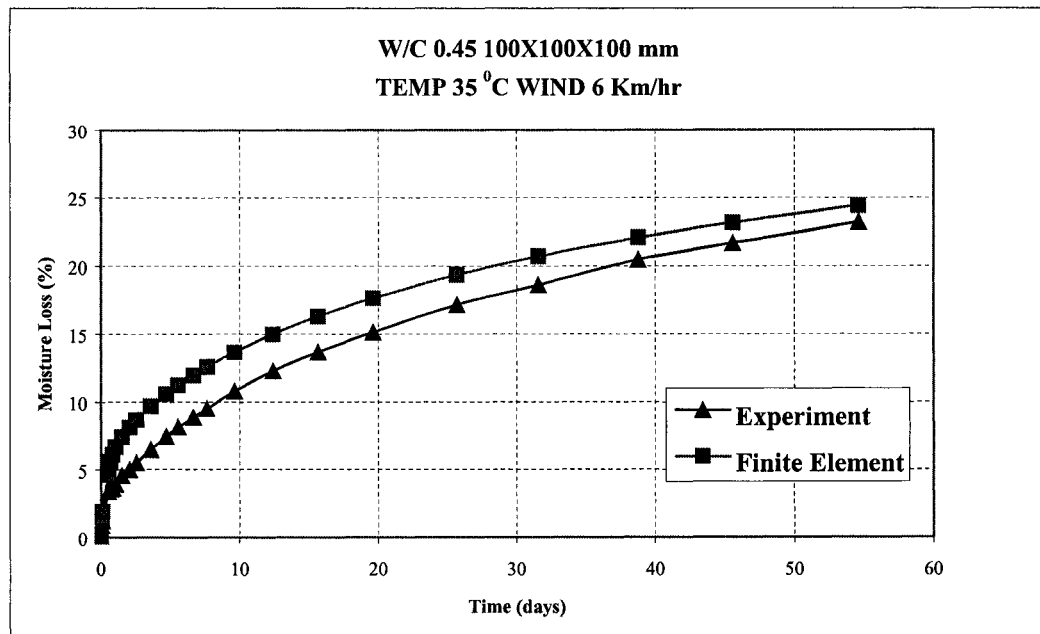


Figure 5.18: Computed & Experimental Mean Moisture Loss (%) for  
W/C 0.45 - 100x100x100 mm Specimen at 35 °C & 6 km/hr Wind

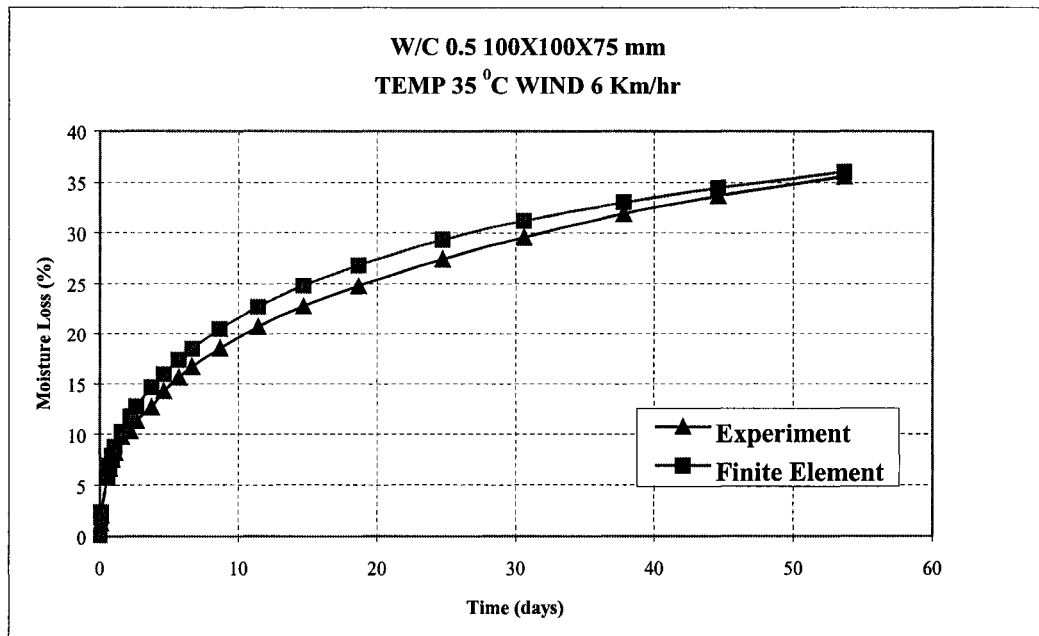


Figure 5.19: Computed & Experimental Mean Moisture Loss (%) for  
W/C 0.5 - 100x100x75 mm Specimen at 35 °C & 6 km/hr Wind

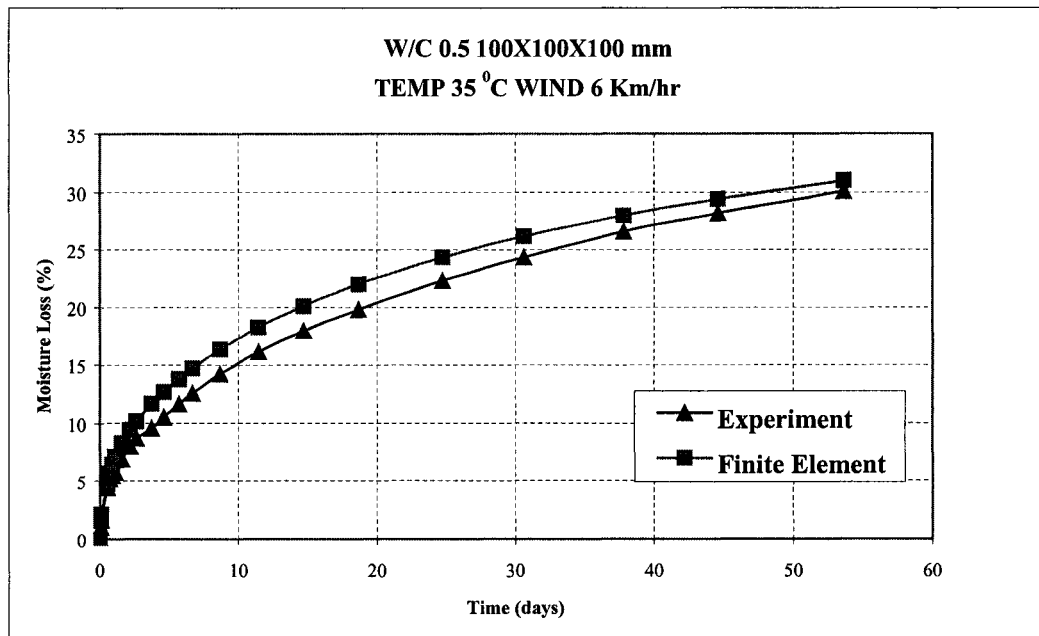


Figure 5.20: Computed & Experimental Mean Moisture Loss (%) for  
W/C 0.5 - 100x100x100 mm Specimen at 35 °C & 6 km/hr Wind

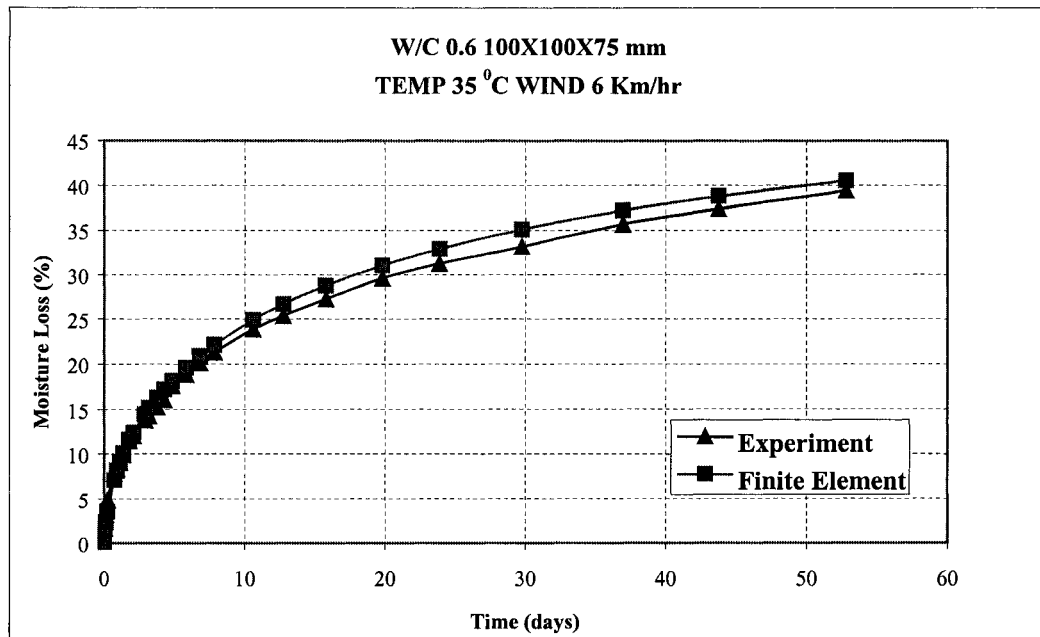


Figure 5.21: Computed & Experimental Mean Moisture Loss (%) for  
W/C 0.6 - 100x100x75 mm Specimen at 35 °C & 6 km/hr Wind

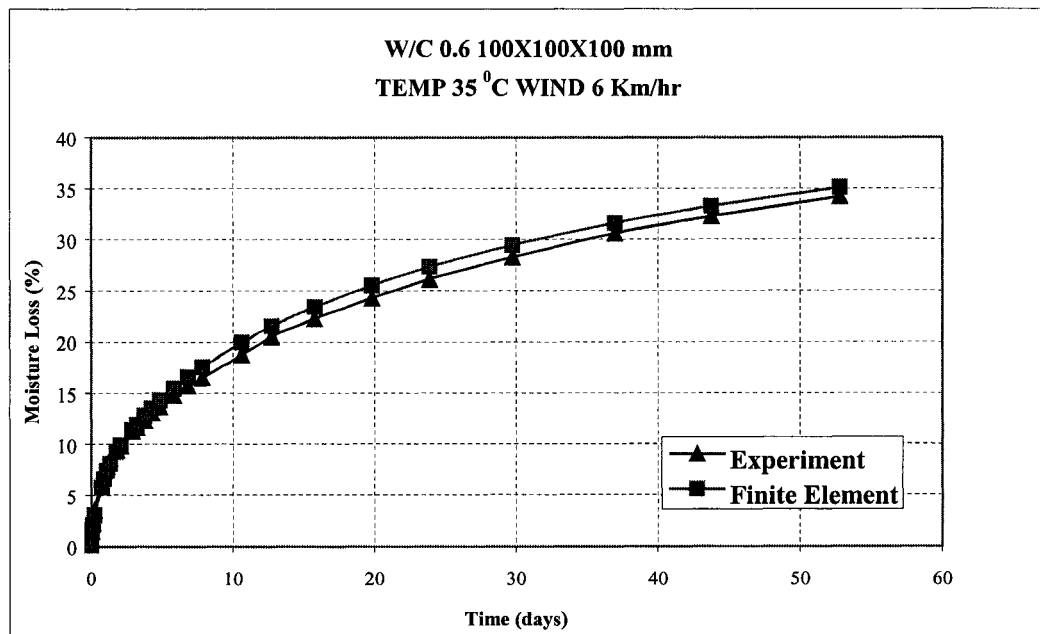


Figure 5.22: Computed & Experimental Mean Moisture Loss (%) for  
W/C 0.6 - 100x100x100 mm Specimen at 35 °C & 6 km/hr Wind

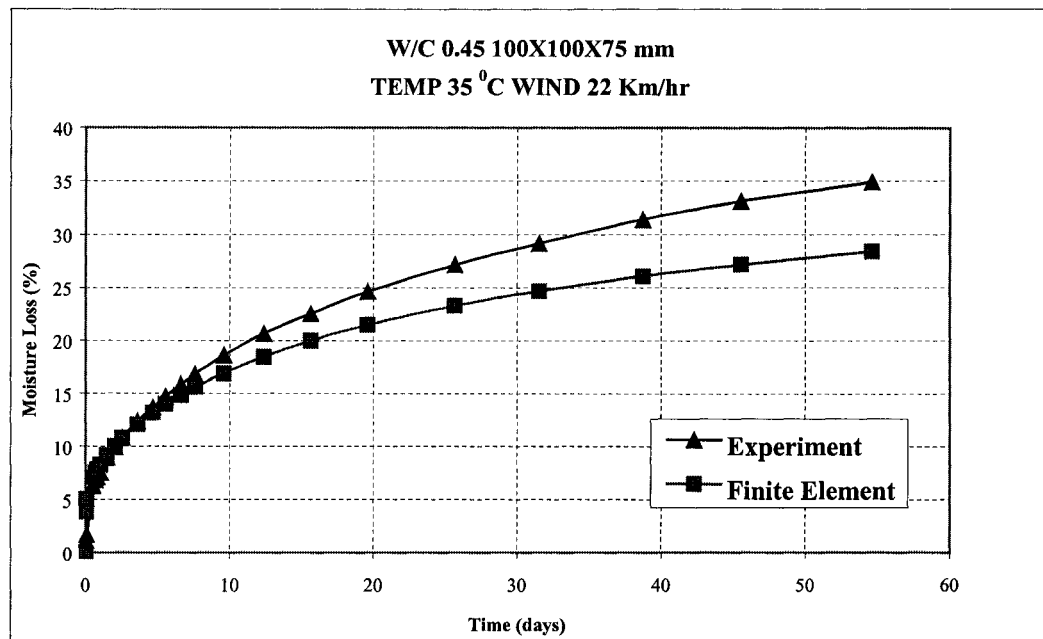


Figure 5.23: Computed & Experimental Mean Moisture Loss (%) for  
W/C 0.45 - 100x100x75 mm Specimen at 35 °C & 22 km/hr Wind

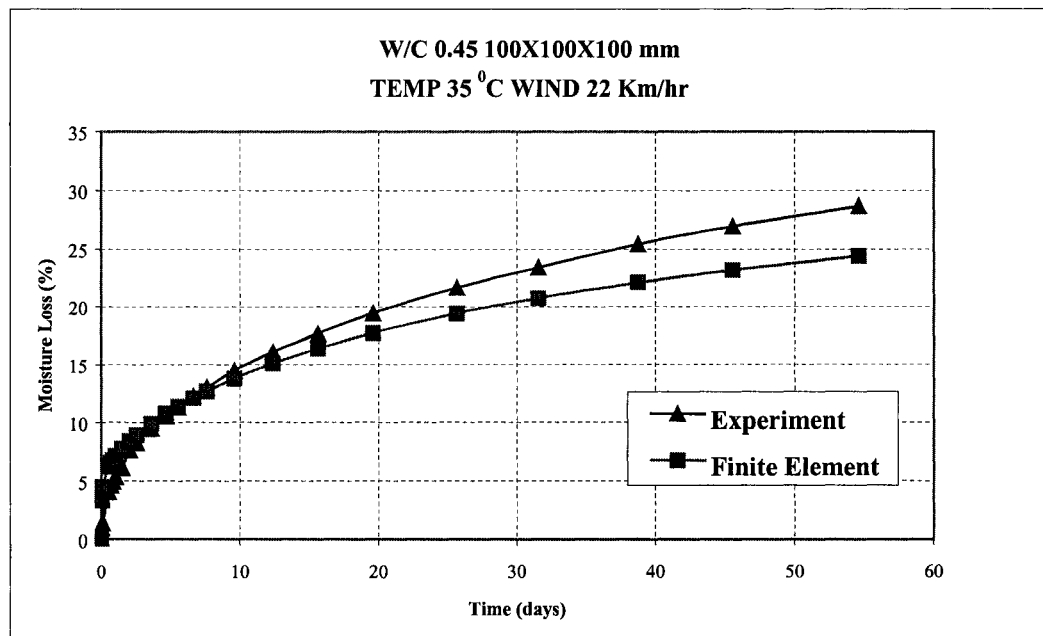


Figure 5.24: Computed & Experimental Mean Moisture Loss (%) for  
W/C 0.45 - 100x100x100 mm Specimen at 35 °C & 22 km/hr Wind

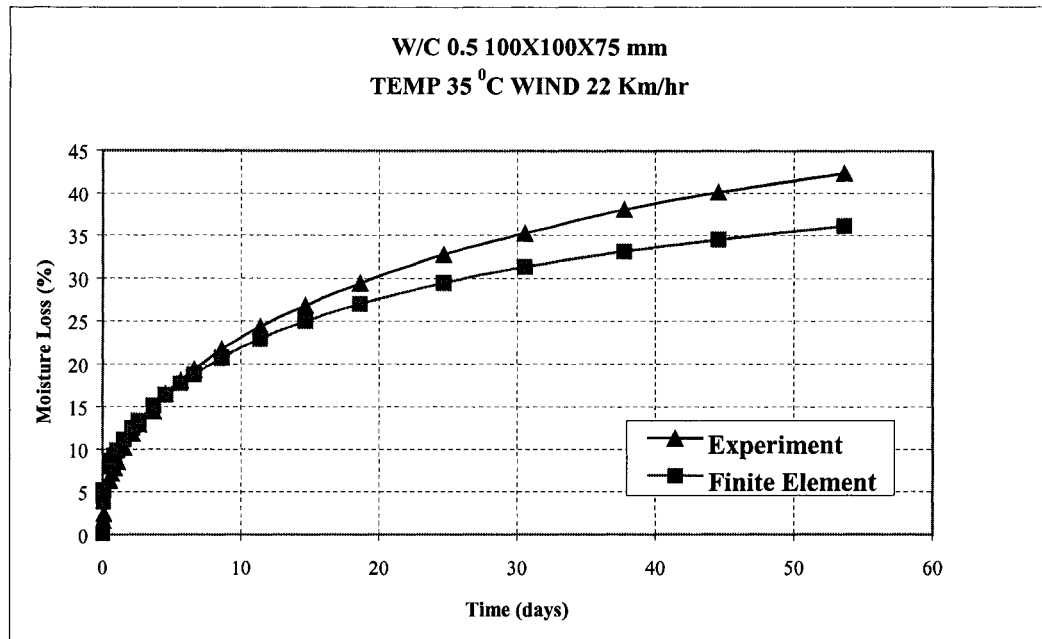


Figure 5.25: Computed & Experimental Mean Moisture Loss (%) for  
W/C 0.5 - 100x100x75 mm Specimen at 35 °C & 22 km/hr Wind

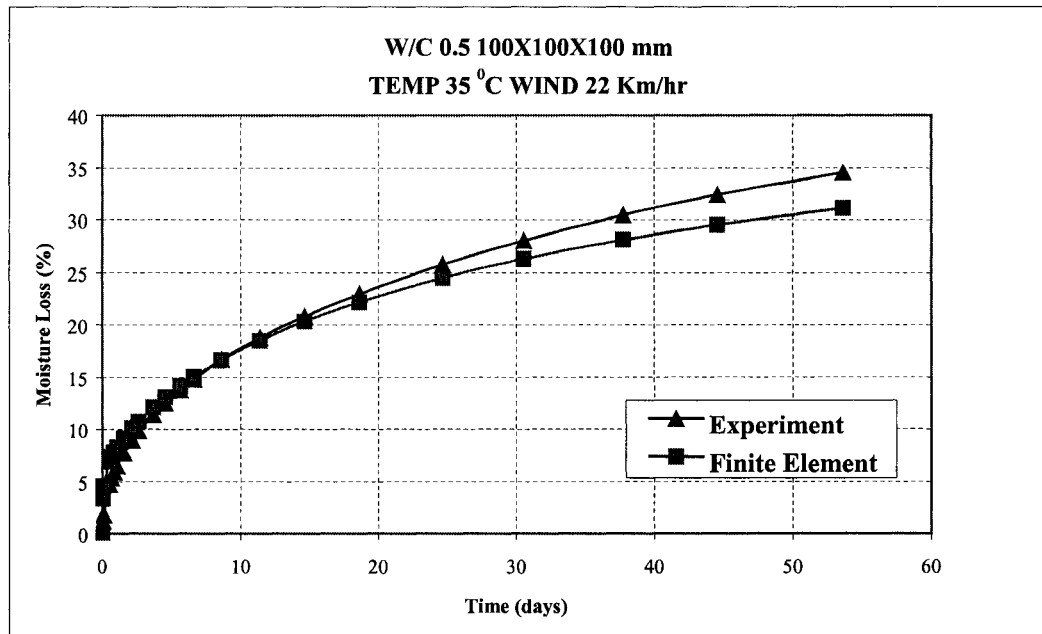


Figure 5.26: Computed & Experimental Mean Moisture Loss (%) for  
W/C 0.5 - 100x100x100 mm Specimen at 35 °C & 22 km/hr Wind

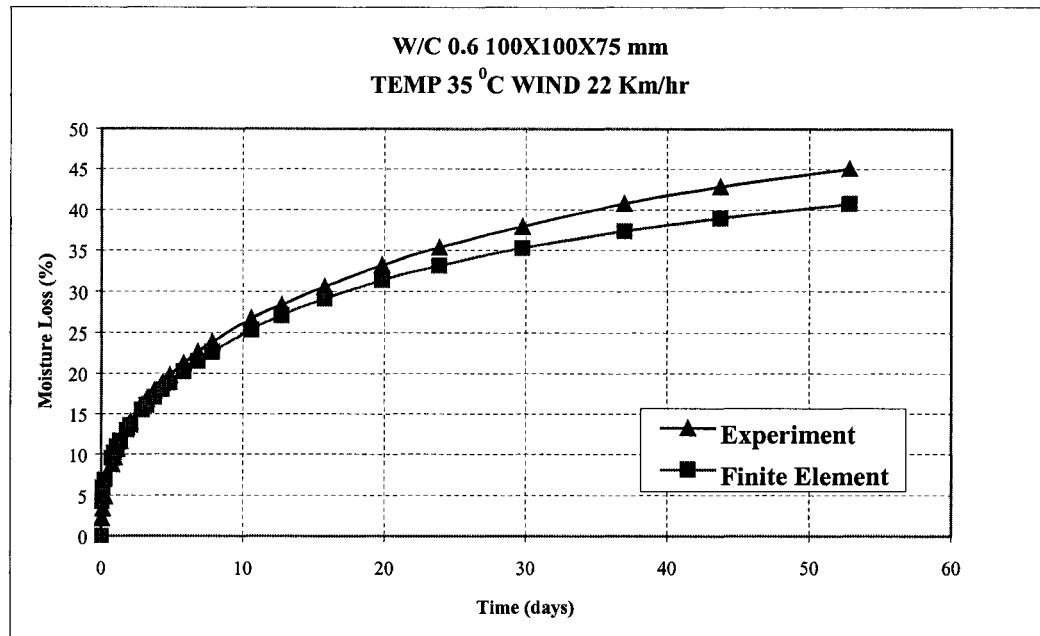


Figure 5.27: Computed & Experimental Mean Moisture Loss (%) for  
W/C 0.6 - 100x100x75 mm Specimen at 35 °C & 22 km/hr Wind

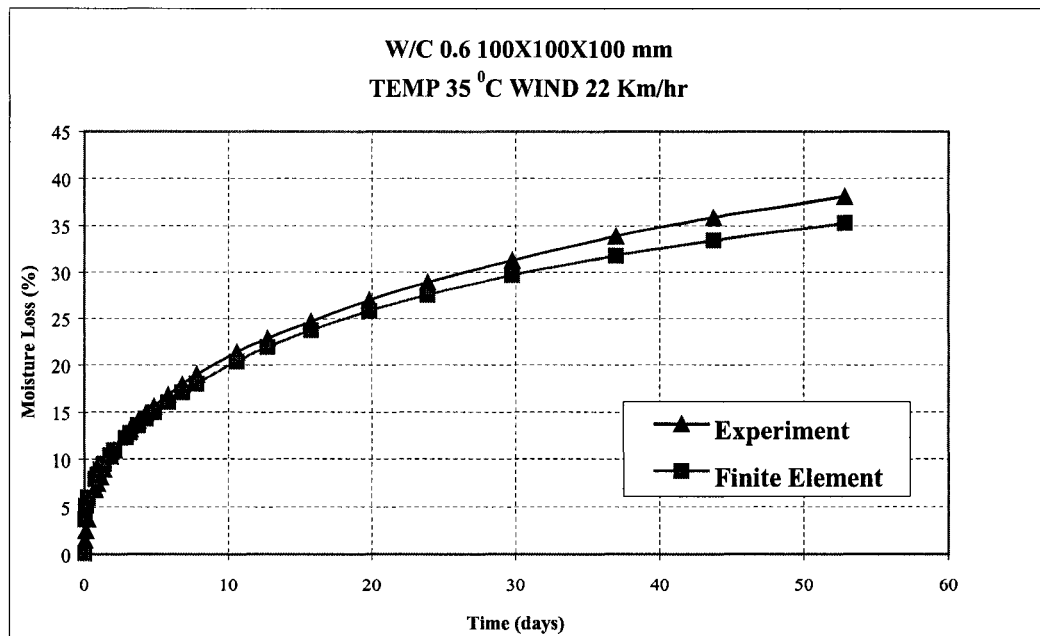


Figure 5.28: Computed & Experimental Mean Moisture Loss (%) for  
W/C 0.6 - 100x100x100 mm Specimen at 35 °C & 22 km/hr Wind

## 5.4 Moisture Diffusivity of Concrete

Table 5.1 reports the values of diffusivity parameters  $b_0$ ,  $b_1$  &  $n$ , convective transfer coefficient ( $h_f$ ) and average diffusivity ( $D_{av}$ ), for each concrete mix under each exposure regime. Diffusivity versus normalized moisture content curves for all cases, are shown in Figures 5.29-5.34. It was observed that the parameter  $b_0$  is merely a measure of amplitude of diffusivity, whereas  $b_1$  and  $n$  control its shape. To simulate higher moisture loss a higher value of  $b_0$  had to be used, which meant a higher average diffusivity of the mix. Also it was noted that higher values of 'n' result in a rapid decay of diffusivity leading to a lower average value of  $D$ . Generic curves for the effect of 'n' on diffusivity versus normalized moisture content are shown in Figure 5.35.

It can be seen from these Figures that diffusivity falls sharply with the decrease in moisture content up to 40-50 %, however below that it either becomes constant or the effect is not that significant. Bazant & Najjar [63] and Wittmann et al [66] reported similar trend for dependence of diffusivity on moisture content.

Table 5.1: Parameters for Diffusivity Law of Concrete,  $D(C) = b_0 \tan(b_1 c^n)$ 

W/C Ratio	Temp. °C	Wind km/hr	$h_f$ cm/day	$b_0$	$b_1$	$n$	$D_{av}$ cm <sup>2</sup> /d
0.45	50	6	0.8	2.9	0.5	3.25	0.358
0.5	50	6	0.8	2.9	0.5	3.1	0.37
0.6	50	6	0.8	2.9	0.5	2.7	0.41
0.45	50	22	7.0	2.9	0.5	3.25	0.358
0.5	50	22	7.0	2.9	0.5	3.1	0.37
0.6	50	22	7.0	2.9	0.5	2.7	0.41
0.45	35	6	0.8	1.35	1.0	9.25	0.162
0.5	35	6	0.8	1.35	1.0	6.5	0.218
0.6	35	6	0.8	1.35	1.0	5.3	0.258
0.45	35	22	7.0	1.35	1.0	9.25	0.162
0.5	35	22	7.0	1.35	1.0	6.5	0.218
0.6	35	22	7.0	1.35	1.0	5.3	0.258

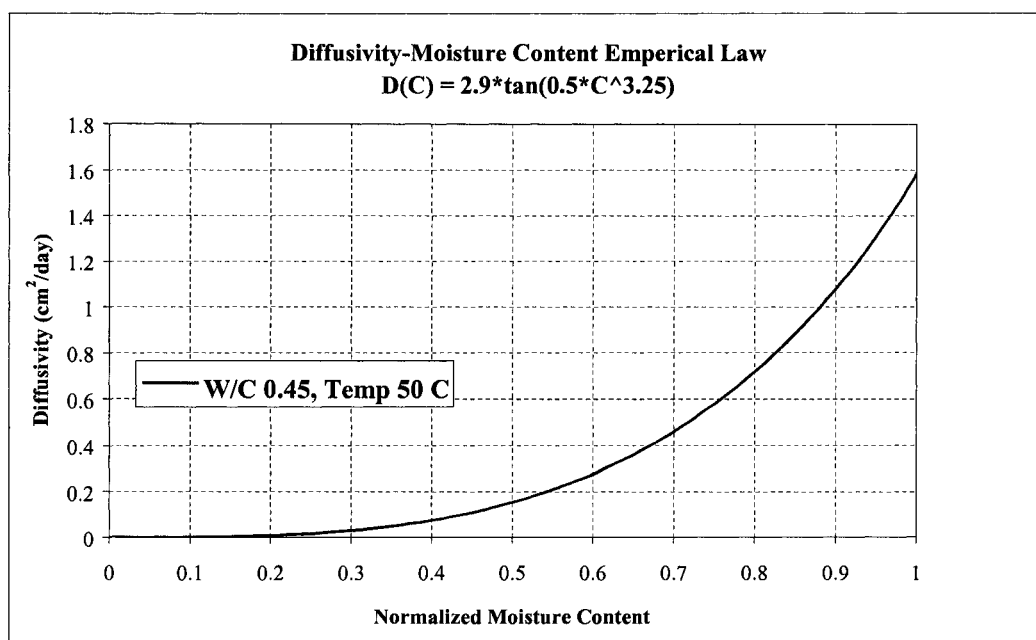


Figure 5.29: Diffusivity-Normalized Moisture Content for Concrete,  
W/C 0.45 at 50 °C

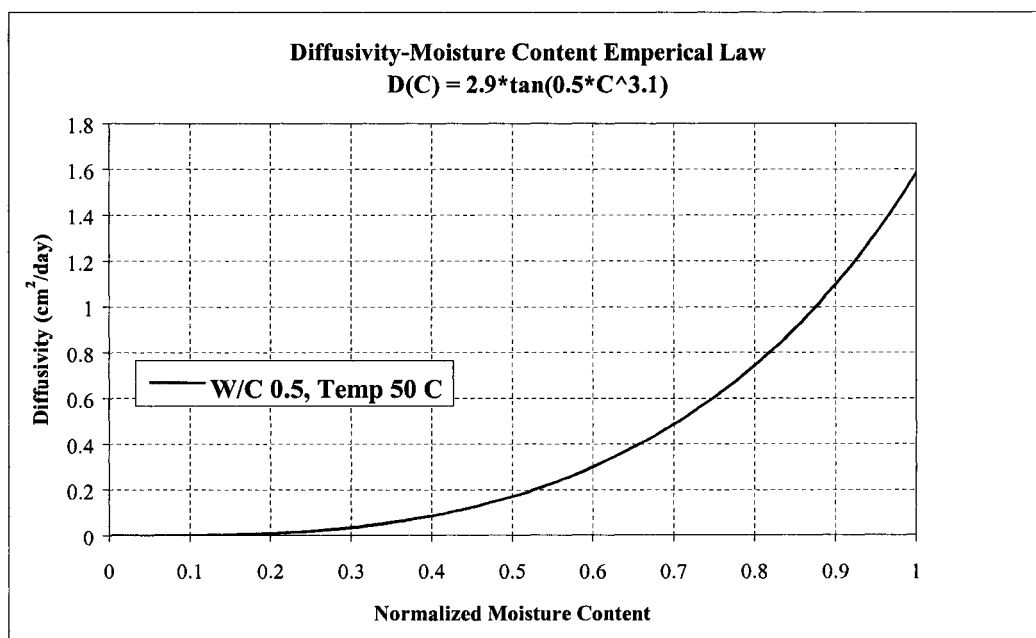


Figure 5.30: Diffusivity-Normalized Moisture Content for Concrete,  
W/C 0.5 at 50 °C

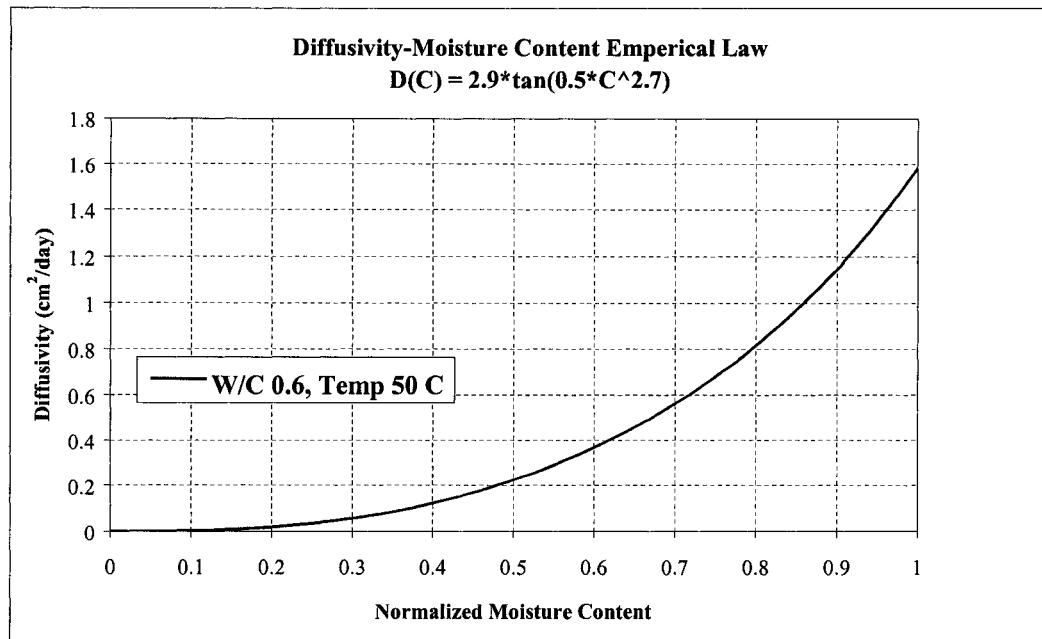


Figure 5.31: Diffusivity-Normalized Moisture Content for Concrete,  
W/C 0.6 at 50 °C

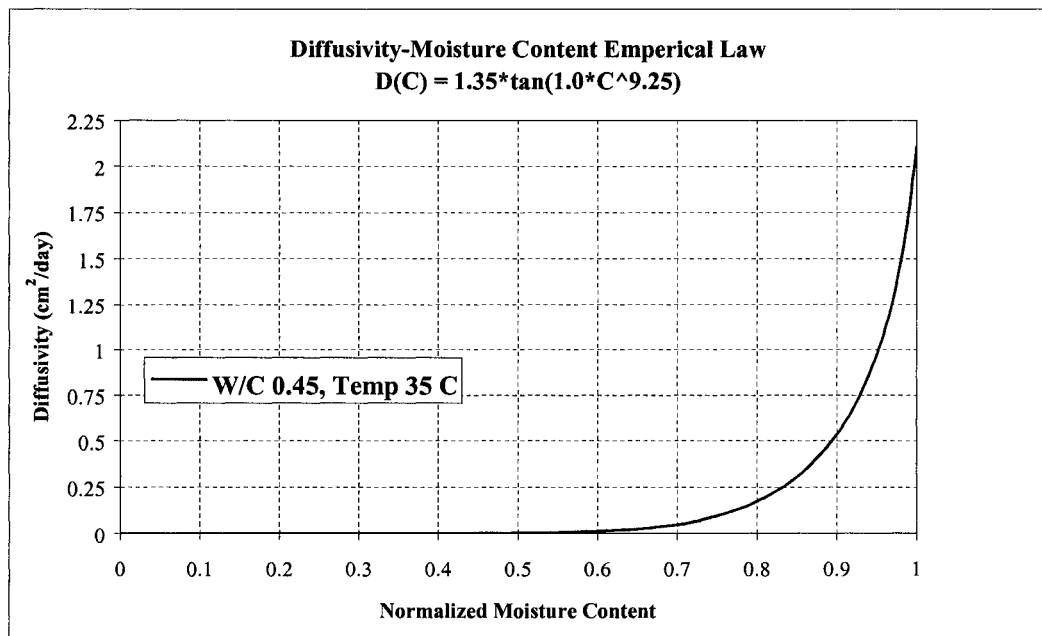


Figure 5.32: Diffusivity-Normalized Moisture Content for Concrete,  
W/C 0.45 at 35 °C

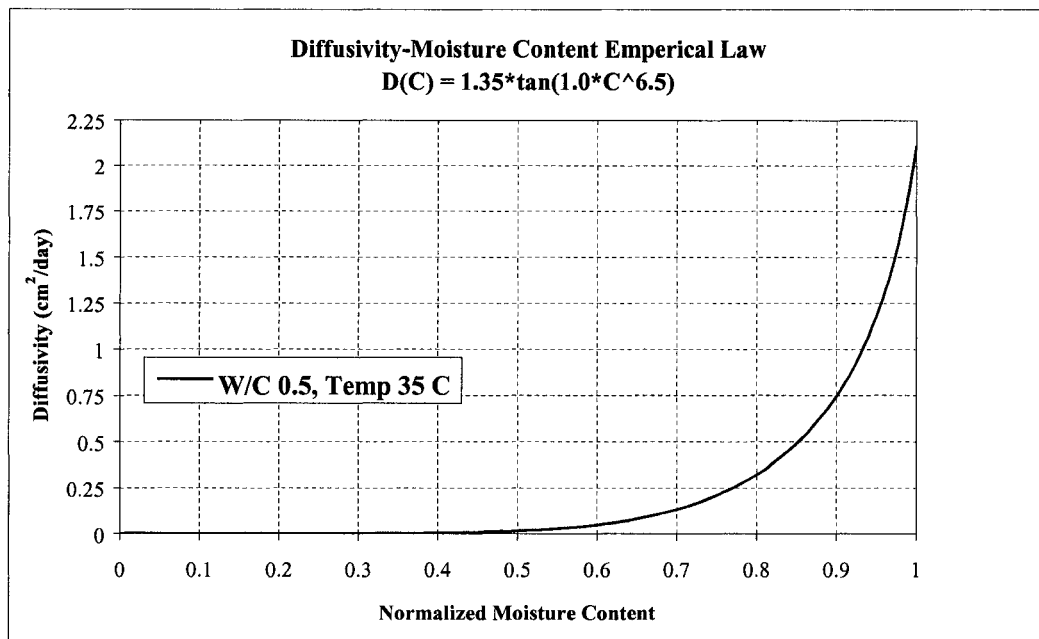


Figure 5.33: Diffusivity-Normalized Moisture Content for Concrete,  
W/C 0.5 at 35 °C

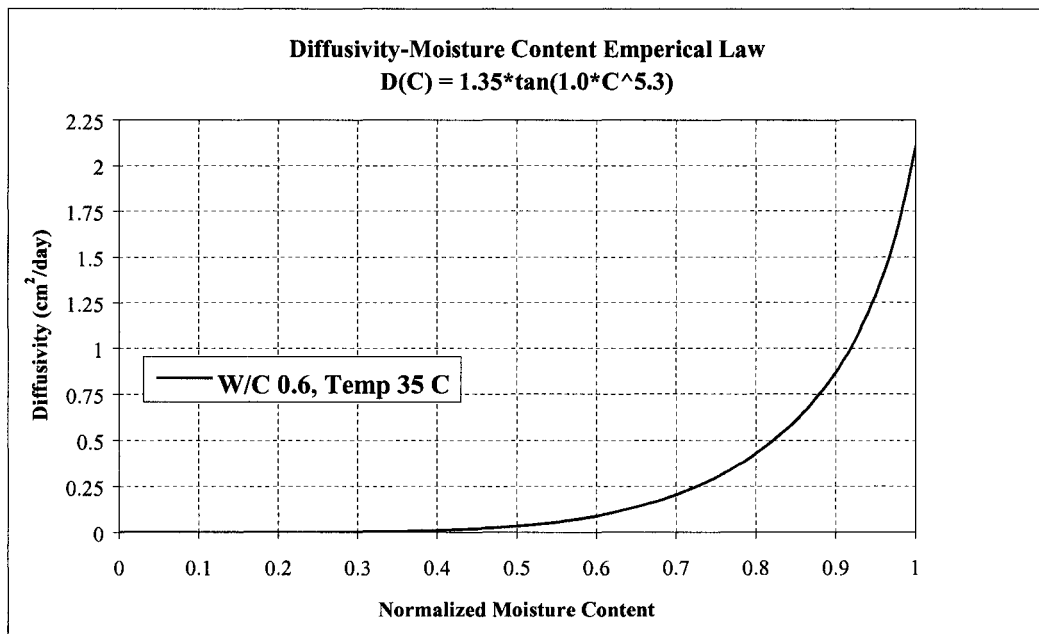


Figure 5.34: Diffusivity-Normalized Moisture Content for Concrete,  
W/C 0.6 at 35 °C

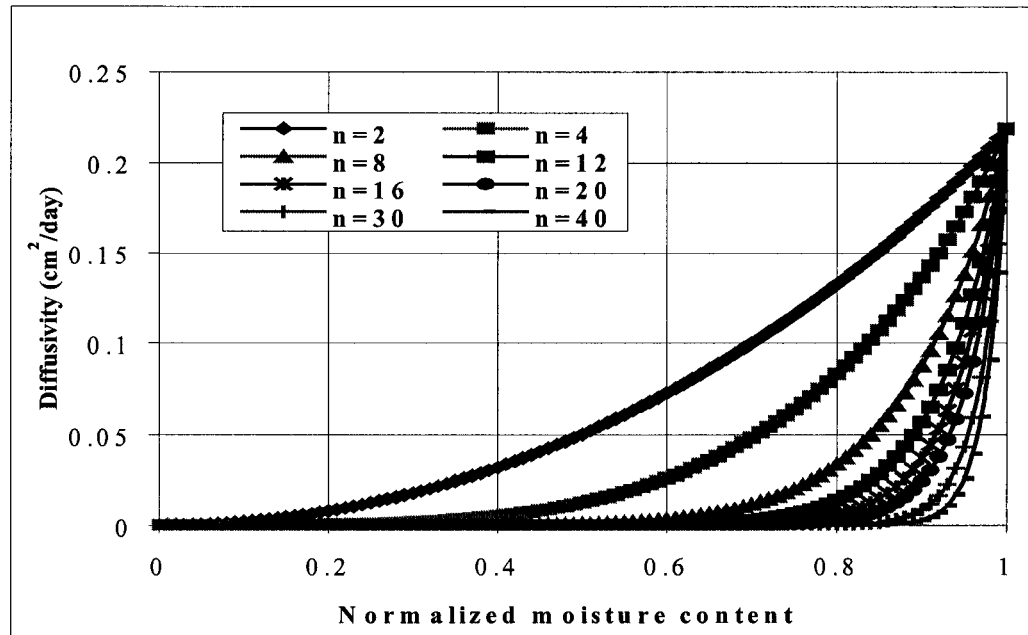


Figure 5.35: Generic Curves for Effect of 'n' on Diffusivity ~ Normalized Moisture Content

### 5.4.1 Effect of Water-Cement Ratio

At an exposure temperature of 50 °C, Figure 5.36 shows the effect of w/c ratio on diffusivity versus normalized moisture content. It can be seen that diffusivity increases with the increase in w/c ratio. An average diffusivity ( $D_{av}$ ) of 0.358 cm<sup>2</sup>/day was obtained for the mix with w/c ratio 0.45, 0.37 cm<sup>2</sup>/day for 0.5 and 0.41 cm<sup>2</sup>/day for that of 0.6.

Figure 5.37 shows similar effect at an exposure temperature of 35 °C. In this case the average diffusivity ( $D_{av}$ ) was found to be 0.162 cm<sup>2</sup>/day for the mix with w/c ratio 0.45, 0.218 cm<sup>2</sup>/day for 0.5 and 0.258 cm<sup>2</sup>/day for that of 0.6

This effect was accounted for in the diffusivity law by using different values of 'n', with the value being lower at higher water-cement ratio, as shown in Table 5.1.

Increase in diffusivity of concrete with the increase in water-cement ratio of the mix can be attributed to increased porosity and connectivity of pores in the hydrated cement paste and hence the decreased tortuosity of the diffusion paths. Also the excess water reduces the amount of cement grains present around the aggregate surface and thus increases the porosity of the interfacial zone. Thus the moisture/water vapors get more and continuous space and hence diffuse with a greater ease.

Average moisture diffusivity of ordinary concrete ( $D_{av}$ ) at 35 °C & 50 °C can be predicted from the water-cement ratio of the mix, by the following general equation:

$$(D_{av})^T = A(T) * (w / c) + B(T) \quad (5.20)$$

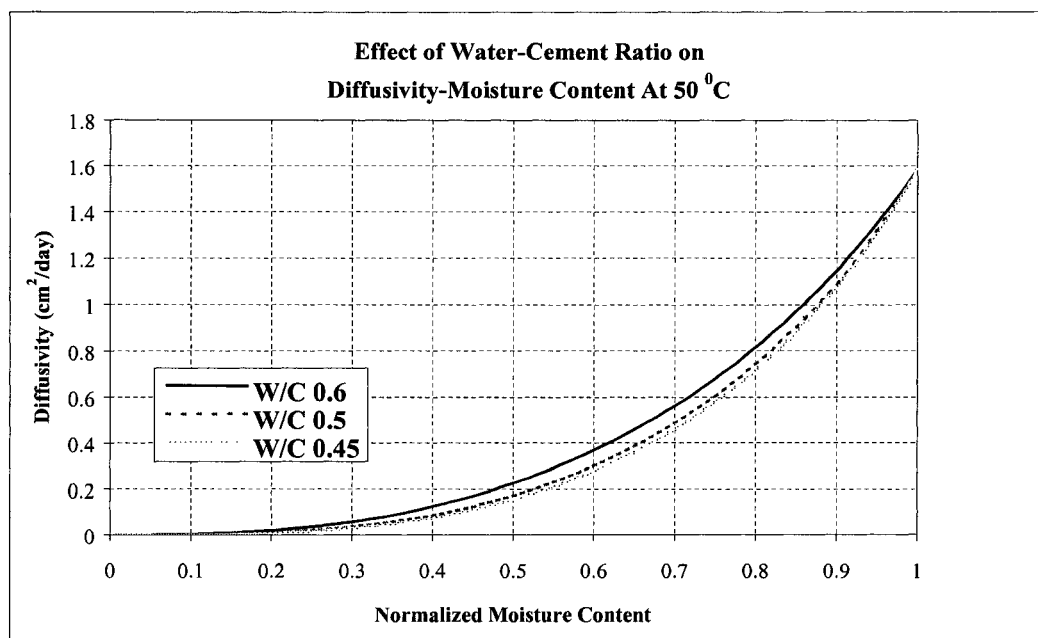


Figure 5.36: Effect of Water-Cement Ratio on Diffusivity-Normalized Moisture Content  
for Concrete at 50 °C

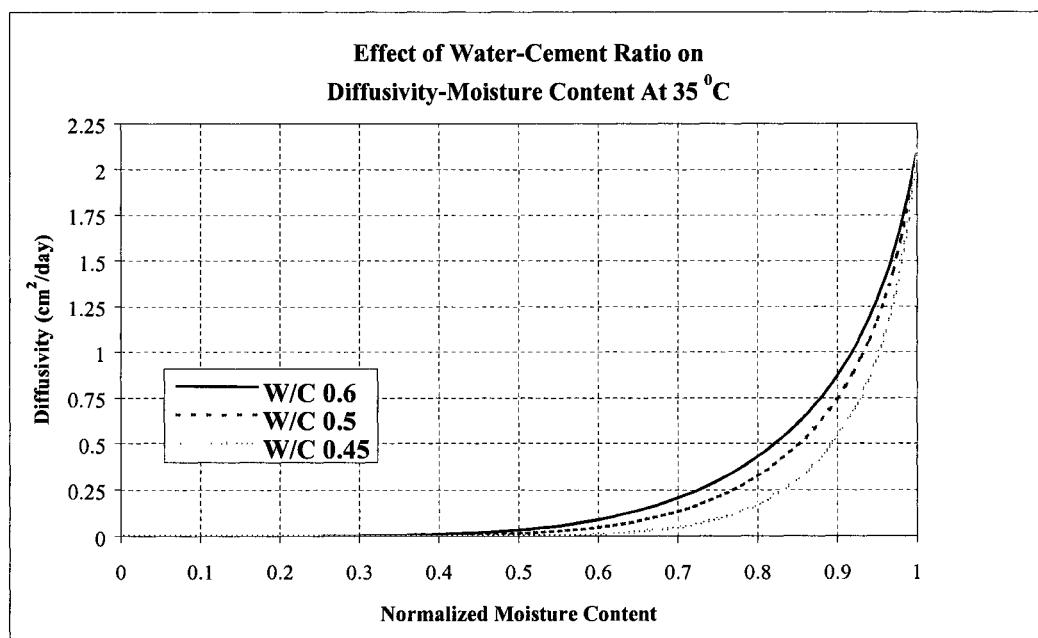


Figure 5.37: Effect of Water-Cement Ratio on Diffusivity-Normalized Moisture Content  
for Concrete at 35 °C

The regressed plots are shown in Figures 5.38 & 5.39. Adopted linear form for the relationship gives good fits with  $R^2$  values well above 90 % in both cases. At an ambient temperature of 35 °C the value of 'A' is found to be 0.6057 & 'B' as -0.1003 and at 50 °C the value of 'A' as 0.3543 & 'B' as 0.1963.

#### 5.4.2 Effect of Ambient Temperature

Figures 5.40-5.42 show the effect of temperature on diffusivity versus normalized moisture content for each mix. A significant increase in diffusivity can be observed with the increase in ambient temperature from 35-50 °C. The diffusivity at 90 % moisture content is about 68-72 % of the value at 100 % moisture content at 50 °C, the drop being only about 30 % in this range of high moisture content. However, at 35 °C this drop is very large being 60-75 %.

Temperature effect was incorporated in the diffusivity law in terms of values of  $b_0$ ,  $b_1$  and  $n$ . It was found that  $b_0$  and  $b_1$  are functions of ambient temperature only, whereas,  $n$  is a function of both w/c ratio and ambient temperature. From Table 5.1 it can be seen that the value of  $b_0$  increased from 1.35 to 2.9 with the temperature rising from 35-50 °C, whereas the value of  $b_1$  decreased from 1.0 to 0.5. On the other hand the value of  $n$  decreased from 9.25-3.25 for w/c ratio 0.45, 6.5-3.1 for w/c ratio 0.5 and 5.3-2.7 for that of 0.6.

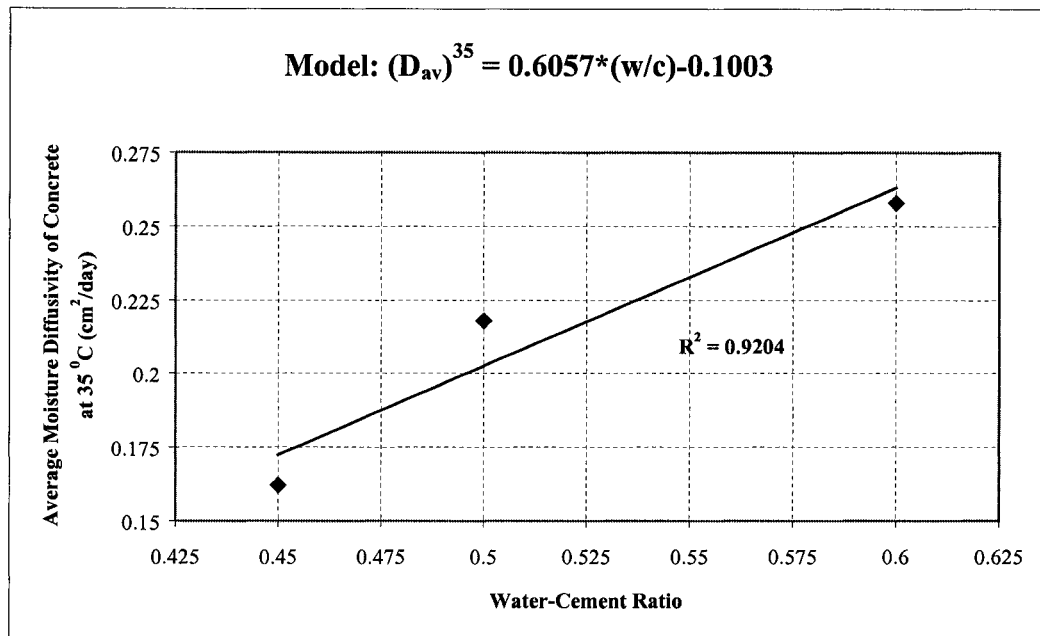


Figure 5.38: Average Diffusivity at 35 °C ~ Water Cement Ratio of Concrete

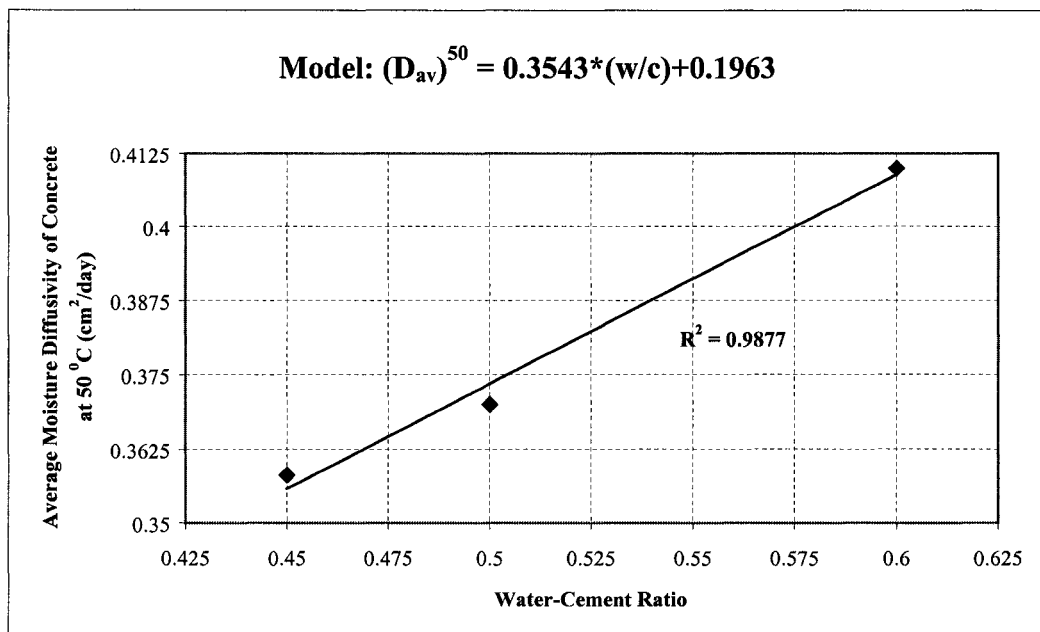


Figure 5.39: Average Diffusivity at 50 °C ~ Water Cement Ratio of Concrete

Increase in moisture diffusivity of concrete with the rising temperature is due to increase in the energy of the water vapor molecules and thermal dilation of pores. Also applying the Kelvin Thomson equation of thermodynamics, relative humidity of pores should increase with the increase in ambient temperature. This promotes transport in the form of liquid water rather than water vapors, which is the more efficient transport mechanism and hence diffusivity increases [24].

The regressed relationship between average diffusivity at 50 °C and 35 °C is shown in Figure 5.43. Exponential form gives the best fit with R<sup>2</sup> value of 0.86. The relationship is found to be as under:

$$(D_{av})^{50} = 0.2836(\exp)^{1.36*(D_{av})^{35}} \quad (5.21)$$

Where

$(D_{av})^{50}$  is the average moisture diffusivity of concrete at 50 °C (cm<sup>2</sup>/day)

$(D_{av})^{35}$  is the average moisture diffusivity of concrete at 35 °C (cm<sup>2</sup>/day)

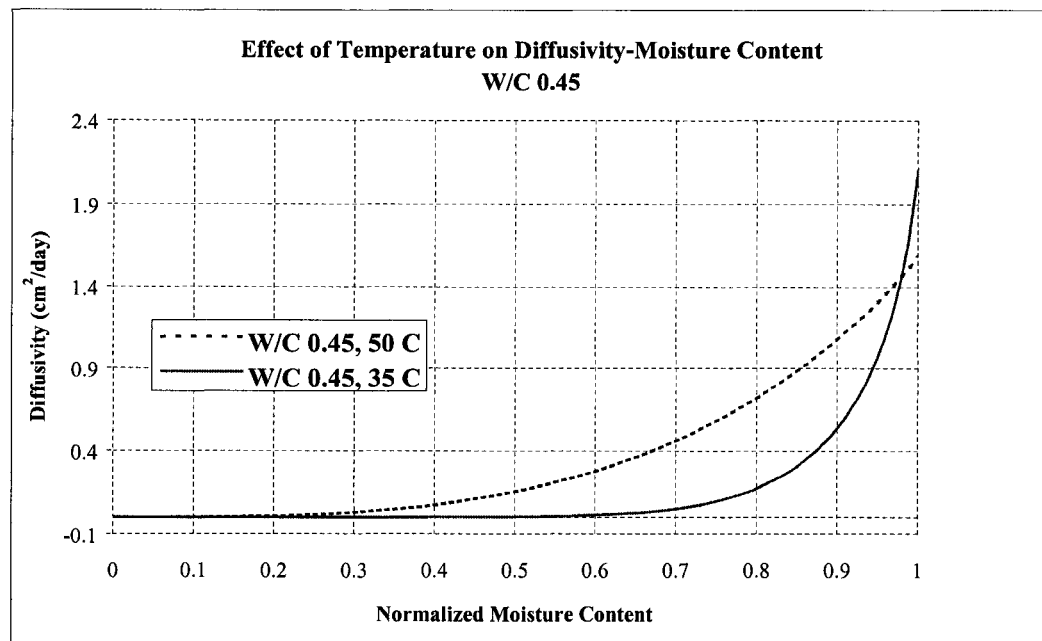


Figure 5.40: Effect of Temperature on Diffusivity-Normalized Moisture Content for  
W/C 0.45

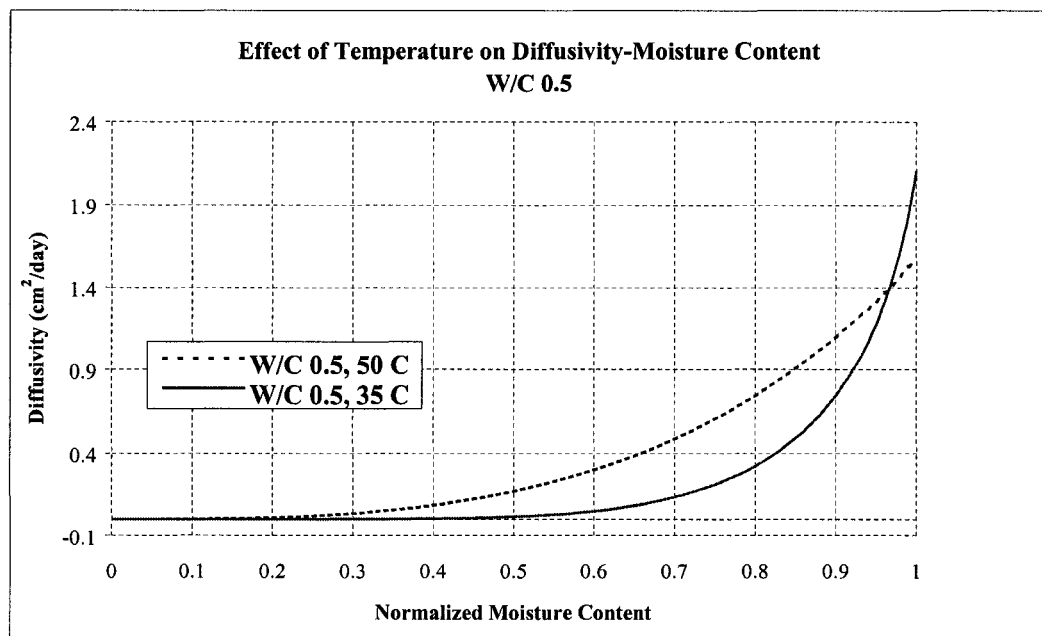


Figure 5.41: Effect of Temperature on Diffusivity-Normalized Moisture Content for  
W/C 0.5

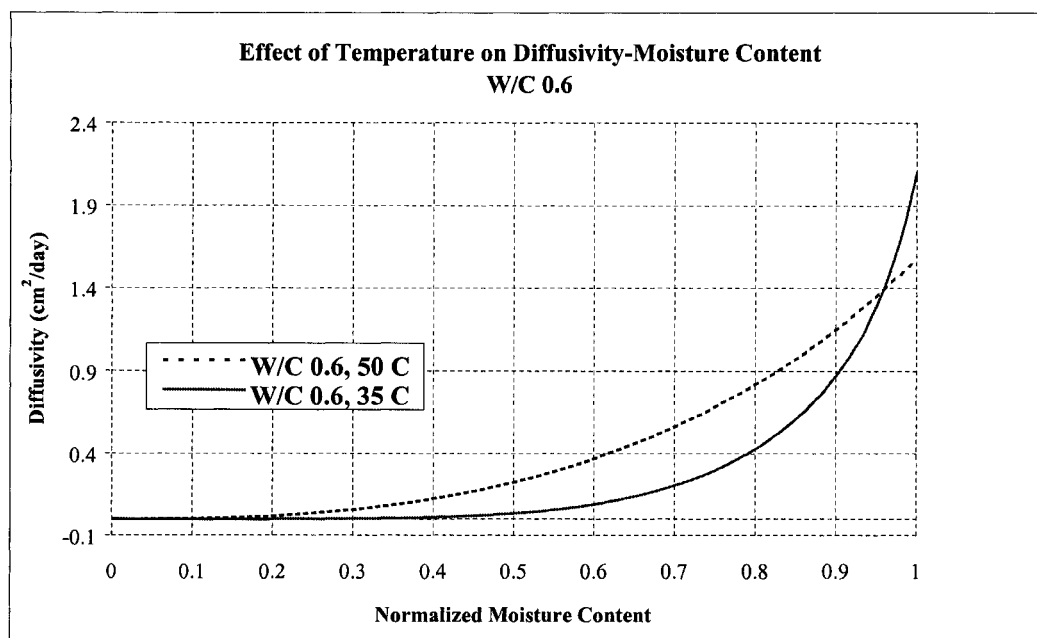


Figure 5.42: Effect of Temperature on Diffusivity-Normalized Moisture Content for  
W/C 0.6

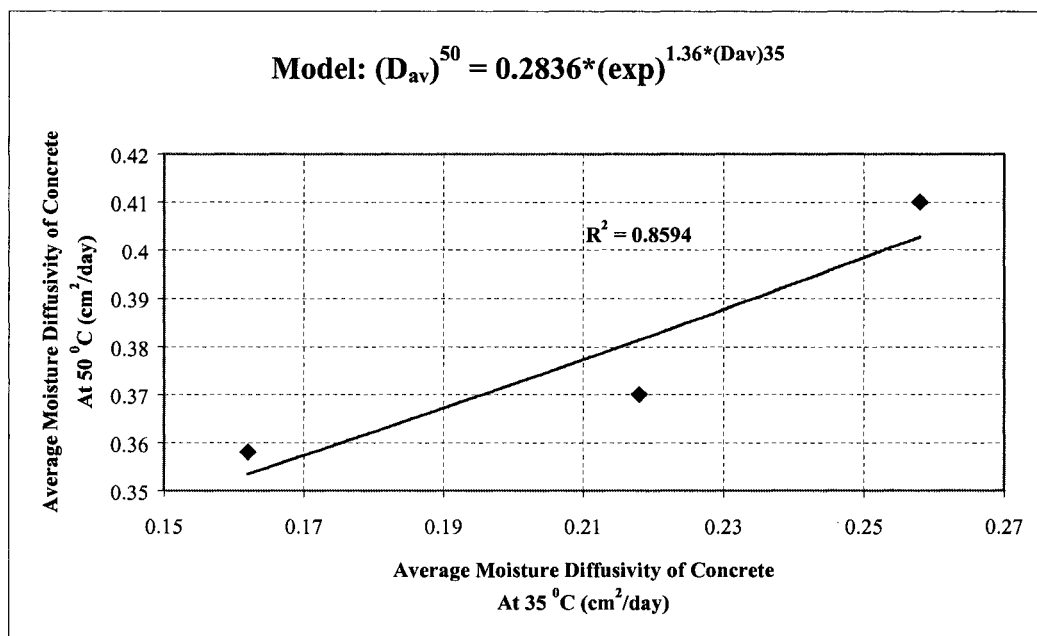


Figure 5.43: Average Diffusivity at 50°C ~ 35°C for Concrete

## 5.5 Diffusivity versus Strength & Permeability of Concrete

Figures 5.44 & 5.45 show the regressed relationships between diffusivity at 50 °C & 35 °C and the 28-day compressive strength, for the selected concrete mixes. It can be seen that higher compressive strengths correspond to a lower diffusivity value. The general form for the relationship can be expressed as follows:

$$(D_{av})^T = A(T) * (fc') + B(T) \quad (5.22)$$

Where

$$A(50) = -0.0025, B(50) = 0.4614, A(35) = -0.0044 \text{ \& } B(35) = 0.355.$$

Figures 5.46 & 5.47 show the regressed relationships between water permeability of concrete in terms of penetration depth 'e' and its diffusivity at 50 °C and 35 °C respectively. It can be seen that higher permeability corresponds to a higher diffusivity value. The proposed general form for the relationship is as under:

$$(D_{av})^T = A(T) * (e) + B(T) \quad (5.23)$$

Where

$$A(50) = 0.002, B(50) = 0.291, A(35) = 0.0032 \text{ \& } B(35) = 0.0714.$$

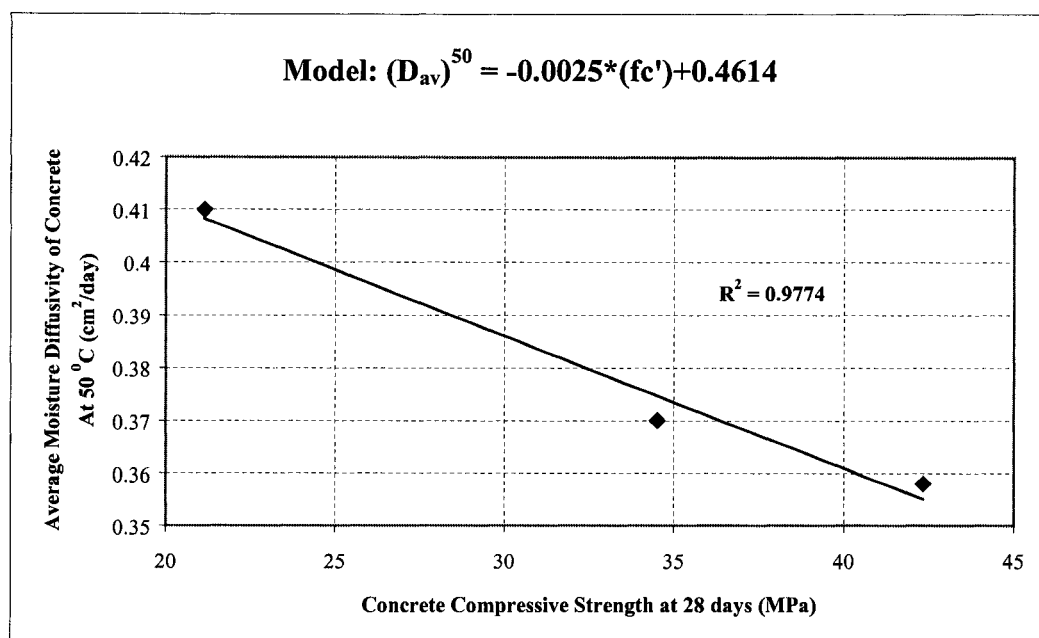


Figure 5.44: Average Diffusivity at 50 °C ~ 28 day Compressive Strength of Concrete

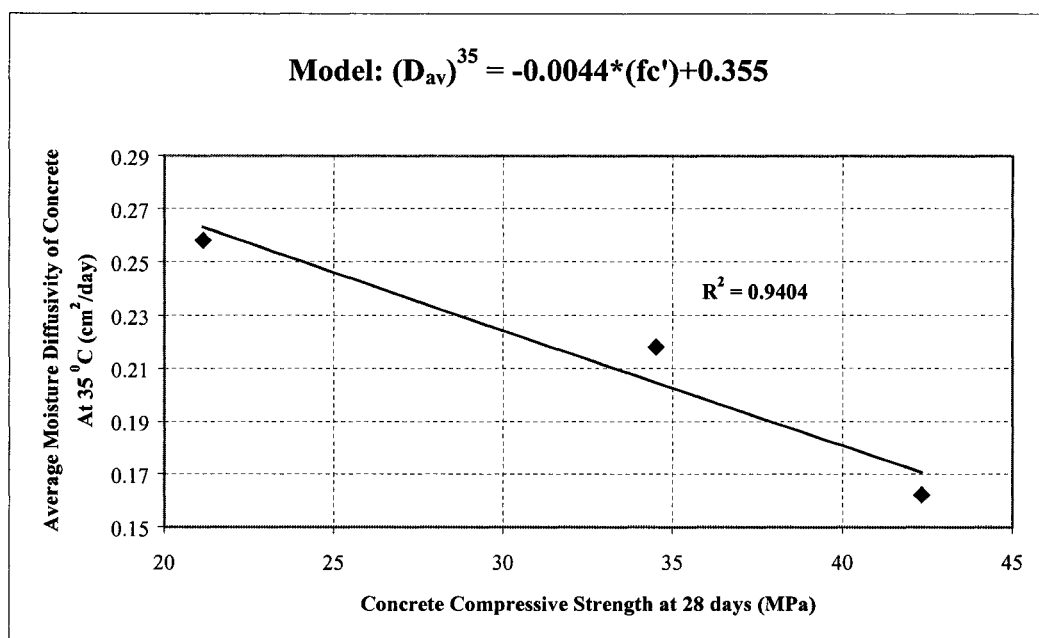


Figure 5.45: Average Diffusivity at 35 °C ~ 28 day Compressive Strength of Concrete

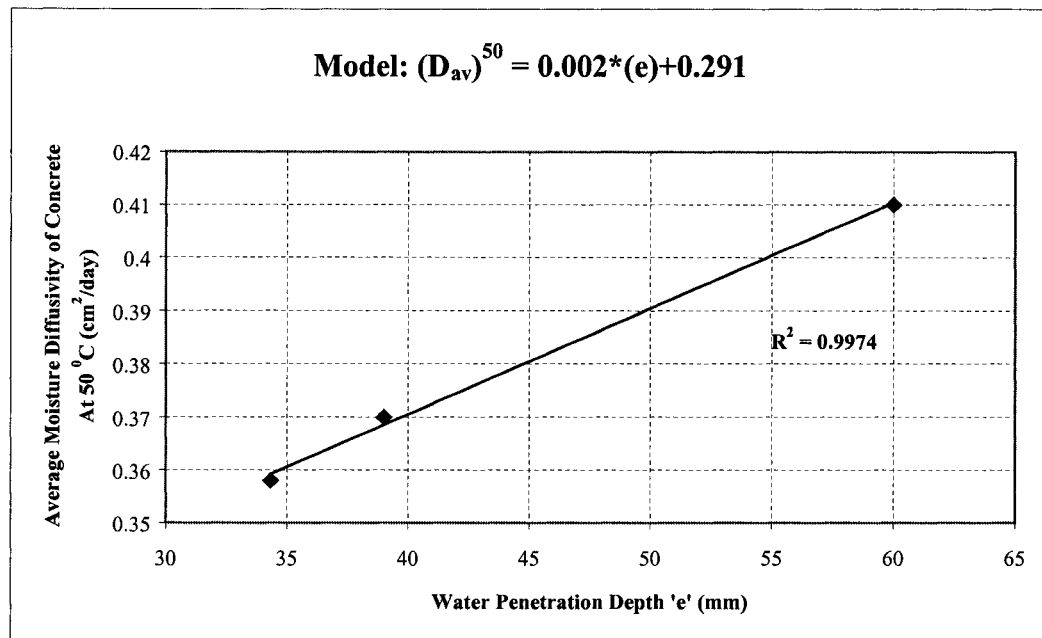


Figure 5.46: Average Diffusivity at 50 °C ~ Permeability of Concrete

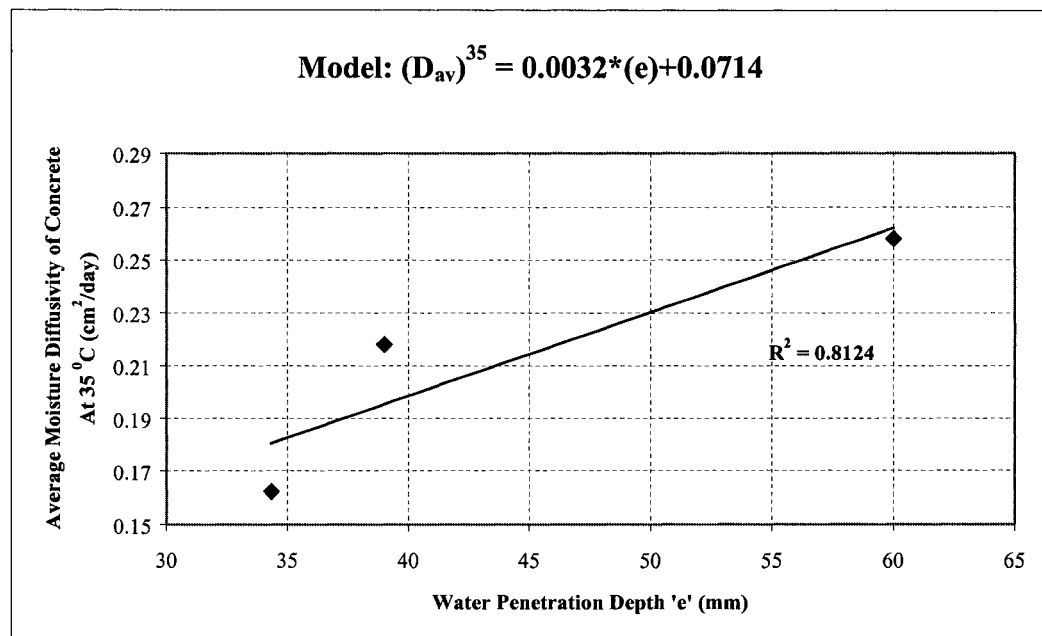


Figure 5.47: Average Diffusivity at 35 °C ~ Permeability of Concrete

## 5.6 A New Approach to Mix Design based upon Moisture Diffusivity

Regressing the data obtained for moisture diffusivity and shrinkage strains in concrete, a new approach to concrete mix design (w/c ratio) for crack free concrete under hot weather conditions is presented in the following paragraphs.

Figure 5.48 shows the regressed relationship between mean moisture loss (%) in concrete at 28 days of exposure (mlp)<sup>28</sup> for the specimen size of 100x100x75 mm and the shrinkage strains (10<sup>-6</sup>) at 45 days ( $\epsilon_{sh}$ )<sup>45</sup>. Each point on this curve corresponds to a particular concrete mix (w/c ratio) for a particular exposure temperature and wind speed at 40 % R.H. The relationship is found to be:

$$(\epsilon_{sh})^{45} = 272.09(\exp)^{0.0121*(mlp)^{28}} \quad (5.24)$$

Equation 5.24 is an invariant relationship in general between  $\epsilon_{sh}$  ( $t = t_1$ ) and the mlp ( $t = t_2$ ), and is independent of other variables. Time  $t_1$  and  $t_2$  may be taken to be the same or different depending upon target objectives. Based upon a threshold value of  $400 \times 10^{-6}$  for shrinkage strain at 45 days to ensure crack free concrete, the mean moisture loss in percentage at 28 days (mlp)<sup>28</sup> for a specimen size of 100x100x75 mm should not be greater than 32 %, as obtained by Equation 5.24.

Next the data is regressed for mlp<sup>28</sup> as a function of average moisture diffusivity of concrete ' $D_{av}$ ' (cm<sup>2</sup>/day) and ambient wind speed ' $\omega$ ' (Km/hr) for the specimen size of 100x100x75 mm, as shown in Figure 5.49. The regression model obtained is as follows:

$$(mlp)^{28} = 7.589 + 90.294(D_{av}) + 0.251(\omega) \quad (5.25)$$

It may be noted that the moisture loss percentage is an invariant relationship of the form,  $mlp = mlp(D_{av}, \omega, R.H, t)$ . However, the data used in this work has fixed the R.H at a relatively conservative 40 % and the time  $t$  for  $mlp$  output as 28 days. From the value of  $mlp^{28}$  obtained from Equation 5.24 and using the ambient wind speed to which the concrete is to be exposed in practice, the required average moisture diffusivity of concrete can be obtained using Equation 5.25.

Figure 5.50 shows the regressed relationship for  $D_{av}$  as a function of ambient temperature 'T' ( $^{\circ}C$ ) and water-cement ratio ( $w/c$ ) of the concrete mix. The model adopted for this relationship is as under:

$$(D_{av}) = -0.424 + 0.48(w/c) + 0.011(T) \quad (5.26)$$

Equation 5.26 is the third of the invariant relations proposed in this model in which other mix design parameters such as aggregate to cement ratio ( $A/C$ ) and curing time could be incorporated. From the value of  $D_{av}$  obtained from Equation 5.25 and the ambient temperature to which the concrete is to be exposed, the required water cement ratio of the mix can be calculated using Equation 5.26.

However as mentioned in the above discussion, the proposed model is only valid for hot weather conditions, i.e. a temperature range of 35-50  $^{\circ}C$ , a wind speed range of 6-

22 Km/hr and relative humidity fixed at 40 %. The model will yield conservative results for higher ambient relative humidity.

The whole of the above-mentioned procedure for concrete mix design can be explained by solving an example. For a crack free concrete ( $\epsilon_{sh}$ )<sup>45</sup> is limited to  $400 \times 10^{-6}$ , which corresponds to an  $mlp$ <sup>28</sup> value of 32 % as obtained from Equation 5.24. Using this value of  $mlp$ <sup>28</sup> and taking a value of say 12 Km/hr for the exposure wind speed, required  $D_{av}$  for the concrete mix as calculated by Equation 5.25 comes out to be  $0.237 \text{ cm}^2/\text{day}$ . From Equation 5.26, using this value of  $D_{av}$  and a value of say  $40^\circ\text{C}$  for the ambient temperature, the required water cement ratio for the concrete mix is calculated as 0.46.

Following this procedure for concrete mix design within the specified limits of ambient temperature 'T' ( $^\circ\text{C}$ ) and wind speed ' $\omega$ ' (Km/hr), a lot of data was generated to regress water cement ratio (w/c) of the concrete mix as a direct function of 'T' and ' $\omega$ '. The best-fit plot is shown in Figure 5.51 and the model obtained is given in the following equation:

$$(w/c) = 1.447 - 0.023(T) - 0.006(\omega) \quad (\text{R.H} = 40\%) \quad (5.27)$$

This model can now be used to directly calculate the required water cement ratio for a crack free concrete mix for given values of ambient temperature and wind speed, an engineering guideline that would be especially useful for concreting in relatively dry and hot weather conditions.

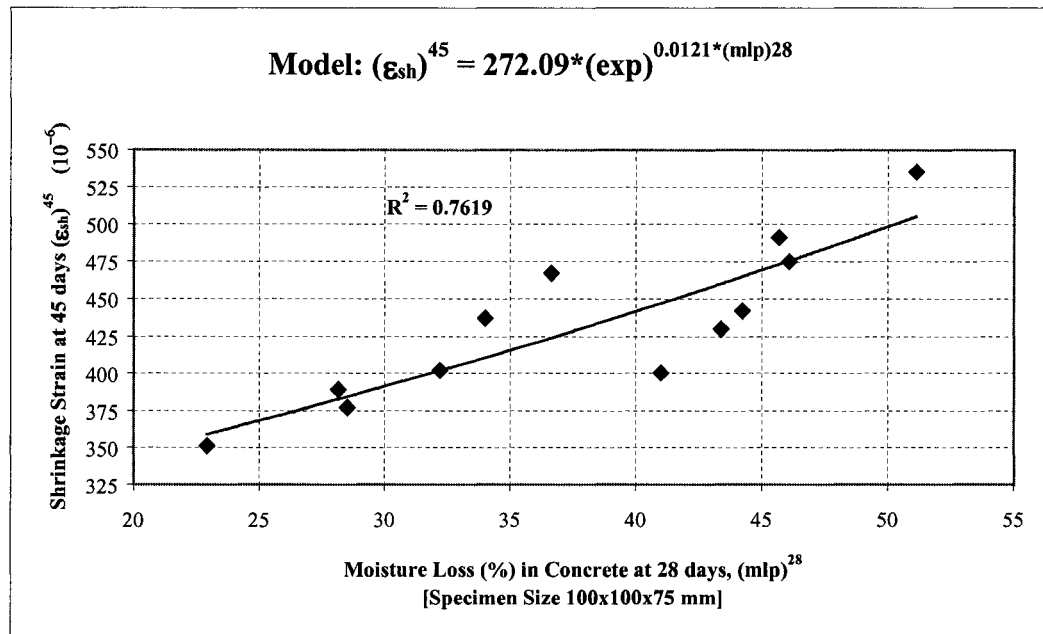


Figure 5.48: Shrinkage Strain in Concrete at 45 days ~ Mean Moisture Loss at 28 days

[Specimen size 100x100x75 mm]

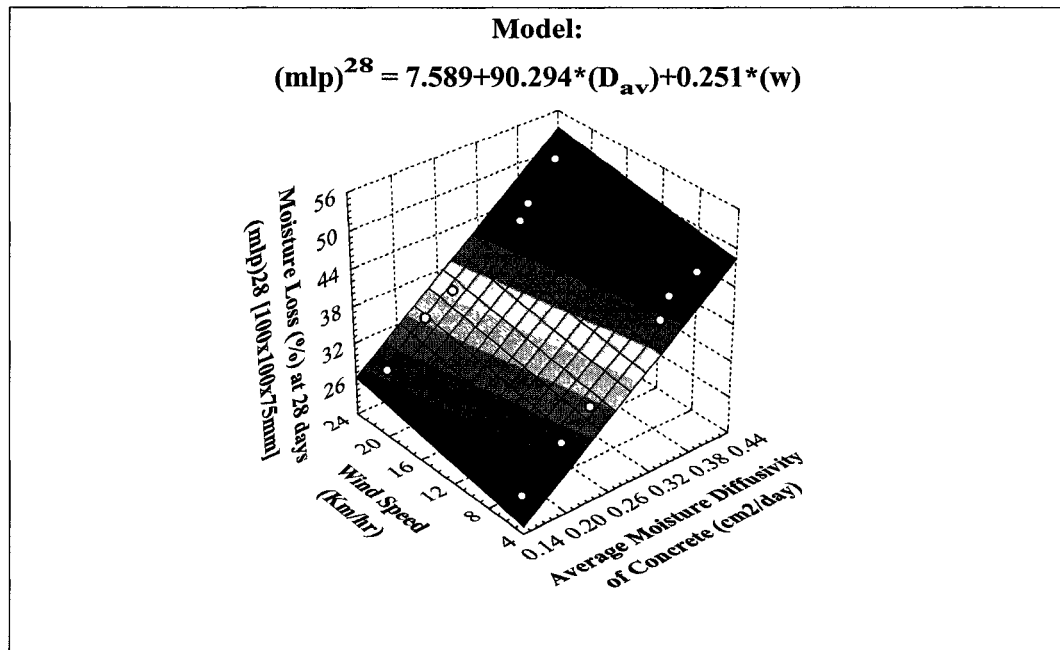


Figure 5.49: Average Moisture Diffusivity of Concrete ~ Mean Moisture Loss at 28 days

and Ambient Wind Speed [Specimen size 100x100x75 mm]

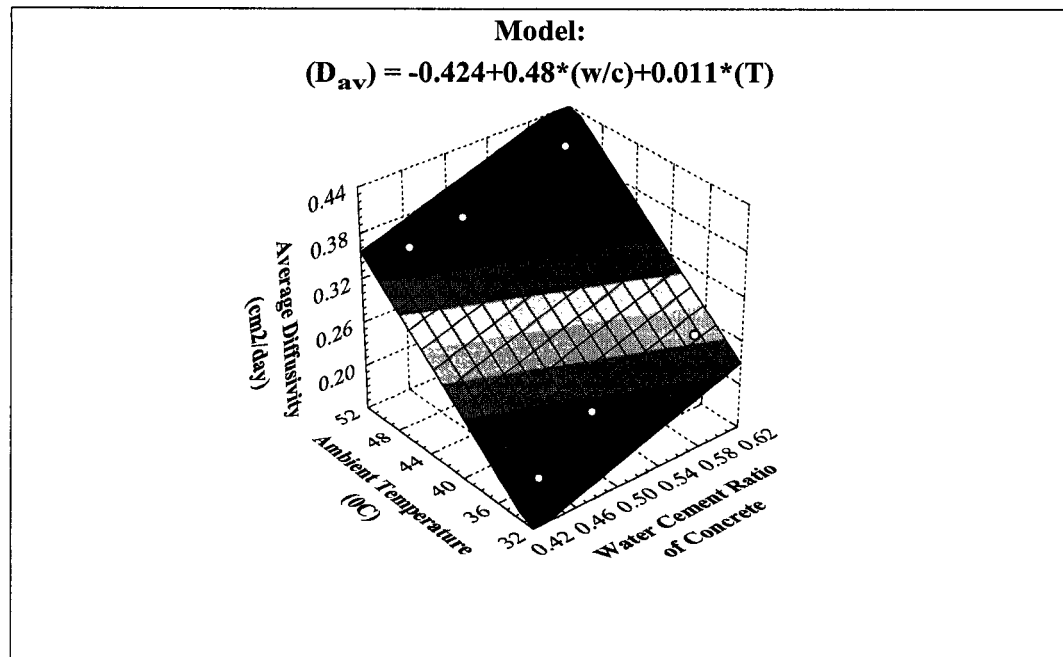


Figure 5.50: Water Cement Ratio of Concrete ~ Average Moisture Diffusivity and Ambient Temperature

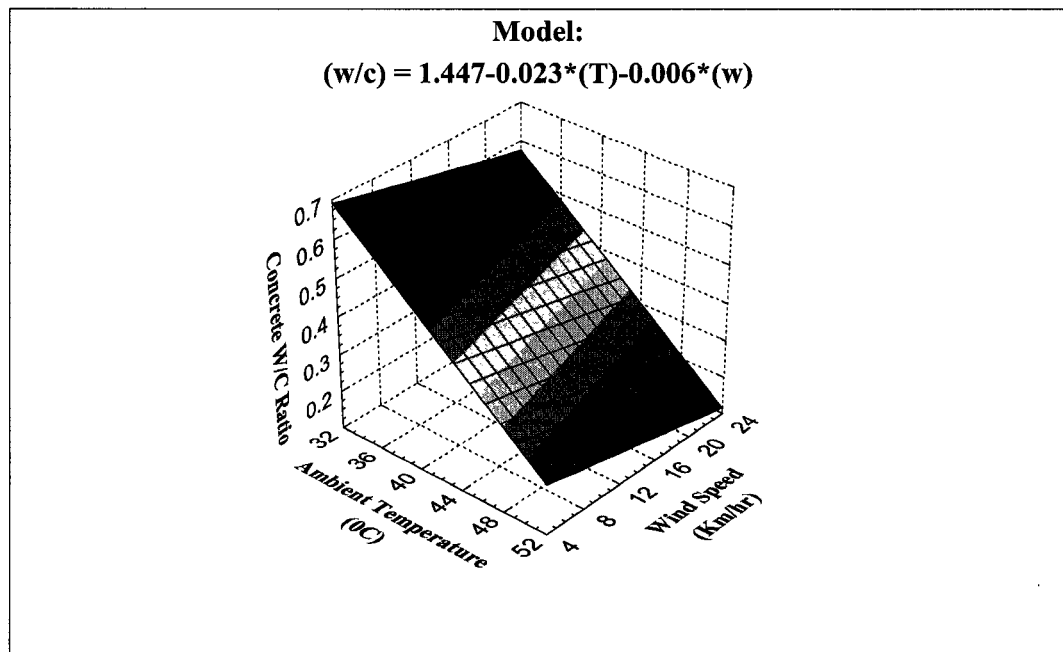


Figure 5.51: Water Cement Ratio of Concrete ~ Ambient Temperature and Wind Speed

## 5.7 Best Fit Diffusivity Law Parameters for Repair Materials

Numerical computation of diffusivity law parameters ( $b_0$ ,  $b_1$  &  $n$ ) and convective transfer coefficient ( $h_f$ ) were carried out for FMC1 & FMC2 under each exposure regime, using DIANA-2D, following the procedure described in section 5.2.4. For each case iterative runs were first carried out for the 100x100x40 mm specimen to ascertain the values of  $b_0$ ,  $b_1$ ,  $n$  &  $h_f$  which best fit the experimental moisture loss data. Computed parameter values were then verified by running the model for specimens of other thickness and hence fine-tuned. However comparison plots for experimental and numerical moisture loss, are presented for 40 mm specimen only.

### 5.7.1 Diffusivity Parameters for FMC1

Diffusivity parameters for FMC1 were first computed under the exposure temperature of 30 °C and 60 % relative humidity. Parameter values were obtained and confirmed following the above-mentioned procedure. Computed mean moisture loss showed a good fit with the experimental mean moisture loss data for each specimen. Figure 5.52 shows the comparison for the 40 mm specimen.

The entire procedure was repeated for ambient temperature of 50 °C (R.H = 50 %). Comparison plot for 40 mm specimen is shown in Figure 5.53. Selected parameter values yielded a good fit.

Next the parameters were evaluated under exposure temperature of 50 °C, relative humidity of 50 % and wind speed of 12 km/hr. For the selected parameter values, reasonable fits were obtained between the experimental and computed moisture loss data

for each specimen size. Figure 5.54 shows the comparison plot for specimen thickness of 40 mm.

### **5.7.2 Diffusivity Parameters for FMC2**

DIANA-2D was used in a similar manner to that for FMC1 to compute the diffusivity parameters for FMC2. Comparison of computed and experimental mean moisture loss data is presented in Figures 5.55-5.57, for the specimen size of 100x100x40 mm. It can be seen that for the selected parameter values good fits were obtained.

Parameter values for all of these cases are reported in Table 5.2.

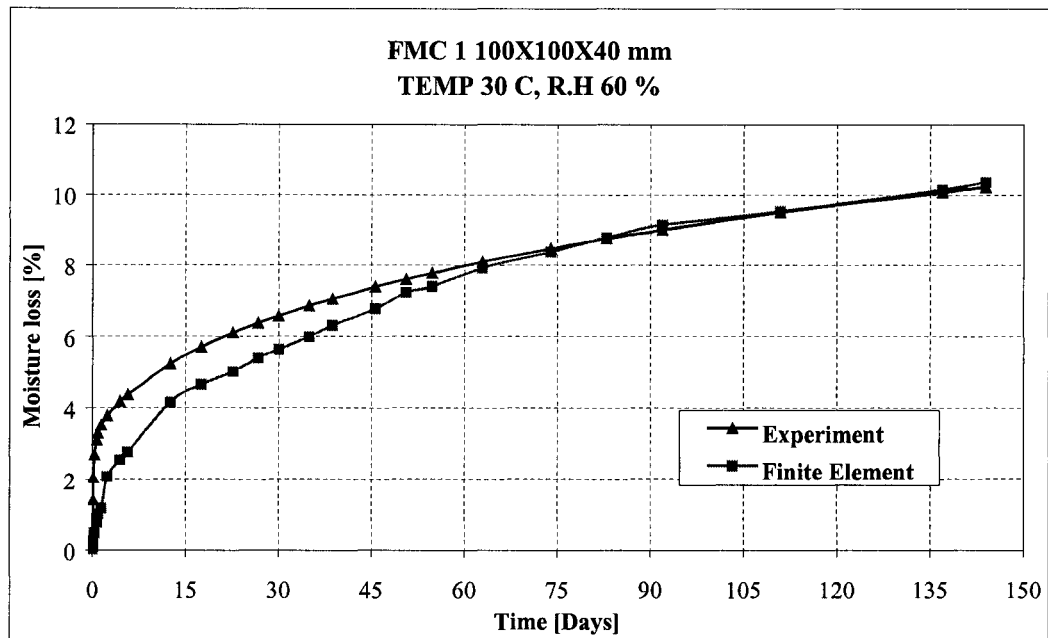


Figure 5.52: Computed & Experimental Mean Moisture Loss (%) for  
FMC1 - 100x100x40 mm Specimen at 30 °C & 60 % R.H

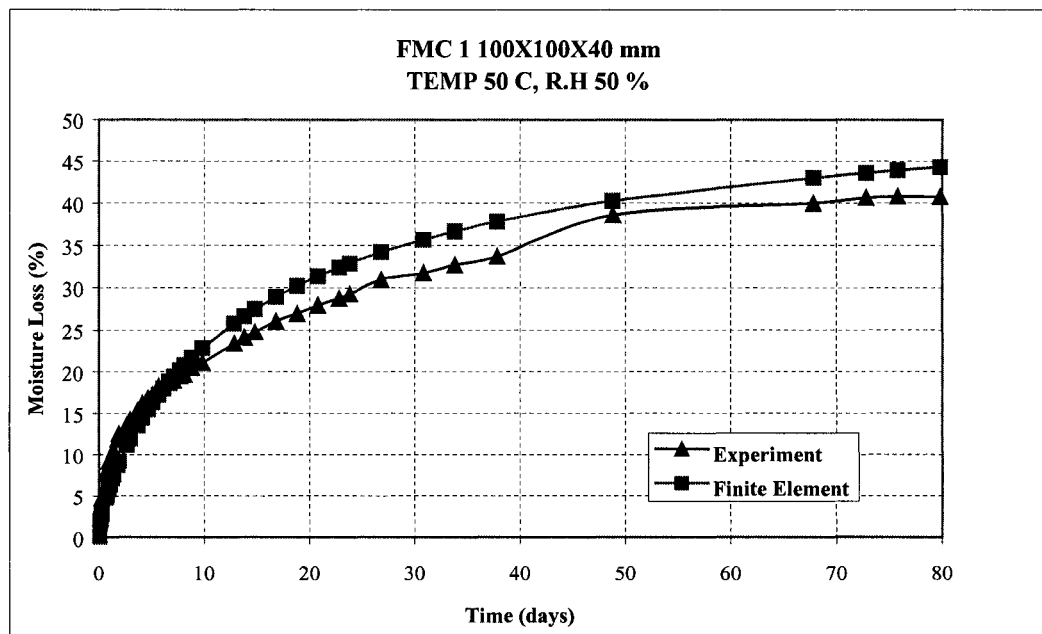


Figure 5.53: Computed & Experimental Mean Moisture Loss (%) for  
FMC1 - 100x100x40 mm Specimen at 50 °C & 50 % R.H

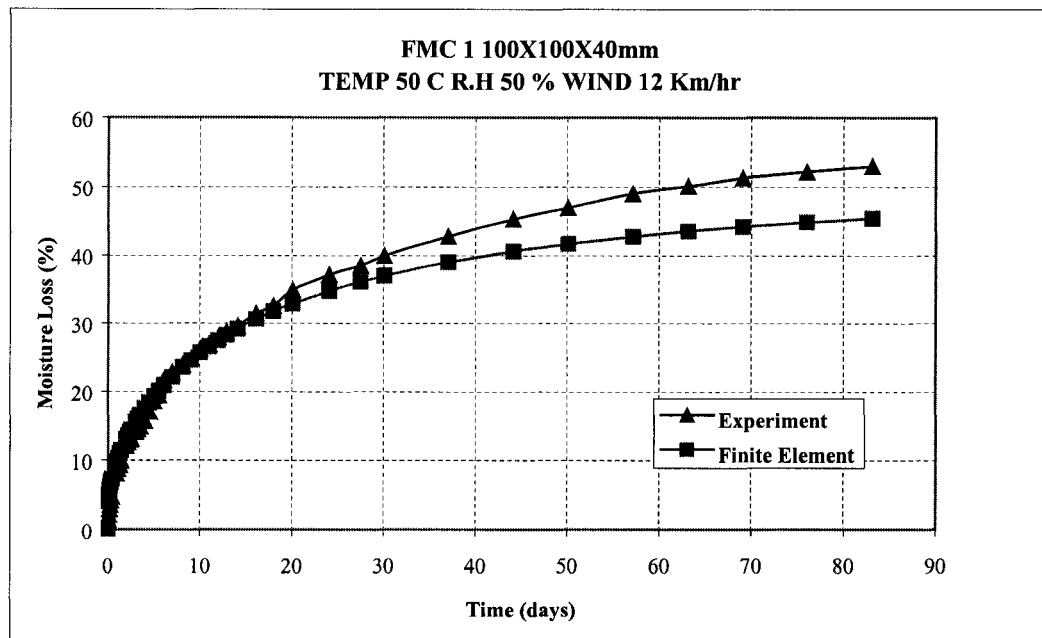


Figure 5.54: Computed & Experimental Mean Moisture Loss (%) for  
FMC1 - 100x100x40 mm Specimen at 50 °C, 50 % R.H & 12 km/hr Wind

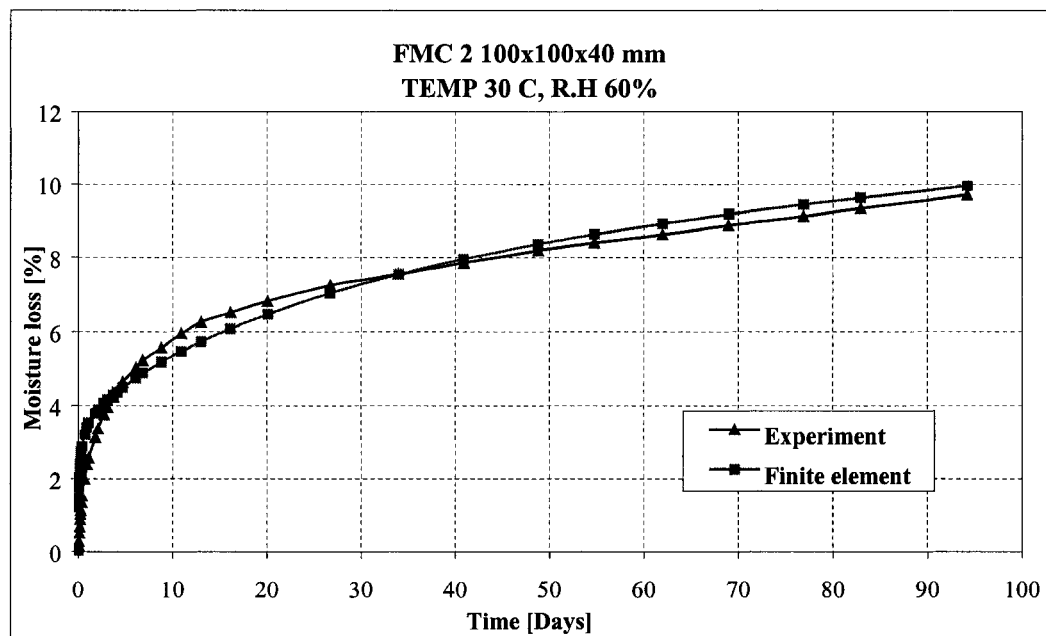


Figure 5.55: Computed & Experimental Mean Moisture Loss (%) for  
FMC2 - 100x100x40 mm Specimen at 30 °C & 60 % R.H

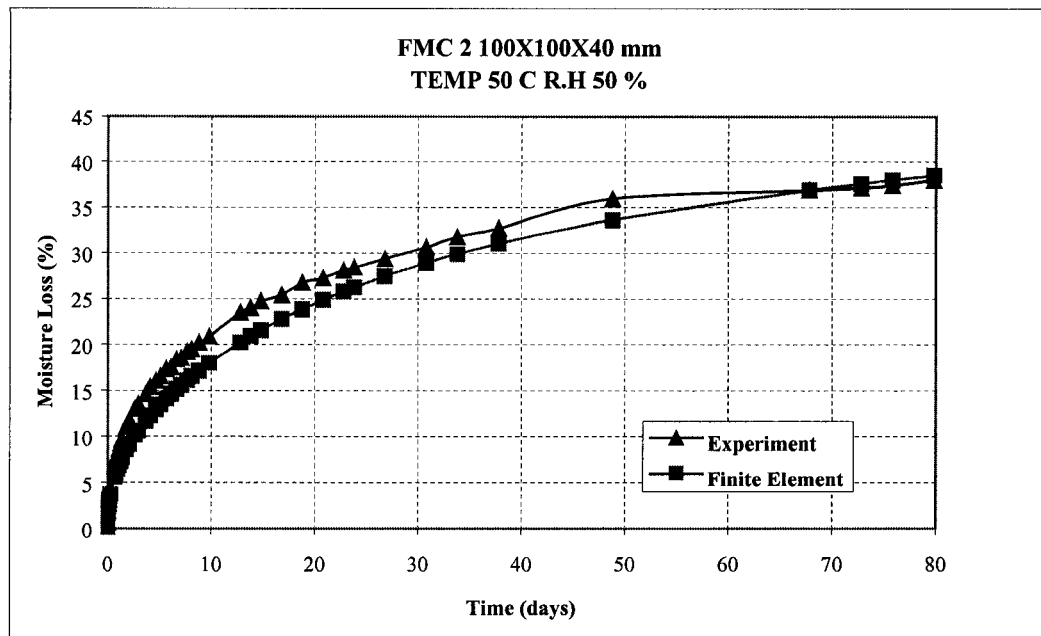


Figure 5.56: Computed & Experimental Mean Moisture Loss (%) for

FMC2 - 100x100x40 mm Specimen at 50 °C & 50 % R.H

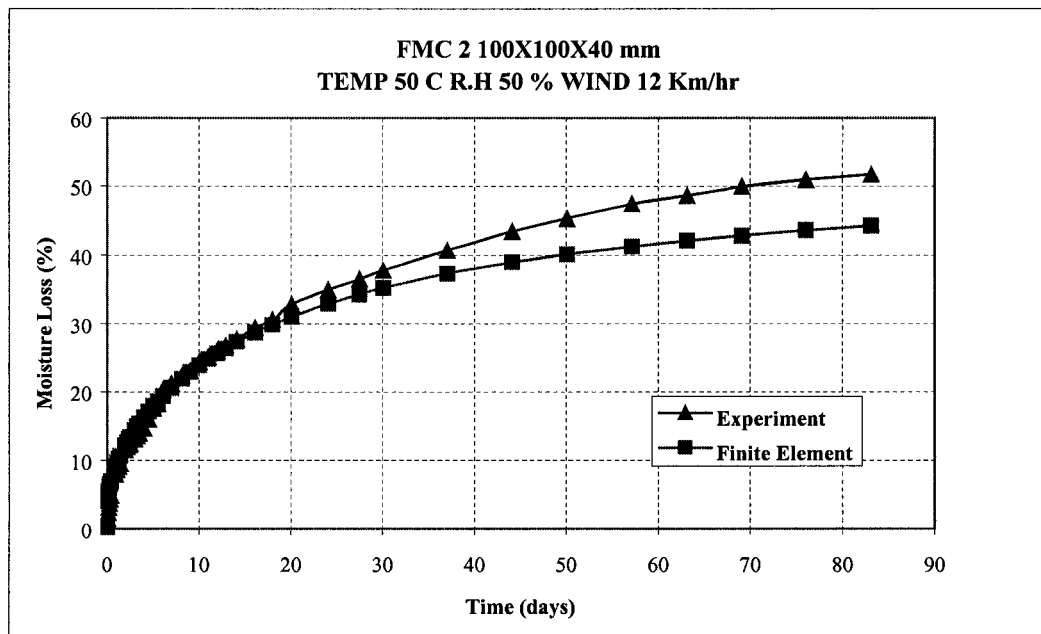


Figure 5.57: Computed & Experimental Mean Moisture Loss (%) for

FMC2 - 100x100x40 mm Specimen at 50 °C, 50 % R.H & 12 km/hr Wind

### 5.7.3 Effect of Temperature

Diffusivity-normalized moisture content curves for FMC1 & FMC2 at the two exposure temperatures are shown in Figures 5.58-5.59. It can be seen that at 30 °C both FMC1 and FMC2 show a very steep fall in diffusivity value as the moisture content is reduced from 100 % to 95 %. Diffusivity of these materials at 95 % moisture content is 20-25 % of the value at 99 % moisture content, and for the moisture content below 90 % it is almost constant. Rahman [25] reported similar behavior for his repair materials under normal temperature of 22 °C. He found the diffusivity at 95 % moisture content to be 30-35 % of the 99 % values.

However at an ambient temperature of 50 °C fall in the diffusivity value is found to be gradual. Diffusivity at 95 % moisture content in this case is about 80 % of the value at 99 % moisture content.

As shown by these graphs, diffusivity at 50 °C is much higher than at 30 °C. This effect is clearly visible between the moisture content of 98-90 %. The effect of higher temperature on diffusivity value is accounted for in the diffusivity law by using a higher value of  $b_0$ , lower value of  $b_1$  and a much lower value of  $n$ .

Average diffusivity value for FMC1 at 30 °C is found to be 0.01 cm<sup>2</sup>/day, while at 50 °C as 0.066 cm<sup>2</sup>/day. Similarly for FMC2 the average diffusivity value at 30 °C is found to be 0.008 cm<sup>2</sup>/day, while at 50 °C as 0.055 cm<sup>2</sup>/day.

Table 5.2: Parameters for Diffusivity Law of Repair Materials,  $D(C) = b_0 \tan(b_1 c^n)$ 

Mater.	Temp.	R.H	Wind	$h_f$	$b_0$	$b_1$	$n$	$D_{av}$
Type	$^{\circ}\text{C}$	%	km/hr	cm/day				$\text{cm}^2/\text{d}$
FMC1	30	60	Nil	0.3	0.05	1.5	26.0	0.01
FMC1	50	50	Nil	0.3	0.6	0.5	3.75	0.066
FMC1	50	50	12	5.0	0.6	0.5	3.75	0.066
FMC2	30	60	Nil	0.3	0.15	1.1	30.0	0.008
FMC2	50	50	Nil	0.3	0.5	0.5	3.75	0.055
FMC2	50	50	12	5.0	0.5	0.5	3.75	0.055

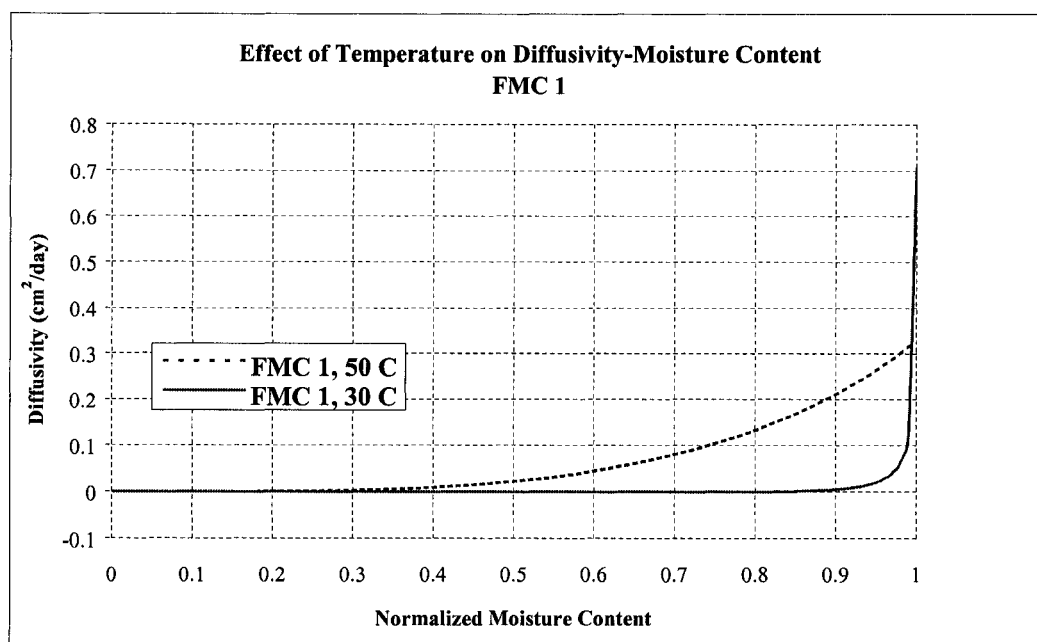


Figure 5.58: Effect of Temperature on Diffusivity-Normalized Moisture Content for  
FMC1

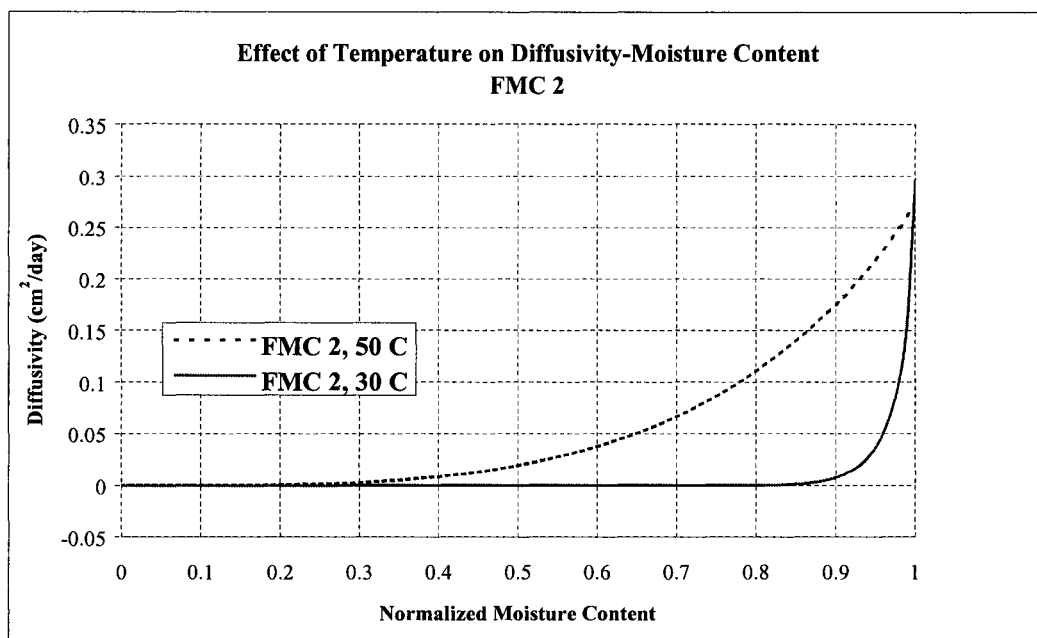


Figure 5.59: Effect of Temperature on Diffusivity-Normalized Moisture Content for  
FMC2

## 5.8 Effect of Wind Speed on Convective Transfer Coefficient

The effect of wind speed on mean moisture loss can be predicted by DIANA-2D through convective transfer coefficient/surface factor ( $h_f$ ). This parameter accounts for rate of drying/evaporation of the moisture that is coming to the specimen surface through diffusion.

From the finite element runs on various diffusivity specimens of concrete and repair, it was found that  $h_f$  depends primarily only on the wind speed and is independent of the material type or water-cement ratio of the mix. To fit the experimental moisture loss data at higher wind speeds, a higher value of  $h_f$  had to be used, values summarized in Table 5.3. The effect is similar in concept to that of forced convection in heat transfer problems, where the value of convective heat-transfer coefficient depends upon the intensity of wind speed. Figure 5.60 shows the regressed relationship between  $h_f$  and wind speed ( $\omega$ ). Linear form gives a good fit with  $R^2$  value of 0.9175. The relationship is found to be as follows:

$$h_f = 0.333(\omega) - 0.051 \quad (5.28)$$

Table 5.3: Convective Transfer Coefficient at Various Wind Speeds

Wind (Km/hr)	0	6	12	22
$h_f$ (Cm/day)	0.3	0.8	5.0	7.0

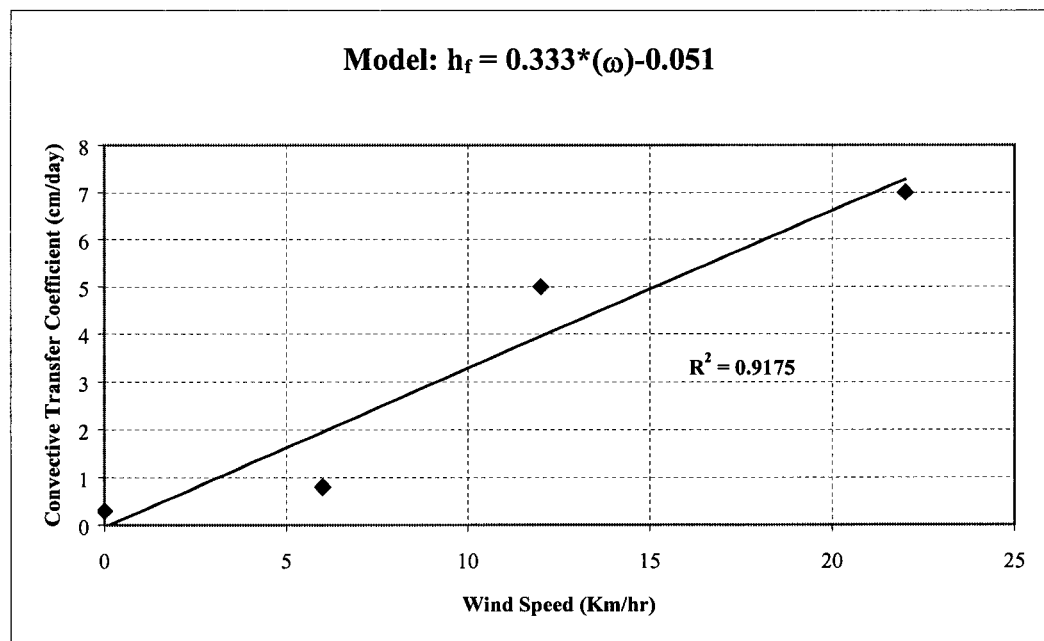


Figure 5.60: Convective Transfer Coefficient ~ Wind Speed

## **CHAPTER 6**

# **CONCLUSIONS AND RECOMMENDATIONS**

### **6.1 Conclusions**

The primary aim of this research was to investigate the influence of water-cement ratio, ambient temperature and wind speed on moisture transport properties of concrete and repair materials, respectively. The main conclusions drawn from the results can be summarized as follows:

1. A combined experimental-Finite element based approach, suggested by Rahman et al. [70] is used to determine the moisture diffusivity of selected materials. Adopted functional form for the moisture diffusivity is found to replicate the experimental moisture loss data for all concrete mixes and repair materials, under each exposure regime, for the selected values of unknown parameters  $b_0$ ,  $b_1$  &  $n$  used in the functional form.
2. Coefficient of moisture diffusivity, for both concrete and repair materials at an exposure temperature of 35 & 30 °C respectively, shows a rapid fall ( $n = 5.3, 6.5, 9.25$  &  $26.0, 30.0$ ) with the reduction in moisture content up to 90 %. However at 50 °C, the drop is observed to be more gradual ( $n = 2.7, 3.1, 3.25$  &  $3.75$ ). Below a

moisture content value of 20-40 % it tends to become zero for all temperature ranges.

3. Moisture diffusivity of concrete and repair materials is found to increase significantly with the rise in ambient temperature.
4. A regression model is proposed in Equation 5.21, to help engineers calculate average moisture diffusivity of ordinary concrete at an ambient temperature of 50 °C knowing the value at 35 °C:

$$(D_{av})^{50} = 0.2836(\exp)^{1.36*(D_{av})^{35}}$$

5. It is found that moisture diffusivity of concrete increases with the increase in w/c ratio of the mix. The effect is more pronounced at low exposure temperatures.
6. To calculate average moisture diffusivity of ordinary concrete at 35 °C & 50 °C from the water-cement ratio of the mix, Equation 5.20 is proposed:

$$(D_{av})^T = A(T)*(w/c) + B(T)$$

At 35 °C the value of 'A' is 0.6057 & 'B' is -0.1003 and at 50 °C the value of 'A' is 0.3543 & 'B' is 0.1963.

7. Diffusivity law parameters  $b_0$  and  $b_1$  are found to be functions of ambient temperature, whereas 'n' varies with both temperature and w/c ratio of concrete. To find regression models for these parameters and hence ultimately express the

diffusivity law for concrete explicitly in terms of moisture content, w/c ratio and ambient temperature, it is proposed to carry out similar study under another set of exposure temperature. A temperature of 70 °C has been recommended for research under a KFUPM funded project.

8. An accelerated rate of moisture loss is observed under high wind speed and is simulated using a higher value of convective transfer coefficient ( $h_f$ ) in the finite element model. Equation 5.28 gives the regression model to predict value of  $h_f$  under any wind speed exposure:

$$h_f = 0.333(\omega) - 0.051$$

9. Average moisture diffusivity of concrete is found to be approximately six times of that of repair materials at comparable compressive strengths under similar exposures.
10. The rate of development of shrinkage strain is found to increase with the increase in moisture diffusivity for both concrete and repair materials.
11. It is found that water permeability of concrete is in direct relation with its moisture diffusivity. Equation 5.23 is proposed to estimate average value of coefficient of moisture diffusivity for ordinary concrete, at an ambient temperature of 35 & 50 °C, based upon the water penetration depth values obtained from the relatively simple water permeability test [DIN 1048]:

$$(D_{av})^T = A(T) * (e) + B(T)$$

Where

$$A(50) = 0.002, B(50) = 0.291, A(35) = 0.0032 \text{ \& } B(35) = 0.0714.$$

12. With the increase in compressive strength of concrete, the moisture diffusivity tends to decrease. Regression model is presented in Equation 5.22 to help engineers get a rough idea of average moisture diffusivity of ordinary concrete at 35 & 50 °C knowing its compressive strength:

$$(D_{av})^T = A(T) * (fc') + B(T)$$

Where

$$A(50) = -0.0025, B(50) = 0.4614, A(35) = -0.0044 \text{ \& } B(35) = 0.355.$$

13. In lieu of diffusivity computations, which are difficult, time consuming and involve approximations, a simplified criterion based upon moisture loss from a specimen is recommended for assessing moisture diffusion characteristics of concrete in hot weather conditions. Mean moisture loss in a 100x100x75 mm specimen can be measured for a period of 28 days at 50±2 °C temperature and 40±3 % R.H. The percentage of diffusible moisture, which is the percentage of moisture lost, based on evaporable moisture content (obtained by heating the specimen at 105±5 °C) is then computed. A moisture loss of ≤ 32 % at 28 days would signify a mix of acceptable diffusivity.

14. A new approach to mix design based upon moisture diffusivity of concrete is presented. A model (Eqn. 5.28) using three invariant relationships linking the primary variables is proposed to calculate water-cement ratio for crack free concrete under various ambient combinations of temperature ( $T$ ) and wind speed ( $\omega$ ), for a relative humidity of 40%. This could be a useful guideline for concreting under dry and hot weather conditions:

$$(w/c) = 1.447 - 0.023(T) - 0.006(\omega)$$

15. It has been shown that moisture diffusivity and hence the shrinkage strain in concrete increases significantly with the rise in ambient temperature. In fresh concrete this would result in a rapid growth of tensile stresses whereas the compressive strength develops at a slower rate, which may result in premature cracking. Thus moisture diffusivity should be considered as a key physical parameter in context to concreting under hot weather conditions.
16. It is recommended to use chilled water for mixing and curing of fresh concrete, use wind-breakers and avoid pouring concrete on hot or windy days when the humidity levels are low. Also based on proposed diffusivity criterion it is recommended to limit the water cement ratio of concrete to a maximum of 0.45 for use in hot arid environments.
17. Same methodology adopted in this research can be extended to the broader problem of mass transport of aggressive species in concrete.

## **6.2 Recommendations for Future Research**

Due to the wide scope of this work, following recommendations for future research in the same area can be made:

- i. The effect of varying other mix proportions, like aggregate content, cement content & maximum aggregate size and the use of different ratios of silica fume and blast furnace slag, on moisture diffusivity of concrete should be investigated.
- ii. Standard concrete mixes used by ARAMCO and SCECO must be tested for moisture diffusivity under the prevalent summer conditions of Eastern Province of Saudi Arabia.
- iii. The effect of cracking on moisture diffusivity of concrete should be investigated experimentally and modeled.
- iv. In order to understand true relationship between concrete microstructure and its moisture transport properties, investigations should be carried out on well-characterized specimens with known degree of hydration, porosity of the cement paste and width of interfacial zones.
- v. Computer simulations should be carried out to make microstructure-transport connection, by comparing digital images of microstructure with computed moisture transport properties.

## APPENDIX-A

### SAMPLE INPUT FILE FOR DIANA-2D

Finite Element Analysis of Moisture Diffusion in 2-D

NPOIN NELEM NVFIX NNODE NMATS NPROP NGAUS NALGO NINCS  
IFORM STMOIS

441 100 0 9 1 2 3 1 36  
1 0.99

Time Period for Computation of Diffusivity

0.00 0.04 0.08 0.16 0.51 0.68 0.84 1.01 1.52 1.81 2.10 2.53  
2.86 3.53 4.67 4.96 5.61 6.06 6.55 7.56 8.55 10.65 13.66 15.14  
19.63 26.63 33.64 39.66 44.52 50.61 57.52 66.66 73.65 80.65 87.65 96.53

Moisture Loss Percentage

0.00 0.58 1.46 2.53 5.88 6.74 7.40 8.23 10.29 11.39 12.22 12.77  
13.18 14.51 16.91 17.34 18.25 18.87 19.47 21.02 22.35 24.62 28.05 28.58  
31.19 35.11 38.16 40.60 42.18 43.79 45.41 47.38 48.74 50.10 51.54 52.16

NITER TOLER NECOD NSCOD NCONC NOUTP

100 0.001 1 0 0 0

Element Connectivity Data

Elem.#	Mat#	Nodes #									
1	1	1	2	3	24	45	44	43	22	23	
2	1	3	4	5	26	47	46	45	24	25	
3	1	5	6	7	28	49	48	47	26	27	
4	1	7	8	9	30	51	50	49	28	29	
5	1	9	10	11	32	53	52	51	30	31	
6	1	11	12	13	34	55	54	53	32	33	
7	1	13	14	15	36	57	56	55	34	35	
8	1	15	16	17	38	59	58	57	36	37	
9	1	17	18	19	40	61	60	59	38	39	
10	1	19	20	21	42	63	62	61	40	41	
11	1	43	44	45	66	87	86	85	64	65	
12	1	45	46	47	68	89	88	87	66	67	
13	1	47	48	49	70	91	90	89	68	69	
14	1	49	50	51	72	93	92	91	70	71	
15	1	51	52	53	74	95	94	93	72	73	

16	1	53	54	55	76	97	96	95	74	75
17	1	55	56	57	78	99	98	97	76	77
18	1	57	58	59	80	101	100	99	78	79
19	1	59	60	61	82	103	102	101	80	81
20	1	61	62	63	84	105	104	103	82	83
21	1	85	86	87	108	129	128	127	106	107
22	1	87	88	89	110	131	130	129	108	109
23	1	89	90	91	112	133	132	131	110	111
24	1	91	92	93	114	135	134	133	112	113
25	1	93	94	95	116	137	136	135	114	115
26	1	95	96	97	118	139	138	137	116	117
27	1	97	98	99	120	141	140	139	118	119
28	1	99	100	101	122	143	142	141	120	121
29	1	101	102	103	124	145	144	143	122	123
30	1	103	104	105	126	147	146	145	124	125
31	1	127	128	129	150	171	170	169	148	149
32	1	129	130	131	152	173	172	171	150	151
33	1	131	132	133	154	175	174	173	152	153
34	1	133	134	135	156	177	176	175	154	155
35	1	135	136	137	158	179	178	177	156	157
36	1	137	138	139	160	181	180	179	158	159
37	1	139	140	141	162	183	182	181	160	161
38	1	141	142	143	164	185	184	183	162	163
39	1	143	144	145	166	187	186	185	164	165
40	1	145	146	147	168	189	188	187	166	167
41	1	169	170	171	192	213	212	211	190	191
42	1	171	172	173	194	215	214	213	192	193
43	1	173	174	175	196	217	216	215	194	195
44	1	175	176	177	198	219	218	217	196	197
45	1	177	178	179	200	221	220	219	198	199
46	1	179	180	181	202	223	222	221	200	201
47	1	181	182	183	204	225	224	223	202	203
48	1	183	184	185	206	227	226	225	204	205
49	1	185	186	187	208	229	228	227	206	207
50	1	187	188	189	210	231	230	229	208	209
51	1	211	212	213	234	255	254	253	232	233
52	1	213	214	215	236	257	256	255	234	235
53	1	215	216	217	238	259	258	257	236	237
54	1	217	218	219	240	261	260	259	238	239
55	1	219	220	221	242	263	262	261	240	241
56	1	221	222	223	244	265	264	263	242	243
57	1	223	224	225	246	267	266	265	244	245
58	1	225	226	227	248	269	268	267	246	247
59	1	227	228	229	250	271	270	269	248	249
60	1	229	230	231	252	273	272	271	250	251

61	1	253	254	255	276	297	296	295	274	275
62	1	255	256	257	278	299	298	297	276	277
63	1	257	258	259	280	301	300	299	278	279
64	1	259	260	261	282	303	302	301	280	281
65	1	261	262	263	284	305	304	303	282	283
66	1	263	264	265	286	307	306	305	284	285
67	1	265	266	267	288	309	308	307	286	287
68	1	267	268	269	290	311	310	309	288	289
69	1	269	270	271	292	313	312	311	290	291
70	1	271	272	273	294	315	314	313	292	293
71	1	295	296	297	318	339	338	337	316	317
72	1	297	298	299	320	341	340	339	318	319
73	1	299	300	301	322	343	342	341	320	321
74	1	301	302	303	324	345	344	343	322	323
75	1	303	304	305	326	347	346	345	324	325
76	1	305	306	307	328	349	348	347	326	327
77	1	307	308	309	330	351	350	349	328	329
78	1	309	310	311	332	353	352	351	330	331
79	1	311	312	313	334	355	354	353	332	333
80	1	313	314	315	336	357	356	355	334	335
81	1	337	338	339	360	381	380	379	358	359
82	1	339	340	341	362	383	382	381	360	361
83	1	341	342	343	364	385	384	383	362	363
84	1	343	344	345	366	387	386	385	364	365
85	1	345	346	347	368	389	388	387	366	367
86	1	347	348	349	370	391	390	389	368	369
87	1	349	350	351	372	393	392	391	370	371
88	1	351	352	353	374	395	394	393	372	373
89	1	353	354	355	376	397	396	395	374	375
90	1	355	356	357	378	399	398	397	376	377
91	1	379	380	381	402	423	422	421	400	401
92	1	381	382	383	404	425	424	423	402	403
93	1	383	384	385	406	427	426	425	404	405
94	1	385	386	387	408	429	428	427	406	407
95	1	387	388	389	410	431	430	429	408	409
96	1	389	390	391	412	433	432	431	410	411
97	1	391	392	393	414	435	434	433	412	413
98	1	393	394	395	416	437	436	435	414	415
99	1	395	396	397	418	439	438	437	416	417
100	1	397	398	399	420	441	440	439	418	419

## Nodal Coordinates

Node #	X-Coord	Y-Coord	Node #	X-Coord	Y-Coord
1	0.00	0.00	35	3.25	0.50
2	0.25	0.00	36	3.50	0.50
3	0.50	0.00	37	3.75	0.50
4	0.75	0.00	38	4.00	0.50
5	1.00	0.00	39	4.25	0.50
6	1.25	0.00	40	4.50	0.50
7	1.50	0.00	41	4.75	0.50
8	1.75	0.00	42	5.00	0.50
9	2.00	0.00	43	0.00	1.00
10	2.25	0.00	44	0.25	1.00
11	2.50	0.00	45	0.50	1.00
12	2.75	0.00	46	0.75	1.00
13	3.00	0.00	47	1.00	1.00
14	3.25	0.00	48	1.25	1.00
15	3.50	0.00	49	1.50	1.00
16	3.75	0.00	50	1.75	1.00
17	4.00	0.00	51	2.00	1.00
18	4.25	0.00	52	2.25	1.00
19	4.50	0.00	53	2.50	1.00
20	4.75	0.00	54	2.75	1.00
21	5.00	0.00	55	3.00	1.00
22	0.00	0.50	56	3.25	1.00
23	0.25	0.50	57	3.50	1.00
24	0.50	0.50	58	3.75	1.00
25	0.75	0.50	59	4.00	1.00
26	1.00	0.50	60	4.25	1.00
27	1.25	0.50	61	4.50	1.00
28	1.50	0.50	62	4.75	1.00
29	1.75	0.50	63	5.00	1.00
30	2.00	0.50	64	0.00	1.50
31	2.25	0.50	65	0.25	1.50
32	2.50	0.50	66	0.50	1.50
33	2.75	0.50	67	0.75	1.50
34	3.00	0.50	68	1.00	1.50

69	1.25	1.50	107	0.25	2.50
71	1.75	1.50	109	0.75	2.50
72	2.00	1.50	110	1.00	2.50
73	2.25	1.50	111	1.25	2.50
74	2.50	1.50	112	1.50	2.50
75	2.75	1.50	113	1.75	2.50
76	3.00	1.50	114	2.00	2.50
77	3.25	1.50	115	2.25	2.50
78	3.50	1.50	116	2.50	2.50
79	3.75	1.50	117	2.75	2.50
80	4.00	1.50	118	3.00	2.50
81	4.25	1.50	119	3.25	2.50
82	4.50	1.50	120	3.50	2.50
83	4.75	1.50	121	3.75	2.50
84	5.00	1.50	122	4.00	2.50
85	0.00	2.00	123	4.25	2.50
86	0.25	2.00	124	4.50	2.50
87	0.50	2.00	125	4.75	2.50
88	0.75	2.00	126	5.00	2.50
89	1.00	2.00	127	0.00	3.00
90	1.25	2.00	128	0.25	3.00
91	1.50	2.00	129	0.50	3.00
92	1.75	2.00	130	0.75	3.00
93	2.00	2.00	131	1.00	3.00
94	2.25	2.00	132	1.25	3.00
95	2.50	2.00	133	1.50	3.00
96	2.75	2.00	134	1.75	3.00
97	3.00	2.00	135	2.00	3.00
98	3.25	2.00	136	2.25	3.00
99	3.50	2.00	137	2.50	3.00
100	3.75	2.00	138	2.75	3.00
101	4.00	2.00	139	3.00	3.00
102	4.25	2.00	140	3.25	3.00
103	4.50	2.00	141	3.50	3.00
104	4.75	2.00	142	3.75	3.00
105	5.00	2.00	143	4.00	3.00
106	0.00	2.50	144	4.25	3.00

145	4.50	3.00	181	3.00	4.00
146	4.75	3.00	182	3.25	4.00
147	5.00	3.00	183	3.50	4.00
148	0.00	3.50	184	3.75	4.00
149	0.25	3.50	185	4.00	4.00
150	0.50	3.50	186	4.25	4.00
151	0.75	3.50	187	4.50	4.00
152	1.00	3.50	188	4.75	4.00
153	1.25	3.50	189	5.00	4.00
154	1.50	3.50	190	0.00	4.50
155	1.75	3.50	191	0.25	4.50
156	2.00	3.50	192	0.50	4.50
157	2.25	3.50	193	0.75	4.50
158	2.50	3.50	194	1.00	4.50
159	2.75	3.50	195	1.25	4.50
160	3.00	3.50	196	1.50	4.50
161	3.25	3.50	197	1.75	4.50
162	3.50	3.50	198	2.00	4.50
163	3.75	3.50	199	2.25	4.50
164	4.00	3.50	200	2.50	4.50
165	4.25	3.50	201	2.75	4.50
166	4.50	3.50	202	3.00	4.50
167	4.75	3.50	203	3.25	4.50
168	5.00	3.50	204	3.50	4.50
169	0.00	4.00	205	3.75	4.50
170	0.25	4.00	206	4.00	4.50
171	0.50	4.00	207	4.25	4.50
172	0.75	4.00	208	4.50	4.50
173	1.00	4.00	209	4.75	4.50
174	1.25	4.00	210	5.00	4.50
175	1.50	4.00	211	0.00	5.00
176	1.75	4.00	212	0.25	5.00
177	2.00	4.00	213	0.50	5.00
178	2.25	4.00	214	0.75	5.00
179	2.50	4.00	215	1.00	5.00
180	2.75	4.00	216	1.25	5.00

217	1.50	5.00	253	0.00	6.00
219	2.00	5.00	255	0.50	6.00
220	2.25	5.00	256	0.75	6.00
221	2.50	5.00	257	1.00	6.00
222	2.75	5.00	258	1.25	6.00
223	3.00	5.00	259	1.50	6.00
224	3.25	5.00	260	1.75	6.00
225	3.50	5.00	261	2.00	6.00
226	3.75	5.00	262	2.25	6.00
227	4.00	5.00	263	2.50	6.00
228	4.25	5.00	264	2.75	6.00
229	4.50	5.00	265	3.00	6.00
230	4.75	5.00	266	3.25	6.00
231	5.00	5.00	267	3.50	6.00
232	0.00	5.50	268	3.75	6.00
233	0.25	5.50	269	4.00	6.00
234	0.50	5.50	270	4.25	6.00
235	0.75	5.50	271	4.50	6.00
236	1.00	5.50	272	4.75	6.00
237	1.25	5.50	273	5.00	6.00
238	1.50	5.50	274	0.00	6.50
239	1.75	5.50	275	0.25	6.50
240	2.00	5.50	276	0.50	6.50
241	2.25	5.50	277	0.75	6.50
242	2.50	5.50	278	1.00	6.50
243	2.75	5.50	279	1.25	6.50
244	3.00	5.50	280	1.50	6.50
245	3.25	5.50	281	1.75	6.50
246	3.50	5.50	282	2.00	6.50
247	3.75	5.50	283	2.25	6.50
248	4.00	5.50	284	2.50	6.50
249	4.25	5.50	285	2.75	6.50
250	4.50	5.50	286	3.00	6.50
251	4.75	5.50	287	3.25	6.50
252	5.00	5.50	288	3.50	6.50

289	3.75	6.50	325	2.25	7.50
290	4.00	6.50	326	2.50	7.50
293	4.75	6.50	329	3.25	7.50
294	5.00	6.50	330	3.50	7.50
295	0.00	7.00	331	3.75	7.50
296	0.25	7.00	332	4.00	7.50
297	0.50	7.00	333	4.25	7.50
298	0.75	7.00	334	4.50	7.50
299	1.00	7.00	335	4.75	7.50
300	1.25	7.00	336	5.00	7.50
301	1.50	7.00	337	0.00	8.00
302	1.75	7.00	338	0.25	8.00
303	2.00	7.00	339	0.50	8.00
304	2.25	7.00	340	0.75	8.00
305	2.50	7.00	341	1.00	8.00
306	2.75	7.00	342	1.25	8.00
307	3.00	7.00	343	1.50	8.00
308	3.25	7.00	344	1.75	8.00
309	3.50	7.00	345	2.00	8.00
310	3.75	7.00	346	2.25	8.00
311	4.00	7.00	347	2.50	8.00
312	4.25	7.00	348	2.75	8.00
313	4.50	7.00	349	3.00	8.00
314	4.75	7.00	350	3.25	8.00
315	5.00	7.00	351	3.50	8.00
316	0.00	7.50	352	3.75	8.00
317	0.25	7.50	353	4.00	8.00
318	0.50	7.50	354	4.25	8.00
319	0.75	7.50	355	4.50	8.00
320	1.00	7.50	356	4.75	8.00
321	1.25	7.50	357	5.00	8.00
322	1.50	7.50	358	0.00	8.50
323	1.75	7.50	359	0.25	8.50
324	2.00	7.50	360	0.50	8.50

361	0.75	8.50	397	4.50	9.00
362	1.00	8.50	398	4.75	9.00
363	1.25	8.50	399	5.00	9.00
367	2.25	8.50	403	0.75	9.50
368	2.50	8.50	404	1.00	9.50
369	2.75	8.50	405	1.25	9.50
370	3.00	8.50	406	1.50	9.50
371	3.25	8.50	407	1.75	9.50
372	3.50	8.50	408	2.00	9.50
373	3.75	8.50	409	2.25	9.50
374	4.00	8.50	410	2.50	9.50
375	4.25	8.50	411	2.75	9.50
376	4.50	8.50	412	3.00	9.50
377	4.75	8.50	413	3.25	9.50
378	5.00	8.50	414	3.50	9.50
379	0.00	9.00	415	3.75	9.50
380	0.25	9.00	416	4.00	9.50
381	0.50	9.00	417	4.25	9.50
382	0.75	9.00	418	4.50	9.50
383	1.00	9.00	419	4.75	9.50
384	1.25	9.00	420	5.00	9.50
385	1.50	9.00	421	0.00	10.00
386	1.75	9.00	422	0.25	10.00
387	2.00	9.00	423	0.50	10.00
388	2.25	9.00	424	0.75	10.00
389	2.50	9.00	425	1.00	10.00
390	2.75	9.00	426	1.25	10.00
391	3.00	9.00	427	1.50	10.00
392	3.25	9.00	428	1.75	10.00
393	3.50	9.00	429	2.00	10.00
394	3.75	9.00	430	2.25	10.00
395	4.00	9.00	431	2.50	10.00
396	4.25	9.00	432	2.75	10.00

433	3.00	10.00
434	3.25	10.00
435	3.50	10.00
436	3.75	10.00
437	4.00	10.00
438	4.25	10.00
439	4.50	10.00
440	4.75	10.00
441	5.00	10.00

## Boundary Conditions

NOFIX          IFPRE          Prescribed Values

## Element Material Properties

Material #   Surface Factor   Env. Humidity

1                   0.8                   0.400

## Diffusivity Paramters

b0      b1      n

2.9      0.5      3.25

## Number of Convecting Edges

10

## Location of Convecting Edges

ELEM	NSCOD	NODEI	NODEJ	NODEK
10	1	21	42	63
20	1	63	84	105
30	1	105	126	147
40	1	147	168	189
50	1	189	210	231
60	1	231	252	273
70	1	273	294	315
80	1	315	336	357
90	1	357	378	399
100	1	399	420	441

## REFERENCES

1. Mehta, P.K., "Concrete Structure, Properties and Materials," Prentice Hall, New Jersey, 1986, p.2.
2. Mehta, P.K., "Concrete Technology at the cross roads-Problems and opportunities," Mohan Malhotra Symposium, Concrete Technology-Past, Present & Future, ACI Publication, SP-1144, ed. P. K. Mehta, 1994, pp. 1-30.
3. Rostam, S., Editor, CEB-RILEM International Workshop on Durability of Concrete Structures, May 1983, Copenhagen, p. 432.
4. "Guide to Evaluation of Concrete Structures Prior to Rehabilitation," ACI Committee 364 Report, ACI Materials Journal, Sept-Oct. 1993, pp. 479-498.
5. Emmons, P.H. and Vaysburd, A.M., "System Concept in Design and Construction of Durable Concrete Repairs," Concrete International, Vol.1, No.1, 1996.
6. Emberson, N.K. and Mays, G.C., "Significance of Property Mismatch in the Patch Repair of Structural Concrete-Part I: Properties of Repair Systems," Magazine of Concrete Research, vol.42, No.152, 1990, pp.147-160.
7. Jones, R., Chiu, W. K. & Hana, S., "Potential Failure Mechanisms of Bonded Composite Repairs for Metal & Concrete," Theoretical & Applied Fracture Mechanics, Vol. 21, 1994, pp. 107-119.

8. Emmons, P.H. and Vaysburd, A.M., "The Total System Concept Necessary for Improving the Performance of Repaired Structures," *Concrete International*, Vol.17, No.3, March 1995, pp.31-36.
9. Cusson, D. and Mailvaganam, V., "Durability of Repair Materials," *Concrete International*, March 1996, pp.34-38.
10. Al-Mandil, M.Y., Azad, A.K., Baluch, M.H. and Sharif, A.M., Jamarat Bridge, First Progress Report, Ministry of Communications Contract, Dept. of Civil Engineering, KFUPM, December 1995, 91 pp.
11. Al-Mandil, M.Y., Azad, A.K., Baluch, M.H., Pearson-Kirk, D., Alfarabi Sharif and Al-Dhalaan, M.A., A Study of Cracking of Concrete Bridge Decks in Saudi Arabia, Ministry of Communications Contract, Dept. of Civil Engineering, KFUPM, 1984-1987.
12. Al-Nufaily, A.I., Repair of Pre-cast Concrete Slabs Subjected to Spalling Due to Corrosion of Reinforcement, Technical Report, Dept. of Civil Engineering, KFUPM, June 1994, 68 pp.
13. Baluch, M.H., Azad, A.K., Alfarabi Sharif, Al-Sulaimani, G.J. and Basunbul, I.A., Diagnosis, Assessment and Repair of Jubail Sports Club, Dept. of Civil Engineering, KFUPM, 1992.
14. Al-Gahtani, A.S., Rasheeduzzafar and Al-Musallam, A.A., "Performance of Repair Materials Exposed to Fluctuation of Temperatures," *Journal of Materials in Civil Engineering*, Vol.7, No.1, 1995.
15. Rizzo, E.M. and Sobleman, M.B. "Selection Criteria for Concrete Repair Materials," *Concrete International*, September 1989, pp.46-49.

16. Malhas, F.A., "The Effect of Drying Shrinkage on Bond Strength between Repair Mortars and Concrete," Second Regional Conference of ASCE-SAS, Beirut, Nov.1995, pp.891-898.
17. Bazant, Z.P. and Najjar, L.J., "Drying of Concrete as a Non-Linear Diffusion Problem," Cement and Concrete Research, Vol.1, 1971, pp.461-473.
18. Pleinert, H., Sadouki, H. and Wittmann, F.H., "Determination of Moisture Distributions in Porous Building Materials by Neutron Transmission Analysis," Materials and Structures, Vol.31, May 1998, pp.218-224.
19. Baluch, M.H., Rahman, M.K. and Al-Gadhib, A.H., "Risk of Cracking and Delamination in Patch Repair," ASCE Journal of Materials in Civil Engineering, Vol.14, No.4, July/August 2002, pp.294-302.
20. Welly, J.R., Wicks, C.E. and Wilson, R.E., Fundamentals of Momentum, Heat and Mass Transfer, John Wiley & Sons, New York, 1984.
21. Meng, B., "Calculation of Moisture Transport Coefficients on the Basis of Relevant Pore Structure Parameters," Materials and Structures, Vol.27, 1992, pp.125-134.
22. Sakata, K., Nishigaki, M. and Kuramoto, O., "Finite Element Analysis of Nonlinear Moisture Transfer Problems in Concrete," Research & Development, Vol.1, No.4, Okayama University, March 1980, pp.11-33.
23. Hirschfelder, J.O., Curtiss, C.F. and Bird, R.B., Molecular Theory of Gases and Liquids, John Wiley & Sons, New York, 1954.

24. Jooss, M. and Reinhardt, H.W. "Permeability and Diffusivity of Concrete as Function of Temperature," *Cement and Concrete Research*, Vol.32, April 2002, pp.1497-1504.
25. Rahman, M.K., "Simulation and Assessment of Concrete Repair System," PhD Dissertation, KFUPM, 1999.
26. Asad, M., *Computational Modeling of Shrinkage in Repaired Concrete*, Master's Thesis, King Fahd University of Petroleum and Minerals, Dhahran, KSA, 1995.
27. Asad, M., Baluch, M.H. and Al-Gadhib, A.H., "Drying Shrinkage Stresses in Restrained Concrete Systems," *Magazine of Concrete Research*, Vol.49, No.181, Dec. 1997, pp.283-293.
28. Atkins, P.W., "Physical Chemistry," Fifth Edition, Oxford University Press, 1994.
29. Janz, M., "Methods of Measuring the Moisture Diffusivity at High Moisture Levels," Report TVBM-3076, Division of Building Materials, University of Lund, 1997.
30. Carlson, R.W., "Drying Shrinkage of Large Concrete Members," *American Concrete Institute Journal* 33, 327, 1937.
31. Pickett, G., "Shrinkage Stresses in Concrete," *Journal of ACI*, Part-I, Vol.17, No.3, 1946, pp.165-203 and Part-II, Vol.17, No. 4, 1946, pp.361-398.
32. Philajavaara, S.E. and Vaisanen, J. "Numerical Solution of Diffusion Equation with Diffusivity Concentration Dependant," *The State Institute for Technical Research*, Helsinki, Publication No.87, 1965.

33. Johansson, J. E., "Analysis of Creep & Shrinkage in Concrete and its Application to Concrete Top Layers," *Cement & Concrete Research*, Vol.8, 1978, pp. 441-454.
34. Garbozyski, M., & Shah, S. P., "Model to Predict Cracking in Fiber Reinforced Concrete due to Restrained Shrinkage," *Magazine of Concrete Research*, Vol.41, No.148, 1989, pp. 125-135.
35. Alvaredo, M. A., "Drying Shrinkage & Crack Formation," Ph.D. Dissertation, Swiss Federal Institute of Technology, Zurich, 1994.
36. Sakata, K., "A Study on Moisture Diffusion in Drying and Drying Shrinkage of Concrete," *Cement & Concrete Research*, Vol.13, No.2, 1983, pp.216-224.
37. Penev, D. and Kawamura, M., "Moisture Diffusion in Soil-Cement Mixtures and Compacted Lean Concrete," *Cement & Concrete Research*, Vol.21, No.1, 1991, pp.137-146.
38. Asad, M., Baluch, M.H., Al-Amoudi, O.S.B., Al-Gadhib, A.H. and Alghamdi, S.A., "Moisture Diffusion & Shrinkage in Concrete Repair Materials," Fourth Saudi Engineering Conference, King Abdulaziz University, Jeddah, Nov. 1995.
39. Asad, M., Baluch, M.H., Al-Amoudi, O.S.B., Al-Gadhib, A.H. and Alghamdi, S.A., "Non-linear Finite Element Model for Moisture Diffusion in Repair Materials," Second Regional Conference of ASCE-SAS, Beirut, Nov. 1995, pp.891-898.
40. Granger, L., Torrenti, J.M. and Acker, P., "Thoughts about Drying Shrinkage: Scale Effects and Modeling," *Materials and Structures*, Vol.30, March 1997, pp.96-105.

41. Allen, A. J., Oberthur, R. C., Pearsons, D., Schofield, P., & Wilding, C. R.,  
“Development of Fine Porosity & Gel Structure of Hydrating Cement Systems,”  
Philosophical Magazine B, Vol.56, No.3, 1987, pp. 263-288.
42. Garboczi, E.J., “Performance Criteria for Concrete Durability,” Edited by Kropp,  
J. & Hilsdrof, H.K., E & FN Spon, London, 1995.
43. Chen, Y., & Odler, I., “On the Origin of Portland Cement Setting,” Cement &  
Concrete Research, Vol.22, 1992, pp. 1130-1140.
44. Bentz, D. P. & Garboczi, E. J., “Percolation of Phases in a 3-D Cement Paste  
Micro Structural Model,” Cement & Concrete Research, Vol.21, 1991, pp. 325-  
344.
45. Ramakrishnan, V., “Latex-modified Concrete and Mortars,” Synthesis of  
Highway Practices 179, NCHRP, Transportation Research Board, 1992, p. 58.
46. Ohama, Y., “Principles of Latex modification & some Typical Properties of  
Latex Modified Mortars and Concretes,” ACI Materials Journal, Nov.-Dec.  
1987, pp. 511-518.
47. Soroka, I., “Concrete in Hot Environments,” E & FN Spon, U.K, 1993, p. 251.
48. Scrivener, K. L., “Micro Structure of Concrete,” Materials Science of Concrete,  
American Ceramic Society, Westerville, 1990.
49. Garboczi, E. J. & Bentz, D. P., “Digital Simulation of Aggregate-Paste  
Interfacial Zone in Concrete,” Journal of Materials Research, Vol.6, No.1, 1991,  
pp. 196-201.

50. Bentz, D.P. & Garboczi, E.J., "Simulation Studies of the Effects of Mineral Admixtures on the Cement Paste-Aggregate Interfacial Zone," *ACI Materials Journal*, Vol. 88, No. 5, 1991, pp. 518-529.
51. Houst, Y. F., Sadouki, H. & Wittmann, F. H., "Influence of Aggregate Concentration on the Diffusion of CO<sub>2</sub> & O<sub>2</sub>," *Interfaces in Cementitious composites*, London, 1992, pp. 279-288.
52. Bentz, D. P., Garboczi, E. J. & Stutzman, P. E., "Computer Modeling of Interfacial Transition Zone in Concrete," *Interfaces in Cementitious Composites*, London, 1992, pp. 107-116.
53. Synder, K. A., Winslow, D. N., Bentz, D. P. & Garboczi, E. J., "Effects of Interfacial Transition Zone Percolation on Cement Based Composite Transport Properties," *Advance Cementitious Systems*, Materials Research Society, Pittsburgh, 1992, pp. 265-270.
54. Synder, K. A., Bentz, D. P., Garboczi, E. J. & Winslow, D. N., "Interfacial Transition Zone Percolation in Cement-Aggregate Composites," *Interfaces in Cementitious Composites*, London, pp. 259-268.
55. Winslow, D. N. & Diamond, S., *ASTM Journal of Materials*, Vol.5, 1970, p.564.
56. Torquato, S. J., *Chem. Phys*, Vol.85, 1986, pp. 624-628.
57. Hall, C., "Barrier Performance of Concrete: A Review of Fluid Transport Theory," *Materials & Structures*, Vol.27, 1994, pp. 291-306.
58. Quenard, D. and Sallee, H., "Water Vapor Adsorption and Transfer in Cement-Based Materials: A Network Simulation," *Materials and Structures*, Vol.25, 1992, pp.515-522.

59. Spooner, D. C., "The Practical Relevance of Mechanism of Water & Water Vapor Transport in Porous Building Materials," Autoclaved Aerated Concrete, Moisture and Properties, Edited by Wittmann, F. H., 1983, Elsevier Scientific Publishing Co., Amsterdam.
60. Coussy, O., Eymard, R. & Lassabatere, T., "Constitutive Modeling of Un-Saturated Drying Deformable Materials," Journal of Engineering Mechanics, June 1998, pp. 658-667.
61. Nilsson, L.O., "Hygroscopic Moisture in Concrete-Drying Measurements and Related Material Properties," Report TVBM-1003, Lund Institute of Technology, Sweden, 1980.
62. Sadouki, H. & Van Mier, J. G. M., "Simulation of Hygral Crack Growth in Concrete Repair Systems," Materials and Structures, Vol. 30, Nov. 1997, pp. 518-526.
63. Bazant, Z.P. and Najjar, L.J., "Nonlinear Water Diffusion in Non-Saturated Concrete," Materials & Structures, Vol.5, No.25, 1972, pp.3-20.
64. Lowe, I.R.G., Hughes, B.P. and Walker, J., "The Diffusion of Water in Concrete at 30°C," Cement & Concrete Research, Vol.1, 1971, pp.547-557.
65. Bazant, Z.P., Sener, S. and Keun Kim, J., "Effect of Cracking on Drying Permeability and Diffusivity of Concrete," ACI Materials Journal, Sept.-Oct. 1987, pp.351-357.

66. Wittmann, X., Sadouki, H. and Wittmann, F.H., "Numerical Evaluation of Drying Test Data," Transaction of the 10th International Conference on Structural Mechanics in Reactor Technology, SMIRT-10, 1989, pp.71-79.
67. Persson, B., "Moisture in Concrete Subjected to Different Kinds of Curing," Materials and Structures, Vol.30, Nov. 1997, pp.533-544.
68. Akita, H., Fujiwara, T. and Ozaka, Y., "A Practical Procedure for the Analysis of Moisture Transfer within Concrete Due to Drying," Magazine of Concrete Research, Vol.49, No.179, June 1997, pp.129-137.
69. Iding, R. & Bresler, B., "Prediction of Shrinkage Stresses & Deformations in Concrete," Fundamental Research on Creep & Shrinkage of Concrete, Wittmann, F.H. (ed.), Martinus Nijhoff Pub, The Hague, 1982, pp. 341-352.
70. Rahman, M.K., Baluch, M.H. and Al-Gadhib, A.H., "Modeling of Shrinkage and Creep Stresses in Concrete Repair," ACI Materials Journal, Vol.96, No.5, September/October 1999, pp.542-559.
71. Al-Gadhib, A.H. and Baluch, M.H., Design Guidelines and Performance Criteria for Concrete Repair Systems, KACST Project No. AR-17-36.
72. Hedenblad, G., "Moisture Permeability of Mature Concrete, Cement Mortar and Cement Paste," Report TVBM-1014, 1993, Division of Building Materials, Lund Institute of Technology.
73. Hedenblad, G., "Material Properties for Calculation of Moisture Transport," Report T 19:1996, Swedish Council for Building Research, Stockholm.

74. Krus, M., "Moisture Transport & Storage Coefficients of Porous Mineral Building Materials, Theoretical Principles & New Test Methods," 1995, der Fakultät Bauingenieur-und Vermessungswesen, University of Stuttgart.
75. Kiebel, K., Krus, M. & Kunzel, H., "Advanced Measuring and Calculative Procedures for Moisture Assessment of Building Elements, Examples of Practical Applications, Bauphysik 15, Heft 2, 1993.
76. Adamson, B., Ahlgren, L., Bergstorm, S. G. & Nevander, L. E., "Moisture-Moisture Related Problems in Buildings," Program-Skrift 12, 1970, Stockholm, Sweden.
77. Wormald, R. & Britch, A. L., "Methods for Measuring Moisture Content Applicable to Building Materials," Building Science, Vol. 3, 1969, pp. 135-145.
78. Sandin, K., "A Method of Measuring the Moisture Distribution in Aerated Autoclaved Concrete," Division of Building Materials, Lund Institute of Technology, 1978.
79. Descamps, F., "Moisture Content Measurement Using Gamma Ray Attenuation," Research Report, Laboratorium Bouwfysica, Katholieke Universitat Leuven, 1990.
80. Nielsen, A. F., "Gamma Ray Attenuation Used for Measuring the Moisture Content & Homogeneity of Porous Concrete," Building Science, Vol. 7, 1972, pp. 257-263.
81. Quenard, D. & Sallee, H., "A Gamma Ray Spectrometer for Measurement of the Moisture Diffusivity of Cementitious Materials," Materials Research Symposium Proceedings, Boston, 28-30 Nov. 1989, Vol. 137, pp. 165-169.

82. Pel, L., "Moisture Transport in Porous Building Materials," Eindhoven University of Technology, 1995.
83. Adan, O. C. G., "Determination of Moisture Diffusivities in Gypsum Renders," *Heron*, Vol. 40, No. 3, 1995, pp. 201-215.
84. Justnes, H., Bryhn-Ingebrigtsen, K. & Rosvold, G. O., "Neutron Radiography: An Excellent Method of Measuring Water Penetration and Moisture Distribution in Cementitious Materials," *Advances in Cement Research*, Vol. 6, No. 22, 1994, pp. 67-72.
85. Dawei, M., Chaozong, Z., Zhiping, G., Yisi, L., Fulin, A. & Quitian, M., "The application of Neutron Radiography to the Measurement of Water Permeability of Concrete," *Proceedings of the Second World Conference on Neutron Radiography*, Paris, 16-20 June 1986, pp. 255-262.
86. Kiebel, K. & Krus, M., "NMR- Measurements of Capillary Penetration Behavior of Water & Hydrophobing Agent in Porous Stone & Derivation of New Capillary Transport Values," Report FTB-12e, Fraunhofer-Institut für Bauphysik, Holzkirchen, 1991.
87. Kopinga, K. & Pel, L., "One Dimensional Scanning of Moisture in Porous Materials with NMR," *Rev. Sci. Instrum.* 65(12), 1994.
88. Freitas, V. P. De, Krus, M., Kunzel, H. & Quenard, D., "Determination of the Water Diffusivity of Porous Materials by Gamma Ray Attenuation and NMR," *Proceedings of the International Symposium on Moisture Problems in Building Walls*, Porto, 11-13 Sept. 1995, pp. 445-460.

89. Brocken, H. J. P. & Pel, L., "Moisture Transport over Brick / Mortar Interface," Proceedings of International Symposium on Moisture Problems in Building Walls, Porto, 11-13 Sept. 1995, pp. 415-424.
90. Bjerkeli, L., "X-Ray Tomography as a Method to Determine the Water Absorption in concrete," Report STF 65 A 90008, FCB, SINTEF, Trondheim, 1990.
91. Volkwein, A., "Investigation of Absorption of Water & Chloride in concrete," Heft 1 / 1991, Institute of Building Materials, Technical University of Munich.
92. Volkwein, A., "The Capillary Suction of Water into Concrete & the Abnormal Viscosity of the Pore Water," Cement and Concrete Research, Vol. 23, 1993, pp. 843-852.
93. Witting, G. & Lingott, H., "Investigation of Moisture Transport in Building Materials by Microwave Beam," Bauphysik 14, Heft 2, 1992, pp. 44-49.
94. Vos, B. H., "Non-Steady-State Method for Determination of Moisture Content in structures," Humidity & moisture, Vol. 4, 1965, pp. 35-47, New York.
95. Sosoro, M. & Reinhardt, H. W., "Thermal Imaging of Hazardous Organic Fluids in concrete," Materials and Structures, Vol. 28, No. 183, 1995, pp. 526-533.
96. Sosoro, M., "A Model to Predict the Absorption of Organic Fluids in Concrete," Deutscher Ausschub fur Stahlbeton, Heft 446, Beuth Verlag Gmbh, Berlin, 1995.
97. Kunzel, H. M., "Simultaneous heat and Moisture Transport in Building Components, 1-D & 2-D Calculation using Simple Parameters," IRB Verlag, Stuttgart, 1995.

98. Johannesson, B. F., "Pre-Study on Diffusion and Transient Condensation of Water Vapor in Cement Mortar," *Cement & Concrete Research*, Vol. 32, 2002, pp. 955-962.
99. Mills, R.H., "Mass Transfer of Water Vapor Through Concrete," *Cement & Concrete Research*, Vol.15, 1985, pp.74-82.
100. Perrin, B., Bouny, V.B. and Chemloul, L., "Method of Determination of Hydric Diffusivity of Hardened Cement Paste," *Materials and Structures*, Vol. 31, May 1998, pp.235-241 (in French).
101. Diaw, M., Perrin, B. & Monlouis-Bonnaire, J. P., "Limit of Validity of Moisture Diffusivity for the Study of Moisture Transfer inside Terracotta," *Materials & Structures*, Vol. 35, Jan. to Feb. 2002, pp. 42-49.
102. Drchalova, J., Palvik, Z. & Cerny, R., "A Comparison of Various Techniques for Determination of Moisture Diffusivity from Moisture Profiles," *Sixth Nordic Symposium on Building Physics*, Czech Republic, 2002.
103. Xin, D., Zollinger, D.G. and Allen, G.D., "An Approach to Determine Diffusivity in Hardening Concrete Based on Measured Humidity Profiles," *Advanced Cement Based Materials*, Vol.2, Part: 4, July 1995, pp.138-144.
104. Kaspar, I., "Moisture Transport in building Materials," D.Sc. Thesis, CVUT Praha, Praha, 1984.
105. Cerny, R. & Toman, J., "A Difference Method for Determining the Thermal Conductivity of Porous Materials in a Wide Range," *High Temp.-High Press.*, Vol. 29, 1997, pp. 51-57.

106. Drchalova, J., "A Transient Method for Determination of Moisture Diffusivity,"  
PhD Dissertation, CVUT Praha, Praha, 1983.
107. Drchalova, J. & Cerny, R., "Non-Steady State Methods for Determining the  
Moisture Diffusivity of Porous Materials," International Comm. In Heat & Mass  
Transfer, Vol. 25, 1998, pp. 109-116.
108. Al-Gadhib, A. H. & Rahman, M. K., "Market Survey of Concrete Repair  
Materials in Kingdom of Saudi Arabia," Symposium on Repair & Rehabilitation  
of Concrete Structures, American concrete Institute, Saudi Arabian Chapter, May  
25, 1998, Riyadh.
109. Robery, P. & Shaw, J., "Materials for the Repair & Protection of Concrete,"  
Construction and Building Materials, Vol. 11, No. 5-6, 1997, pp. 275-281.
110. Williams, T. J. & Parker, A. K., "Reinforced Concrete Structural Considerations  
and Choice of Products for Repair," Proceedings of the International Conference  
on Protection of Concrete Structures, University of Dundee, Scotland, September  
1990, pp. 819-830.
111. Emberson, N. K. & Mays, G. C., "Design of Patch Repair: Measurements of  
Physical & Mechanical Properties of Repair Systems for Satisfactory Structural  
Performance," Proceedings of the International Conference, University of  
Dundee, Scotland, September 11-13, 1990, pp. 936-953.
112. Fulton, "Concrete Technology," Edited by Addis, B. J., Seventh Edition,  
Portland Cement Institute, 1994, South Africa.
113. Holt, E. & Jansen, D., "Influence of Early Age Volume Changes on Long Term  
Concrete Shrinkage," Transportation Research Board, Washington, D. C., 1998.

114. Hansen, W., "Constitutive Model for Predicting Ultimate Drying Shrinkage of Concrete," *Journal of American Ceramic Society*, Vol. 70, pp. 329-332, 1987.
115. Hansen, W., "Drying Shrinkage Mechanisms in Portland Cement Paste," *Journal of American Ceramic Society*, Vol. 70, pp. 323-328, 1987.
116. Neville, A. M., "Properties of Concrete," Fourth Edition, John Wiley & Sons, Inc. 1999.
117. Aitcen, P. C., "Does Concrete Shrink or Does it Swell," *Concrete International*, Vol. 21, No. 12, pp. 77-80, 1999.
118. Bazant, Z. P., "Creep and Shrinkage Prediction Model for Analysis and Design of Concrete Structures-Model B3," *Materials & Structures*, Vol. 28, pp. 357-365, 1995.
119. Bhal, N. S. & Jain, J. P., "Effect of Age at the Time of Loading on Creep of Concrete," *The Indian Concrete Journal*, September 1995.
120. Bhal, N. S. & Mital, M. K., "Effect of Relative Humidity on Creep and Shrinkage of Concrete," *The Indian Concrete Journal*, pp. 21-27, January 1996.
121. Gardner, N. J. & Lockman, M. J., "Design Provisions for Drying Shrinkage and Creep of Normal Strength Concrete," *ACI Materials Journal*, Vol. 98, March-April 2001, pp. 159-167.
122. Sakata, K., "Prediction of Concrete Creep and Shrinkage," *Creep and Shrinkage of Concrete*, Proceedings of the Fifth International RILEM Symposium, 1993.
123. ACI Committee 308, "Standard Practice for Curing Concrete," *ACI Manual of Concrete Practice*, Part 2, 2001.

124. "Drying Shrinkage of Cement and Concrete," Cement and Concrete Association of Australia, July 2002.
125. Torrenti, Michael, J. & Granger, "Modeling of Concrete Shrinkage under Variable Ambient Conditions," ACI Materials Journal, Vol. 96, No. 1, pp. 35-39, 1999.
126. Al-Sayed, S. H., "Effect of Curing Conditions on Strength, Porosity, Absorptivity and Shrinkage of Concrete in Hot and Dry Climate," Cement & Concrete Research, Vol. 24, No. 7, 1994.
127. Al-Mudaiheem, J. A. & Hansen, W., "Effect of Specimen Size and Shape on Drying Shrinkage of Concrete," ACI Materials Journal, Vol. 84, No. 2, pp. 130-135, 1987.
128. Troxell, G., Davis, H. & Kelly, J., "Composition and Properties of Concrete," Second Edition, New York, pp. 290-320.
129. Soroka, I., "Portland Cement Paste and Concrete," Macmillan Press Ltd., 1979.
130. Mokarem, D. W., "Development of Concrete Shrinkage Performance Specifications," PhD Dissertation, Virginia State University, May 2002.
131. Dinku, A. & Reinhardt, H. W., "Gas Permeability Coefficient of Cover Concrete as a Performance Control," Materials & Structures, Vol. 30, 1997, pp. 387-393.
132. Meziani, H. & Skoczylas, F., "An Experimental study of the Mechanical Behavior of a Mortar and of its Permeability under Deviatoric Loading," Materials & Structures, Vol. 32, 1999, pp. 403-409.

133. Helene, L., Zoubeir, L. & Frederic, S., "Experimental study of Gas and Liquid Permeability of a Mortar," *Cement & Concrete Research*, Vol. 32, 2002, pp. 1357-1363.
134. Larbi, L. A., "Micro-structure of the Interfacial Zone around Aggregate Particles in Concrete," *Heron*, Vol. 38, No. 1, Page 69, 1993.
135. Roy, D. M., "Concrete Micro-structure and its Relationship to Pore Structure, Permeability and general Durability," *Durability of Concrete*, G. M. Idorn International Symposium, ACI SP-131, pp. 137-149, Detroit, Michigan, 1992.
136. Reinhardt, H. W. & Pfingstner, A., "Fuel Penetration compared to Water Penetration into concrete," *Otto-Graf-Journal*, Vol. 9, 1998.
137. Glasser, F., "Concrete Durability and the role of Porosity," *Network News No. 3*, EPSRC Engineering Network for the application of NMR Techniques to improve Concrete Performance, 2001.
138. Miyazawa, S. & Monteiro, P. J. M., "Volume Change of High Strength Concrete in Moist Conditions," *Cement & concrete Research*, Vol. 26, No. 4, 1996, pp. 567-572.
139. Ollivier, J. P., Massat, M. & Parrott, L., "Parameters influencing Transport Characteristics," *Performance Criteria for Concrete Durability*, RILEM Report 12, 1995.
140. ACI 211.1-91, "Standard Practice for Selecting Proportions for Normal, Heavyweight and Mass Concrete," *ACI Manual of Concrete Practice*, Part I: Material & General Properties of Concrete, P. 38, Detroit, Michigan, 1994.

141. ACI Committee 209, "Prediction of Creep, Shrinkage and Temperature Effects in Concrete Structures," Designing for Effects of Creep, Shrinkage and Temperature, ACI Special Publication No. 27, 1971, pp. 51-93.
142. Mensi, R., Acker, P. and Attolu, A., "Seepage in Concrete: Analysis and Modeling," Materials and Structures, Vol.21, 1988, pp.3-12.

## **VITAE**

- Salman Zafar
- Born in Sargodha, Pakistan in 1976
- Received Bachelor of Science (B.Sc.) in Civil Engineering from University of Engineering and Technology, Lahore, Pakistan in 1999
- Served as Site Engineer at NLC, Pakistan, on Jail Road Lahore Project, from July 1999 to August 1999
- Served as Design Engineer, Structures, at Izhar Group of Companies, Pakistan, from September 1999 to August 2000
- Served as Research Engineer at Council for Works and Housing Research, Ministry of Science and Technology, Government of Pakistan, from September 2000 to August 2001
- Received Master of Science (MS) in Civil Engineering from King Fahd University of Petroleum and Minerals, Dhahran, Saudi Arabia in December 2003